NASA CR-120920

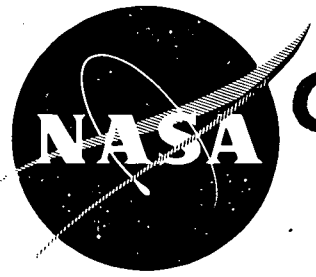

DESIGN, CONSTRUCTION AND EVALUATION OF A 12.2 GHZ, 4.0 KW-CW COUPLED-CAVITY TRAVELING WAVE TUBE

by W.R. Ayers and W.A. Harman

VARIAN ASSOCIATES

prepared for
NATIONAL AERONAUTICS AND SPACE ADMINISTRATION

NASA Lewis Research Center
Contract NAS 3-13728

1. Report No.	2. Government Accession No.	3. Recipient's Catalog No.
NASA CR-120920		

4. Title and Subtitle	5. Report Date
DESIGN, CONSTRUCTION AND EVALUATION OF A 12.2 GHz, 4.0 kW-CW COUPLED-CAVITY TRAVELING WAVE TUBE	March 1973
	6. Performing Organization Code

7. Author(s)	8. Performing Organization Report No.
W. R. Ayers and Ward A. Harman	
	10. Work Unit No.

9. Performing Organization Name and Address	11. Contract or Grant No.
Varian Associates Palo Alto Tube Division 611 Hansen Way Palo Alto, California 94303	NAS 3-13728
	13. Type of Report and Period Covered

12. Sponsoring Agency Name and Address	13. Type of Report and Period Covered
National Aeronautics and Space Administration Washington, D. C. 20546	Final Report
	14. Sponsoring Agency Code

15. Supplementary Notes

Project Manager, G. J. Chomos, Spacecraft Technology Division, NASA Lewis Research Center, Cleveland, Ohio

16. Abstract

This report describes an analytical and experimental program to study design techniques and to utilize these techniques to optimize the performance of an X-band 4 kW, cw traveling wave tube ultimately intended for satellite-borne television broadcast transmitters.

The design is based on the coupled-cavity slow-wave circuit with velocity resynchronization to maximize the conversion efficiency. The design incorporates a collector which is demountable from the tube. This was done to facilitate multistage depressed collector experiments employing a NASA designed axisymmetric, electrostatic collector for linear beam microwave tubes (Ref. 1, 2) after shipment of the tubes to NASA.

17. Key Words (Suggested by Author(s))	18. Distribution Statement
Traveling Wave Tube Coupled-Cavity Slow-Wave Circuit Velocity Resynchronization Demountable Collector Multistage Depressed Collector	Unclassified — Unlimited

19. Security Classif. (of this report)	20. Security Classif. (of this page)	21. No. of Pages	22. Price*
Unclassified	Unclassified	180	

* For sale by the National Technical Information Service, Springfield, Virginia 22151

FOREWORD

The work described herein was done by Varian Associates, Palo Alto Tube Division under NASA Contract NAS3-13728 with Dr. W. R. Ayers as principal investigator. Others working on the project included Dr. J. A. Ruetz, Dr. Ward A. Harman, and Mr. C. Miller. Mr. G. J. Chomos, Spacecraft Technology Division, NASA-Lewis Research Center, was Project Manager.

ABSTRACT

This report describes an analytical and experimental program to study design techniques and to utilize these techniques to optimize the performance of an X-band 4 kW, cw traveling wave tube ultimately intended for satellite-borne television broadcast transmitters.

The design is based on the coupled-cavity slow-wave circuit with velocity resynchronization to maximize the conversion efficiency. The design incorporates a collector which is demountable from the tube. This was done to facilitate multistage depressed collector experiments employing a NASA designed axisymmetric, electrostatic collector for linear beam microwave tubes (Ref. 1, 2) after shipment of the tubes to NASA.

TABLE OF CONTENTS

LIST OF ILLUSTRATIONS

LIST OF ILLUSTRATIONS (Cont.)

LIST OF ILLUSTRATIONS (Cont.)

LIST OF ILLUSTRATIONS (Cont.)

Page Intentionally Left Blank

LIST OF TABLES

DESIGN, CONSTRUCTION AND EVALUATION OF A 12.2 GHz, 4.0 kW, CW COUPLED-CAVITY TRAVELING WAVE TUBE

By: W. R. Ayers and Ward A. Harman
Varian Associates
Palo Alto, California

1.0 SUMMARY

A theoretical design for a high efficiency coupled-cavity traveling wave tube is described. The objective was to obtain 4 kW, cw with 1% bandwidth at 12.2 GHz and with 50% conversion efficiency.

Computer programs, both small and large signal, were employed to analyze the design and to adjust design parameters for maximum conversion efficiency. Velocity resynchronization employing both voltage jump and velocity taper methods have been analyzed.

Five traveling wave tubes were built to verify the analytical design.

The first experimental tube (SN 101) was intended to be used as a test vehicle to check the preliminary circuit design, the adequacy of beam focusing, and techniques for dissipation of heat from the tube body and sever loads. This tube exhibited performance in substantial agreement with analytic prediction. It failed due to an electron gun malfunction which led to excessive beam interception in the output circuit. This high value of beam interception caused sufficient buckling of the output cavity wall to destroy the rf output match.

The second experimental tube (SN 102) was designed to correct the difficulties observed in the first tube. The cavity wall was made slightly thicker to improve the circuit thermal capacity. The circuit cold bandwidth was increased in order to reduce the thermal tuning which had destroyed the rf output match in the first tube. A circuit velocity taper was incorporated into this tube in order to verify the analytic taper design and/or provide experimental data which would aid in refining the taper design. Under test, this tube was found to be electronically unstable, oscillating at a

frequency of 27.6 GHz. This electronic instability was caused by an interaction with the slot mode, a higher order circuit passband in the neighborhood of the coupling slot resonant frequency. The slot resonant frequency had been lowered relative to that in the first tube in order to provide the additional coupling required by the increased bandwidth. Although it was not possible to test this tube to design ratings, operation at reduced beam current showed adequate bandwidth and gain in agreement with predictions. Maximum measured conversion efficiency was 30% running at approximately three-quarters of rated beam current.

The second experimental tube exhibited acceptable beam transmission and performed in a predictable manner at reduced beam current. It operated without arcs, and except for the instability already noted, exhibited no performance anomalies operating at 2 kW, cw.

A third experimental tube (SN 103) was built based on the prediction that, by eliminating the slot mode instability, it would be possible to confirm the analytical predictions of efficiency at rated beam current and verify the design principles employed, as well as providing experimental data for further optimization of the final design. Iron powder was sprayed and sintered in four of the slots in the output circuit section to provide distributed attenuation of power on the interactive circuit in order to achieve the required stability.

SN 103 exhibited the increased electronic stability which the additional loss was intended to provide. This tube was operated at rated beam voltage and current with zero drive to saturated drive across the entire cold passband without oscillations. While stability had been much improved, relative to SN 102, efficiency had suffered, both because of too little small signal gain beyond the sever and because of too much loss in the output circuit. During cw test the performance of SN 103 deteriorated rapidly and testing was discontinued pending analysis of the cause of this deterioration. The output match had deteriorated to such a degree that further hot testing was abandoned. The collector was removed but no circuit melting was revealed. A check of gap spacing, however, showed cavity wall warping near the center of the output circuit.

In SN 103 as in SN 101 failure had occurred as a result of similar thermal deformation of the cavity wall. SN 102, on the other hand, had run at higher power levels than either of the other tubes without exhibiting thermal deterioration. It was concluded from this evidence that the circuit thermal design was marginal. It was decided to build the two final tubes with cavity walls twice as thick as those employed in SN 103.

The final two tubes were designed with the maximum velocity taper which could be accommodated without seriously diminishing the interaction impedance of the output cavities. The shape of the coupling slots was changed in order to achieve a higher slot resonant frequency, thereby reducing the need for circuit loss required to obtain electronic stability. The resultant reduction in output circuit loss was deemed essential to maximize the efficiency of the tube.

Test data from SN 104 established the predicted electronic stability and produced cw power levels up to 3.7 kW without deterioration in performance due to thermal effects. The measured efficiency was less than 30% against a predicted conversion efficiency of 38%. The power dissipated on the body of the circuit was approximately 25% of the output power, from which it was deduced that excessive rf circuit losses probably accounted for the lower than predicted efficiency.

SN 105 was identical to SN 104 except for the removal of circuit loss from one more cavity in the output section. This modification was expected to increase efficiency and decrease electronic stability although the latter was still expected to be adequate.

Test results on SN 105 showed a slight increase in efficiency and a decrease in body power compared to those measurements on SN 104. The maximum efficiency measured at the microwave calorimeter was 29%. With reasonable allowances for power dissipated in the output waveguide and window and in the external waveguide components, the estimated maximum intrinsic conversion efficiency of the TWT is 31%. The measured efficiency was found to increase with beam voltage. This fact, almost certainly indicates a nonoptimum circuit velocity taper.

In all, three different circuit configurations were tested: SN 101 employed thin tapered cavity walls and circular coupling slots and possessed about 2% cold bandwidth. SN 102 and 103 employed 0.020 in. thick cavity walls and long thin coupling slots and possessed about 4% cold bandwidth. SN 104 and 105 employed 0.040 in. thick cavity walls with short thick coupling slots and possessed about 3.5% cold bandwidth.

The desired goal of 50% conversion efficiency has not been achieved. Theoretical predictions of efficiency, however, are in reasonable agreement with experiment when it is considered that the theoretical model assumed that the desired circuit velocity taper could be achieved without compromising circuit impedance to the extent actually measured later. It is felt that a considerable increase in efficiency could be achieved by an improved taper design. Further analysis should be performed to optimize the velocity taper subject to the constraints imposed by thermal and mechanical considerations. Interaction efficiency of about 40% should be achievable in an extension of the present design.

2.0 INTRODUCTION

This report describes an analytic and experimental program for a high efficiency traveling wave tube for use in a satellite television transmitter. The primary objective of this program was to demonstrate the feasibility of obtaining very high interaction efficiency in a narrowband TWT operating at 4 kW, cw and at 12.2 GHz. Two tubes and ten demountable guns were to be delivered to Lewis Research Center to be operated in a space chamber and to be used for operation with a NASA designed multistage depressed collector. In addition to delivery of the hardware items it was intended to experimentally verify analytic design techniques for high efficiency based on a number of Varian designed computer programs.

The first task on the program was the development of a design and the analytic optimization of this design. This was followed by the fabrication and test of five traveling wave tubes. Each tube provided data which were used to modify the design of subsequent tubes, to better meet the performance objectives or to eliminate experimentally observed defects.

Computed small signal gain and efficiency was in substantial agreement with experimentally measured gain and efficiency. Predicted efficiency was somewhat optimistic compared with experimental measurements although, to some extent, experimental difficulties may have masked the predicted performance.

3.0 DESIGN APPROACH AND TRADE-OFF CONSIDERATIONS

The basic design approach chosen was to use a staggered-slot coupled-cavity slow-wave circuit in conjunction with convergent confined flow beam optics. At the frequency, power level and beam voltage specified, no other circuit type was deemed appropriate for consideration. The requirement for high efficiency mandated the use of a strongly focused electron beam. The factors which influenced the initial choice of parameters are outlined in this section.

3.1 SUMMARY OF SPECIFICATIONS

The major TWT specifications are summarized in Table 3.1. Those specifications which most directly effect the choice of design parameters are frequency, power and efficiency. Frequency and power, taken together, place limits on the mechanical design due to thermal considerations; the choice of circuit and beam parameters for high efficiency, as will be shown, is often in conflict with these thermal considerations.

3.2 INITIAL ELECTRICAL DESIGN

To achieve the specified 4 kW output power at 50% conversion efficiency would require a beam power of 8 kW. To insure that the initial design would not be marginal, it was decided to base the design on a beam power of 9 kW.

The choice of beam voltage, within the specified 16 kv maximum, is controlled by the requirement for high efficiency and the need for thermal stability weighed against the requirement of long life. Life considerations imply limits on cathode current density. Parameter optimization for maximum efficiency typically requires the maximization of the Pierce (Ref. 3) gain parameter C so long as a small space charge parameter QC can be maintained.

Other things being equal, the beam voltage should be chosen to maximize C. The gain parameter is defined by:

TABLE 3.1

MAJOR TWT SPECIFICATIONS

Electronic Conversion Efficiency	50% min
Frequency	12.2 GHz
Bandwidth	120 MHz
Power	4.0 kW min
Gain	40 ± 1.5 dB
Design Life	2 yr min
Phase Linearity $(d^2\phi/df^2)$	$0.005°/MHz^2$ max
Collector Magnetic Leakage	0.5% max
Dc Beam Transmission	99.5% min
Beam Transmission at Saturation	98% min
Maximum Beam Voltage	16 kv
Tube and Focusing Magnet must be capable of operation inside vacuum chamber	
Demountable Collector	
Demountable Electron Gun	

$$C^3 = \frac{K\ I_o}{4\ V_o} \tag{3.1}$$

where K is the Pierce impedance, I_o is the beam current, and V_o is the beam voltage. Eliminating I_o from Equation 3.1 yields:

$$C^3 = \frac{K\ P_o}{4\ V_o^2} \tag{3.2}$$

where P_o is the beam power. The Pierce impedance is proportional to the cavity R/Q, which in turn is approximately proportional to cavity height. Neglecting the thickness of the web between cavities, the cavity height is proportional to beam velocity, hence, Equation 3.2 may be written in the form:

$$C^3 \propto \frac{P_o}{V_o^{3/2}} \tag{3.3}$$

which reduces to

$$C \propto \frac{P_o^{1/3}}{V_o^{1/2}} \tag{3.4}$$

It is thus clear that the gain parameter increases slowly as the beam voltage is reduced at constant beam power. Decreasing the beam voltage, however, also increases the required beam current and the magnetic field required to focus the beam.

For fixed beam and drift tube radii, the space-charge parameter can be shown to take the form:

$$QC \propto \frac{S}{C^2} \tag{3.5}$$

where S is the beam perveance defined by:

$$S = \frac{P_o}{V_o^{5/2}} \tag{3.6}$$

Combining Equations 3.4, 3.5 and 3.6 we obtain:

$$QC \propto \frac{P_o^{1/3}}{V_o^{3/2}} \tag{3.7}$$

At constant beam power, the space-charge parameter is seen to vary three times more rapidly than the gain parameter. The effect of the increase in C which could be achieved by reducing the beam voltage would tend to be neutralized by the concurrent increase in the space-charge parameter. Gerchberg and Niclas (Ref. 4) have made experimental measurements which show that η/C decreases as the beam perveance is increased. It must be concluded that assumptions and constraints other than those assumed above will have an important bearing on the choice of beam voltage.

Listed below are two other factors which play an important role in the choice of operating beam voltage:

1. The web thickness is determined by mechanical and thermal considerations. In no case would it be feasible to diminish the web thickness as the beam velocity is reduced. Hence, as the beam voltage is lowered, the cavity height and the Pierce impedance would diminish more rapidly than was assumed in the above analysis.

2. In order to maximize the efficiency, it will be necessary to employ some method of velocity resynchronization. This will probably require a reduction in the cavity height at the output of the TWT. The tube should thus be designed with the greatest cavity height possible, and consequently should run at the highest permissible beam voltage.

Based on the above arguments, a beam voltage of 15 kV was chosen for the initial design. This choice allowed for some flexibility in the actual operating voltage without exceeding the maximum allowable voltage. The design beam current corresponding to the selected beam voltage and beam power is 600 mA.

It is necessary to examine the repercussion of the above choices on the electron gun and beam focusing system. To obtain long life, the cathode current density must be kept low. To obtain good beam optics the beam convergence must also be kept to a minimum. A trade-off between these parameters may be made after the beam diameter has been chosen.

The normalized beam radius is $\beta_e r_o$ where $\beta_e = \omega/u_o$ is the electronic propagation number and r_o is the beam radius. There is extensive emperical evidence that the beam must be kept small to maximize conversion efficiency. If the beam is large the center of the beam will contribute little to the interaction process. The minimum practical drift tube diameter is determined by the beam size, and since the cavity R/Q is influenced by drift tube size, it is doubly important to minimize the diameter of both the beam and drift tube. On the other hand, a lower limit on beam size is set by space charge effects and by beam optics and focusing considerations.

The initial design has assumed a value of $\beta_e r_o = 0.6$. This value is near optimum from the standpoint of the interaction process. It remains to be shown that this choice does not place unrealistic demands on the gun design.

The above assumed normalized beam radius corresponds to a beam diameter of 0.044 in., a beam current density of 61.2 A/cm^2, a beam perveance of 0.327 μpervs and a Brillouin field of 1040 gauss.

The area convergence of the beam must be chosen large enough to assure tolerable loading of the cathode, yet small enough to provide reasonable gun optics. Experience has shown that area convergences as high as 50:1 are reasonable, in the theoretical design of a gun, capable of producing a beam with excellent laminarity at low perveance. The major problem in low perveance guns stems from the fact that

the location of the focus electrode relative to the cathode is more critical than in higher perveance designs. High area convergence generally complicates magnetic design in a convergent confined flow system since it is necessary to find a magnetic flux pattern which duplicates the trajectories of the electrons in the cathode-anode region.

At lower area convergence ratios, cathode current density becomes a problem. The use of impregnated tungsten cathodes will allow long life expectation at 2 A/cm^2. In the design under consideration, for example, with an area convergence ratio of 20:1, the average cathode current density would be 3 A/cm^2; a value somewhat higher than believed to be desirable for tube life.

An area convergence of approximately 40:1 was chosen as a reasonable compromise in the initial tube design. At the selected cathode diameter of 0.282 in., the predicted maximum cathode current density would be less than 1.75 A/cm^2, a value entirely compatible with the required design life of two years minimum.

The drift tube diameter must be chosen as small as possible in order to maximize the circuit interaction impedance. The high beam transmission required in the present design could be readily assured by choosing a drift tube diameter 1.5 times the nominal beam diameter. However, for the present design, a tunnel diameter 1.43 times the nominal beam diameter has been chosen as a reasonable trade-off between the need for high efficiency and the requirement for high beam transmission. The resultant drift tube diameter is 0.0625 in. based on filling factor 0.7.

The three remaining major design parameters are: cavity period, gap length and intercavity web thickness. A preliminary estimate of the cavity period is 0.150 in. This parameter will be further refined by analytical computation.

The gap length δ should be kept small in order to maximize the beam coupling coefficient. Because the cavity R/Q increases with gap length, the interaction impedance does not depend too critically on the choice of gap length. A normalized

gap length of one radian would correspond to a gap spacing of 0.032 in. It would not be prudent to use such a gap spacing in the present design. The high gap tuning rate associated with such a small gap would make it difficult to fabricate circuit parts to the required precision, as well as aggravating thermal tuning effects. A normalized gap length of two radians would mean a sacrifice in interaction impedance which could not be tolerated in a design where efficiency is so important. An initial choice of 0.040 in. gap spacing was selected, with the option of later increasing the spacing if analytic or experimental data should so indicate.

The web thickness is perhaps the most difficult parameter to select. For maximum R/Q and maximum conversion efficiency the web must be thin. However, if the web is too thin the structure will be thermally unstable. In order to estimate the required thermal capacity of the web it is necessary to first estimate the maximum beam power incident on a single drift tube. The specified minimum beam transmission at saturated drive is 98%. If 2% of the beam current is intercepted on the circuit at full dc energy, it would be necessary to design for a total beam dissipation of 180 W. At zero drive, the specification limits the total beam dissipation to 45 W. The majority of electrons collected on the circuit at saturated drive would be electrons which had lost a significant fraction of their energy. It would be reasonable to assume, therefore, a maximum total beam dissipation of 100 W.

Rf dissipation is estimated to be less than 0.1 dB per cavity in the output cavities. This corresponds to approximately 100 W of rf dissipation in the output cavity, and if the tube is overdriven, an equal amount of rf dissipation should be anticipated in any of the last three or four cavities of the output circuit. The spatial distribution of rf heating is rather complex but, except in the case of cavities which are extremely reentrant, the preponderance of rf dissipation is toward the outer surfaces of the cavity. In order to estimate the effect of rf heating, we assume that the total estimated rf dissipation is injected into the web at a radius equal to one-half the cavity radius. Assuming a cavity radius of 0.350 in. and a copper web 0.020 in. thick, the calculated temperature drop between the injection radius and the cavity radius is 20°C. It will be shown that this rf heating component is essentially negligible compared with the anticipated temperature gradients due to beam interception.

Having estimated the total thermal flux from beam interception at 100 W, it is now necessary to make a plausible assumption regarding the spatial distribution of this heat. It is difficult to generalize how and where the beam will be intercepted because each tube will tend to behave individualistically. In most cases it would be reasonable to guess that one-quarter to one-half the power is intercepted in the driver section of the tube, in such a way that no adverse thermal effects will result. The remainder of the power might be expected to impinge on two or three of the final drift tubes in the output section of the tube. For estimation purposes it has been assumed that 50 W of thermal power is incident on a single drift tube tip. Figure 3-1 shows a typical representative drift tube and cavity web. The estimated thermal impedance, assuming power input at the tip of the drift tube, is 3.77°C/W. The effect of the coupling slot in the web would be to increase the estimated thermal impedance to approximately 4°C/W with an assumed web thickness of 0.020 in. Incident power of 50 W would therefore increase the temperature of the drift tube tip by 200°C above the cavity wall temperature, which can be assumed not to exceed 100°C. A maximum temperature of 300°C would appear to be reasonable, based on test performance of other high power coupled-cavity TWTs.

A summary of the selected preliminary design parameters is given in Table 3.2. It should be emphasized that these parameters are chosen to guide the design of the first experimental tube. They reflect a strong emphasis on the need for high conversion efficiency and therefore may lead to a design with unforeseen shortcomings. Test data from the first experimental tube will be used as basis for design refinement.

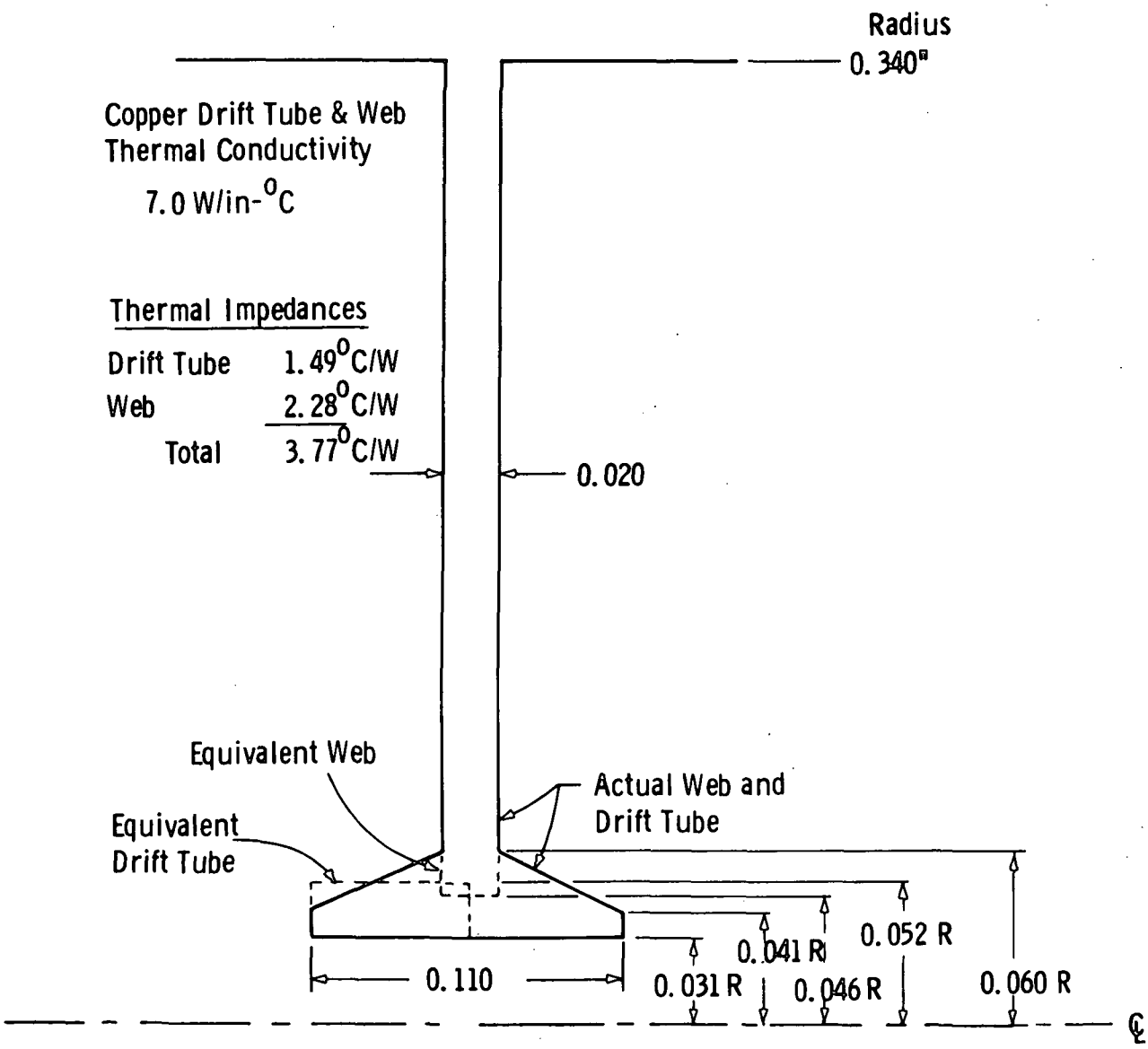

Figure 3-1. Estimated Thermal Capacity of Drift Tube and Web for Initial Tube Design

TABLE 3.2

PRELIMINARY DESIGN PARAMETERS

Beam Voltage	15	kV
Beam Current	600	mA
Beam Perveance	0.327	μperv
Normalized Beam Radius ($\beta_e r_o$)	0.6	rad
Beam Diameter	0.044	in.
Beam Current Density	61.2	A/cm^2
Brillouin Field	1040	G
Magnetic Focusing Field	2500	G
Cathode Diameter	0.282	in.
Beam Convergence	40:1	
Maximum Cathode Current Density	1.75	A/cm^2
Drift Tube Diameter	0.062	in.
Beam Filling Factor	0.70	
Gap Spacing	0.040	in.
Cavity Period	0.150	in.
Web Thickness	0.020	in.

4.0 ANALYTICAL DESIGN

The analytical design procedure is based on a number of Varian computer programs which model the rf interaction process in a coupled-cavity traveling wave tube. These programs are used to refine the initial design; i.e., to ensure that the TWT will perform at the required frequency when operated at the desired beam voltage and beam current, as well as to predict the efficiency as a function of the particular velocity resynchronization scheme being used. Because the programs are basically analytic rather than synthetic in nature, it is necessary, in order to synthesize a design, to compute a number of designs in order to systematically optimize a given parameter.

4.1 REVIEW OF ANALYTIC CAPABILITY

Figure 4-1 outlines the steps and procedures typically employed in optimizing a coupled-cavity tube design. Not all of these steps are employed in every design, depending upon the design starting point and upon the design objectives. As seen in the figure, many steps are used. A brief description of the various steps follows:

1. "CCAV" is a timeshare program which generates major design parameters through a generalized set of scaling relationships.
2. "CCEQCT" is a timeshare program which generates equivalent circuit elements to match a given set of circuit characteristics, such as phase, impedance, and loss.
3. "SSCAV" timeshare program uses the equivalent circuit generated by "CCEQCT" to calculate the complete small signal characteristics of the coupled-cavity tube including gain, gain ripple, phase characteristics and stability of each section. The number of severs, number of cavities per section, gap-to-period ratios, loss patterns, etc., may all be optimized with the aid of this program.
4. Cold circuit measurements of actual circuit sections are made. These include dielectric rod perturbation measurements for determining circuit impedance. Circuit matching characteristics are also measured

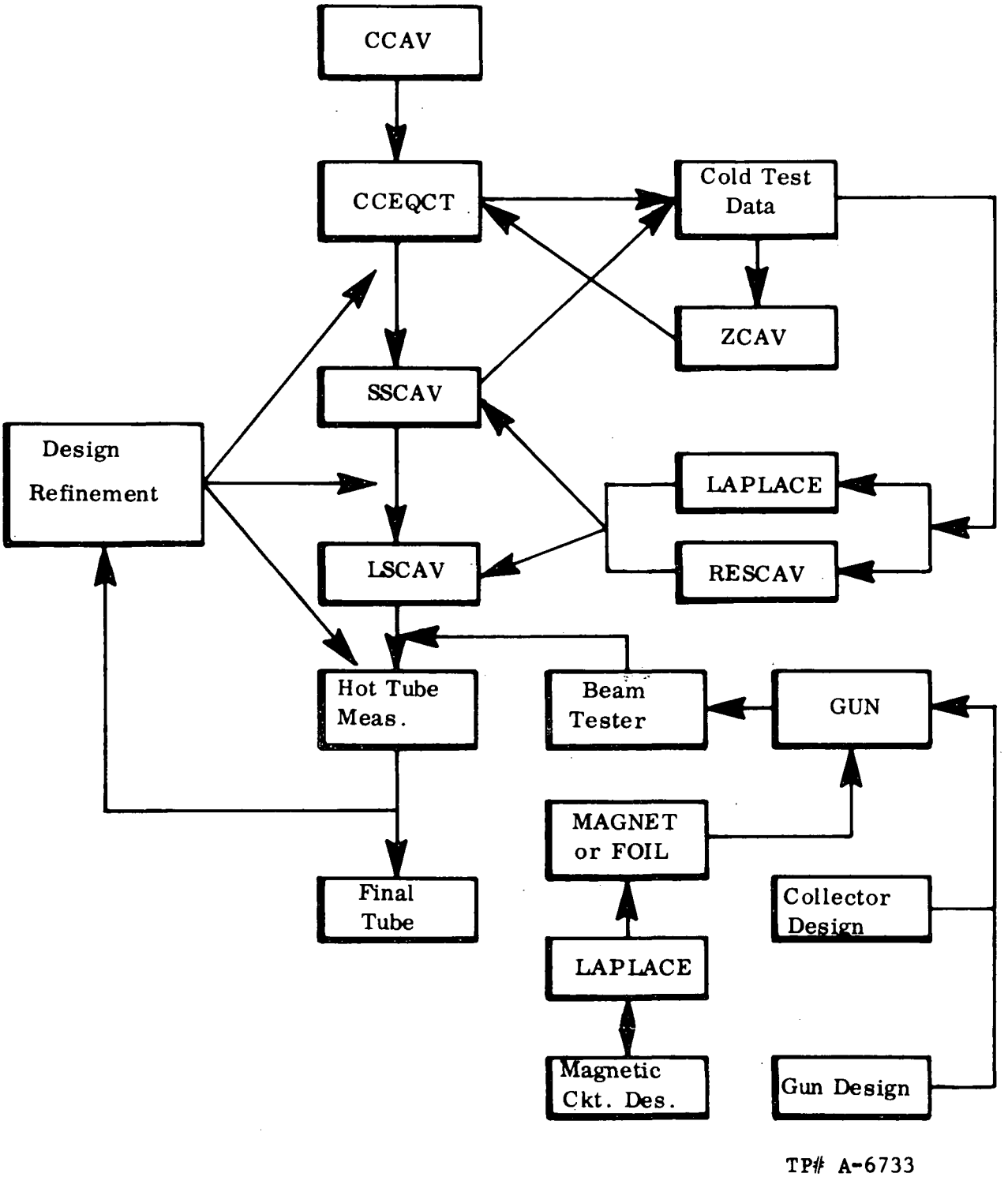

Figure 4-1. Procedure for Optimizing Coupled-Cavity TWT Design

and can either be used directly or simulated in the equivalent circuit models of the cavities.

5. "ZCAV" timeshare program reduces perturbation data to actual impedance data useful for refining any initially assumed circuit model. Equivalent circuits can be generated by "CCEQT" which accurately represent any of the measured circuit sections, including their loss characteristics.

6. The exact cavity field shape for use in either the large or small signal Varian program is obtained either from "LAPLACE" which solves the Laplace equation for arbitrary boundaries or from "RESCAV" which solves the wave equation inside a cavity of arbitrary shape. A one-dimensional field shape is used in the Varian computer model of the cavities. This field shape is obtained by averaging the actual field over the cross section of the beam. Electrons are numerically integrated through this total gap field, so that in effect, all of the space harmonic fields are accounted for in the analysis.

7. "LSCAV" calculates the large signal performance of coupled-cavity tubes.

8. "GUN" solves the electron trajectories for arbitrary beam flow problems including space charge, axially symmetric magnetic fields, relativistic effects (including the self-magnetic field of the beam) and the effects of thermal velocities. Collector beam spread calculations may also be performed with this program in addition to the design of electron guns. The "LAPLACE" program may also be used in conjunction with the "GUN" program for calculating the magnetic field configurations in the gun and collector regions of the tube.

9. Varian's beam tester thoroughly evaluates the performance of actual gun configurations. Normally, a beam test is not required except in the case of gridded guns or guns of unusual design where it is desirable to perform an experimental verification of the computed design.

10. "FOIL" is a timeshare program which will calculate either an aluminum or a copper foil solenoid design. "MAGNET" is an additional program for calculating wire-wound soelnoids.

These represent the principal design steps which would typically be employed leading up to a "hot" test tube. Once a tube is tested the actual performance data are available for refining portions of the design if necessary.

To compute the interaction in a TWT it is necessary to adequately model the circuit and the beam. Both the Varian large and small signal programs employ a common circuit model. The beam models differ: for the large signal case it is necessary to model the nonlinear beam processes whereas, in the small signal case, a linear beam model suffices.

Circuit parameters are taken from actual cold test measurements which are used to obtain an equivalent circuit representation of the coupled-cavity circuit as proposed by Curnow (Ref. 5). This particular equivalent circuit models the actual coupled-cavity circuit extremely well, both with regard to phase characteristics and to the circuit interaction and matching impedances. When the coupled-cavity TWT program is operated such that it derives all of the basic circuit quantities from the equivalent circuit representation of the cavity, it is capable of accurately calculating both inside and outside performance of the propagating passbands. In addition, the equivalent circuit representation (with lossy elements) allows a more accurate calculation to be made by using complex interaction impedances rather than real impedances. Operated in this manner, programs have been used to accurately predict the start-oscillation conditions for band edge oscillations even when these oscillations occur outside of the propagation band of the main interaction circuit.

One of the important features of the Varian programs is that the beam interacts with the total gap field of the cavity so that interaction with all space harmonic components of both forward and backward propagating waves is fully taken into account. The shape of the actual gap fields (used as program input data) may be obtained either

from actual measurements or by means of additional Varian computer programs capable of solving either the Laplace or the wave equation for arbitrary cavity geometries.

It has become increasingly clear that the usual small and large signal programs, based upon the Pierce concept of interaction with single space harmonic field components, is entirely inadequate for describing the coupled-cavity tube in which the electrons interact with gap-type fields. In addition, the Varian programs have been designed to work with the actual tube parameters in terms of circuit dimensions, velocities, currents, voltages, etc., rather than in terms of generalized design parameters such as QC, b, γa, etc. Also, since the total electronic interaction is accounted for within the theory, it is unnecessary to adjust any of the input data parameters to compensate for the effects of beam loading upon the impedance or the propagating characteristics of the circuit. With dispersive circuits, for example, there is no need to artificially adjust parameters like Pierce's "b" parameter to account for changes in synchronization conditions within the tube. In place of Pierce's C parameter, which is artificially tied to only one component of the total interaction impedance, the Varian program uses a total $V^2/2P$ gap impedance comparable to that used in klystron theory. In fact, this program works equally well for TWTs or for klystrons, and calculations have checked favorably with some of the more sophisticated klystron programs, both for small signal and for large signal.

The gap voltage that is used in the calculation for any specific gap is that which results from both the forward and backward propagating wave at any given instant of time, so that the complete interaction is calculated. In the large signal calculation, where a step-by-step forward integration process is employed, the proper backward wave must be obtained through an iteration process. In coupled-cavity tubes with large gains per cavity the backward wave accounts for much of the observed behavior. Programs that do not properly account for the backward wave will generally be in serious error at most all frequencies, with the possible exception of band center. (The backward wave effects are very often minimal at band center where all backward components are far from synchronism with the beam.)

Typical input data to the programs are circuit voltage, beam current, circuit and beam dimensions, matching conditions, cold circuit impedance and phase data, description of the circuit field shape averaged over the beam cross section, and the cavity Q and associated loss characteristics.

The beam and wave velocities are calculated from the input data, space charge depression of the beam is calculated from the circuit and beam dimensions, space charge forces are calculated directly from the geometry of the model, and gap coupling is automatically calculated by integrating the electrons through the prescribed circuit fields, all of which is accomplished in a fully relativistic manner. In place of the usual QC, C, b, K, etc., Pierce parameters, the Varian program uses quantities such as ω_q/ω, u_o/c, v_p/c, $V^2/2P$ and other parameters related specifically to the physical tube under analysis rather than to a generalized set of parameters.

Since the disc electron beam model (properly treated) has proven accurate for the case of distributed circuit interactions (as in a helix-type tube) it was also used for modeling the beam in the large signal coupled-cavity programs. Although numerous improvements have been made over the original Tien (Ref. 6) model, the discs used in the Varian program are rigid, fixed charge, representing laminar one-dimensional flow. Overtaking of electrons is allowed in the program. So far, it has not been considered necessary to go to ring or other more elaborate electron models, although this step has been given serious consideration and may well be implemented in the future. However, the effects of specific electron models are not considered to be as important as obtaining a proper description of the space charge forces between the electron discs. This is particularly true in the regions of the gap where the boundary conditions are considerably more complicated than for a drift tube.

Constant improvements are being made on the space charge modeling of the beam forces, to achieve as close agreement with experiment as possible. Approximations have been removed from the original Tien model, both with respect to evaluating the plasma frequency reduction factor and with respect to calculating the range of the space charge forces between discs. Consideration has been given to

models proposed by Kino and others which reduce the rather high force that is obtained in the Tien model when two electrons approach each other. It is apparent that a force of this type between two rather large "lumped" charges is not truly representative of the forces that exist in a beam when it contains a very large number of electrons, each having a very small charge. One solution is to employ a "thick" electron model with a linearly varying force that passes through zero as the two electrons pass through each other. The electron thickness in this model approaches zero as the total number of electrons is increased. A model has also been implemented, that was proposed by S. Wallender, in which the space charge fields are obtained by summing the field contributions from the various harmonics which make up the total beam current. Since it takes approximately 2N electron discs to accurately represent N beam harmonics, Wallender sums only the N lowest beam harmonics, to achieve a more consistent force relationship between the electron discs when a finite number of discs are used. The effect of limiting the number of harmonics is to round off the discontinuity in the force curve, as illustrated in Figure 4-2.

The large signal calculations carried out in the present investigation have employed the Wallender space charge model. In this formalism the space charge field components are derived from the Fourier components of the rf convection current which relates to the time of arrival of the discs at a given location. Since the beam convection current at a point is a periodic function of time, there is no explicit limit imposed by this formalism on the number of rf cycles of discs employed. In the previously used thick disc model, three rf cycles of discs were employed.

For the beam sizes generally encountered in most TWTs and klystrons, it is felt that the large signal beam model used in the Varian program is as good as, if not better than, the model used in other programs. Actually, a one-dimensional model has been successfully used in Varian's large signal klystron programs to calculate efficiencies in the 50% to 75% range with good experimental agreement. One Varian klystron with a measured conversion efficiency of 75% has a computed conversion efficiency of 83% (Ref. 7). Another klystron with a measured conversion efficiency of 60% has a computed conversion efficiency of less than 62% (Ref.; Goldfinger, A.; Lien, Erling L.:

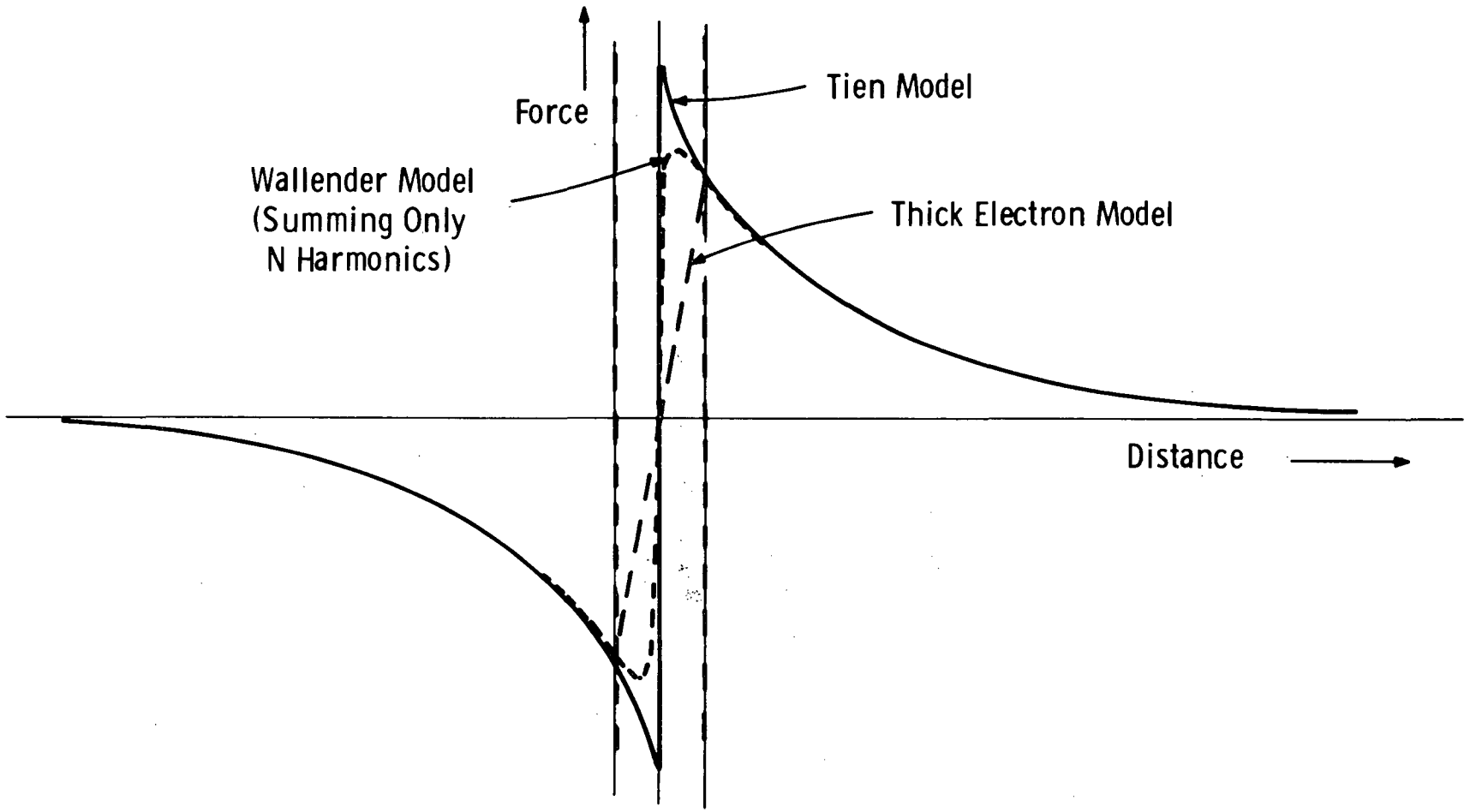

Figure 4-2. Force Fields of Various Disc Models

Private communication regarding design, fabrication and test of Varian 2 kW cw, S-band klystron, Oct. 1972). In the former case, a program which properly took into account radial rf fields and radial beam modulation could be expected to substantially reduce the computed error. In the latter case, at the 60% efficiency level, little improvement could be expected, certainly not enough to justify the increased computer costs. These data would tend to verify the prediction that the effect of radial rf fields in confined flow klystrons is significant only when the normalized gap voltage is extremely high.

In high efficiency coupled-cavity traveling wave tubes the output cavity normalized gap field will not likely reach the levels encountered in the 60% efficiency klystron cited earlier. So long as the normalized beam diameter is small, as it must be, and the beam is well confined, the one-dimensional rigid disc model which was used in the present study should predict efficiency accurately. It is Varian's position that most programs err because of inadequacies in the circuit models and in space charge force calculations rather than because of the short-comings of the rigid disc model. For examples in which very large variations in field occur over the beam cross section, or for tubes employing Brillouin or PPM focusing, a ring model may very well improve the calculation. It is possible that this and other improvements may be added as the program capabilities are improved. Based on Varian's large signal klystron program, failure to account for radial interaction effects, leads to no appreciable effect until efficiencies greater than 60% are reached.

4.2 SMALL SIGNAL ANALYSIS

The initial small signal analysis begins with the assumed initial design parameters given in Table 3.2. A four-times scale model of the cavity was built in order to obtain impedance data for the small signal computer simulation. The scaled circuit permits ease of measurement and will be used to experimentally adjust the size of the coupling iris required to obtain the desired cold bandpass characteristics of the circuit.

The preliminary circuit design employs a circuit with approximately 2% cold bandwidth. This choice, based on experience, should provide the required hot

bandwidth of approximately 1%, while yielding the highest possible interaction impedance.

The design of the slow wave circuit coupling slot is empirical. Analytical design techniques have not been developed to aid in the selection of the optimum coupling slot. Generally a trial slot is cut somewhat smaller than experience would predict is required. After measuring the bandwidth produced by the first trial slot it is usually possible to enlarge the slot for successive trials until the required bandwidth is achieved.

The four-times scale model used in the first trial cold-test circuit is shown in Figure 4-3. The cavity walls have been tapered in order to achieve the highest possible impedance. Figure 4-4 shows the measured normalized phase curve for the cold-test circuit. The frequency and bandwidth of this circuit are quite close to the desired values. Perturbation measurements of this cold-test circuit yielded a measured cavity R/Q of 65.

The equivalent circuit for the preliminary design was obtained using computer programs "ZCAV" and "CCEQT". Figure 4-5 shows the assumed normalized phase curve for the preliminary circuit. Figure 4-6 shows the computed interaction impedance, $V^2/2P$. Figure 4-7 shows the computed Pierce impedance for the space harmonic of interest.

To compute the circuit performance it is necessary to generate a gap field shape function. This is done by solving the wave equation for a single cavity with extended drift tubes. The axial electric field in the gap at the tunnel radius is assumed to be the mean of the field which would exist in an ideal gridded gap and the field which would exist between the tips of infinitesimally thin cylinders. The Fourier coefficients for these assumed fields are sin (nx)/(nx) and $J_o(nx)$ respectively. The Fourier period is chosen long enough to assure an accurate representation of the fields within the tunnel to a point where the axial field is less than 2% of the gap. A sufficient number of Fourier terms are used to assure the required accuracy. The resultant normalized gap field

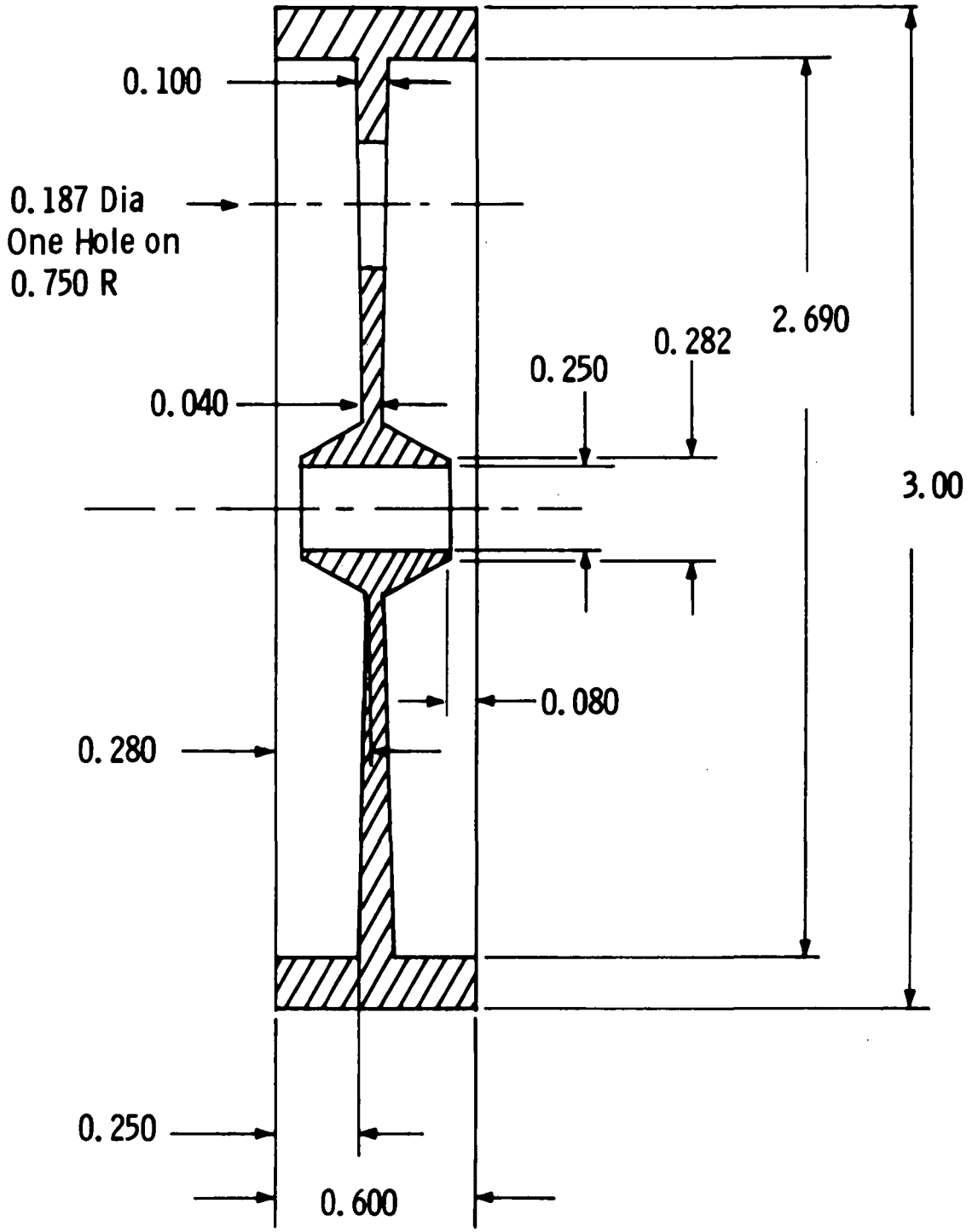

Figure 4-3. Four Times Scale Model Cavity Web and Drift Tube for Preliminary Circuit Design

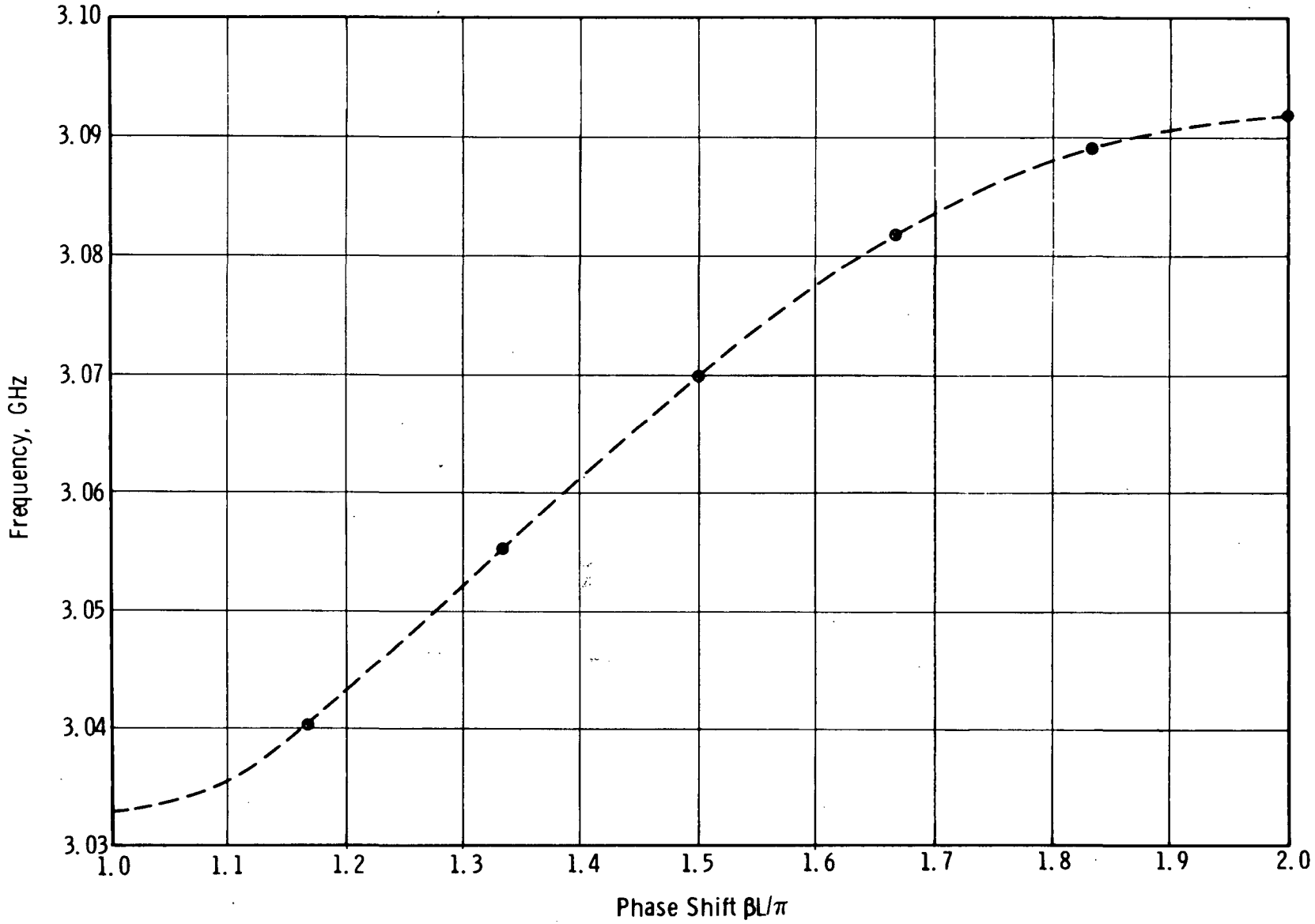

Figure 4-4. Measured Phase Characteristics of Scaled Circuit

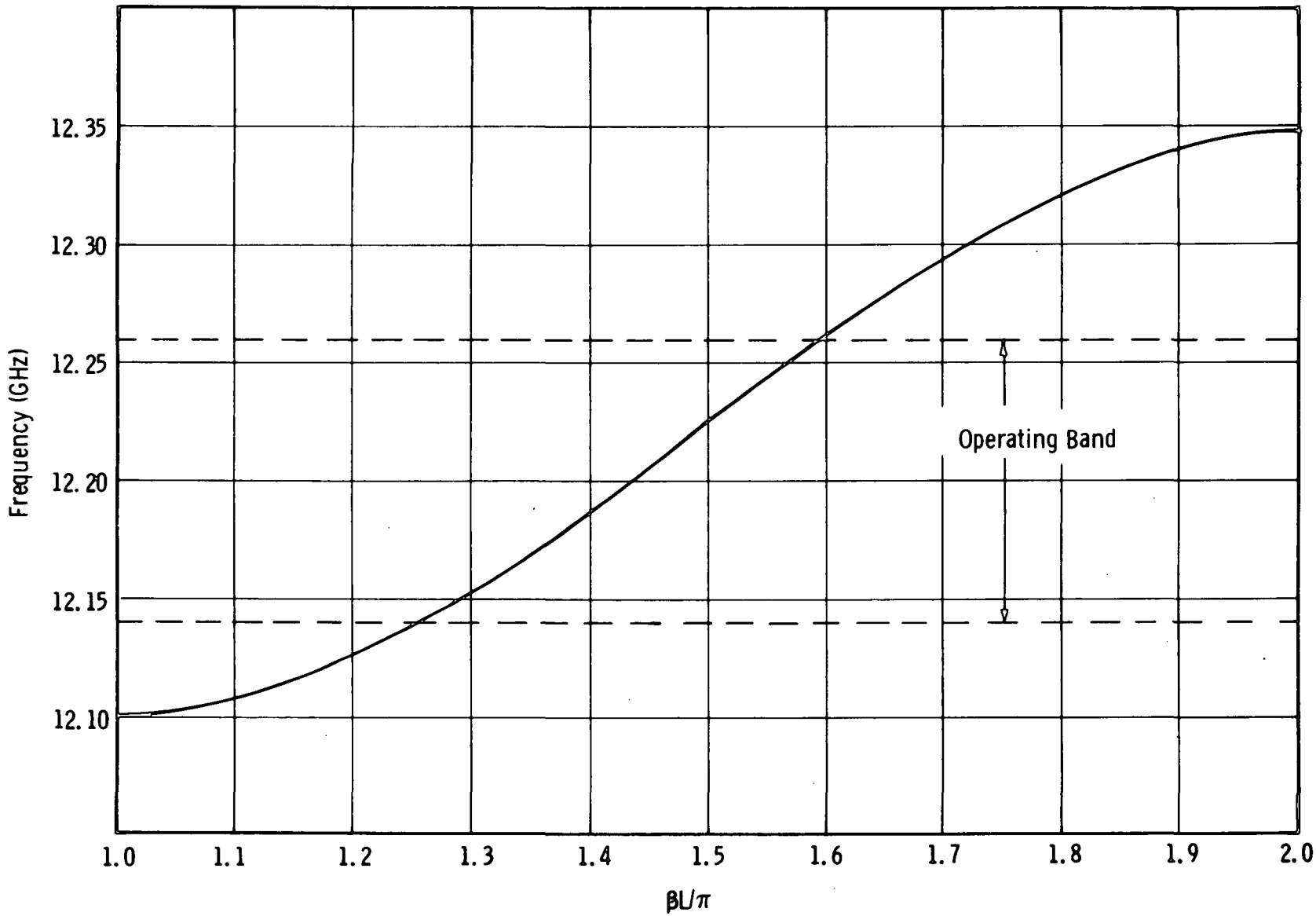

Figure 4-5. Normalized Phase Curve for Preliminary Design

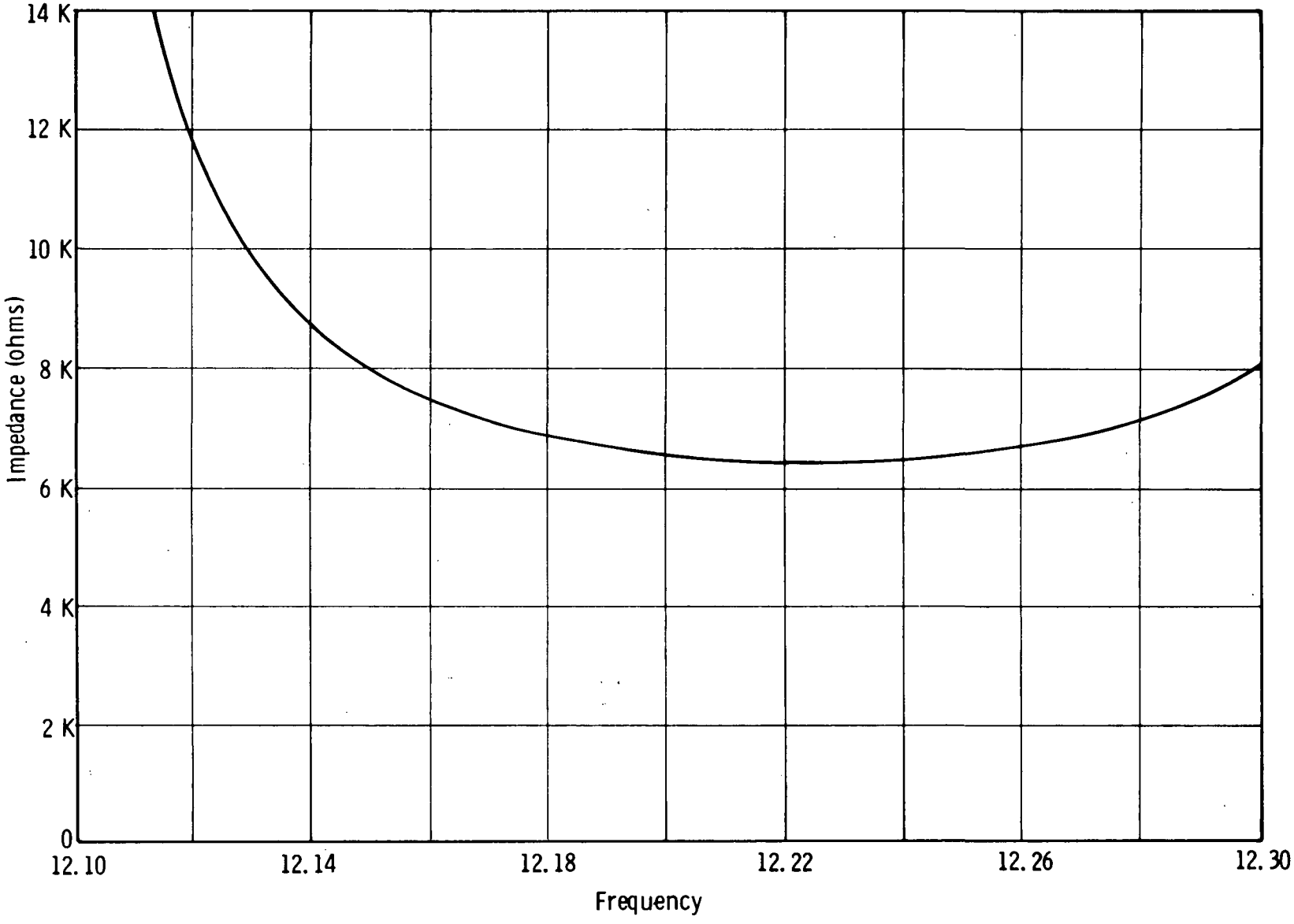

Figure 4-6. Computed Interaction Impedance $V^2/2P$ for Preliminary Design

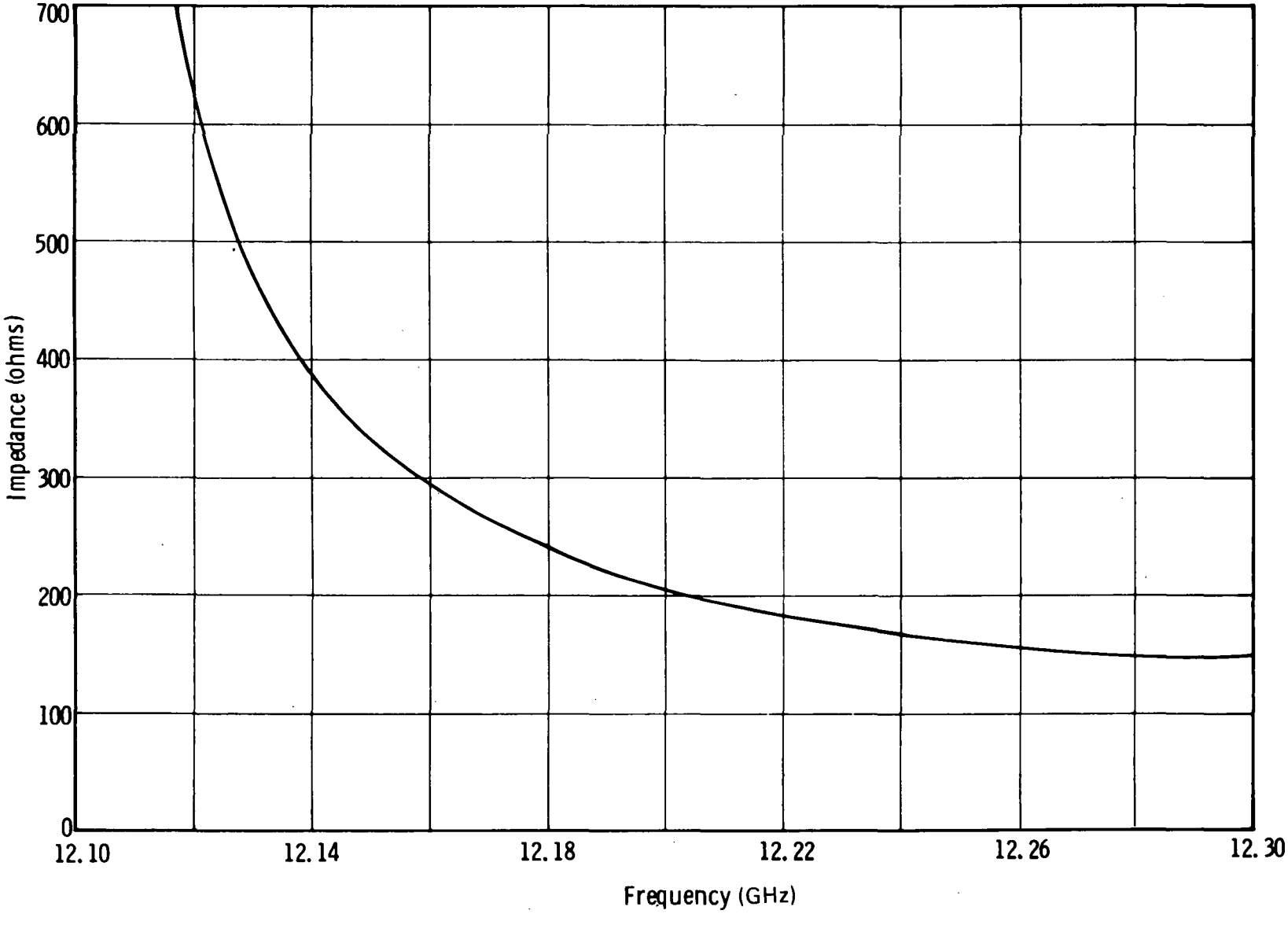

Figure 4-7. Computed Pierce Impedance on Axis of Preliminary Design Circuit

is plotted in Figure 4-8. The field plotted is the axial electric field averaged over the assumed beam area (70% filling factor) assuming unity peak gap voltage and unity circuit period.

Starting with an estimated gain per cavity of approximately 4 dB and assuming a required small signal gain of 46 dB (in order to meet the 40 dB saturated gain requirement) and assuming a three section tube with launching loss of 10 dB and sever loss of 5 dB per sever, a requirement of approximately 17 cavities in the circuit is established. In order to achieve high efficiency it is desirable to have more than 26 dB gain beyond the final sever. A seven cavity output section was thus indicated. To minimize gain ripple it is desirable to use one less cavity in the center section than in the output section. This leaves four cavities for the input section.

A number of preliminary calculations of small signal gain employing program "SSCAV" were used to adjust the cavity period so as to center the hot passband at 12.2 GHz and to find out how to distribute the circuit loss to achieve stability and minimize gain ripple.

The final iteration of the initial design provides the results shown in Figure 4-9. The computed small signal gain is approximately 46 dB and varies less than 1.6 dB over the required operating band. Figure 4-10 shows the computed stability diagram for the output circuit. It is a plot to start oscillation current vs beam voltage for the two lowest current oscillation modes. These data are obtained by operating "SSCAV" in a search mode which automatically locates the frequency and beam current for which the small signal gain is infinite for any given beam voltage.

Figure 4-11 is a plot of computed phase shift through the tube. It shows the relative change in output phase as a function of frequency. A linear component of 2.7°/MHz has been subtracted from the total phase shift through the tube. At no point in the operating band does $\Delta\phi(\omega)$ deviate more than the required 1.2° maximum over any 10 MHz segment of bandwidth. Figure 4-12 presents $d^2\phi(\omega)/d\omega^2$ as a function of frequency. It can be seen that this quantity remains below the $0.05°/MHz^2$ required maximum for each of the 40 MHz segments of interest.

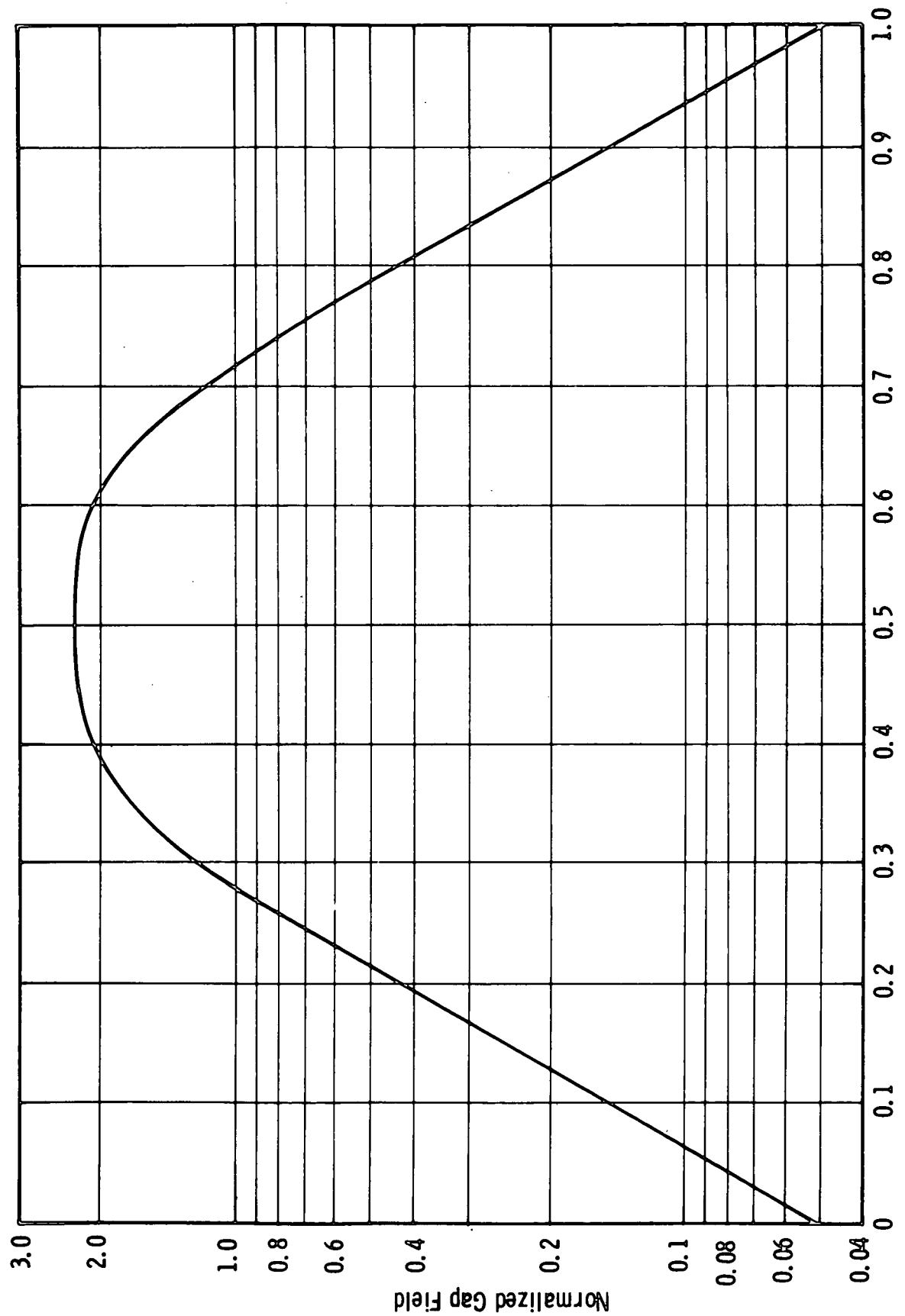

Figure 4-8. Normalized Gap Field for Preliminary Design

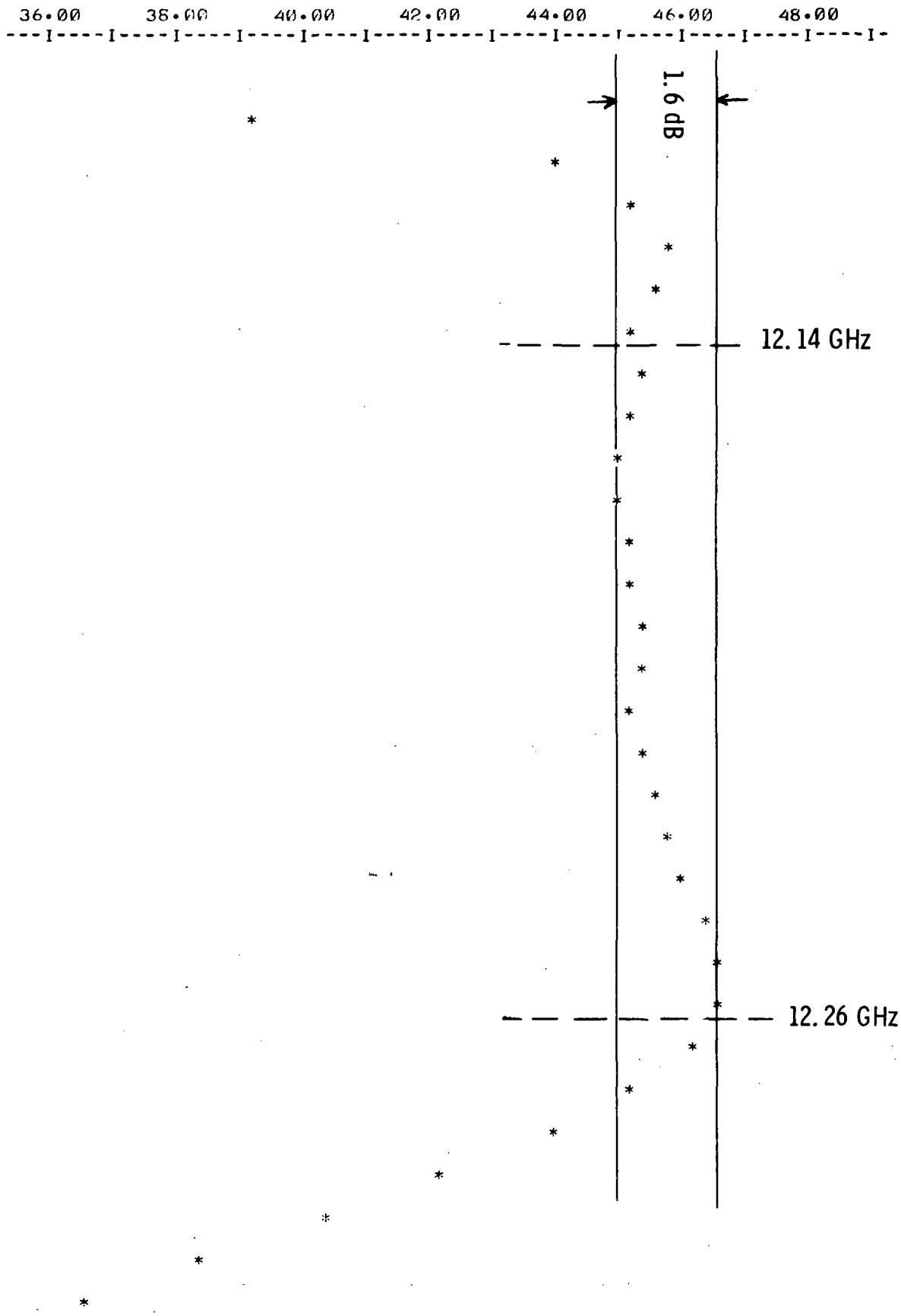

Figure 4-9. Computed Small Signal Gain for First Prototype Circuit (From Teletype)

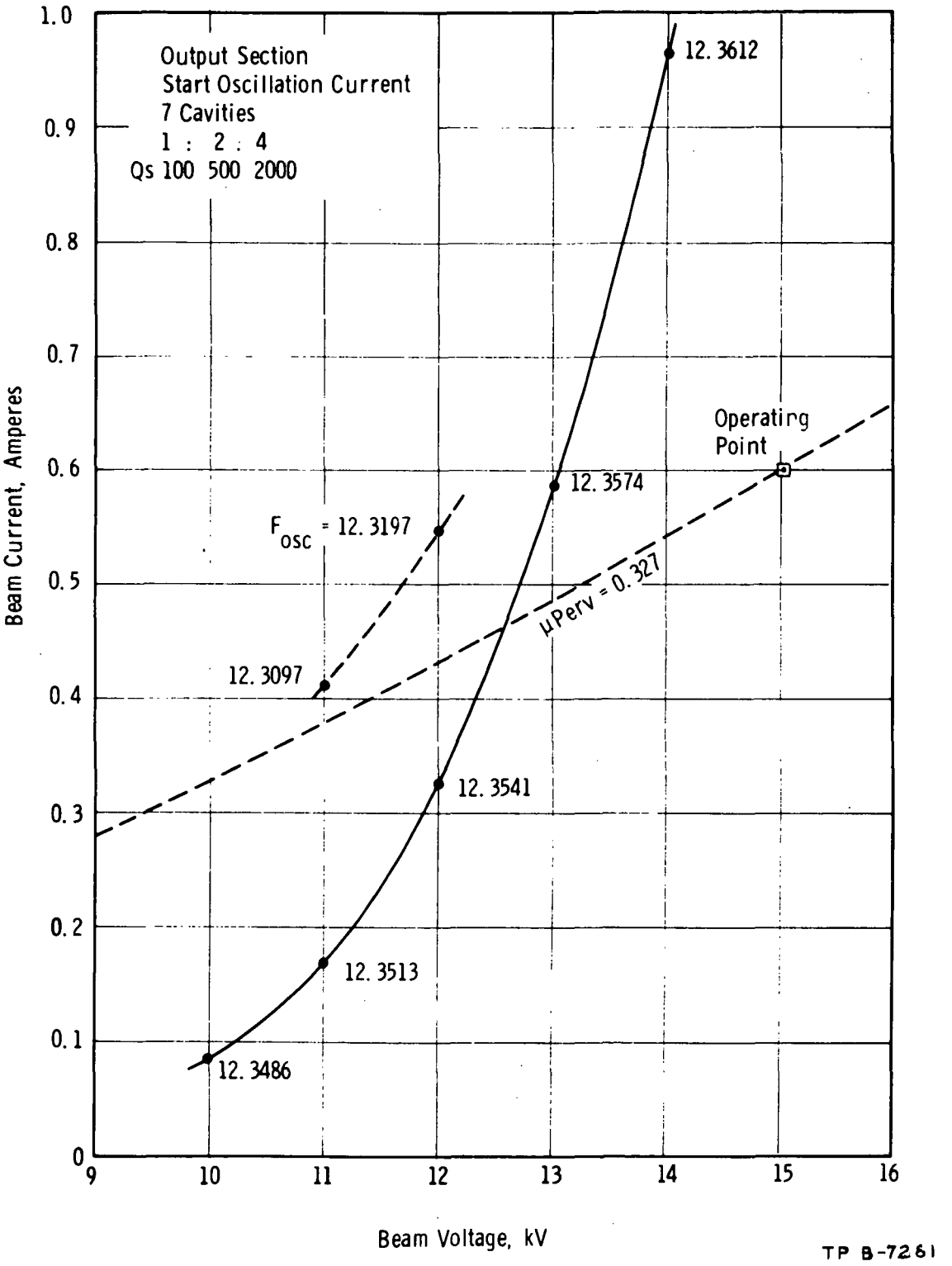

Figure 4-10. Stability Diagram for First Prototype Circuit

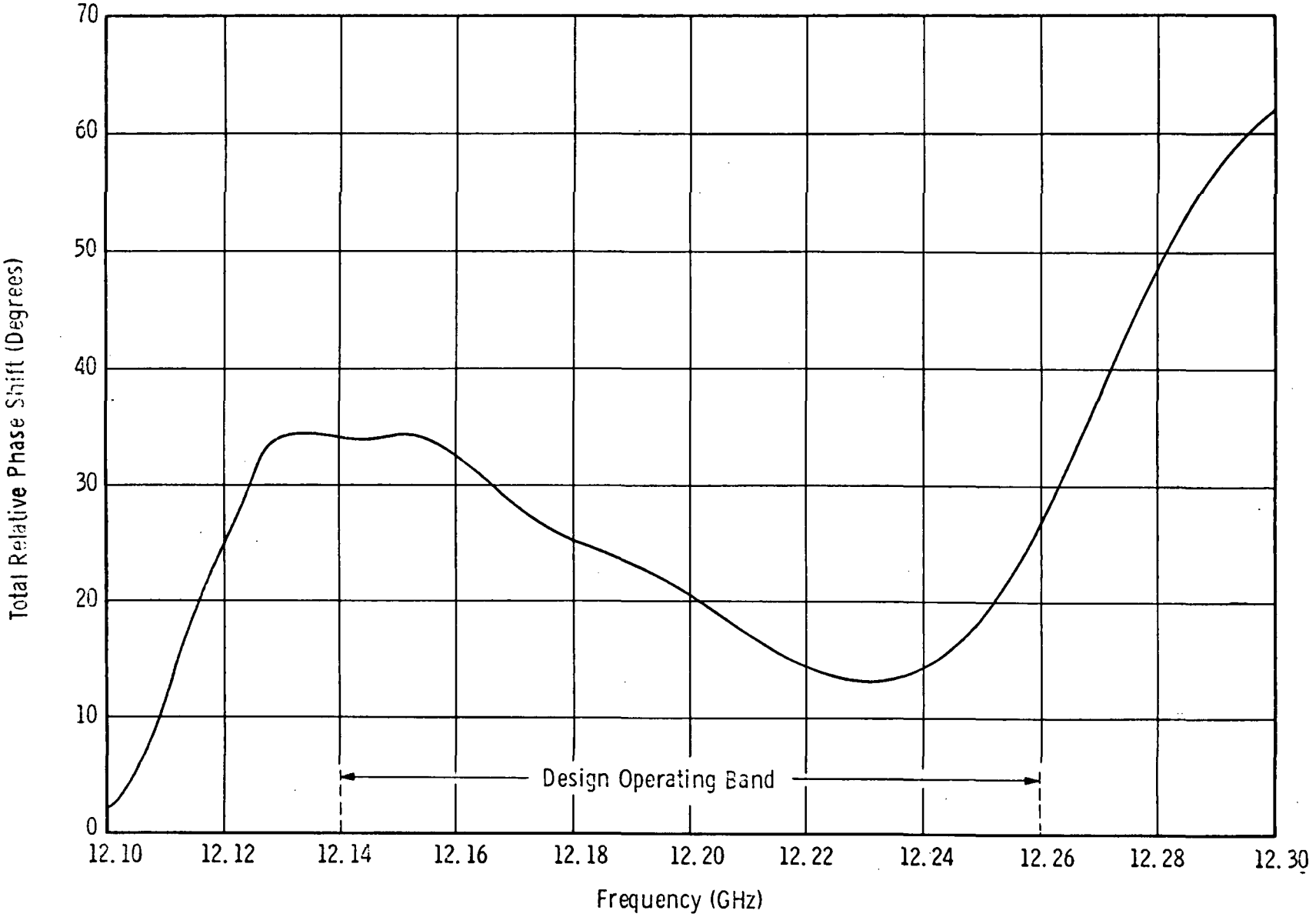

Figure 4-11. Calculated Small Signal Phase Shift of Design Example as a Function of Frequency

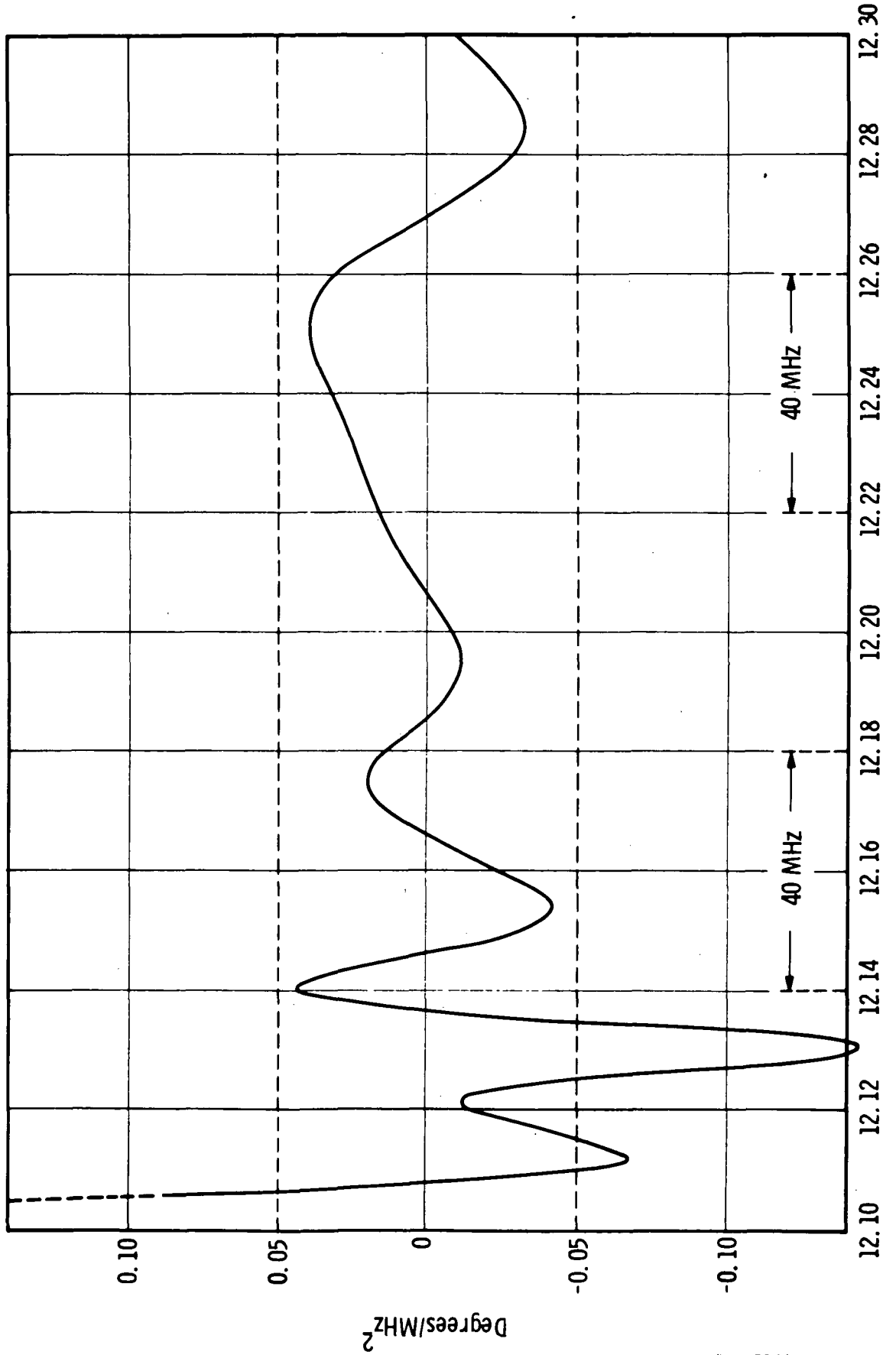

TP # B-7364

Figure 4-12. Calculated Values for $d^2\phi(\omega)/d\omega^2$ as a Function of Frequency for Design Example

The small signal gain computer program has been used to provide some design modification and to fill in those small signal design parameters which could not be chosen at the time of the initial electrical design. A complete compilation of small signal parameters for the first experimental tube is given in Table 4.1.

The use of the small signal computer program and other related programs has been illustrated in this section. Further refinements or changes in design dictated by large signal computer results or from tests of an actual TWT can be incorporated into the design as needed. This small signal design is a starting point for the large signal calculations which follow.

4.3 LARGE SIGNAL ANALYSIS

The large signal analysis is used primarily to investigate those design parameters which determine the conversion efficiency of the TWT. While many tube parameters influence efficiency to some extent, there are two areas of principal concern:

1. The design of a velocity resynchronization section near the output of the tube, which may involve changes in the circuit velocity, in the beam velocity, or both.

2. The gain in the output section of the tube and the distribution of circuit loss in this section of the tube.

The large signal analysis of the preliminary design was used to predict the performance of the first experimental tube, a tube which did not incorporate velocity resynchronization, as well as to provide circuit velocity taper design information, which, in conjunction with the test results from the first experimental tube would provide the design basis for subsequent tubes.

Figure 4-13 is a plot of output power vs drive power at midband for the design example derived in Section 4.2. The computed saturated efficiency is 19.6% with drive power of 158 mW at 40.5 dB gain. Figure 4-14 shows, for the same example,

TABLE 4.1

FINAL SMALL SIGNAL DESIGN

Beam Voltage	15	kV
Beam Current	600	mA
Beam Perveance	0.327	μperv
Beam Diameter	0.044	in.
Drift Tube Diameter	0.062	in.
Beam Filling Factor	0.70	
Brillouin Field	1040	G
Magnetic Focusing Field	2500	G
Gap Spacing	0.040	in.
Cavity Period	0.164	in.
Average Web Thickness	0.020	in.
Cold Passband	12.10 – 12.35	GHz
Hot Band Center	12.2	GHz
Small Signal Gain	46	dB
Number of Sections	3	
Input Section	4	cavities
Cavity Q	500	
Center Section	6	cavities
Cavity Q	500	
Output Section	7	cavities
Cavity Q — First Cavity	100	
Second and Third Cavities	500	
Final Four Cavities	2000	
Total Number of Cavities	17	

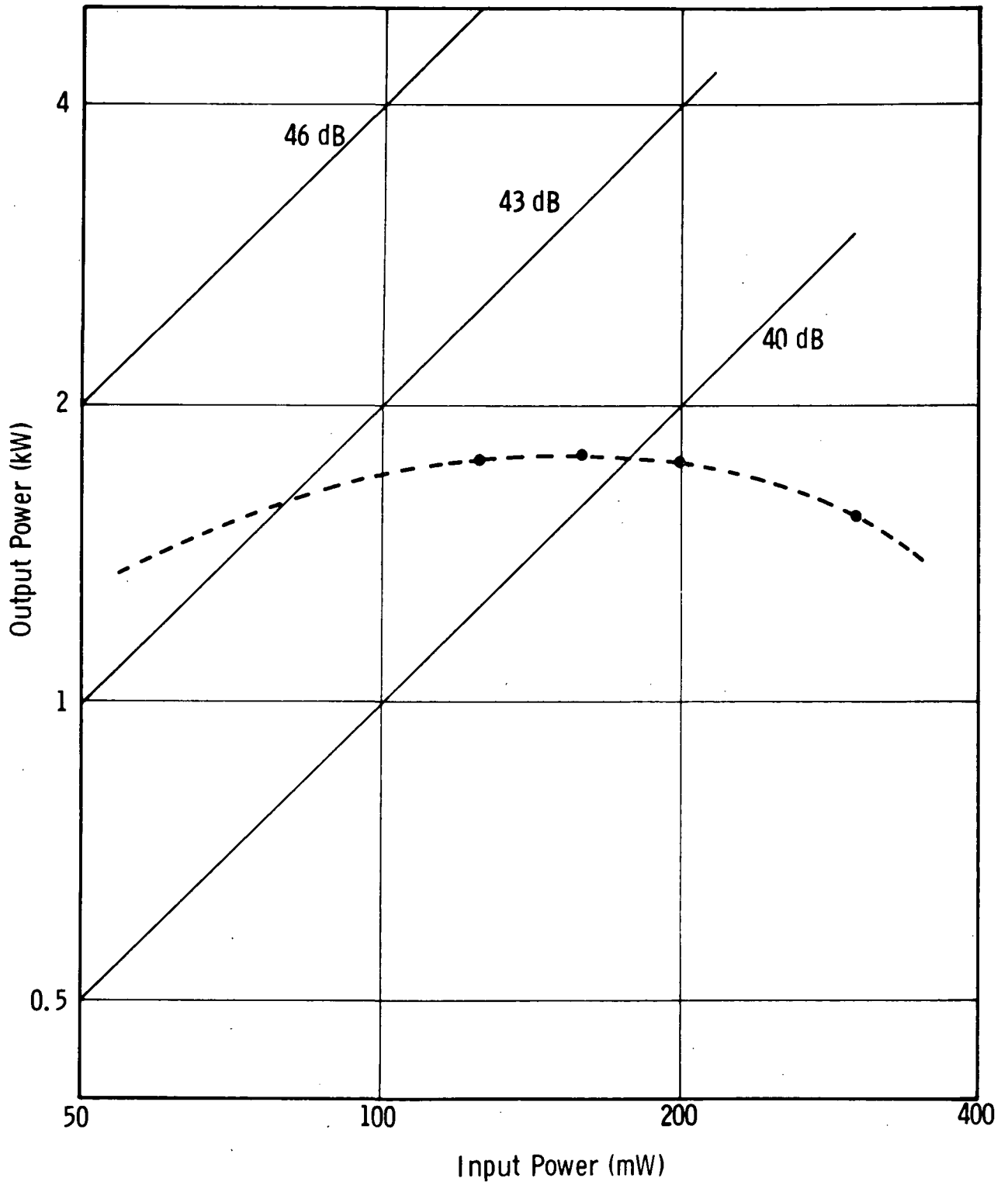

Figure 4-13. Computed Output Power vs Drive Power for Preliminary Design (No Velocity Resynchronization)

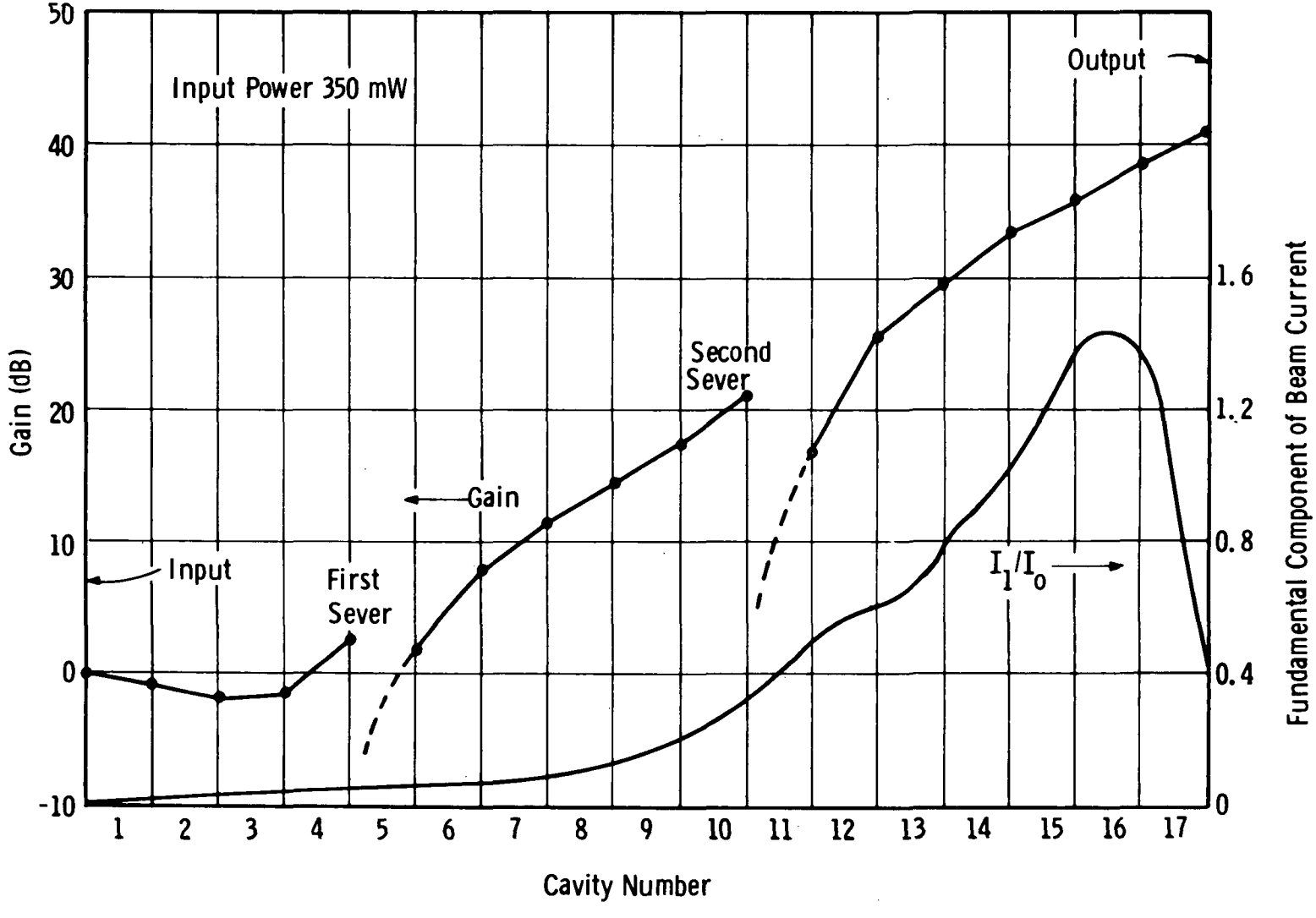

Figure 4-14. Power and Rf Current Buildup Along Circuit for Preliminary Design (No Velocity Resynchronization)

how the power and fundamental component of beam current build up along the circuit at saturation. This figure shows the adequacy of the gain in the output section; i.e., the power level at the second sever is about 21 dB above drive level. The forward wave power being delivered into the second sever load is therefore approximately 20 W or about 1% of the output power. Additional gain in the output section would decrease the electronic stability of the tube without a significant increase in efficiency. The fundamental component of rf convection current is seen to reach a maximum value of 1.44 just past the center of the 16th cavity. This very high value of rf current results from employing synchronous bunching; the low efficiency demonstrates the need for velocity resynchronization.

A search was made for an optimum velocity taper using the above described circuit as a starting point. One-, two-, and three-cavity tapers were studied. The optimum taper for this circuit was found to be one in which the 16th cavity was reduced to 0.75 normal period and the 17th cavity to 0.50 normal length. For ease of computation it was assumed that the tapered cavities would have identical impedance and loss to those they replaced. In actual practice it would be difficult to achieve the required taper without compromising impedance.

The computed performance of the 75-50 tapered TWT is illustrated in Figure 4-15. The saturated drive level at 12.2 GHz is 350 mW compared with the untapered tube which required only 158 mW. The build up in power and rf beam current is shown in Figure 4-15. This figure is superficially similar to the previous figure for the untapered design, however, the conversion efficiency in the latter case has risen to 48%. The fundamental current reaches a maximum value of 1.43 in the middle of the 16th gap, then abruptly decays as the resynchronized circuit wave extracts power from the bunched beam. The net gain in the output section of the tapered tube is approximately 0.5 dB greater than in the untapered case.

The computed efficiency of the initial tapered design is close to the 50% specified conversion efficiency. This estimate is probably optimistic since it assumes that the tapered cavities have not lost interaction impedance. A more detailed analysis of

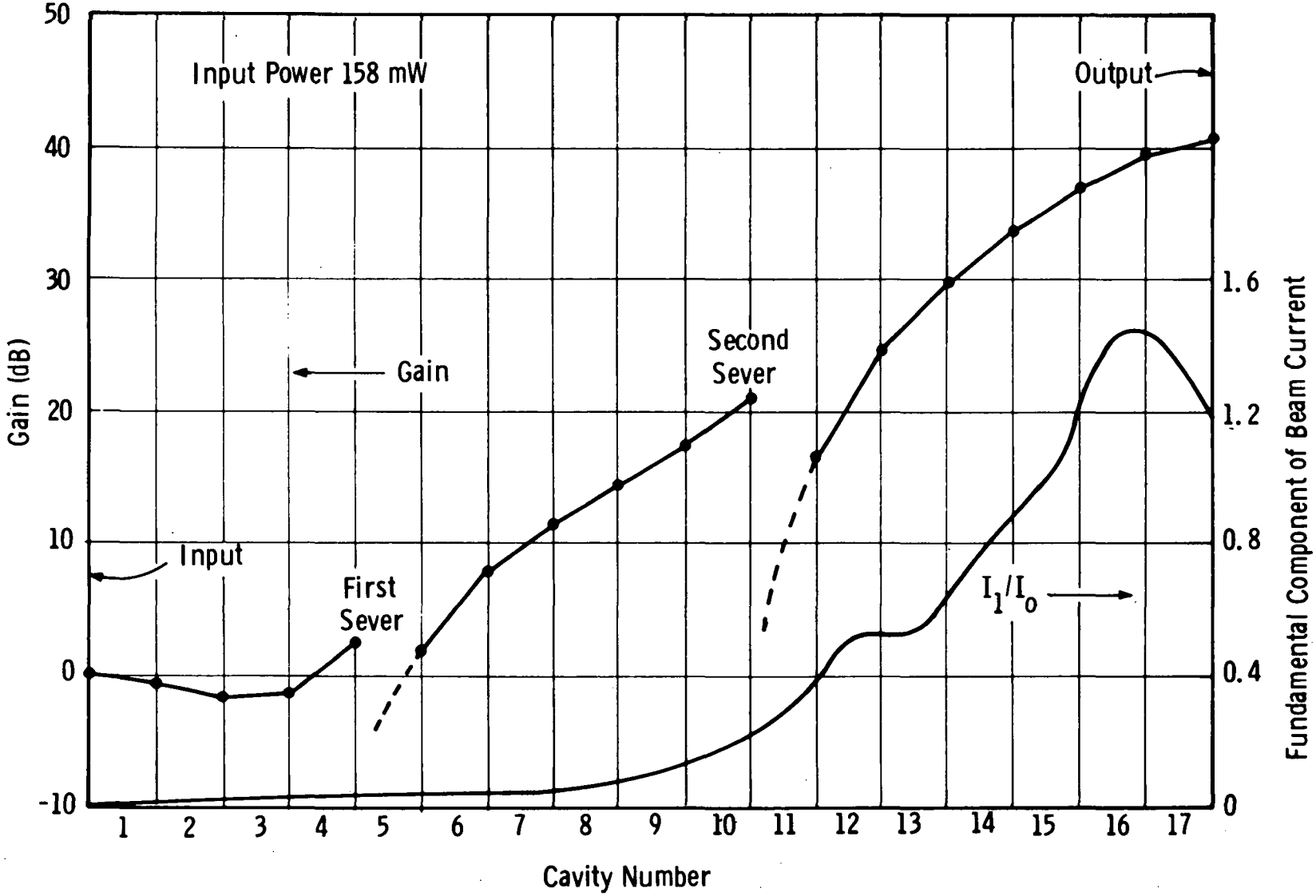

Figure 4-15. Power and Rf Current Buildup Along Circuit Employing Velocity Resynchronization

other factors which effect the conversion efficiency of a coupled-cavity TWT, including analysis of the phase trajectories of the electron discs and the anomalous effect of the backward wave on the gap voltages, is offered in a later section. An examination of voltage jump performance is also presented.

4.4 GUN AND BEAM ANALYSIS

The electron gun is of the type commonly called "convergent confined flow" but perhaps more accurately named "space charge balanced flow." The object of the design is to obtain a beam which is laminar and unscalloped and maintained in equilibrium with a magnetic focusing field approximately 2.5 times the Brillouin field. Gittens (Ref. 8) has shown that to produce and maintain a cylindrical beam in space charge balanced flow it is necessary (but not sufficient) to satisfy the following equation.

$$\frac{R_o}{r_o} = \left[1 - \left(\frac{B_b}{B_o}\right)^2\right]^{1/4} \tag{4.1}$$

where r_o is the beam radius, B_b is the Brillouin field for a beam of radius r_o with uniform current density, B_o is the magnetic focusing field and R_o is the radius of the flux line which cuts the outer edge of the cathode which produced the beam. In addition, the beam injected into the focusing field must have been laminar, of uniform current density and without a radial component of velocity. In practice it is not possible to satisfy these conditions exactly, nevertheless they may be satisfied well enough to provide an adequate beam.

For the present design $B_o = 2.5\ B_b$ and Equation (4.1) reduces to:

$$\frac{R_o}{r_o} = 0.96$$

i.e., the flux line which cuts the outer edge of the cathode has a final radius only slightly less than the radius of the beam.

One procedure used to design electron guns for space charge balanced flow starts with an electrostatic gun design which produces a highly laminar beam of uniform current density with minimum beam radius equal to the desired final beam radius. If a magnetic field can be found which has flux lines which exactly follow the electrostatic beam trajectories from the cathode to the beam minimum, then the application of this magnetic field will not perturb the electron trajectories. If, at the electrostatic beam minimum, the magnet field can be made to abruptly increase so as to satisfy Equation (4.1) then all the conditions for space charge balanced flow will have been met. While it is not possible to abruptly change the magnetic field, it is usually possible, in practice, to find a field shape which produces the same effect.

An alternative design procedure starts with an electrostatic gun which produces a beam having a minimum radius slightly larger than the desired beam. A magnetic field is applied, the flux lines of which are tangent to the electron trajectories at the cathode, but which converge very slightly more rapidly than the electrostatic trajectories. The resultant magnetic forces cause a slight adiabatic compression of the beam and, when properly implemented, can produce a relatively scallop-free space charge balanced beam.

The computer aided design procedure for the electron gun comprises the following steps:

1. A trial gun is designed based on Pierce (Ref. 9) theory or on existing gun designs.

2. A computer run of the electrostatic trial gun is made to determine whether this gun will produce an adequately laminar beam of the correct perveance and convergence.

3. Adjustments are made and the gun is recomputed until a satisfactory electrostatic beam is produced.

4. A polepiece configuration which will produce the desired magnetic field shape is derived from design curves which have been produced by the solution of Laplace's equation for a large number of pole-piece configurations.

5. Beam trajectories are computed for the gun in the presence of the chosen magnetic field.

6. Adjustments are made, if needed, until the computed beam trajectories satisfy the requirements of the design.

7. The computer designed gun is tested in the beam analyzer. Further modifications to the design are made, if needed, to bring the gun up to the required performance levels.

The computed electrostatic beam trajectories for the fourth trial gun design are shown in Figure 4-16. This design shows good laminarity and a minimum beam diameter of 0.046 in. The computed perveance is 0.3314 μperv and the maximum cathode loading is 1.75 A/cm^2.

After three trial runs in the beam analyzer a polepiece configuration was found which produced the results shown in Figure 4-17. This figure shows a sequence of cross sections of beam current density as the beam proceeds downstream from the anode. The gun has been scaled-up in size in order to increase the accuracy of measurement in the beam analyzer. Some spiralling of the beam is evident. The beam analyzer is built to accommodate adjustment of the cathode anode spacing in order to adjust the gun perveance. This valuable feature unfortunately limits the accuracy of cathode anode alignment. In an actual gun it should be possible to completely eliminate this spiralling effect. With the spiralling eliminated, this design will provide a beam with a nominal diameter of 0.044 in. with 7% ripple.

The electron beam is required to exit into a magnetically field-free collector. The maximum collector field at a position two exit hole diameters beyond the collector polepiece face must be less than 0.5% of the focusing field.

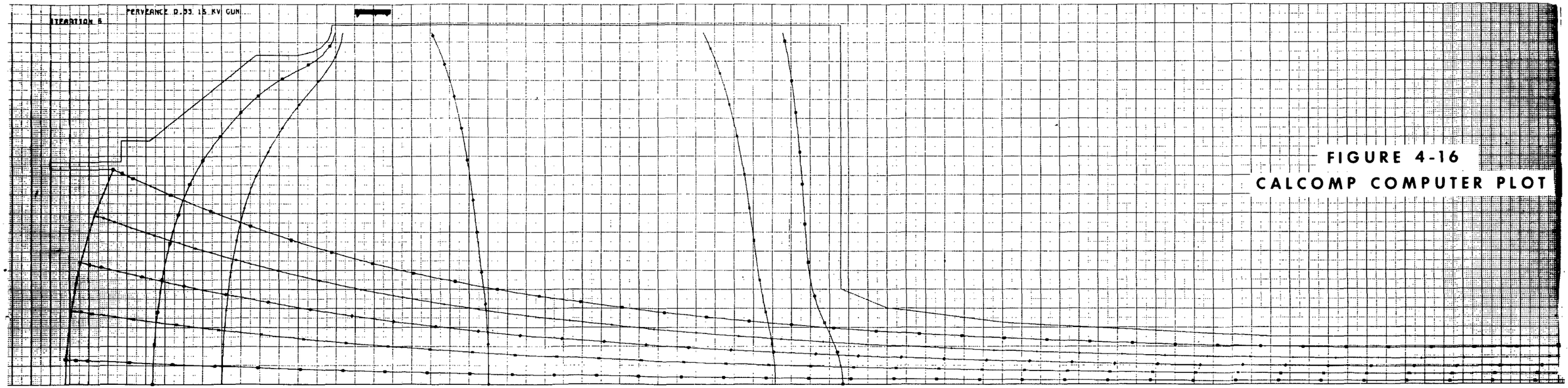

FIGURE 4-16
CALCOMP COMPUTER PLOT

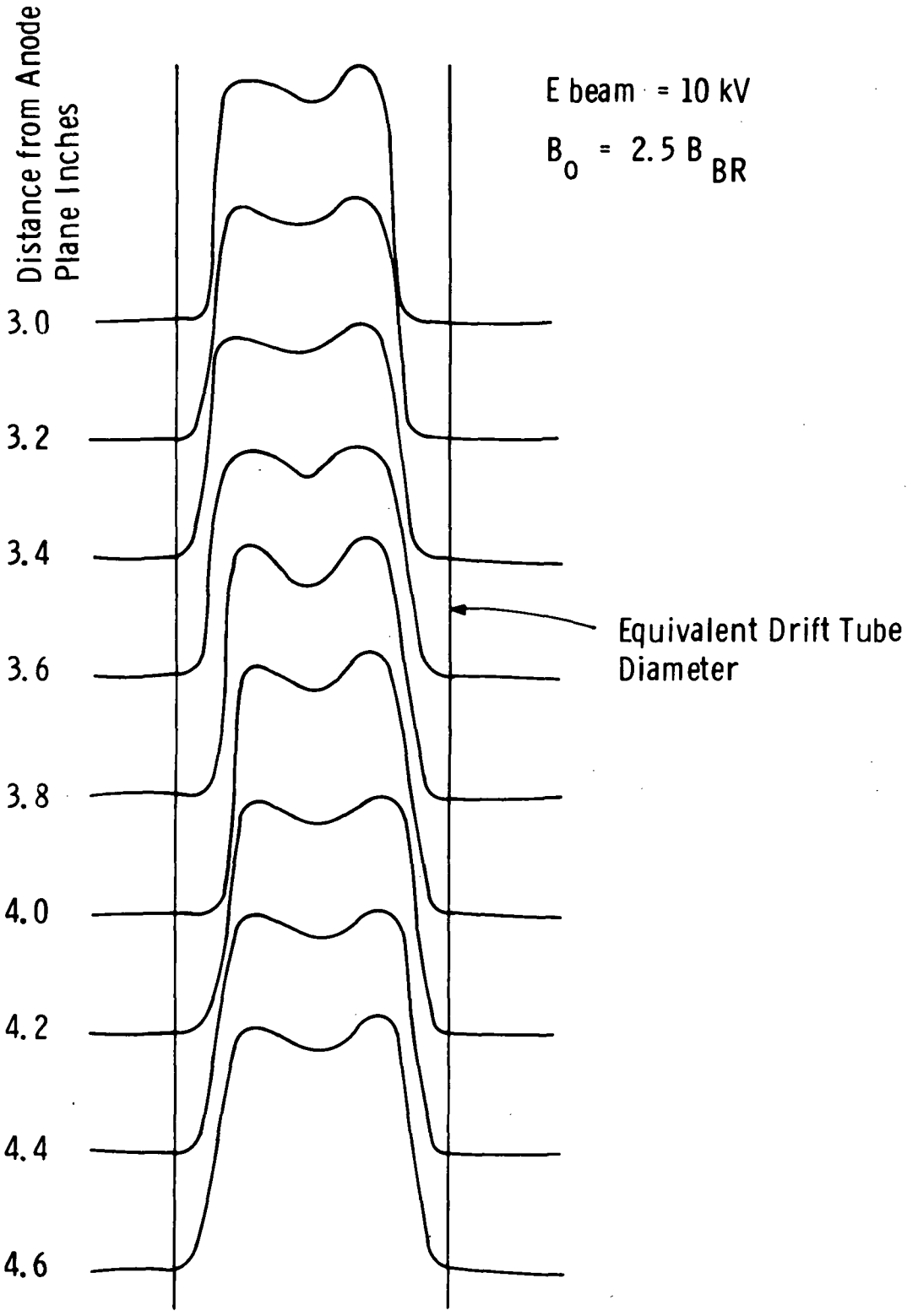

Figure 4-17. Beam Current Density Profile vs Distance

The inner collector polepiece design is shown in Figure 4-18. The polepiece material is annealed CRS. The measured axial magnetic field is shown in Figure 4-19. This polepiece configuration produces a maximum collector field less than 0.4% of the focusing field. These measurements show the collector field reaching a maximum one-half inch beyond the outer face of the solenoid end cap which would indicate that the solenoid shield is as important as, if not more important than, the internal polepiece in providing the required overall shielding.

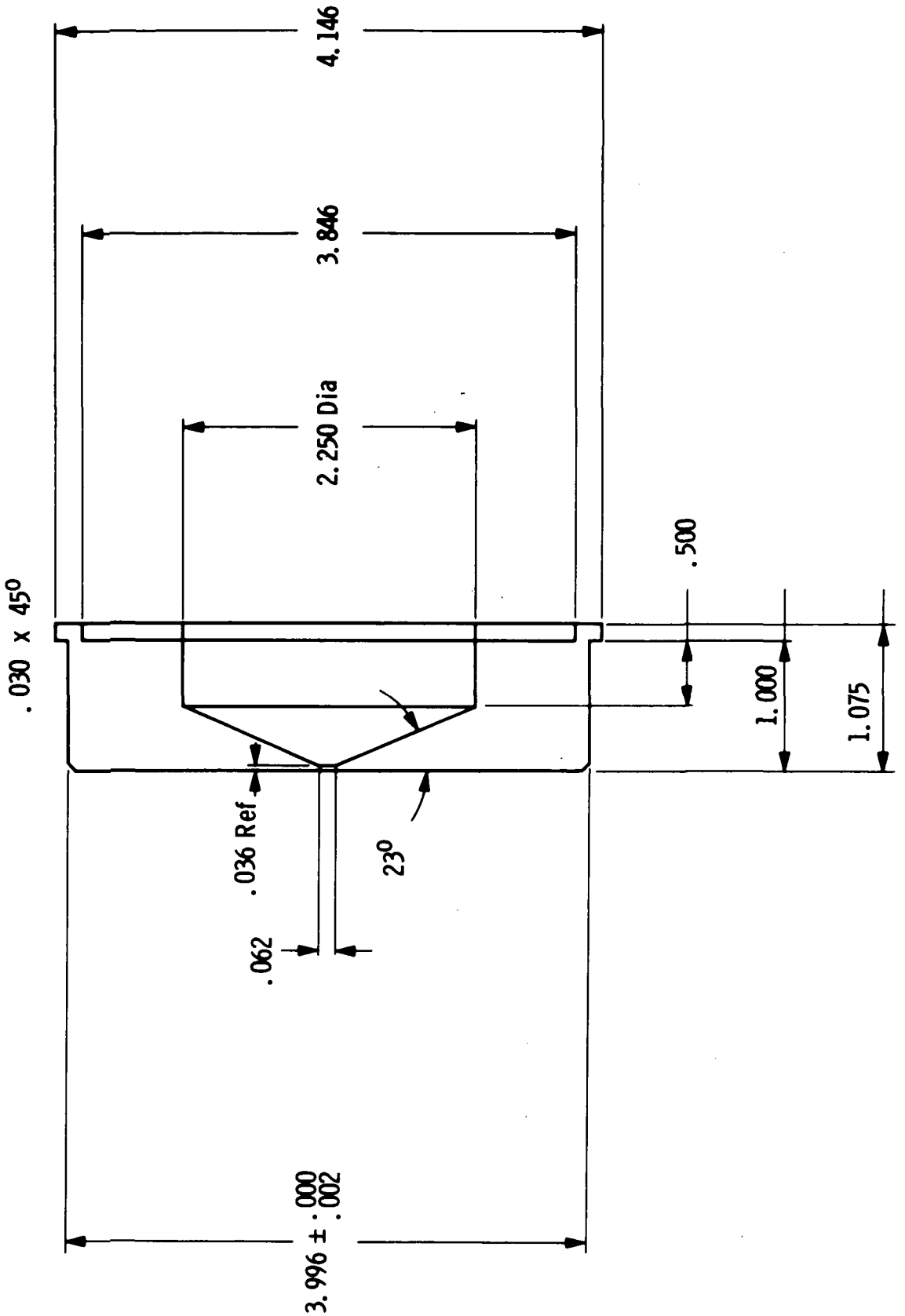

Figure 4-18. Collector Polepiece

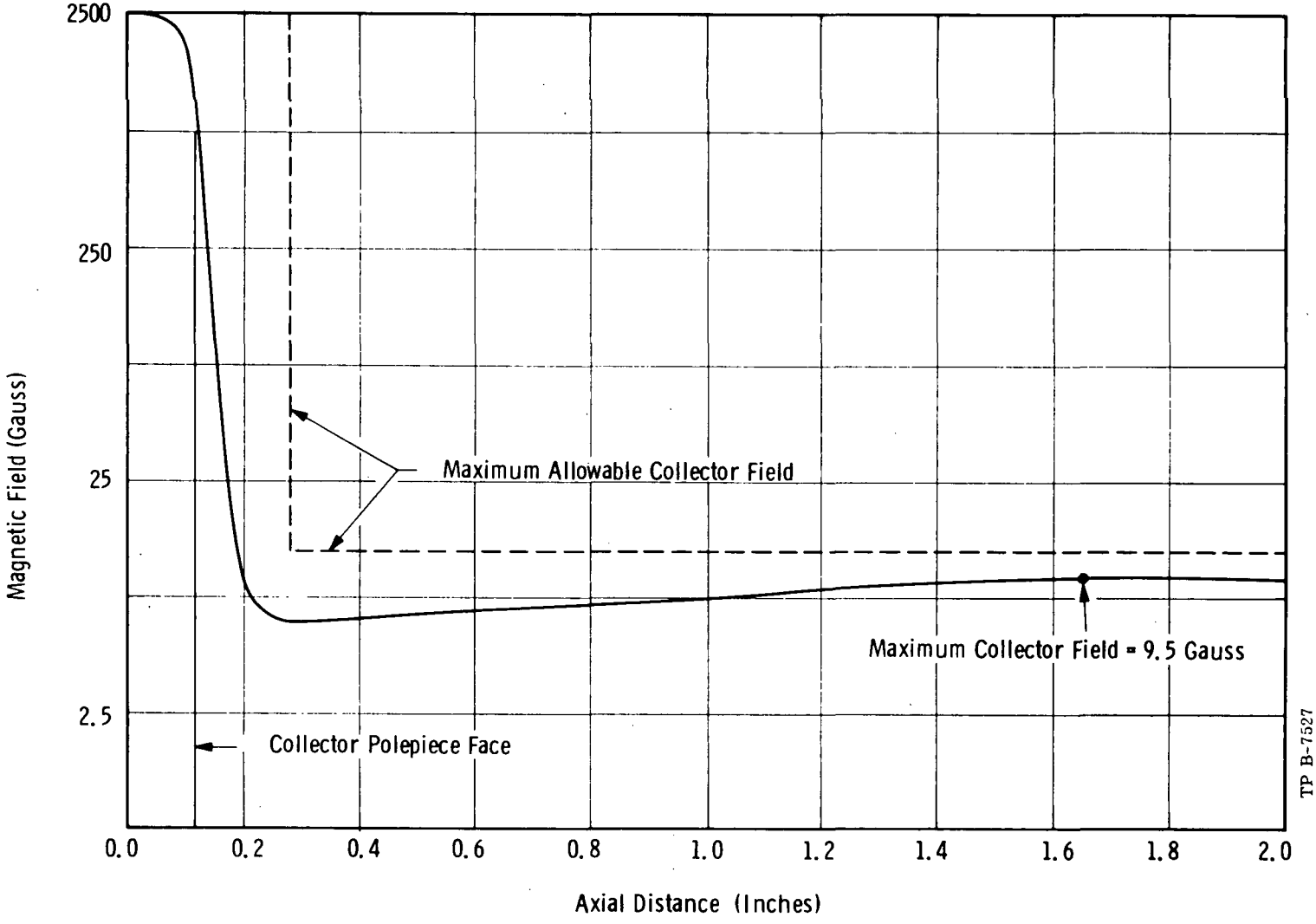

Figure 4-19. Collector Magnetic Shielding for VTX-6681A1, S. N. 101

5.0 MECHANICAL DESIGN

The VTX-6681A1 resembles other coupled-cavity traveling wave tubes in most respects. The major departures from normal design are brought about by the requirement that this tube be operable inside a space-simulating vacuum chamber. It is necessary to provide a removable collector which for experimental purposes, is to be replaced by a multistage depressed collector for efficiency enhancement studies.

The electron gun is also required to be demountable so that it may be replaced in case it is inadvertently damaged in operation by loss of vacuum.

The focusing solenoid is also unusual in that it must be capable of being baked out so that the system may be evacuated to the pressure levels appropriate to traveling wave tube operation.

5.1 CIRCUIT CONSTRUCTION

The circuit is constructed of copper discs. Machined into the discs are a drift tube, an intercavity web with coupling slot, and an outer rim which forms the cavity wall. These discs are stacked, with coupling slots alternated, and brazed together inside an alignment fixture. The circuit stack is then brazed inside a copper sleeve which provides additional stiffness and may be used as a coolant manifold. Figure 5-1 shows a typical output circuit section including coolant tubings.

Each end of each circuit section is matched to a low height waveguide. At the sever end of the circuit section this waveguide is part of a sever load such as shown in Figure 5-2. At the input and output ends of the circuit the waveguide is tapered into a window assembly as shown in Figure 5-3. The window is of the thick poker chip variety. The sever load employs a number of lossy ceramic wedges brazed to a plate, which is backed by a coolant chamber. This sever load is capable of dissipating 500 W of rf power without gassing.

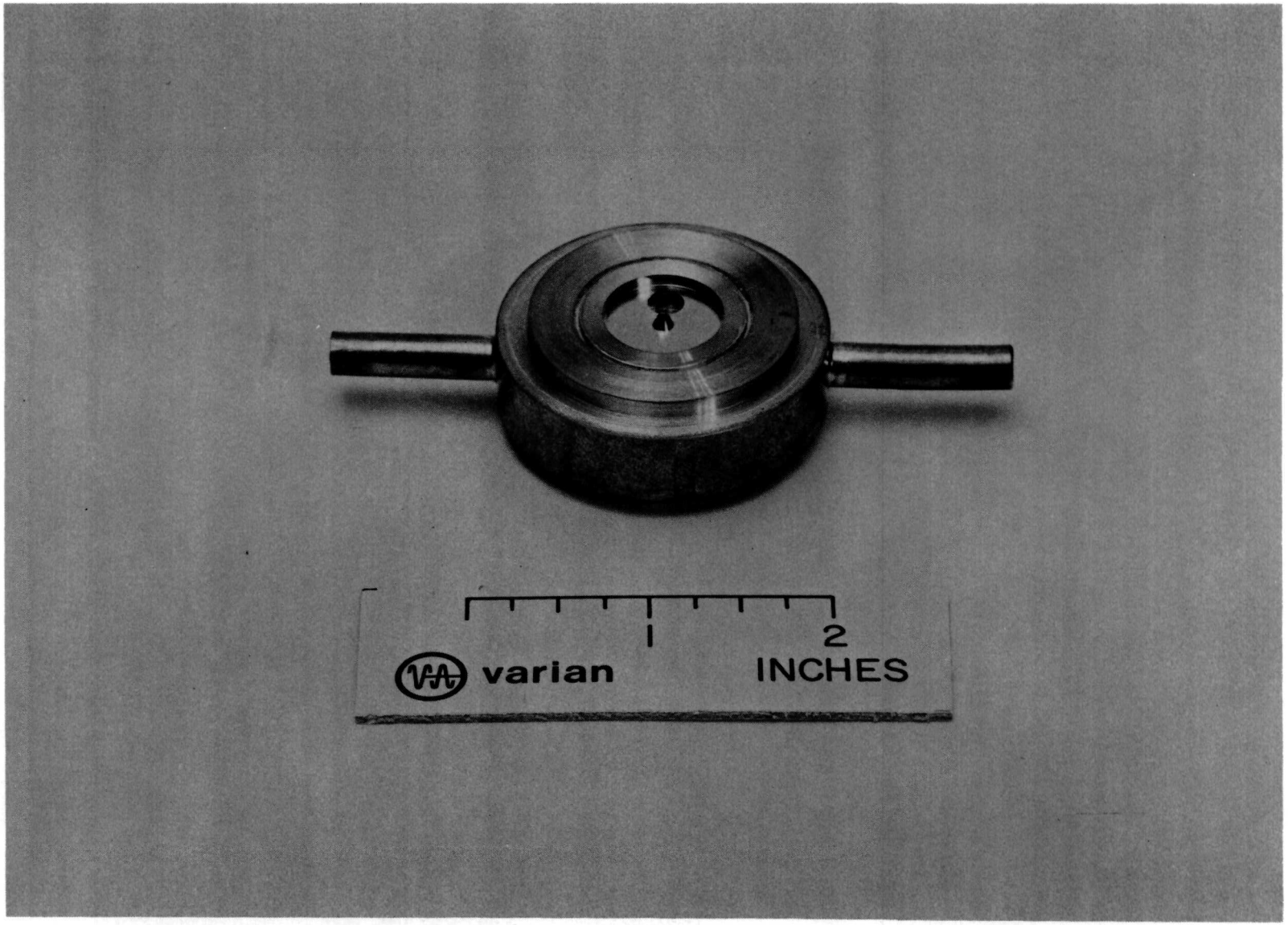

Figure 5-1. Output Circuit Section

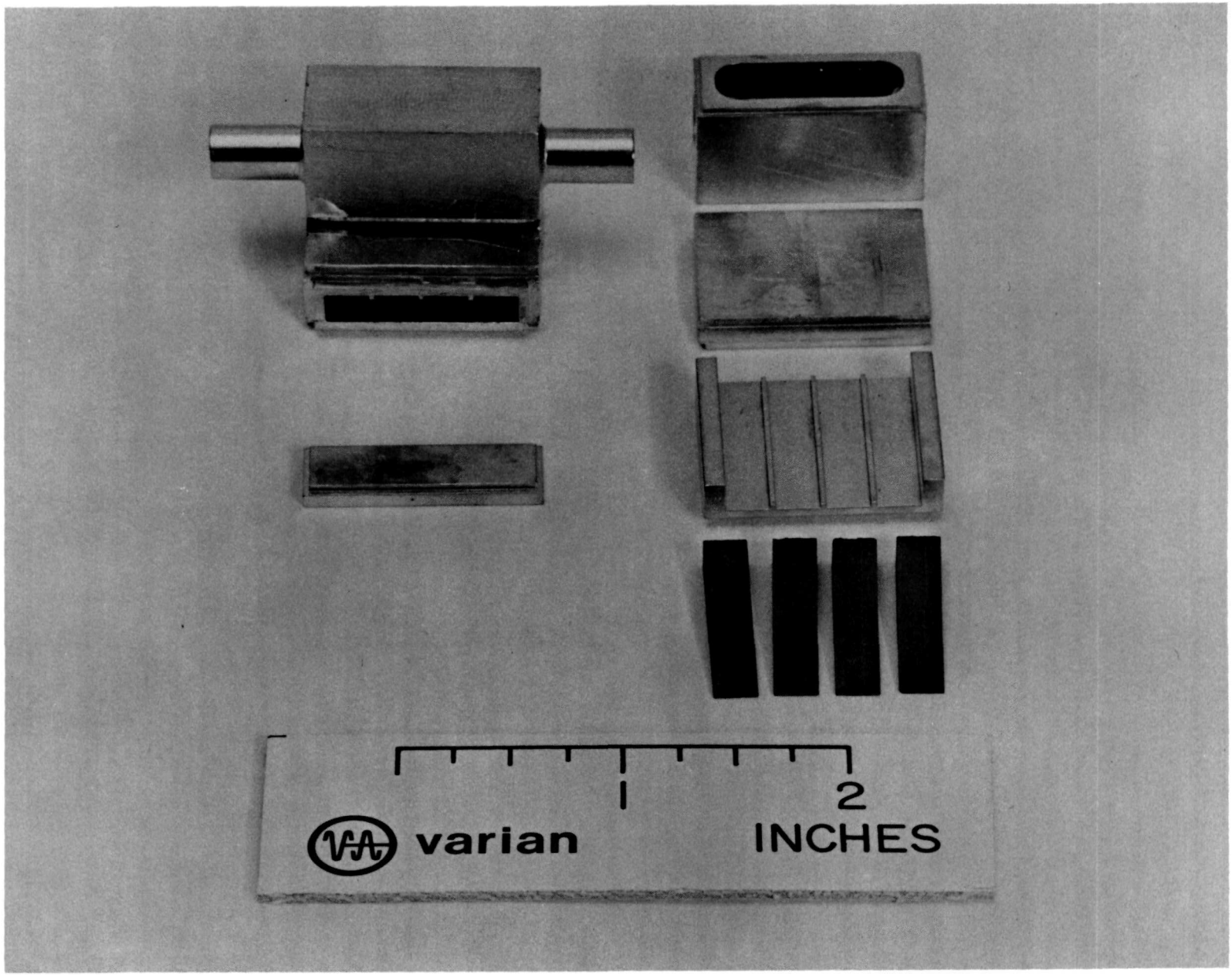

Figure 5-2. Sever Load Assembly

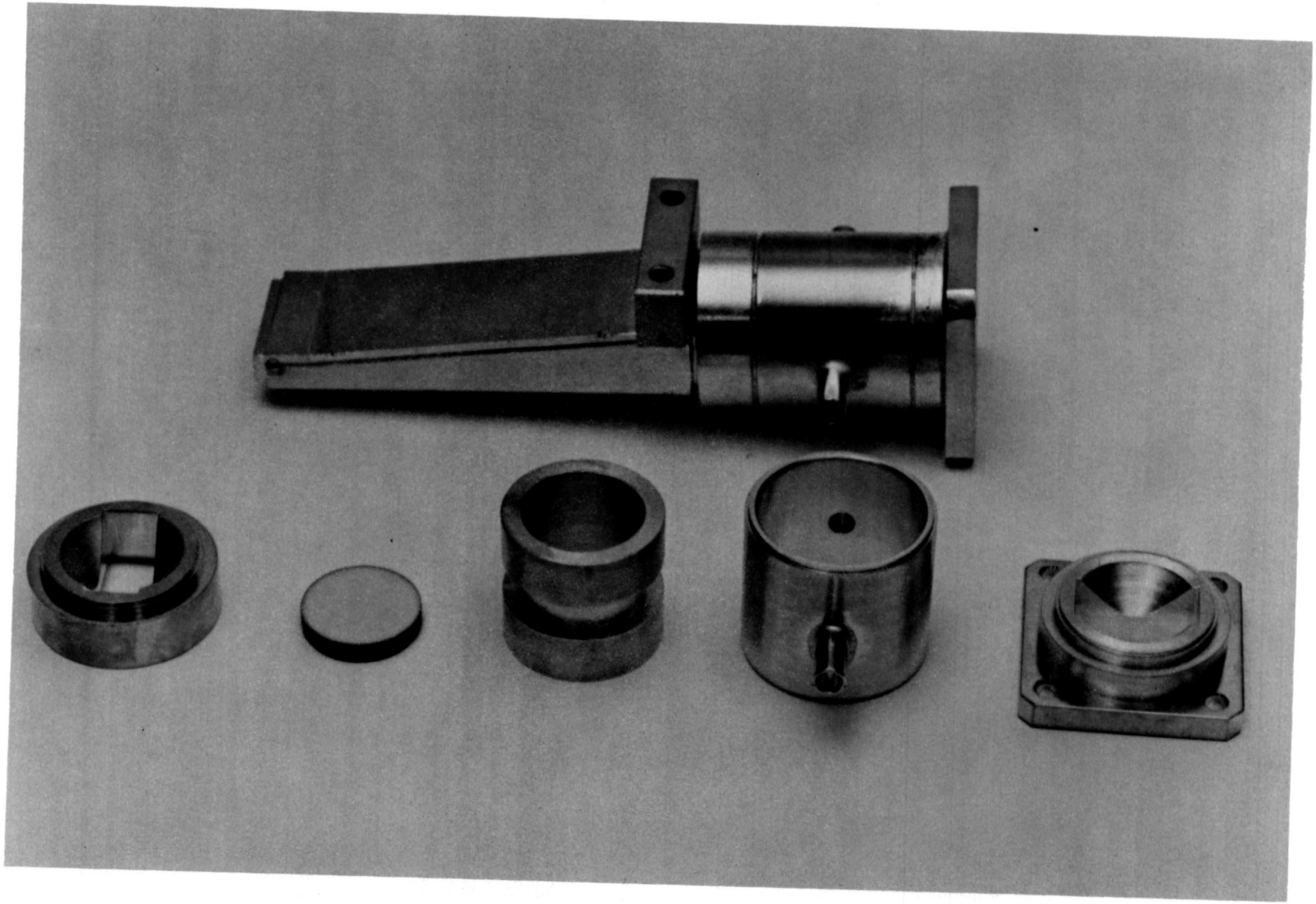

Figure 5-3. Output Window Assembly

The input and output waveguides are brought out at the gun end of the tube as shown in Figure 5-4. This inverted arrangement allows the tube to be inserted into the focusing solenoid, leaving the collector region free of cumbersome waveguide assemblies which would interfere with mounting of the experimental depressed collector.

Gun and collector polepieces made of soft iron are brazed to the circuit assembly and machined to mount snugly within the solenoid end caps, thereby completing the magnetic circuit of the solenoid. The collector polepiece is made very thick to minimize stray flux within the collector.

Figure 5-5 is a preliminary layout showing the tube mounted in the focusing solenoid.

5.2 COLLECTOR CONSTRUCTION

Figure 5-6 shows the demountable collector mounted on the collector polepiece. The collector is of conventional design, taken from a 10 kW klystron. It is supported by a ceramic insulator in order to allow measurement of beam transmission.

The major feature of the collector design is the heliarc flange by which it is mounted to the collector polepiece. This is designed to provide maximum unimpeded access to the beam exit tunnel upon removal of the collector.

5.3 ELECTRON GUN CONSTRUCTION

Figure 5-7 shows the demountable electron gun. The gun ceramic is made large in order to minimize leakage in a less than optimum environment. The ceramic is shielded from the cathode assembly by the focus electrode support and by the deep magnetic shield which extends back from the gun polepiece. The magnetic shield serves the additional purpose of shielding the electron gun from stray external fields.

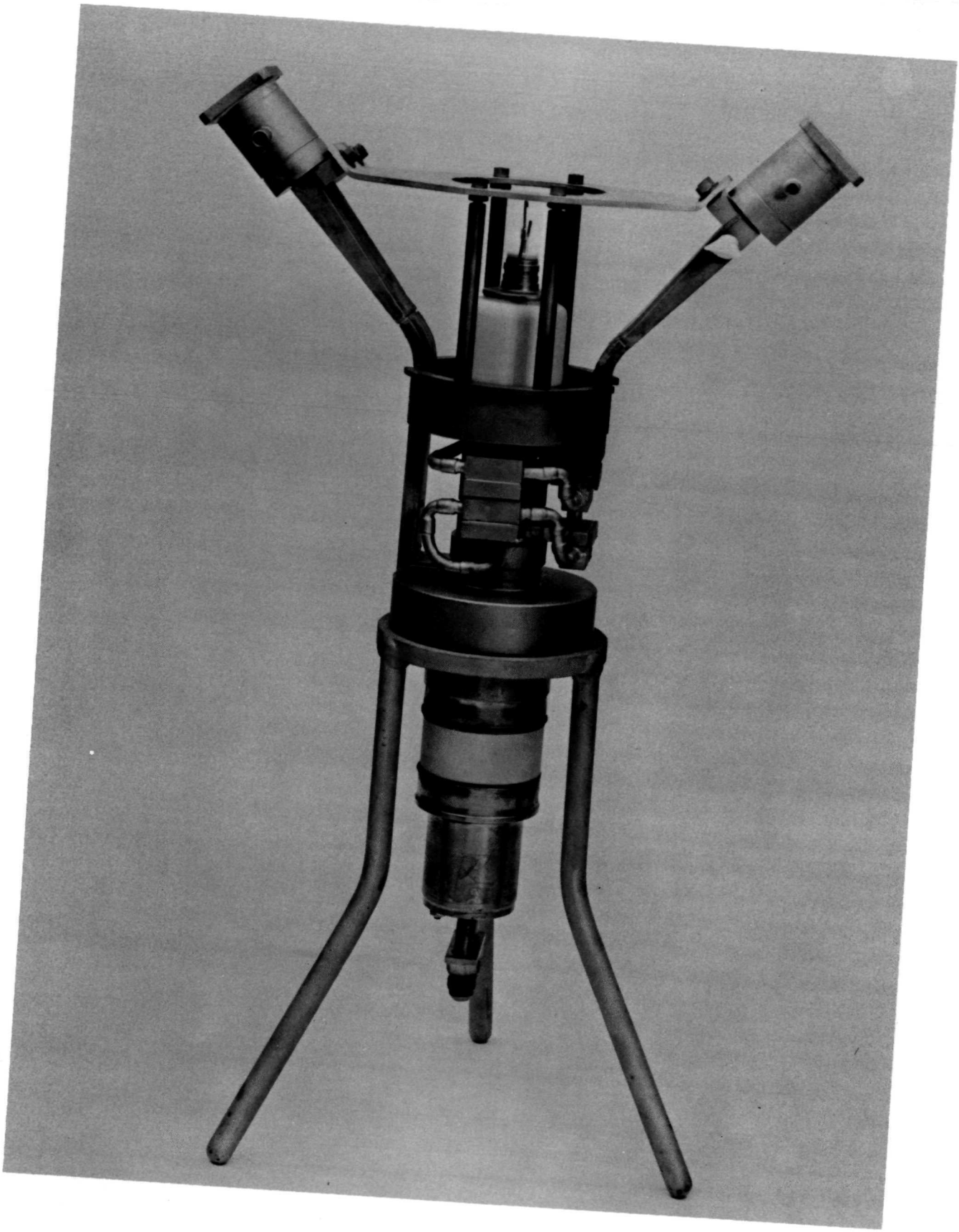

Figure 5-4. Photo of VTX-6681A1, S. N. 101

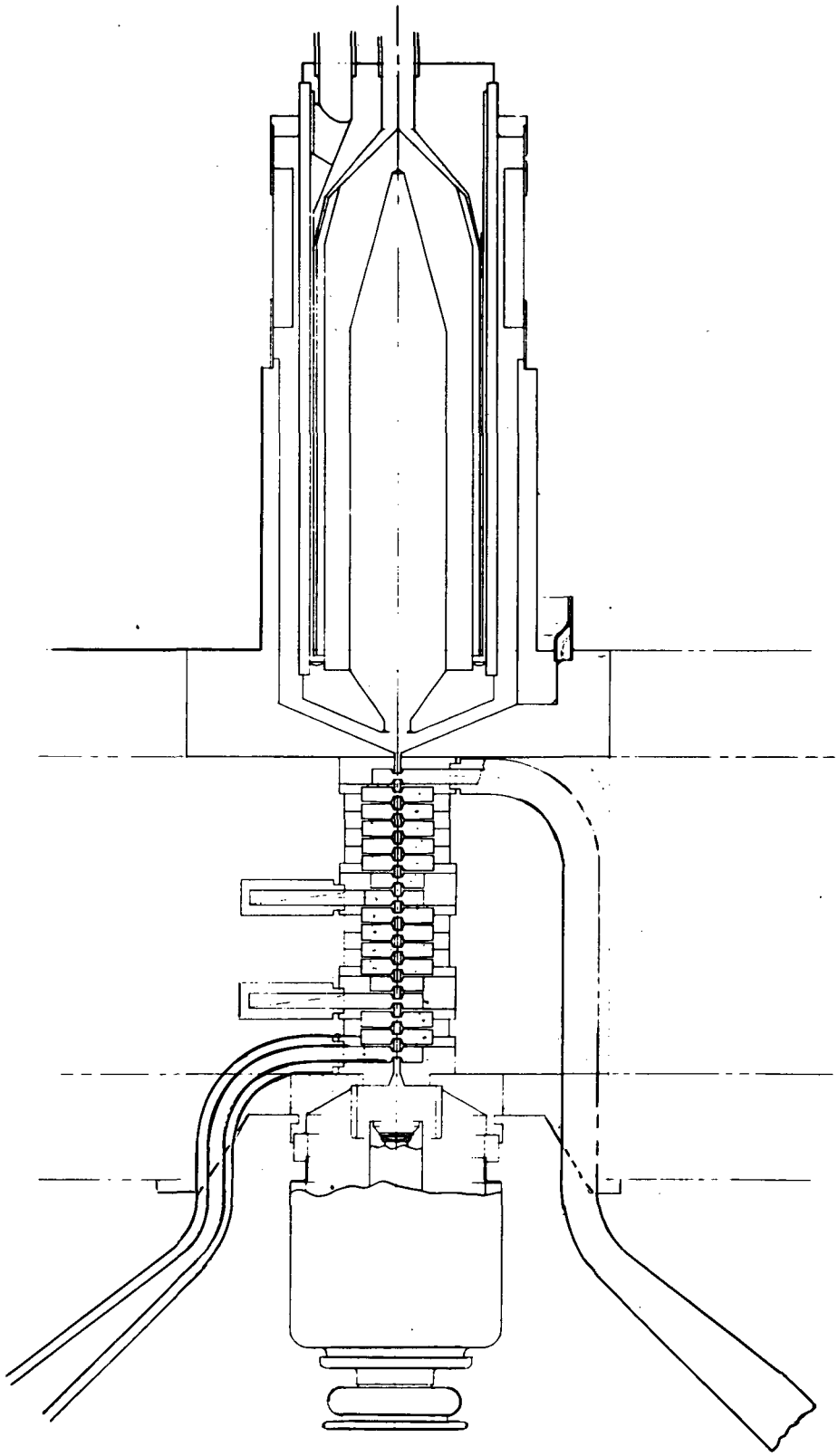

Figure 5-5. Preliminary Layout of First Experimental Tube

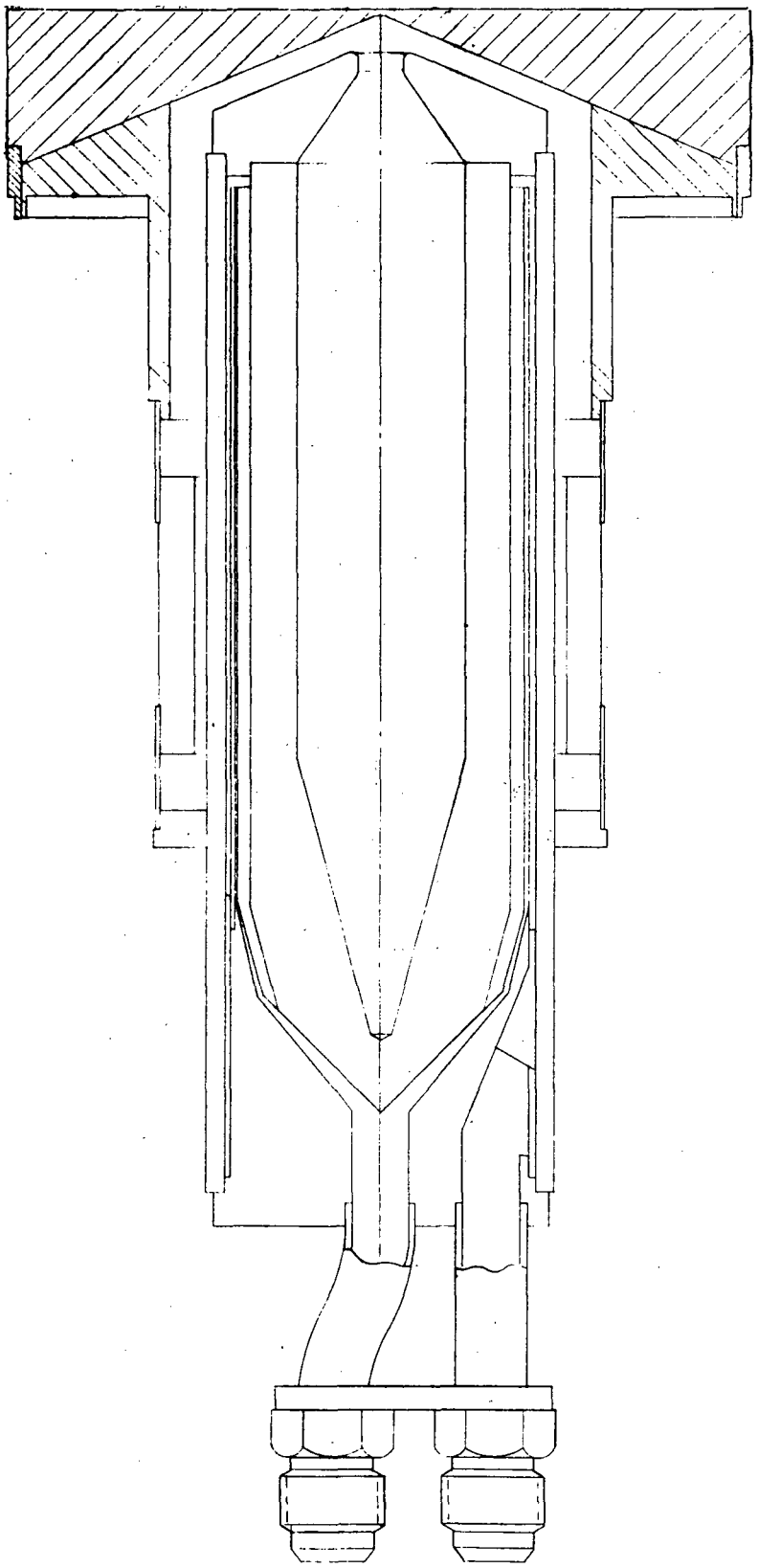

Figure 5-6. Collector Assembly

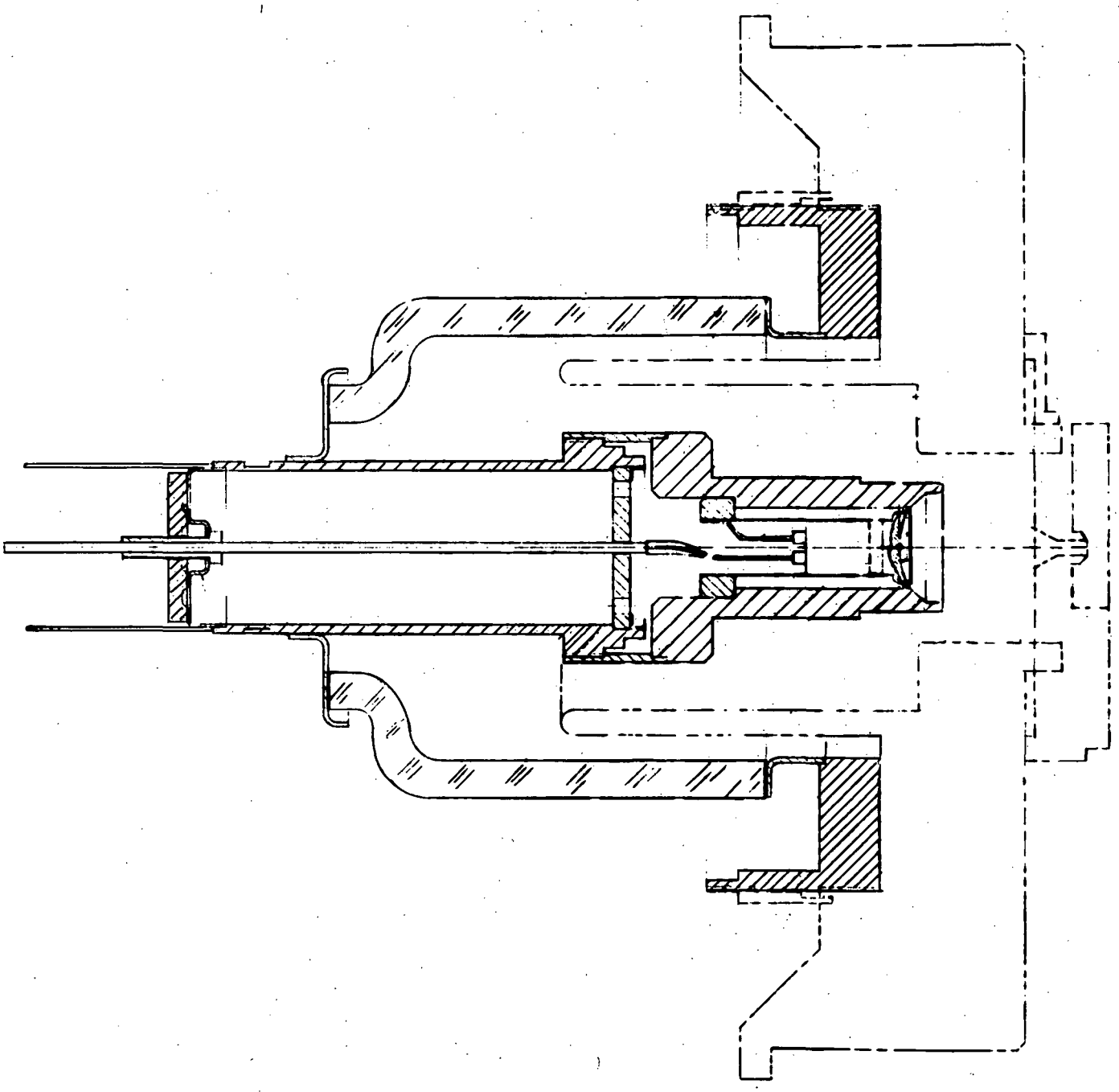

Figure 5-7. Electron Gun Assembly

The cathode employed is a dispenser cathode, because an oxide coated cathode could not be expected to provide the cathode current density required in this application. The cathode is supported by a cylindrical sleeve which is mounted inside the focus electrode support sleeve and brazed to a diaphragm at the base of the gun ceramic. During operation it is possible to make small adjustments to the cathode using a fixture which clamps on the gun base and provides a means of distorting the mounting diaphragm in a carefully controlled manner.

The original gun is mounted on the gun polepiece by means of a heliarc sleeve on the gun flange. Replacement guns are provided with holes drilled through the gun flange. These guns are mounted by means of machine screws which pass through the gun flange and engage tapped holes in the gun polepiece.

5.4 SOLENOID CONSTRUCTION

The focusing solenoid is required to be bakeable in a vacuum chamber to 250°C minimum. The solenoid used in this program has been designed to withstand bakeout temperatures to 300°C. To minimize the evolution of gasses during bakeout the solenoid is completely free of all plastics or other high vapor pressure materials. The magnet coils are made of aluminum foil insulated with aluminum oxide, formed by anodizing the foil. The coils are insulated from the magnet case and magnet coolant plate with mica. Although the cooling efficiency is relatively poor, the ability of the magnet to operate at high foil temperatures minimizes the need for good thermal contact between the magnet coils and the magnet cooling plate.

The focusing solenoid core or bobbin is made of nonmagnetic stainless steel. The solenoid case is made of annealed cold rolled steel coated with electrodeposited nickel, to avoid corrosion. The end plates of the case are made 1 in. thick in order to avoid flux leakage in the collector region.

The focusing solenoid mechanical and electrical characteristics are summarized in Table 5.1.

TABLE 5.1

FOCUSING SOLENOID APPLICATION DATA

Magnetic Field	3000	G
Current	25	A
Voltage (Winding Temperature of 120°C)	69	V
Resistance at 20°C	1	Ohm (max)
Nonoperating Temperature	300	°C
Coolant	Water	
Flow	1.5	gpm
Weight	175	lb
Length of Gap	3.0	in.
Length of Magnet	5.0	in.
Inner Diameter	4.0	in.
Outer Diameter	16.0	in.

6.0 EXPERIMENTAL RESULTS

This section is divided into two parts. The first part contains a review of the results obtained from testing the five tubes which were built. The second part is a review of analytical results based on use of the Varian large signal computer program.

6.1 RESULTS OF TUBE TESTS

For ease of testing, the initial cold test work was carried out using scaled up cavities based on an assumed actual cavity period of 0.150 in. Computer calculations described in Section 4.0 indicated a required period of 0.164 in. The cavity section for the first tube is shown in Figure 6-1. The cavity walls are tapered for maximum interaction impedance. The gap length has been increased from the initially estimated 0.040 in. to 0.044 in. to maintain the gap-to-period ratio of 0.268.

The Brillouin diagram for the circuit is shown in Figure 6-2. The passband is centered around 12.1 GHz and the bandwidth is approximately 2%. The circuit had scaled about 1% low in frequency because of the increase in the cavity period. Rescaling the circuit for better band-centering would have delayed the program without enhancing our ability to meet the program objectives for the first experimental tube.

The interaction impedance of the cold test circuit was measured by standard perturbation techniques. An equivalent circuit was fitted to the cold test data as a first step in building a model for computer simulation. The computed interaction impedances are shown in Figure 6-3. The total impedance is $V^2/2P$, where V is the peak gap voltage and P is the power flowing in the equivalent circuit. The Pierce impedance is derived from the total impedance with a knowledge of the field shape in the gap. The gap field shape is needed to relate the cold test perturbation data to the total impedance and is derived by solving the wave equation for $r \leq a$, where a is the drift tube radius. Solving the wave equation requires an assumption of the field shape at $r = a$. We assume a field shape which is intermediate between a constant field and a field with

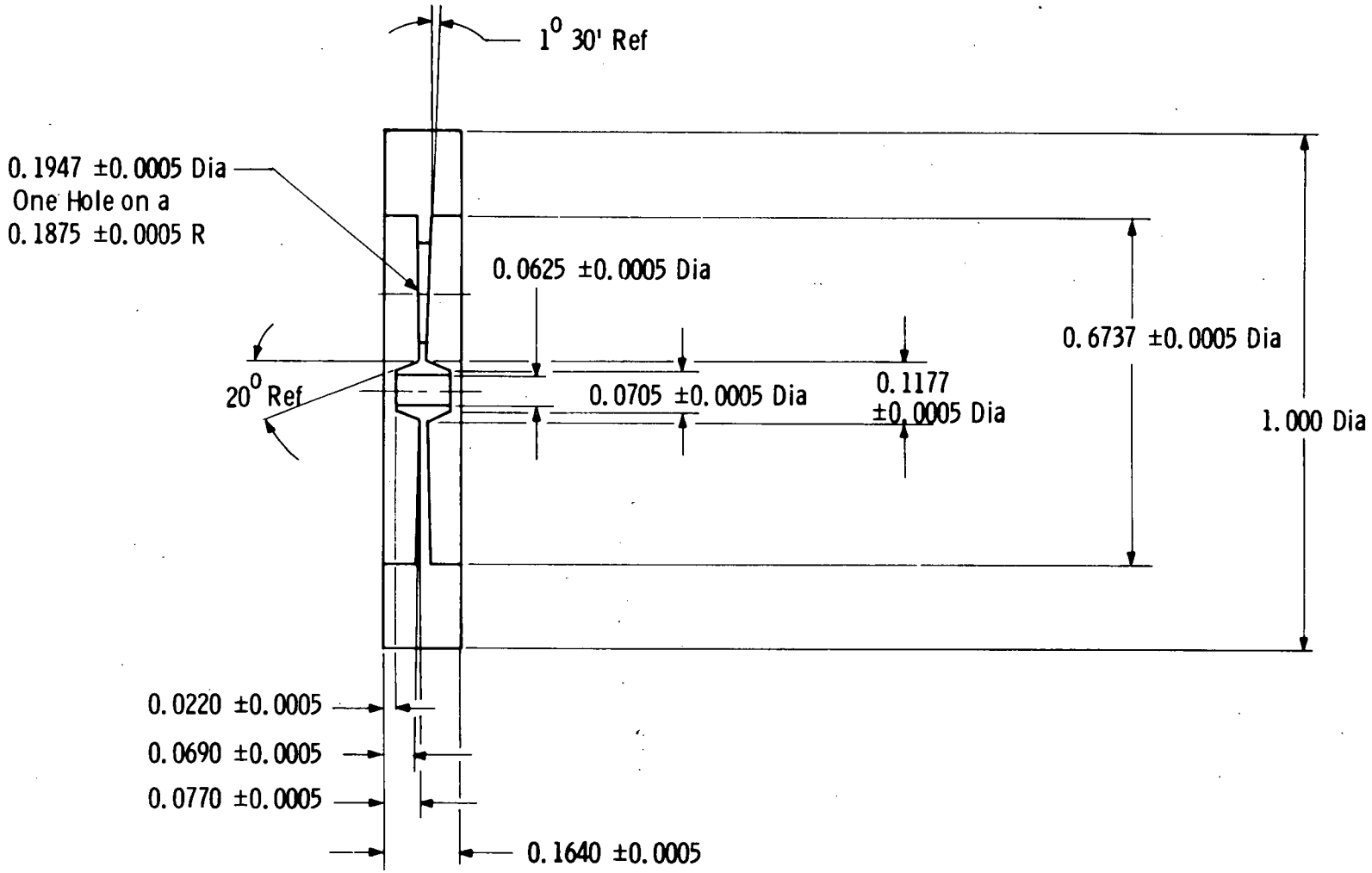

Figure 6-1 Cavity Web and Drift Tube for VTX-6681A1, S.N. 101

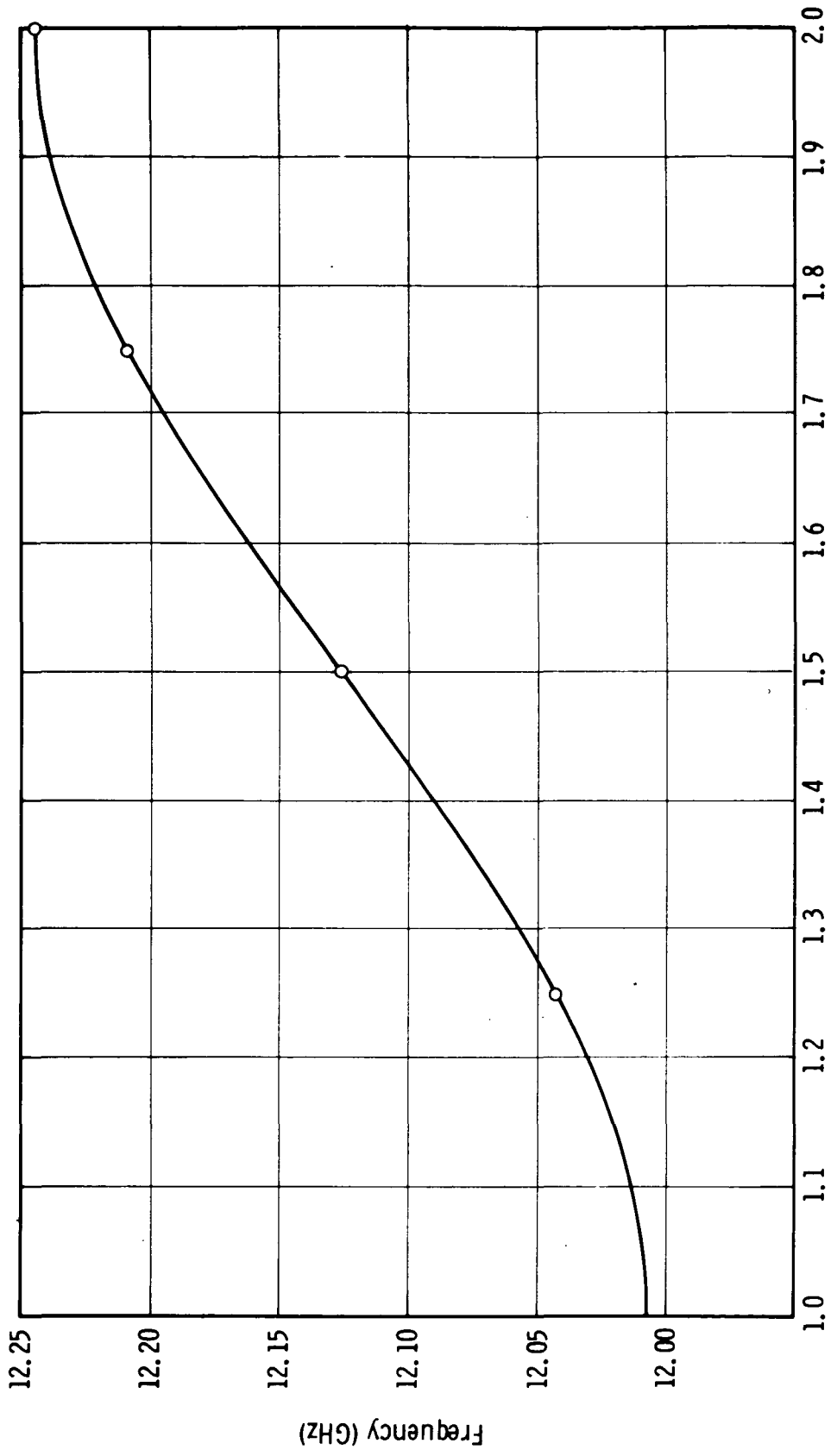

Figure 6-2. Brillouin Diagram for VTX-6681A1, S. N. 101

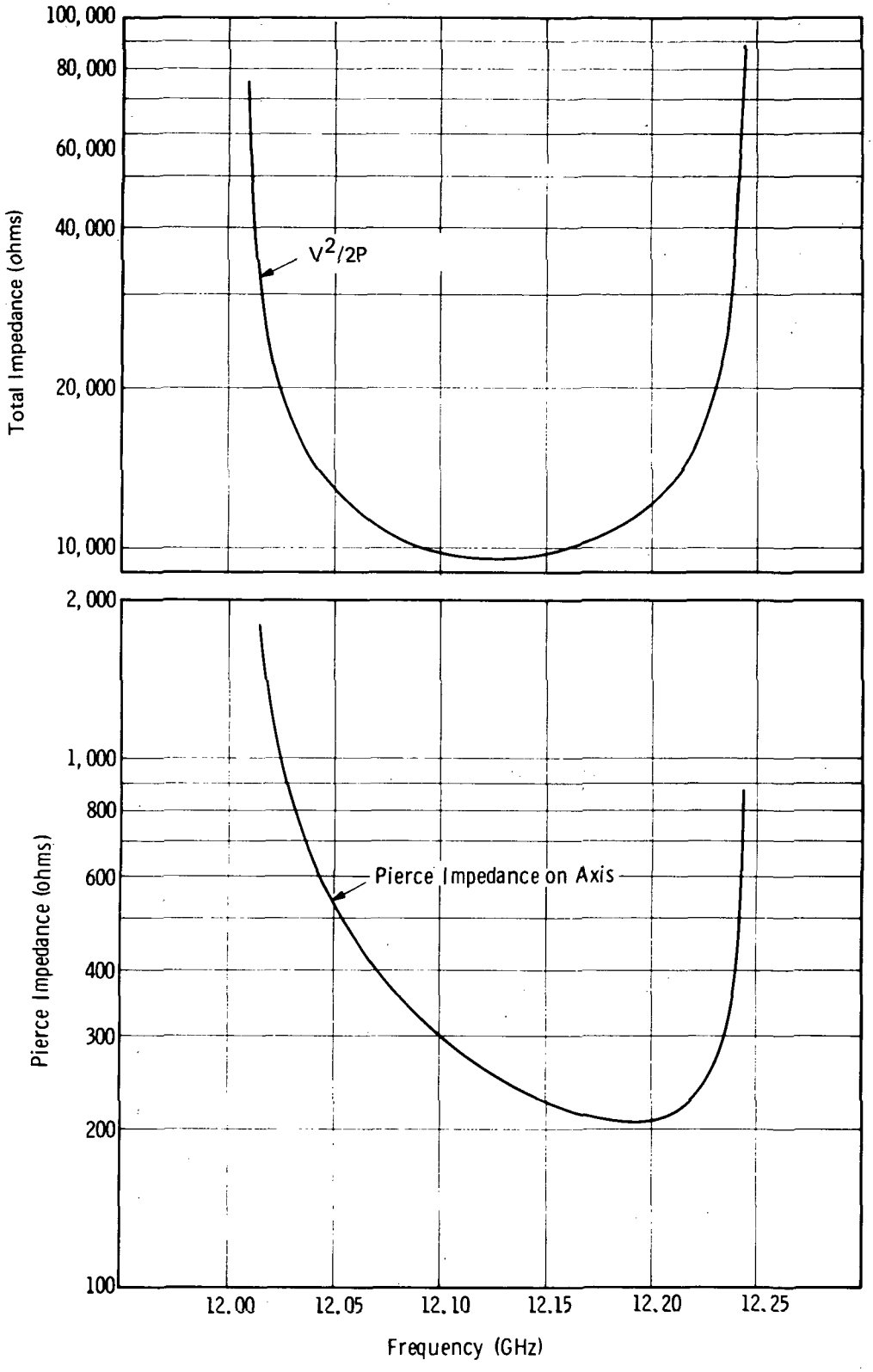

Figure 6-3. Measured Total Impedance and Pierce Impedance for VTX-6681A1, S. N. 101

sharp "horns" which would occur if the drift tips were infinitely sharp. Using this technique, the calculated field shape near the middle of the gap is virtually indistinquishable from the Laplace field for the exact gap geometry, and the calculated field near the middle of the drift tube is known to be accurate, since it satisfies the wave equation and is noncritical with respect to the assumed field shape. The Pierce impedance shown in Figure 6-3 is that for the first forward-wave space harmonic of the circuit. It is presented here for comparison and not used in the computer simulation of the TWT. The Pierce impedance of the n^{th} space harmonic is defined by

$$K_n = \frac{E_n^2}{2\beta_n^2 P} \tag{6.1}$$

where

$$E_n = \frac{V}{L} \frac{\int_0^L e^{j\beta_n z} e(z)\, dz}{\int_0^L e(z)\, dz} \tag{6.2}$$

and V = peak gap voltage

L = periodic length of circuit

β_n = propagation number of n^{th} space harmonic

$e(z)$ = total axial electric field of the slow-wave circuit

P = power propagating on slow-wave circuit

Combining Equations (6.1) and (6.2) we obtain

$$K_n = \frac{V^2}{2P} \cdot \left(\frac{M_n}{\beta_n L}\right)^2 \tag{6.3}$$

where

$$M_n = \frac{\int_0^L e^{j\beta_n L} e(z)\, dz}{\int_0^L e(z)\, dz} \tag{6.4}$$

Equation (6.3) relates each of the Pierce space harmonic impedances to the total impedance $V^2/2P$.

The circuit of the first experimental tube contains seventeen identical cavities with two severs. There is no velocity taper and no attempt has been made to equalize the gain by controlling the mismatch at the severs. No additional loss has been added to the circuit. The measured Q of a very lightly coupled cavity was approximately 1000. Pierce (Ref. 10) shows a relation between Q and loss per wavelength in a coupled-cavity circuit in the form:

$$\text{dB/wavelength} = \frac{27.3}{Q} \cdot \frac{Vp}{Vg} \tag{6.5}$$

This expression may be converted to a more usable form by multiplying by $\beta L/2\pi$ to obtain

$$\text{dB/cavity} = \frac{27.3}{Q} \cdot \frac{Vp}{Vg} \cdot \frac{\beta L}{2\pi} \tag{6.6}$$

Using Equation (6.6) the midband loss is found to be 0.43 dB/cavity.

The sever load VSWR is shown in Figure 6-4. This is a relatively broadband sever load which has been tuned to an almost perfect match over the hot design bandwidth.

The electron gun was designed for 0.325 μperv. The gun of the first experimental tube exhibited a μperv of 0.300, and represented a slight error in estimating the thermal expansion of the gun assembly. Figure 6-5 is a plot of body current versus focusing magnet current for the tube operating under cathode pulsed conditions. At the design value of the focusing field, 2500 G, the body interception was less than 0.7%. These tests under pulsed conditions appear slightly pessimistic in view of subsequent cw measurement which yielded 2 mA of interception at 15 kV with 550 mA of beam current and a focusing field of 2500 G; i.e., 99.6% transmission. The smooth variation of interception current with focusing magnet current is evidence of a satisfactory gun design and proper magnetic field shaping.

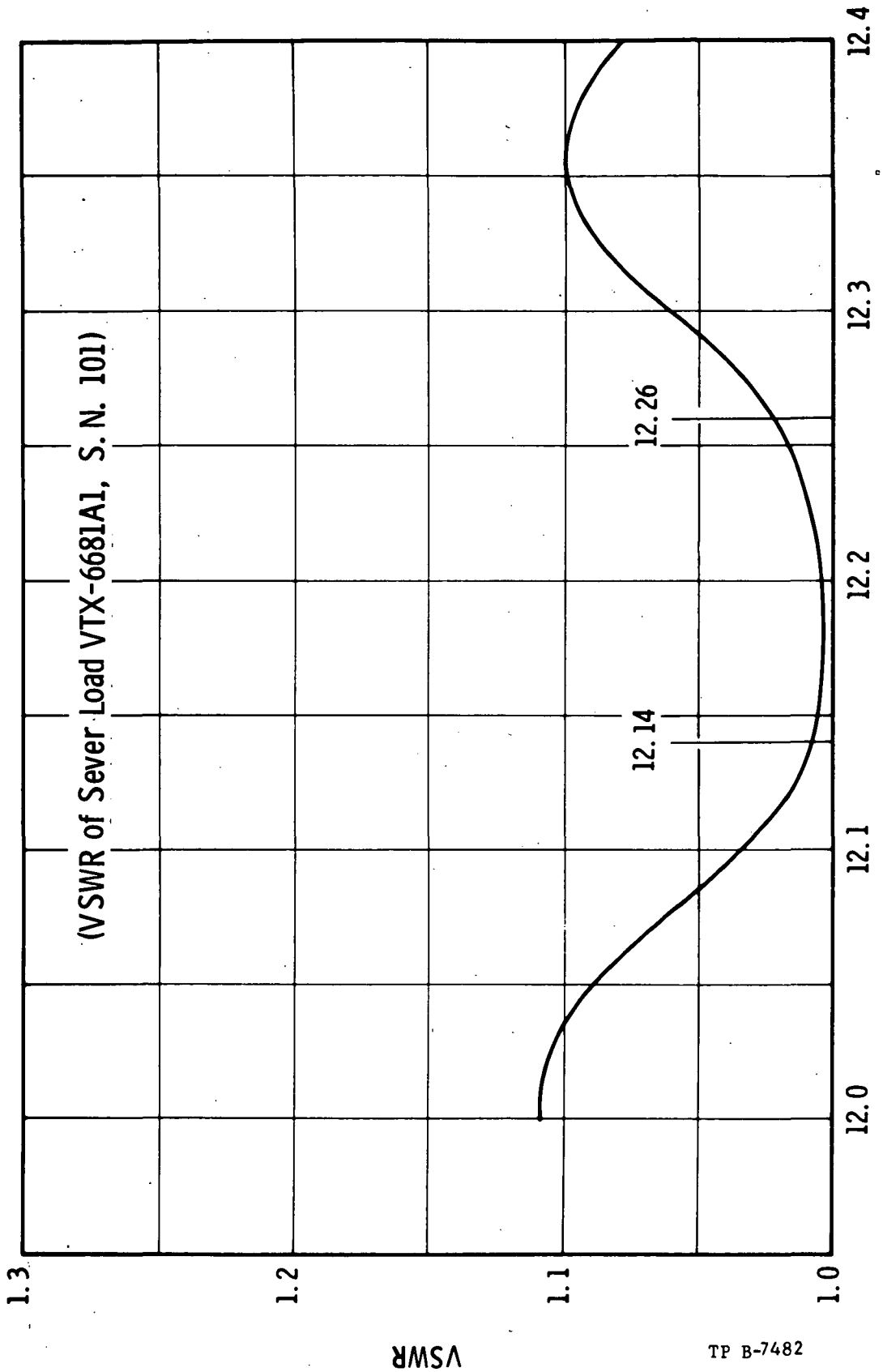

Figure 6-4. Cold Test Match of Sever Load for First Experimental Tube

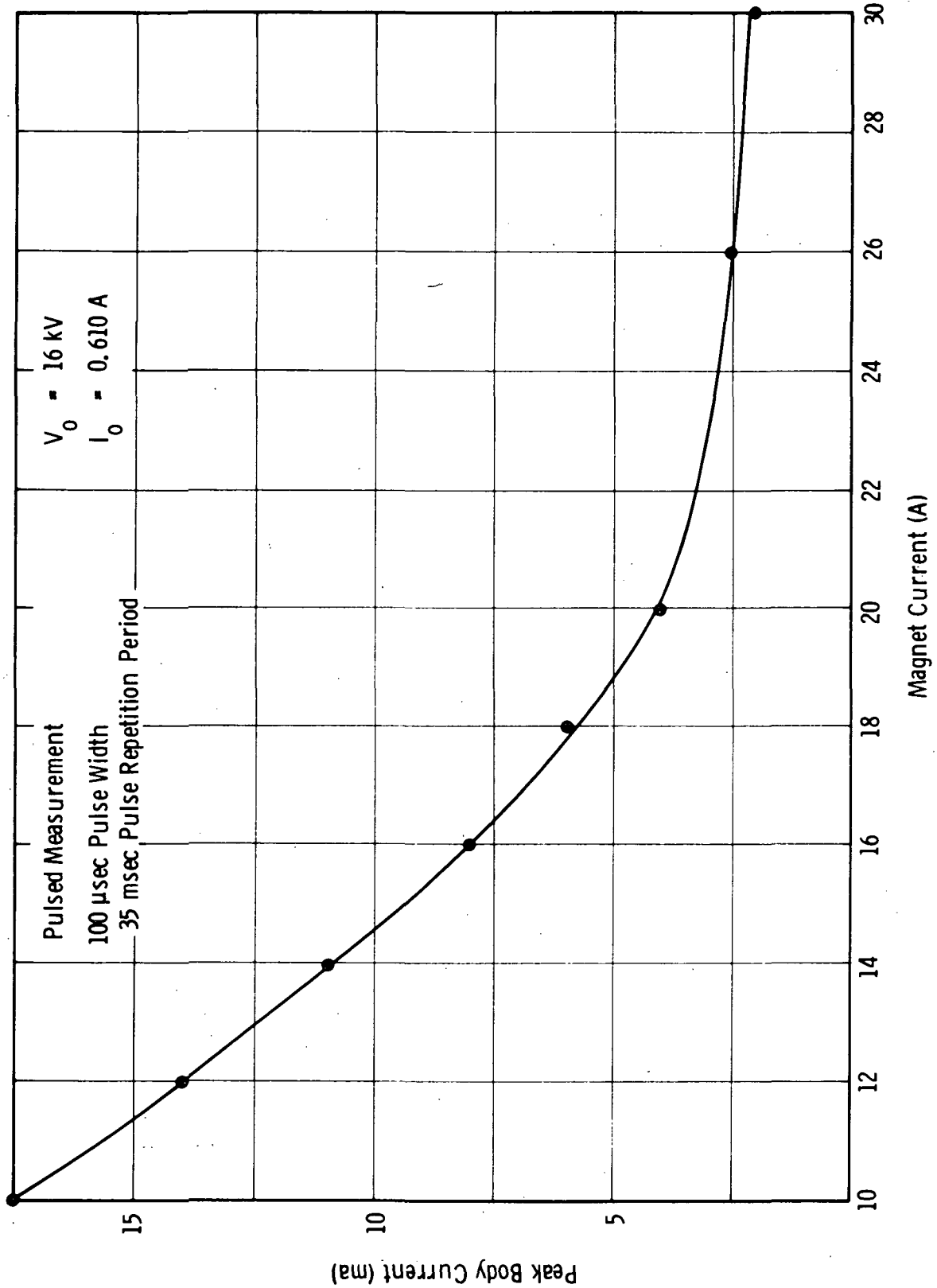

Figure 6-5. Measured Interception Current Under Pulsed Operation

6.1.1 Serial Number 101 Test Results

The first experimental tube was initially operated under pulsed conditions to check for instability without thermally overstressing the circuit and sever loads. Band edge oscillation was encountered at a beam voltage of 12 kV $\pm$ 100 V. Figure 6-6 shows the peak power output versus frequency at a drive power of 50 mW. The saturated gain at maximum power output is 47 dB with 30% conversion efficiency. Drive-induced oscillation is evident at 12.25 GHz.

Figure 6-7 shows the small signal gain under cw operation at three different beam voltages. The computed small signal gain at 15 kV is superimposed for comparison. Two factors stand out: (1) the tube exhibits significant gain above the upper band edge, and (2) large gain variations within the band are indicative of poor matching.

The measured saturated efficiency under cw operation is shown in Figure 6-8. The output power was measured calorimetrically and is perhaps a little conservative. The discrepancy between the efficiency measured here and the pulsed measurements is believed to be due to a deterioration in the output match. The computed efficiency for this tube at 12.18 GHz, under the operating conditions specified, is 24.4%. Low efficiency is not surprising since the tube is operating near synchronism. At 16 kV and full perveance, drive-induced oscillations were encountered because of higher gain and poor matches.

The tube was operated with a temperature-limited cathode at 16 kV beam voltage, a voltage more favorable for high efficiency with an untapered circuit. The results of this test are shown in Figure 6-9. During these tests, with 400 mW drive power at 12.25 GHz, the body current exceeded 30 mA and the power supply shut down.

Several attempts were made to turn the tube on, but in each case the body current, without drive, was about 10% of the beam current and the power supply was shut down automatically.

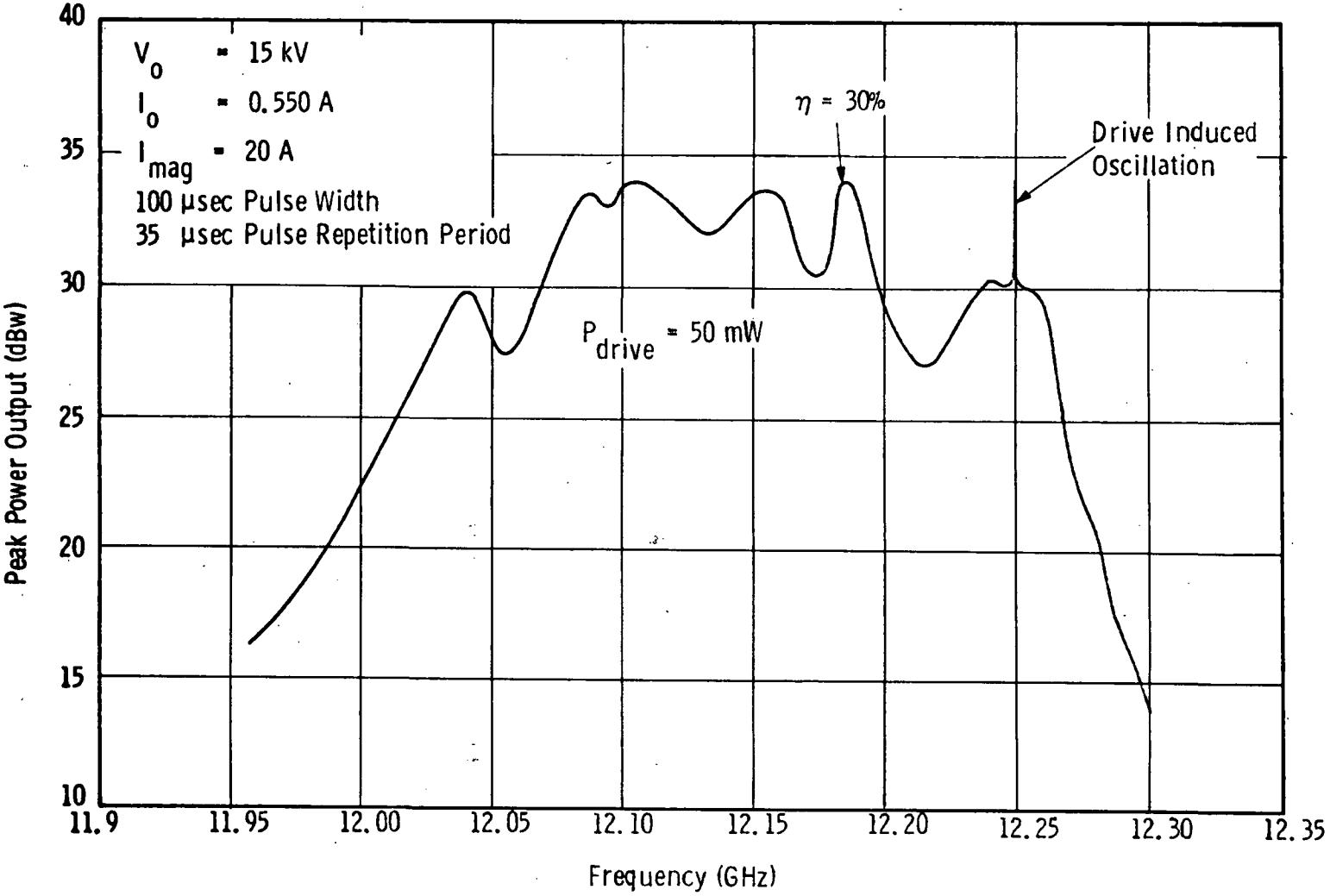

Figure 6-6 Peak Power Output vs Frequency

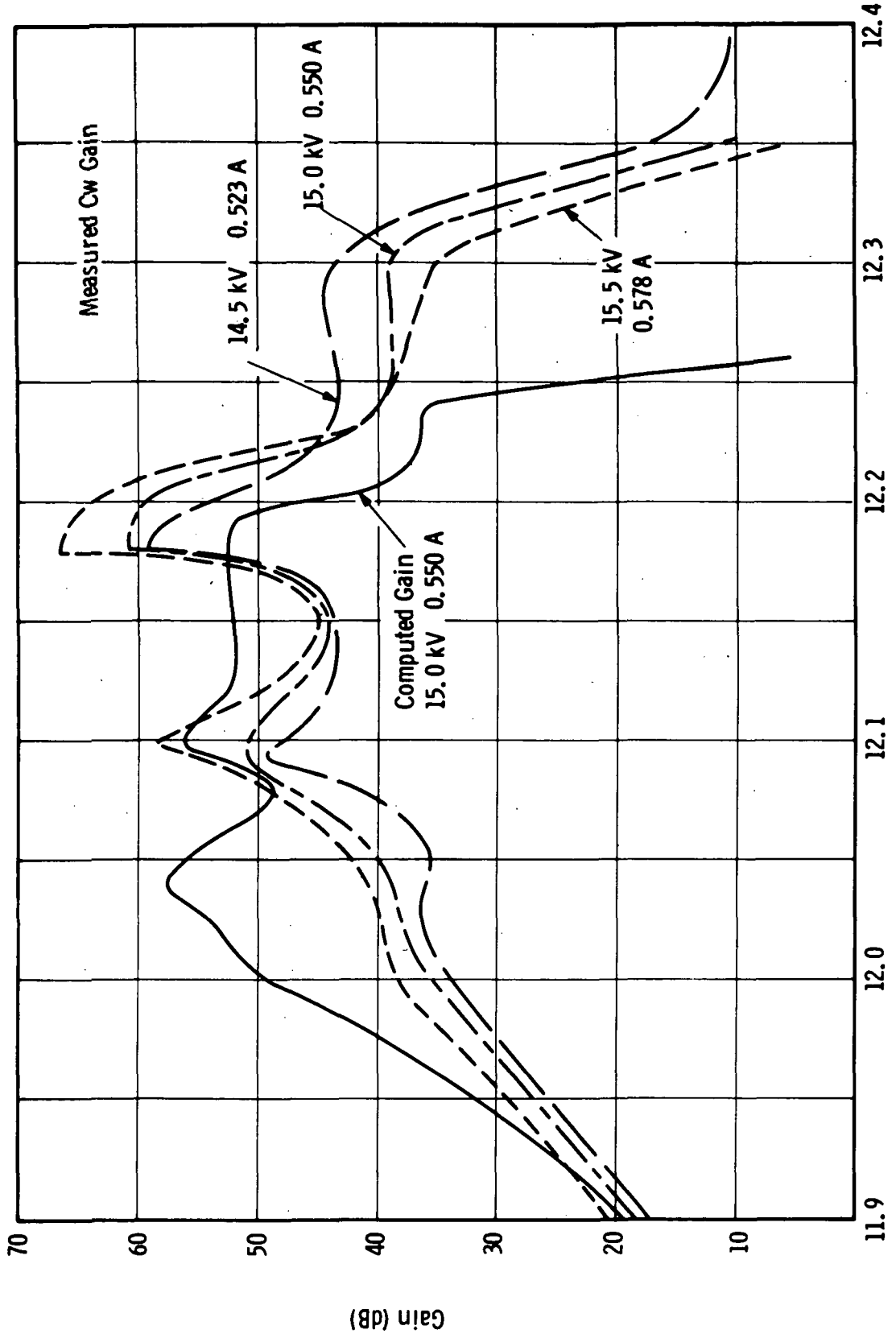

Figure 6-7. Measured and Computed Small Signal Gain of VTX-6681A1, S. N. 101

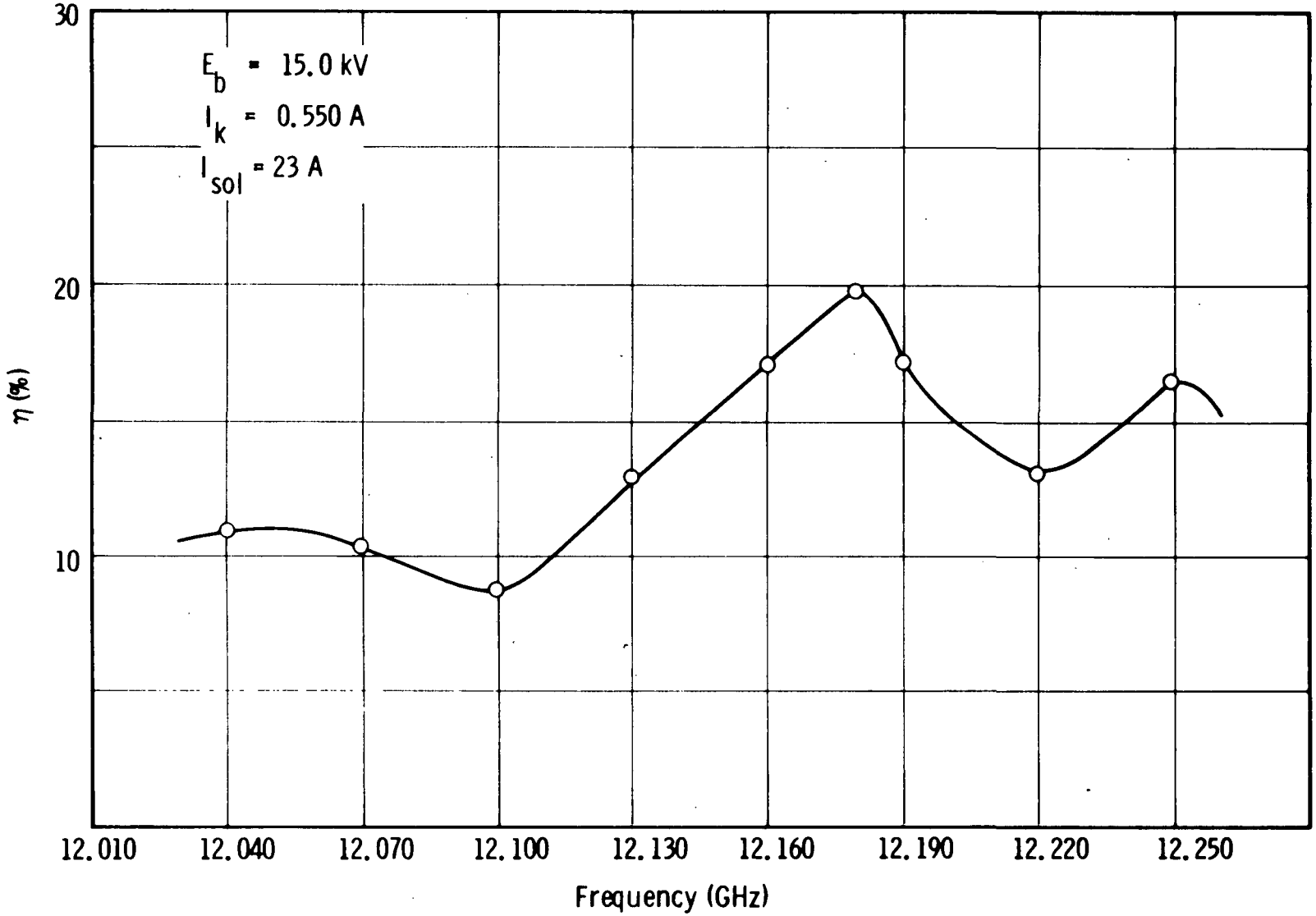

Figure 6-8. Measured Saturated Efficiency of VTX-6681A1, S. N. 101

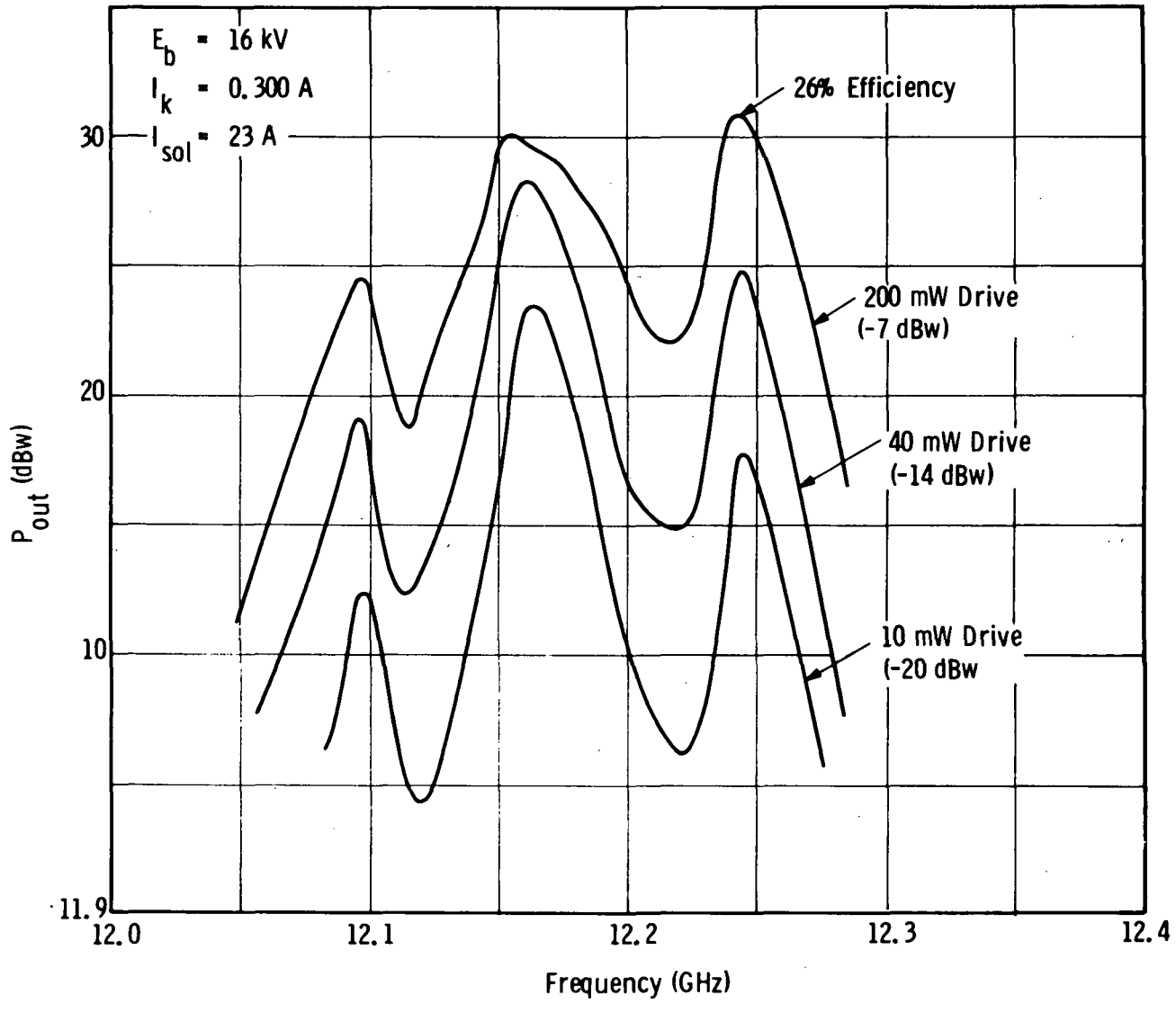

Figure 6-9. Measured Performance of VTX-6681A1, S. N. 101, at Reduced Perveance

The VSWR looking into the output was then measured and found to be very poor. The measured output VSWR before and after hot testing is shown in Figure 6-10.

The tube was disassembled and examined. No melted drift tubes were encountered; however, the output gap spacing was found to have decreased by 0.001 in., which is sufficient to explain the poor output match. An examination of the electron gun showed that the cathode was eccentric with respect to the focus electrode by approximately 0.003 in. This was the apparent cause of poor beam transmission.

The test data from SN 101 are in substantial agreement with analytical predictions. These tests have demonstrated the adequacy of the collector, the sever loads, the focusing solenoid and the beam optics. A mechanical defect in the cathode support structure requires correction.

The irreversible thermal detuning of the output cavity shows a weakness in the design which must be dealt with. The thin cavity web, which was chosen to maximize circuit impedance is mechanically and thermally inadequate. The narrow band circuit, which was also chosen to maximize circuit impedance, is least tolerant of thermal detuning. A larger gap spacing might improve the situation by reducing the gap tuning rate.

6.1.2 Serial Number 102 Test Results

The design of SN 102 takes account of the inadequacies of the first experimental tube and is also intended to provide necessary experimental information on velocity tapering.

The cathode support structure was modified to correct the defect detected in the first tube.

To improve the thermal capacity and mechanical strength of the cavity web, its thinnest part, near the hub, was increased in thickness from 0.010 and 0.020 in. To decrease the gap tuning rate the gap length was increased from

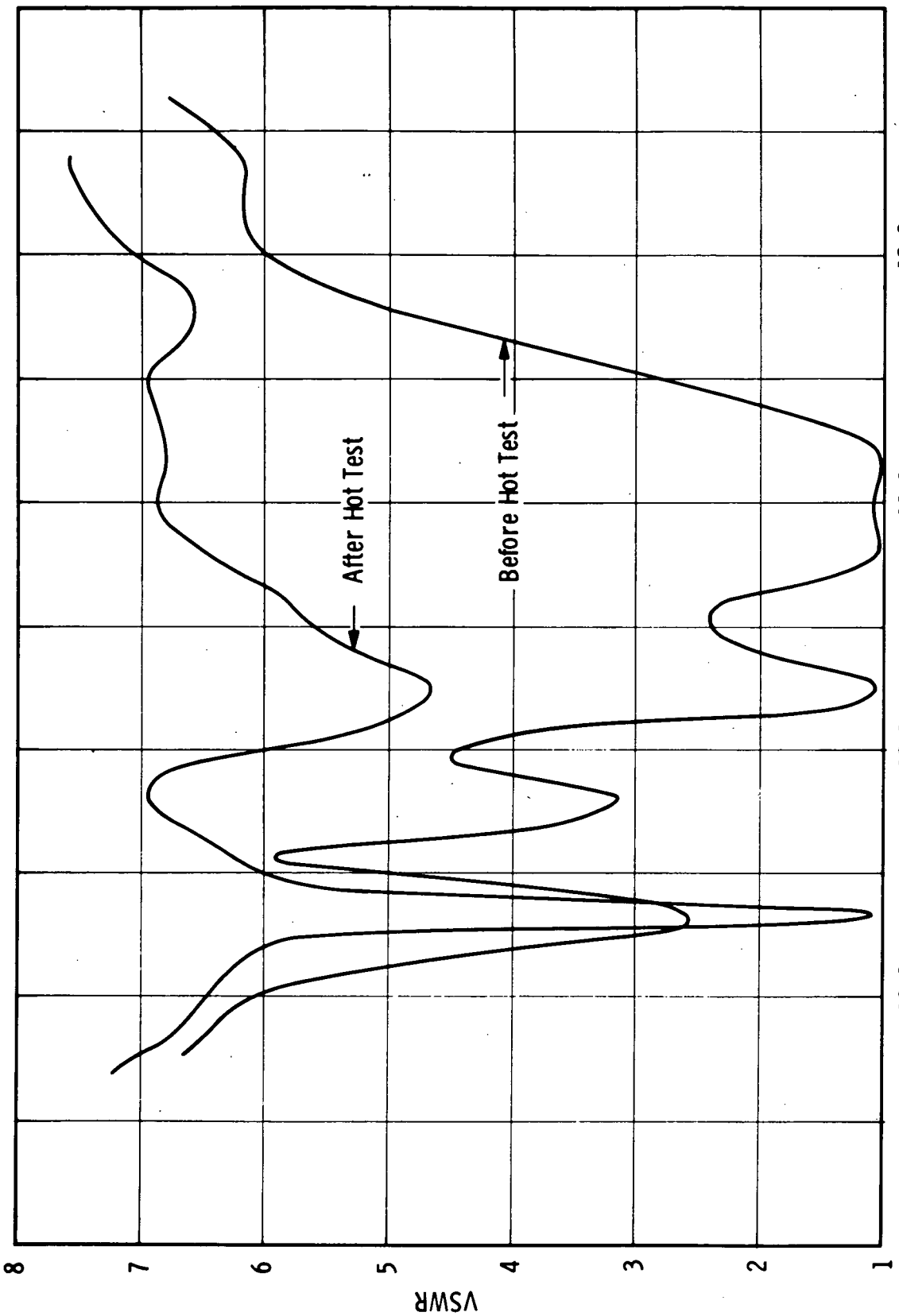

Figure 6-10. Rf Match at Output of VTX-6681A1, S.N. 101

0.044 to 0.050 in. To improve the rf circuit match the coupling slot impedance was lowered. The cold bandwidth of the circuit was increased to 4% in order to make the circuit less dimensionally critical.

A five-times scale model of the circuit was built to facilitate cold testing. The measured Brillouin diagram for the cold test circuit is shown in Figure 6-11. The interaction impedance computed from measurements of the cold test circuit is shown in Figure 6-12.

The rf match to the new circuit is illustrated in Figure 6-13. This figure shows how the match changes when the input gap spacing is varied $\pm$ 0.005 in., which in the X-band circuit would represent a gap change of $\pm$ 0.001 in. The match is seen to be relatively noncritical and the tube should thus be less susceptable to thermal detuning.

In order to fit within the existing focusing solenoid it has been necessary to design the second tube with less gain than the first tube. The output section has been increased to eight cavities to ensure sufficient gain beyond the final sever. There are 18 cavities in all with five cavities in both the input and center sections. Figure 6-14 illustrates the configuration of the cavity and coupling slots. Figure 6-15 is the measured Brillouin diagram for this circuit. The insertion loss was measured to be 0.35 dB/cavity at midband. A schematic of the output velocity taper is shown in Figure 6-16. The two-cavity velocity taper is achieved by reducing the height of the penultimate cavity and offsetting drift tubes. An effort has been made to maintain the highest possible impedance in the reduced velocity section, particularly in the output cavity.

The computed small signal gain is shown in Figure 6-17. The gain variation over the operating band is approximately 1 dB. The computed efficiency for this design is 38%. The last two drift spaces have velocity ratios of 0.90 and 0.70. A two-cavity taper with velocity ratios of 0.75, 0.70 shows a computed efficiency of 40%. The highest computed efficiency for this circuit is 42% which is

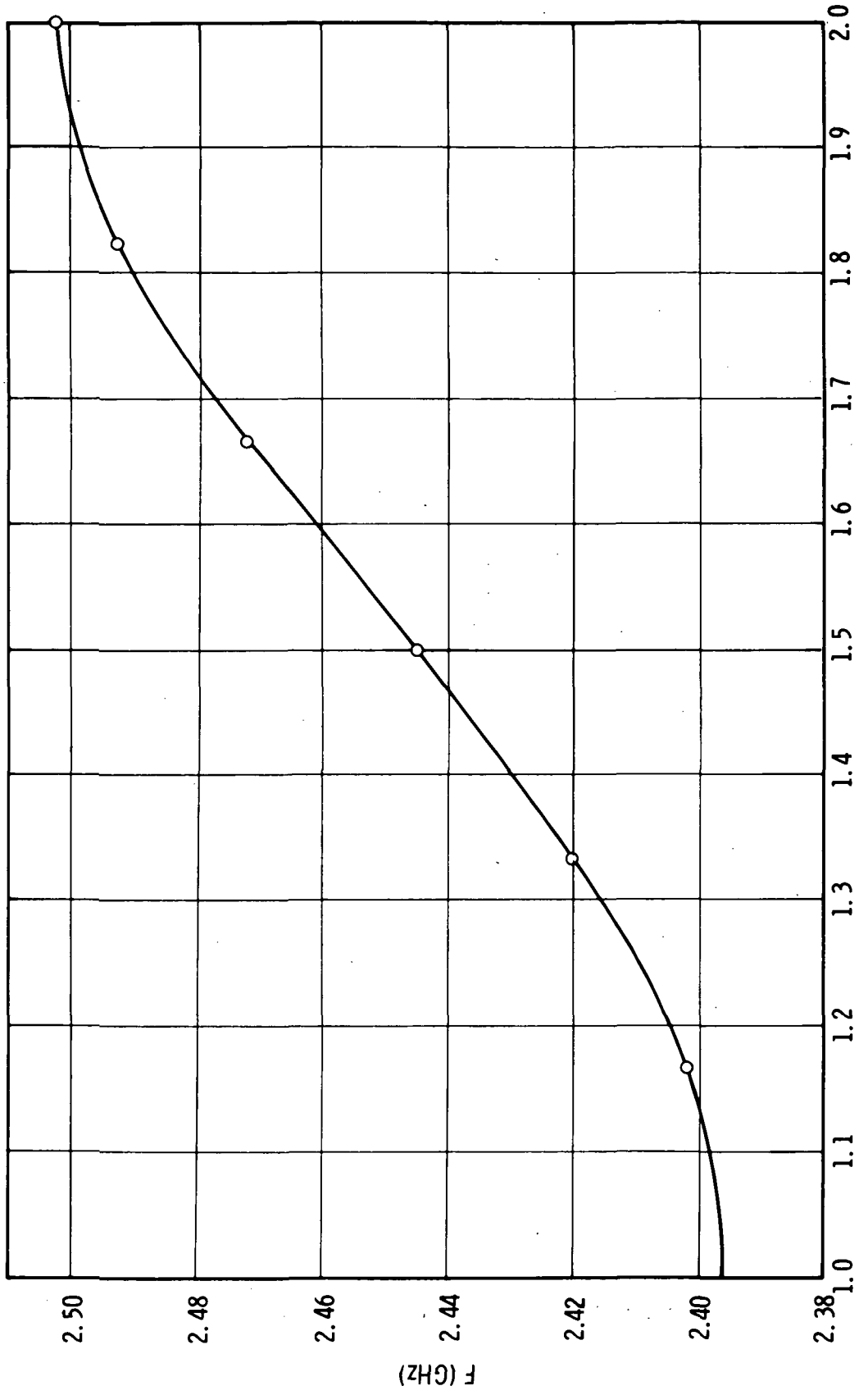

Figure 6-11. Brillouin Diagram for Cold Test Circuit with Bandwidth Equal to Four Times Required Hot Bandwidth

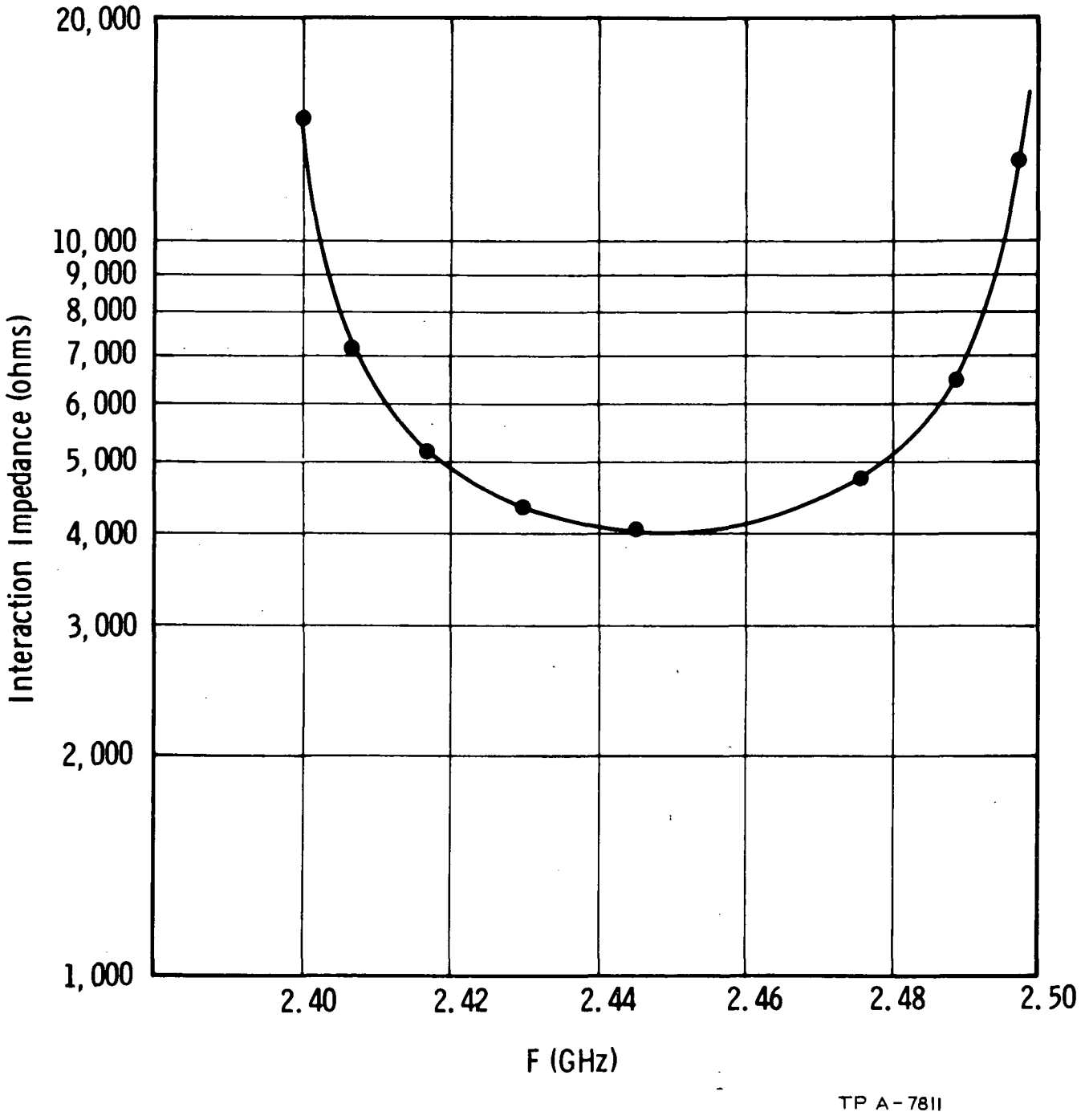

Figure 6-12. Interaction Impedance ($V^2/2P$) of 5:1 Scaled Cold Test Circuit

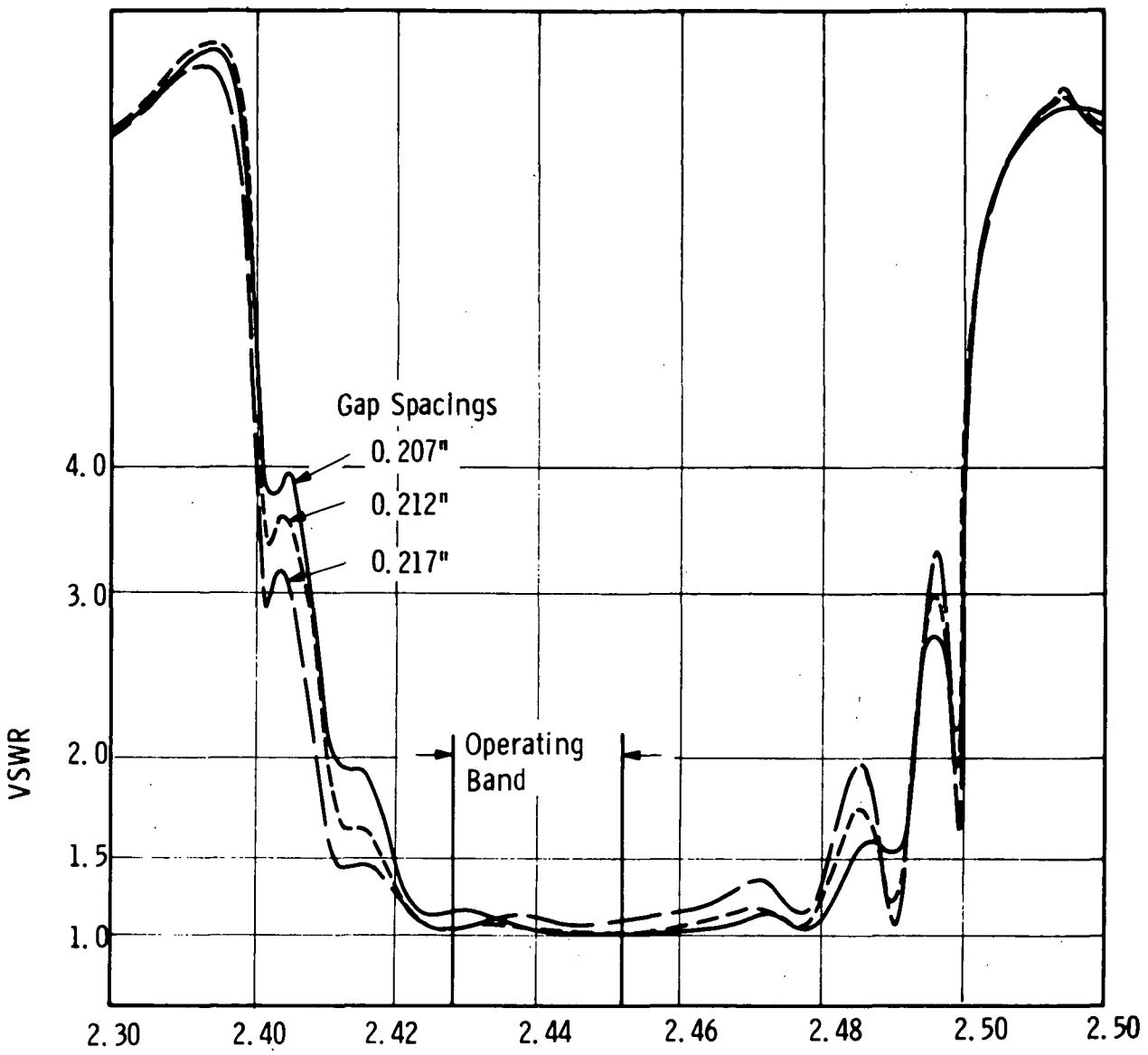

Figure 6-13. Input VSWR of Prototype Cold Test Circuit with Three Different Gap Spacings in First Cavity

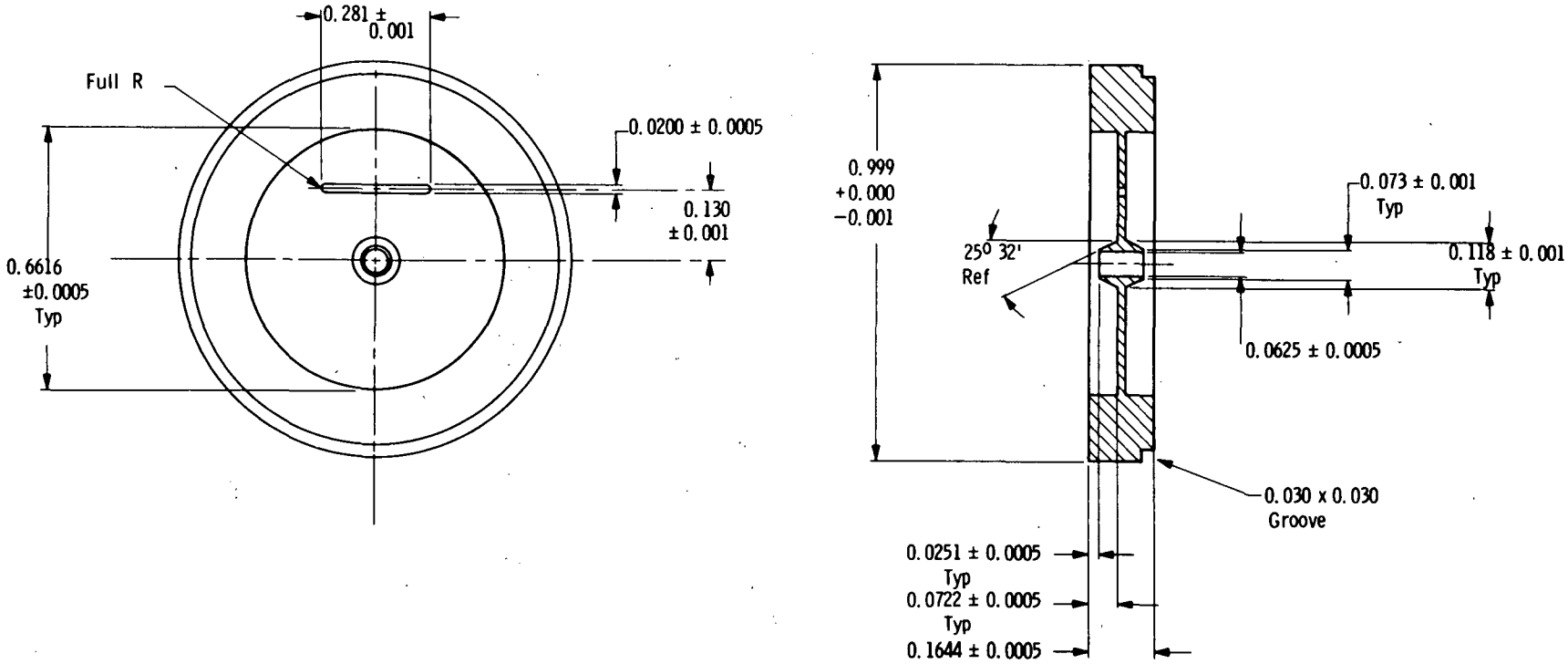

Figure 6-14. Cavity Web and Drift Tube for VTX-6681A1, S. N. 102

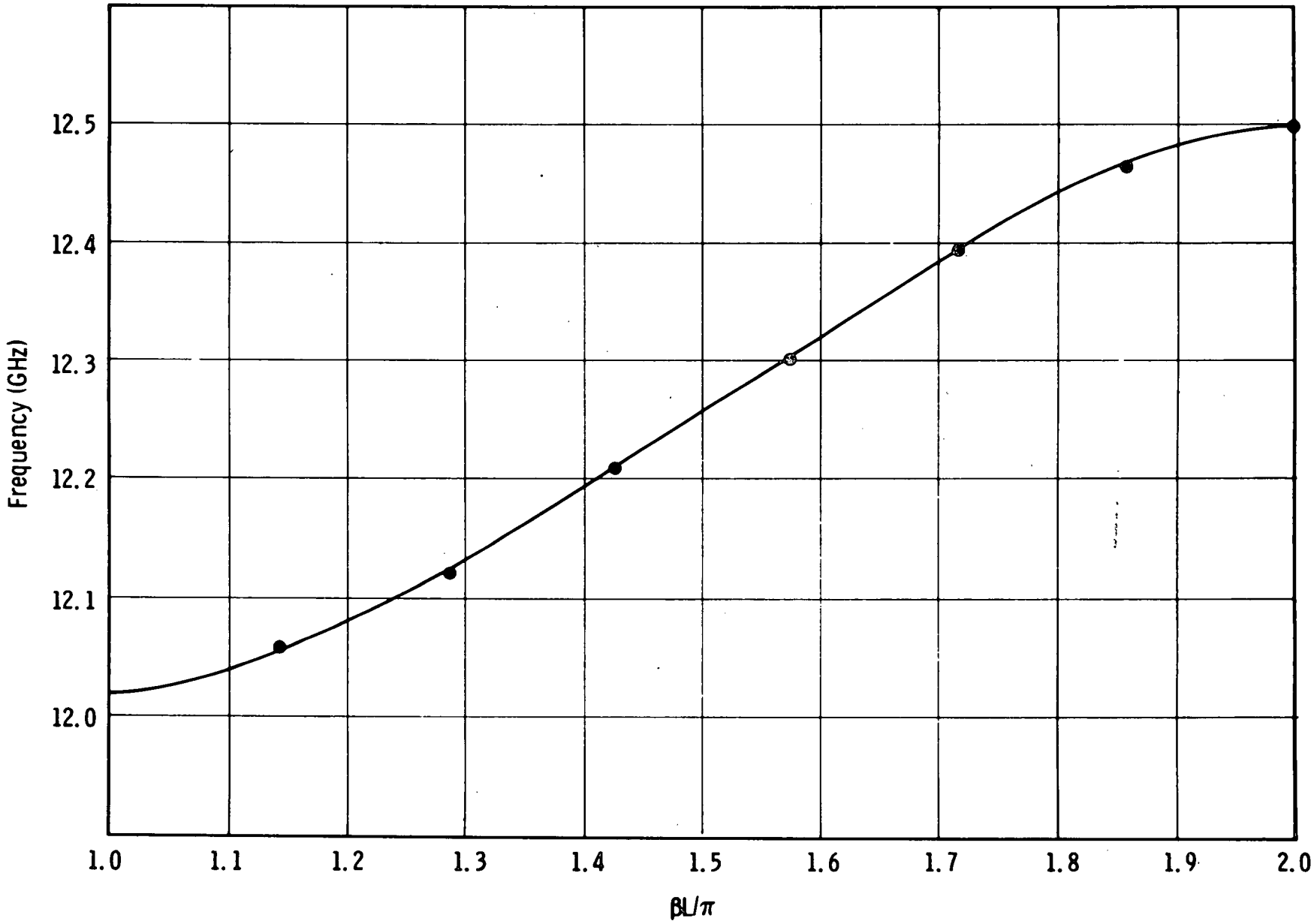

Figure 6-15. Measured Brillouin Diagram of VTX-6681A1, S.N. 102

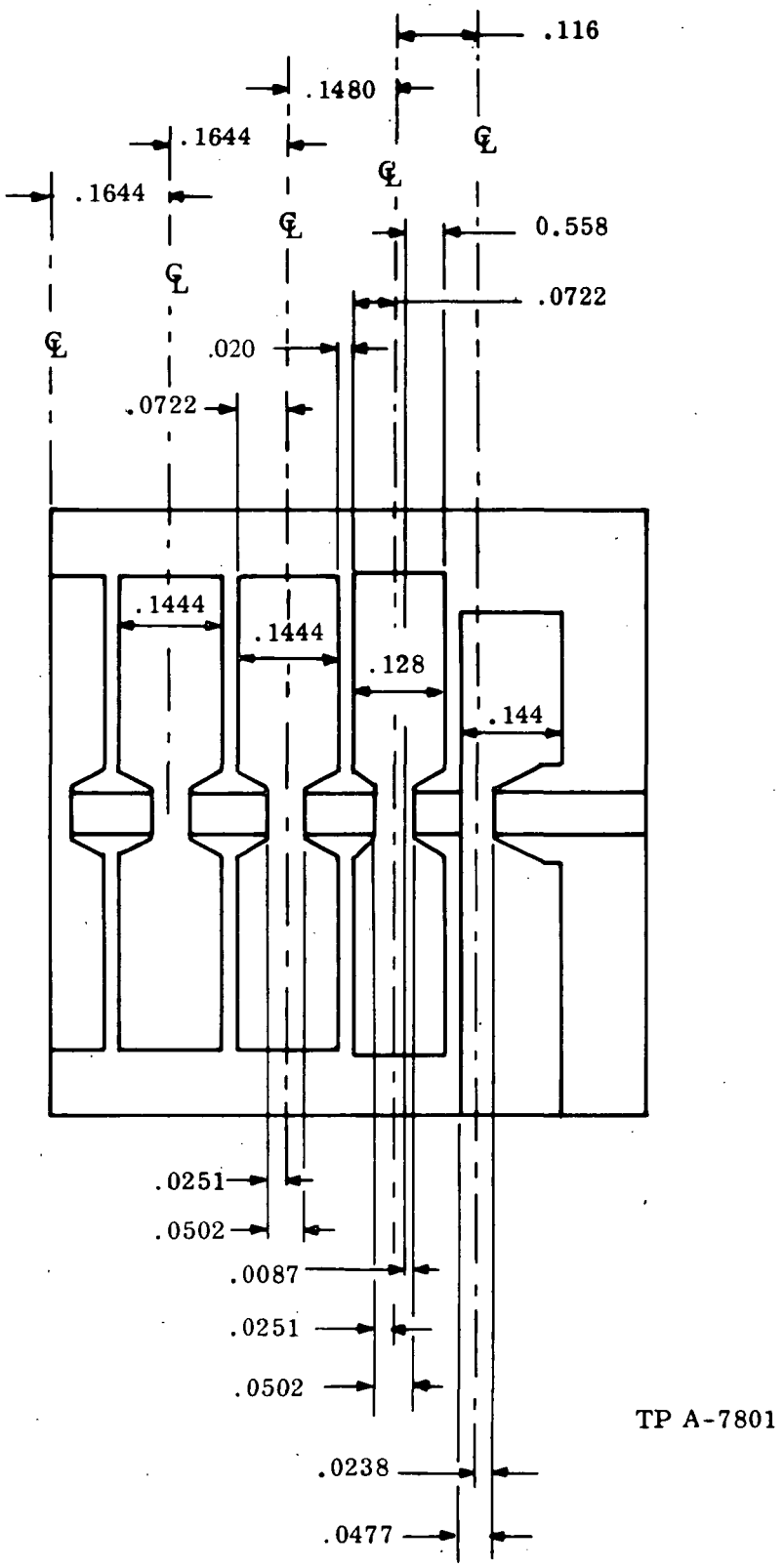

Figure 6-16. Schematic of Output Velocity Taper for VTX-6681A1, S. N. 102

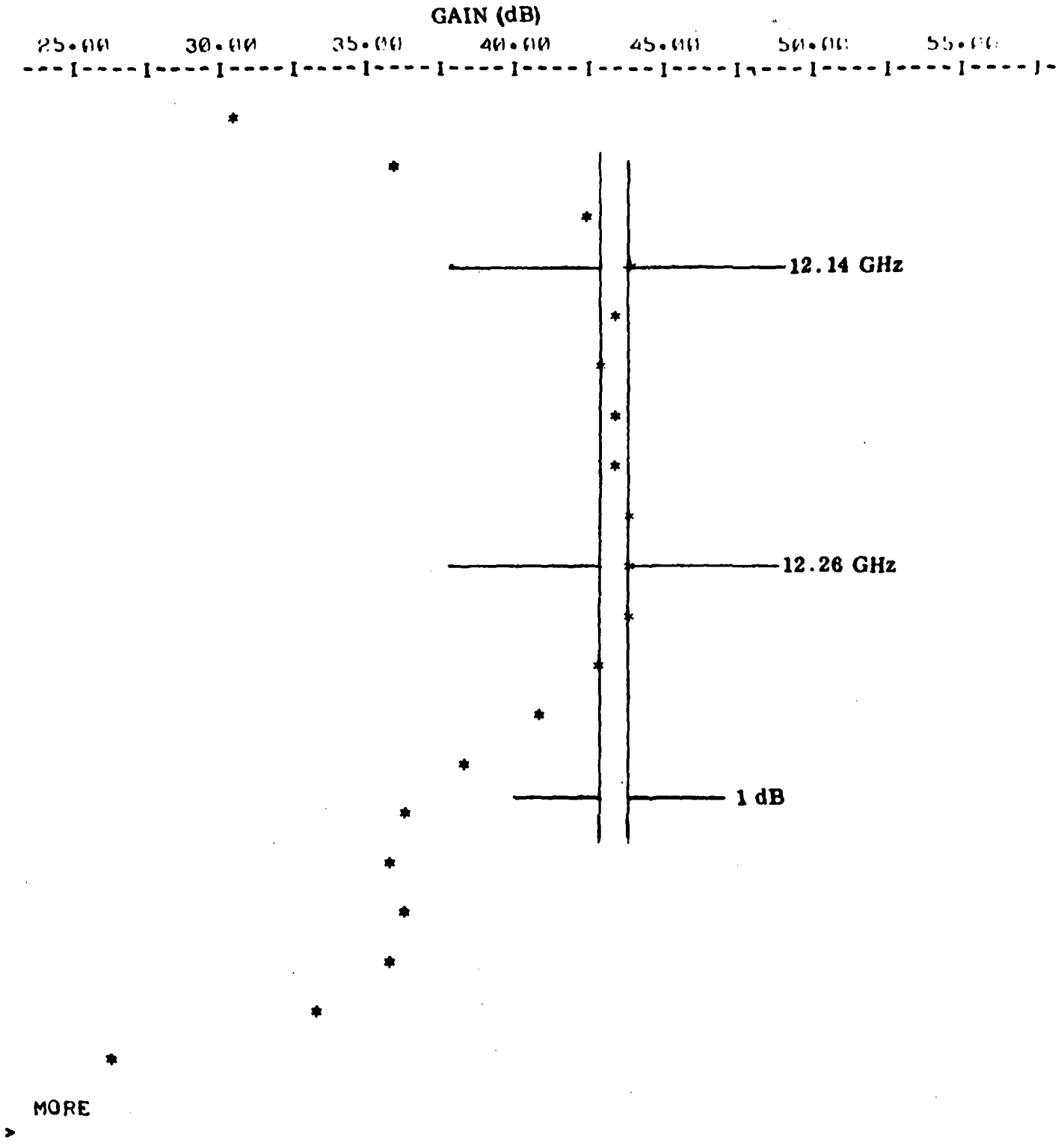

Figure 6-17. Computer Plot of Small Signal Gain for VTX-6681A1, S. N. 102

achieved using a three-cavity taper with velocity ratios of 0.90, 0.85, 0.70. This compares with the computed 48% efficiency of the high impedance circuit used in the first experimental tube and indicates the price that must be paid as a result of doubling the cold circuit bandwidth.

Figure 6-18 is a plot of measured start oscillation current versus beam voltage with experimental points superposed on the computed curve. The measured instability "tongue" above 15 kV is not in agreement with the theory. This instability was found to be a slot mode oscillation at 27.6 GHz. Below 14 kV, oscillation occurs near the upper band edge at 12.5 GHz. This is a so-called band edge oscillation. These oscillations imply insufficient rf loss in the output circuit.

Figure 6-19 is a plot of power output versus frequency at a beam voltage of 15 kV and a beam current of 250 mA. Over a 120 MHz band centered at 12.2 GHz the power output varies by 1.9 dB.

Further measurements were carried out under cw operating conditions. The onset of instability, or instability threshold, was difficult to measure because it depends critically on the magnetic focusing field. The relationship between focusing field and instability is unpredictable. Sometimes stability is improved by increasing solenoid current, in other instances increased solenoid current causes stability deterioration.

The most noticeable and reproducible characteristic of the tube is an abrupt reduction in the "slot mode" starting current at a beam voltage near 14.8 kV. Figure 6-20 shows the measured effect of changing beam voltage at constant beam current. It is a plot of power output versus frequency at constant drive power, with beam voltage as a parameter. Below 14.75 kV, a small change in beam voltage produces a slight offset in the passband, as predicted. At 15 kV, the midband gain has dropped by 1 dB due to the onset of the "slot mode" oscillation. At 15.25 kV the "slot mode" has become sufficiently strong to reduce midband gain by 6 dB. At higher

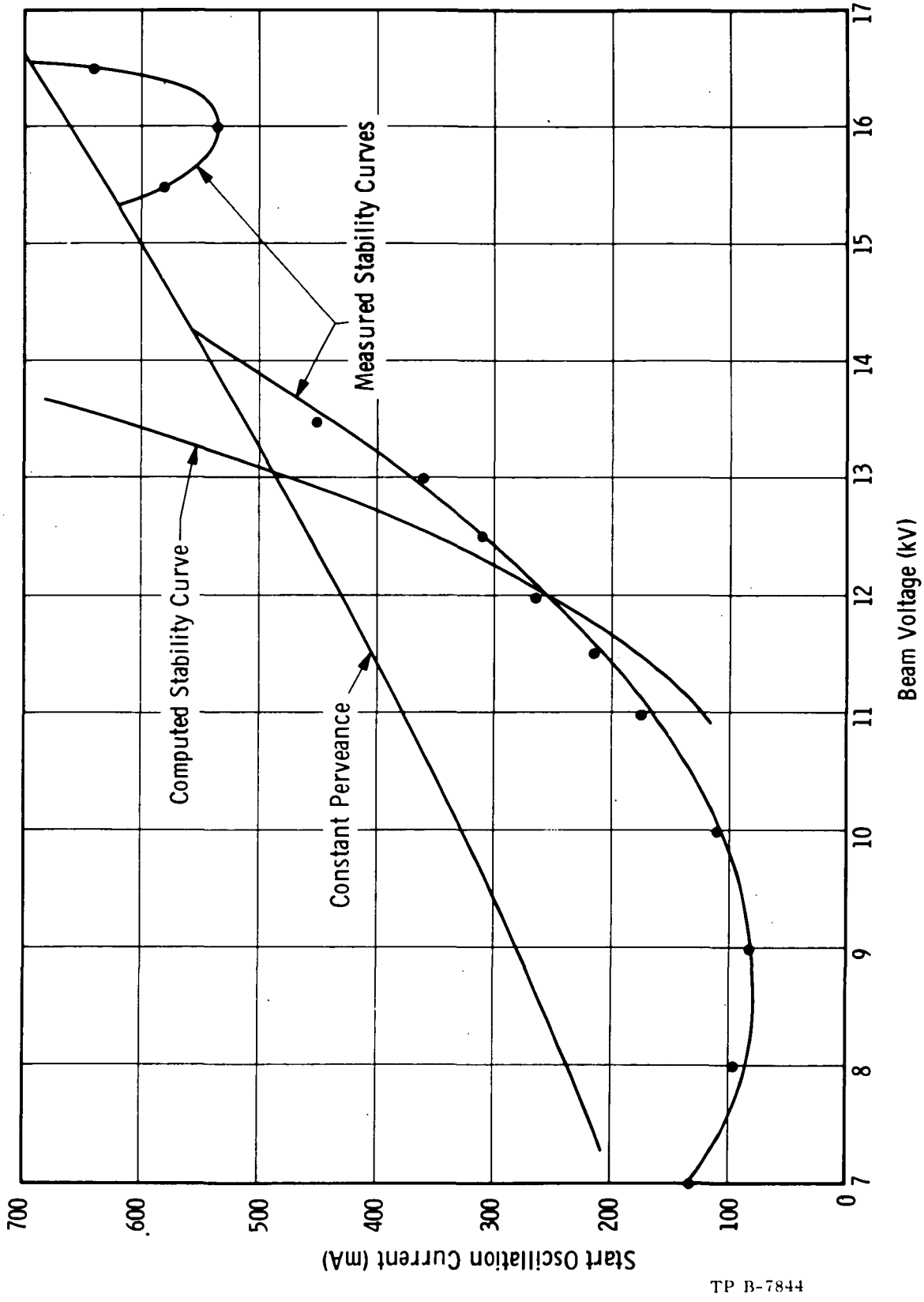

Figure 6-18. Measured and Computed Stability Curves for VTX-6681A1, S.N. 102

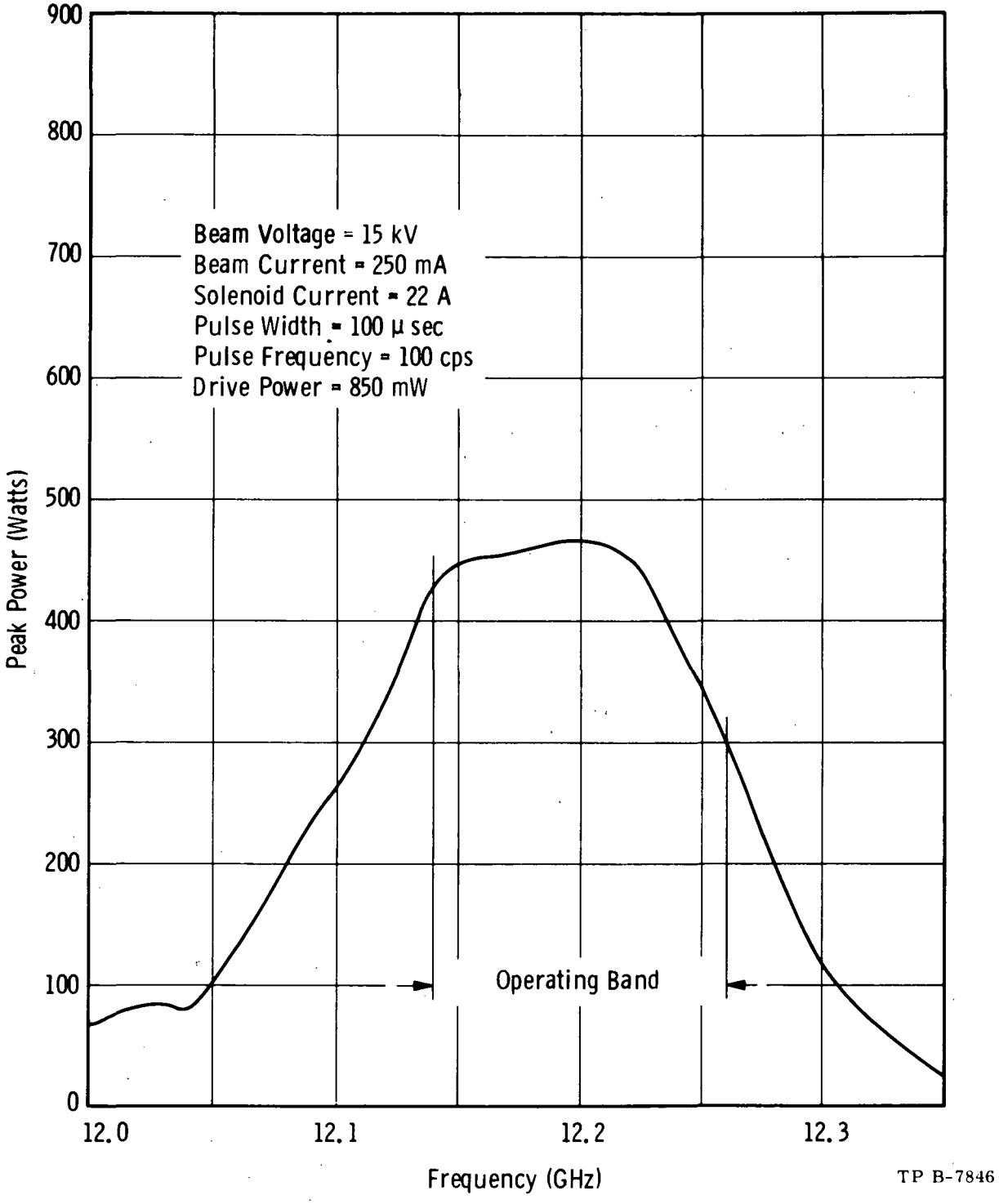

Figure 6-19. Power Output vs Frequency for Constant Drive Power

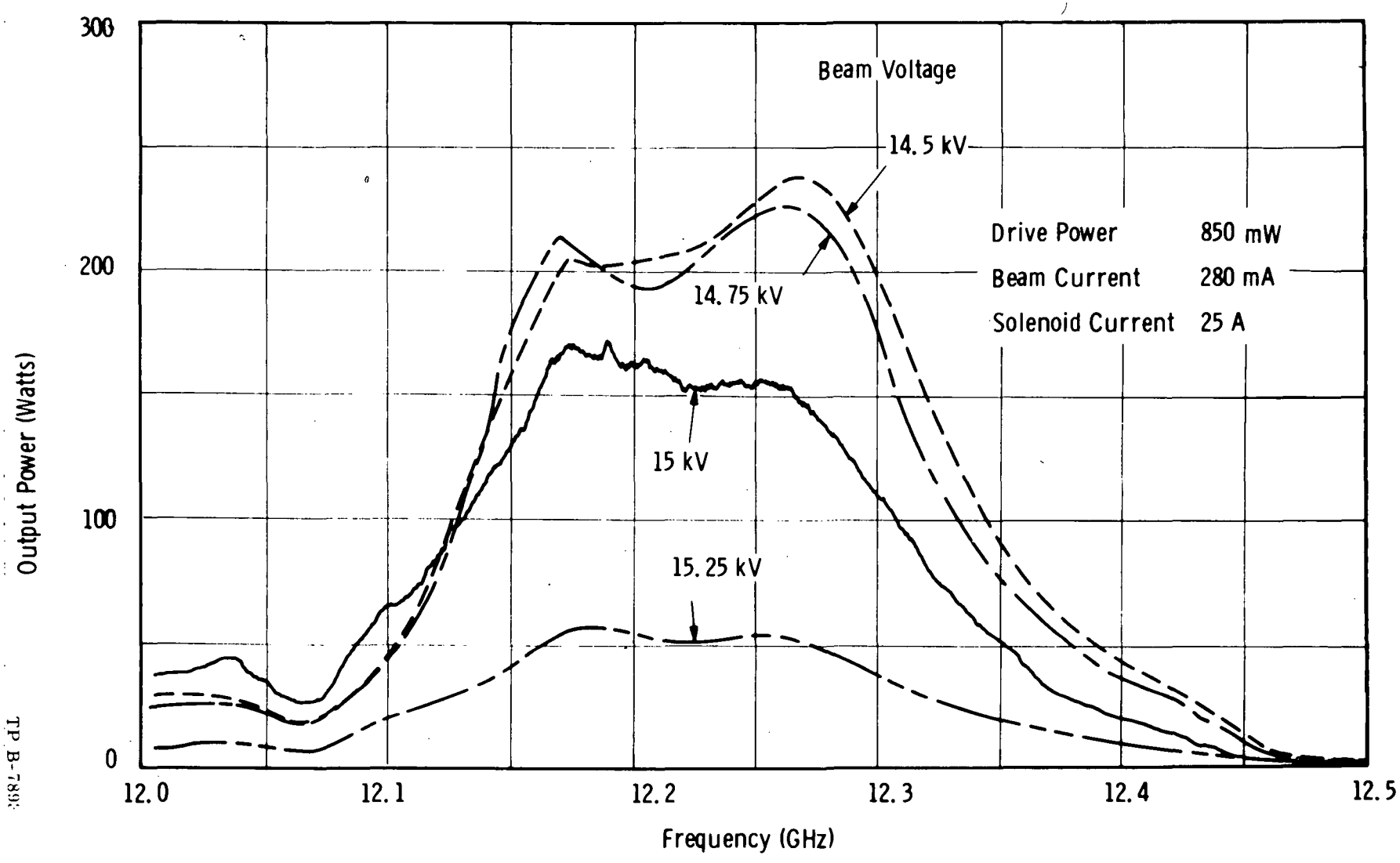

Figure 6-20. Power Output vs Frequency with Beam Voltage as a Parameter

beam currents the "slot mode" is encountered at lower beam voltages. The maximum gain shown in Figure 6-20 is approximately 24 dB.

Figure 6-21 shows the power output vs frequency with drive power as a parameter. The beam current has been reduced to 170 mA to ensure stability. The slight increase in gain with drive is normal for an overvoltage tube. Figure 6-22 shows power output vs drive for a case in which the beam current is sufficiently high to cause instability at zero drive. For drive levels below 2.4 W the instability causes the output to vary erratically. Above 2.4 W drive the "slot mode" is suppressed by the interaction of the fundamental mode and the tube saturates in normal fashion. The maximum power output is 2 kW at a conversion efficiency of 30%. Higher conversion efficiencies were not measured, because at higher beam currents it was not possible to drive through the instability region.

Figure 6-23 is a plot of beam interception vs solenoid current. The cathode is space charge limited although the beam current is slightly low because the cathode has been retracted to maximize beam transmission. Since the tube is oscillating, the rf fields can be expected to be large throughout the entire output section and rf defocusing might be worse than that anticipated in a stable tube at full drive. The beam transmission is better than 98% over a range of almost 4 A of solenoid current.

6.1.3 Serial Number 103 Test Results

SN 103 was built with lossy material sprayed on some of the coupling slots in order to avoid the electronic instability encountered in SN 102. In other respects it is essentially identical to its predecessor. The coupling slot loss was applied by spraying powdered iron through a mask which results in a film of iron powder 0.005 in. thick, in and around the coupling slot. This iron powder was sintered to the copper web to ensure good adhesion. Figure 6-24 illustrates how the lossy material is applied to the coupling slots. Figure 6-25 shows the insertion loss of an eight cavity test circuit before and after the application of slot loss to five of the seven cavity slots. The end slots have been left uncoated to facilitate matching the

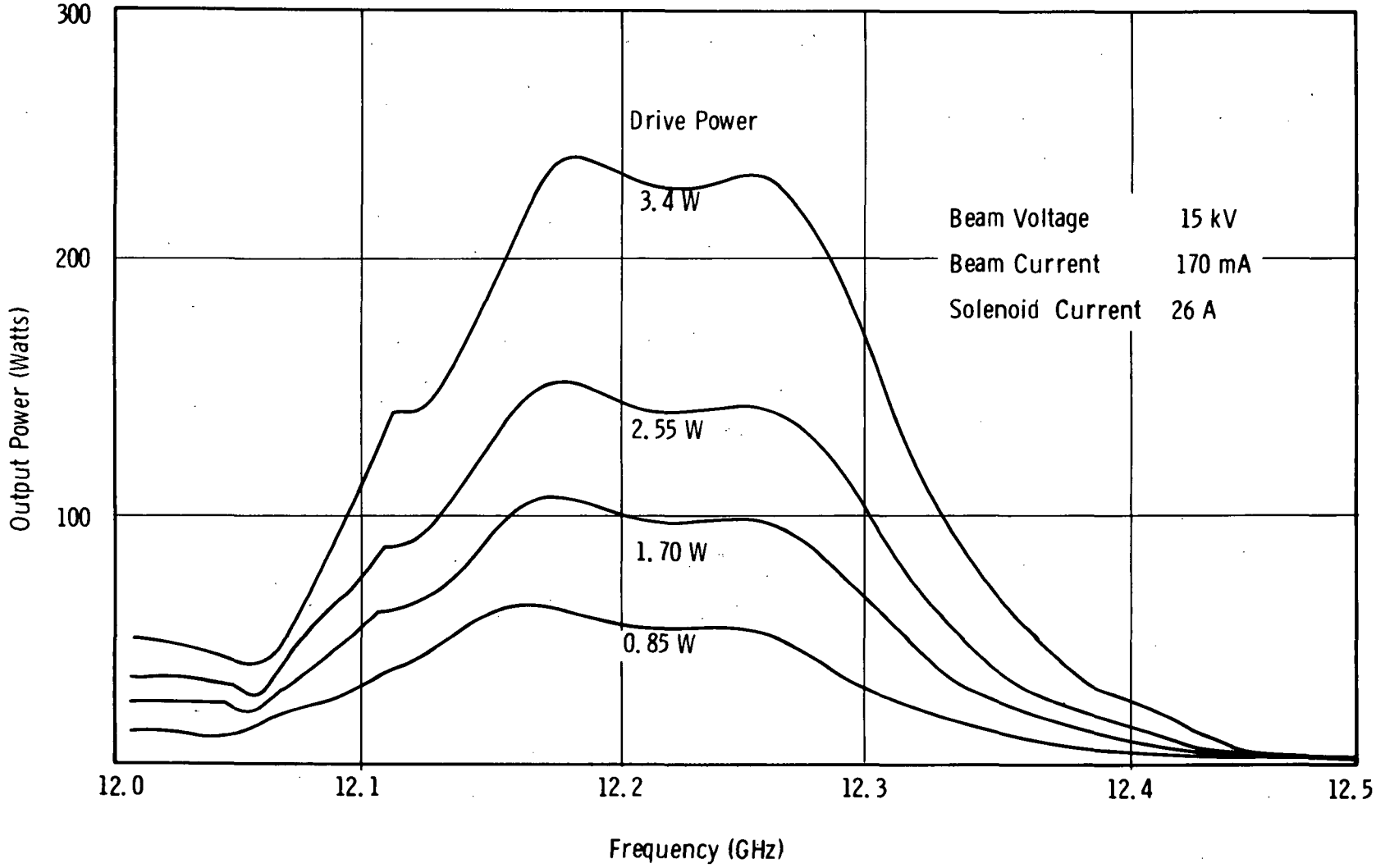

Figure 6-21. Power Output vs Frequency with Drive Power as a Parameter

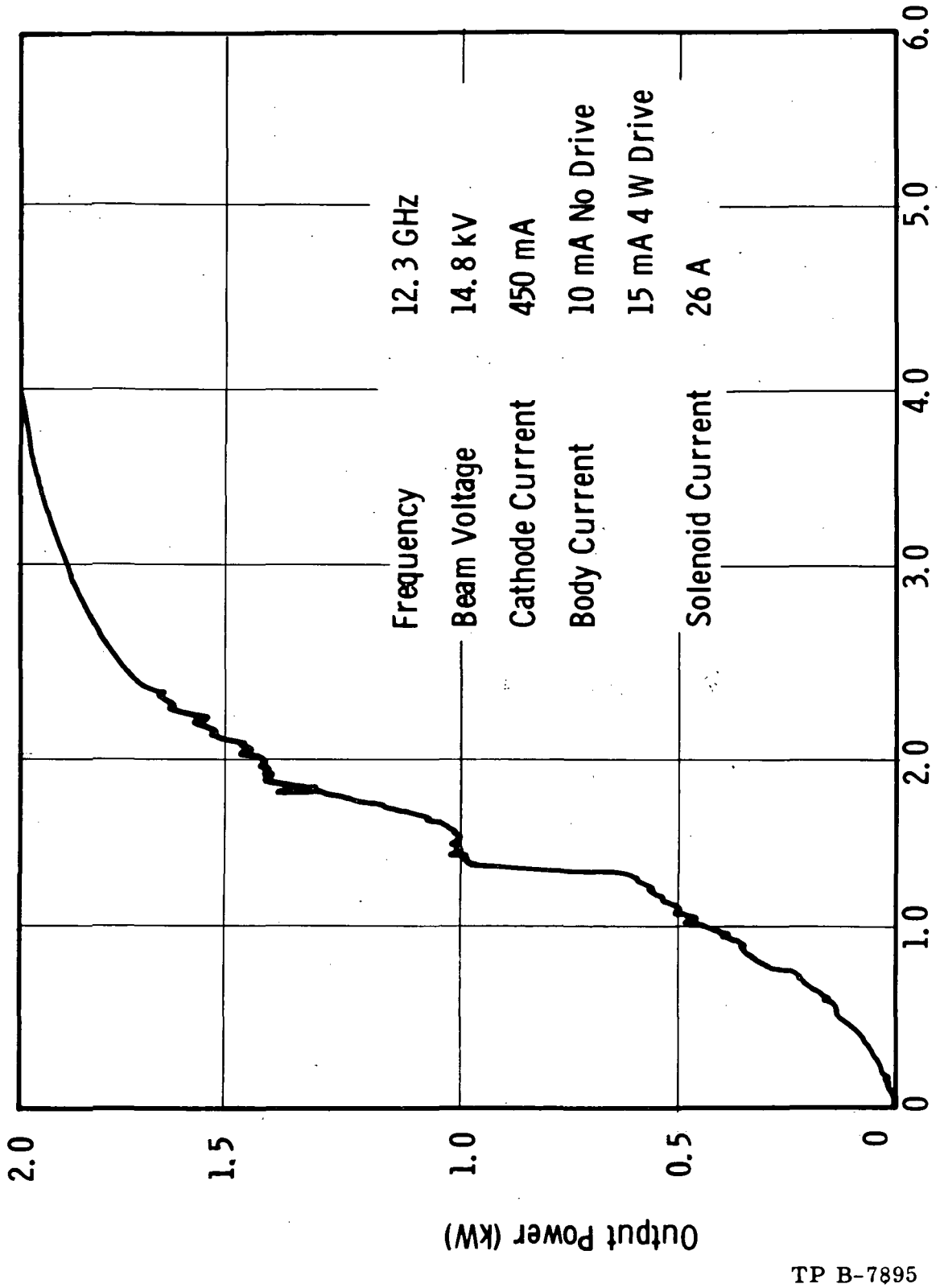

Figure 6-22. Power Output vs Drive

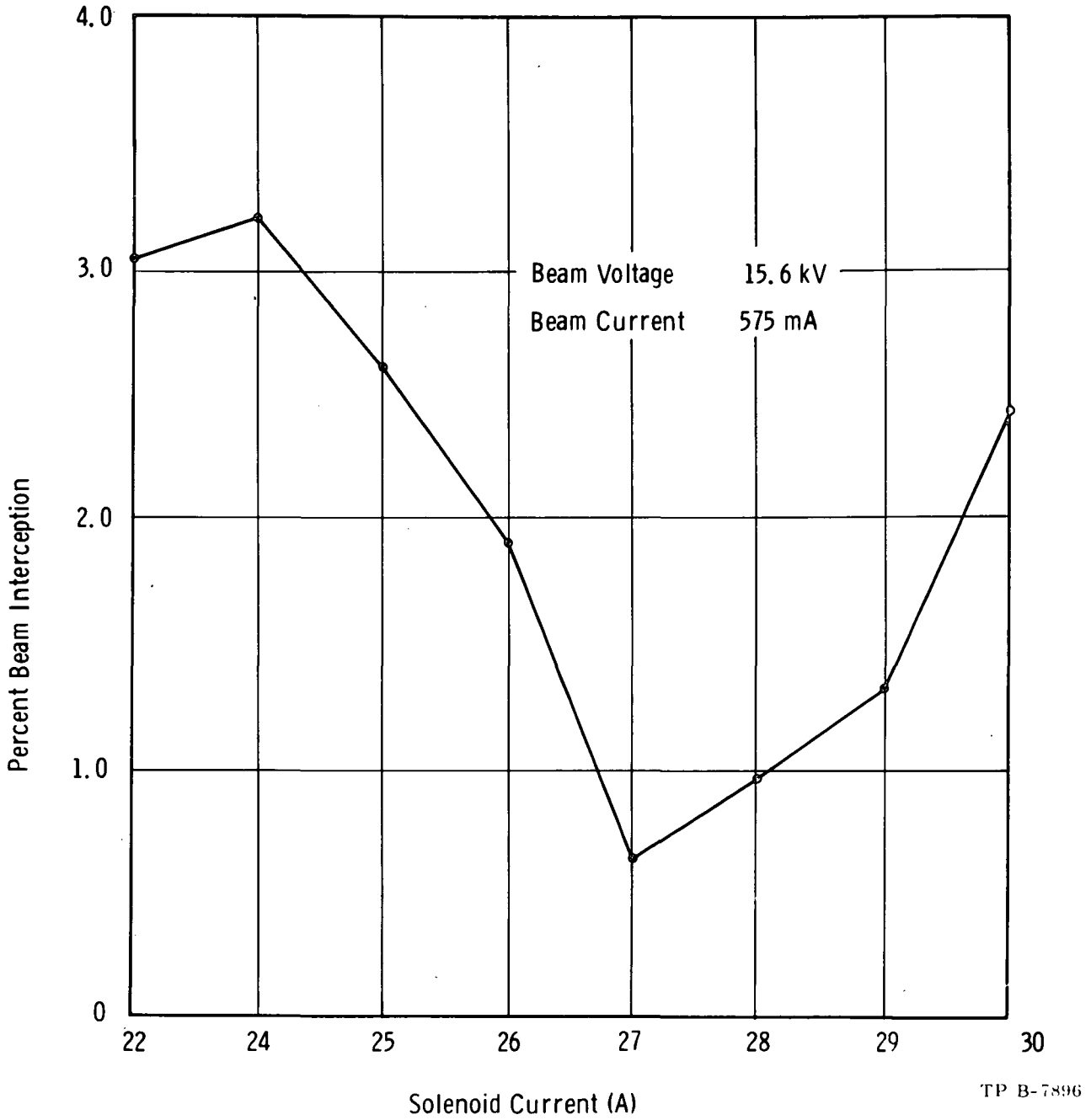

Figure 6-23. Beam Transmission as a Function of Solenoid Current

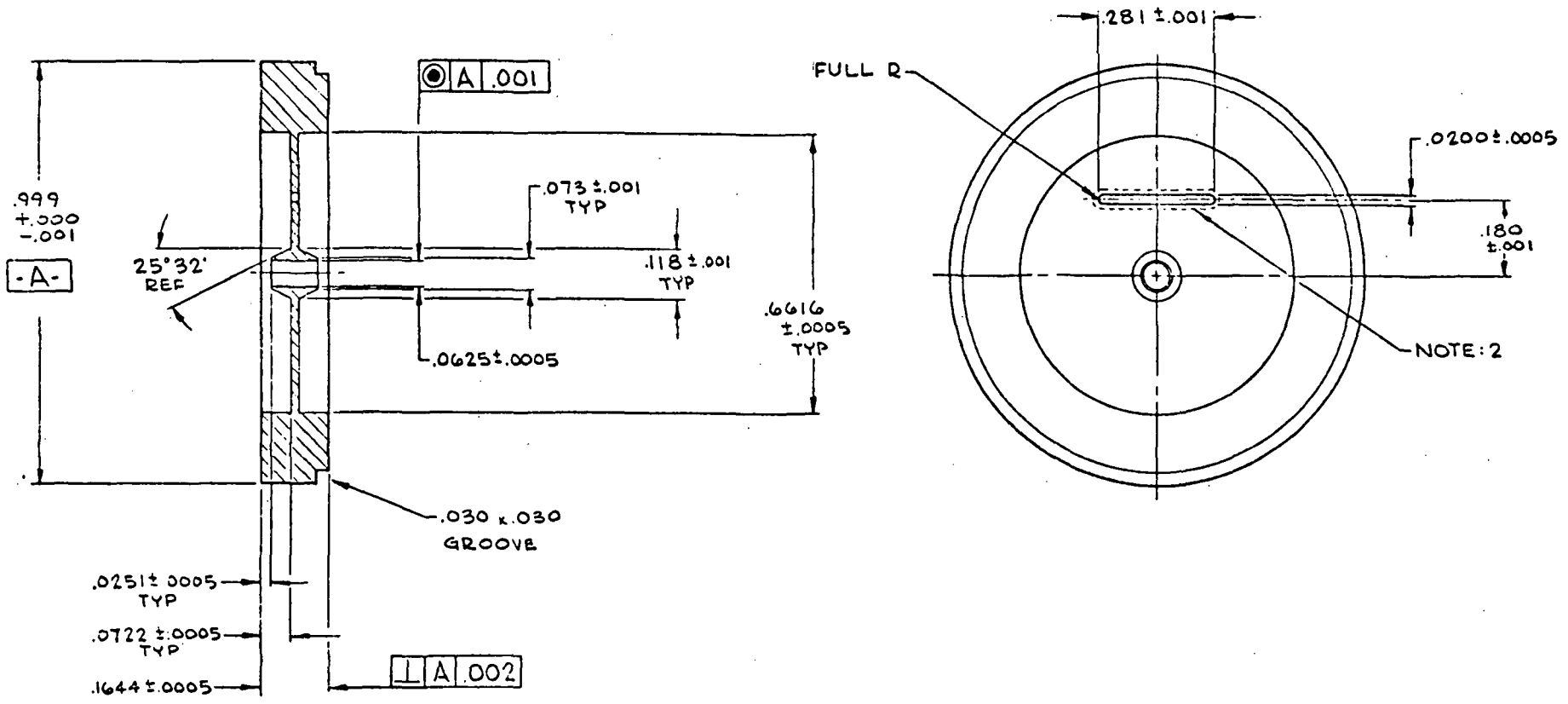

Figure 6-24. Diagram Showing Loss Pattern on Coupling Slots

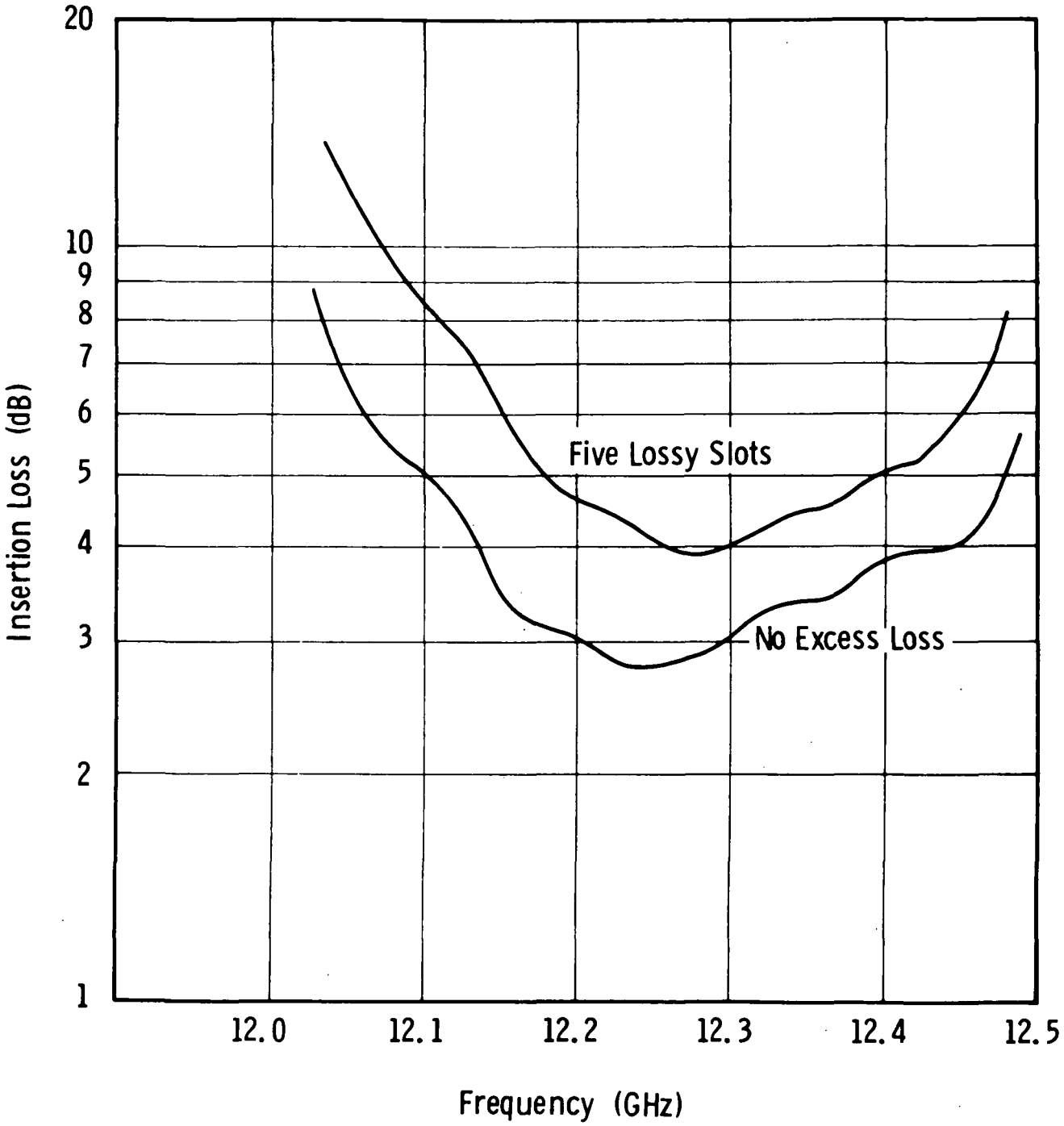

Figure 6-25. Measured Insertion Loss of Eight-Cavity Test Circuit

test circuit. The midband insertion loss can be seen to have increased by approximately 1.5 dB or 0.3 dB per coated slot. The uncoated circuit exhibits a midband insertion loss of approximately 0.35 dB per cavity. The eight cavity output circuit of the tube is designed with four lossy slots in order to minimize slot mode instability. The output cavities are left lossless in order to maintain high efficiency.

The measured output rf match is shown in Figure 6-26. The perturbation of the cavity parameters due to the lossy slots has degraded the match near the band edges. The match over the operating band is better than 1.5:1 and should be adequate to demonstrate the performance of the tube.

Pulse tests on SN 103 at 1% duty showed the tube to be electronically stable at beam voltages between 11 and 16 kV. This compares with SN 102 which was stable only between 14.2 and 15.2 kV. In both tubes band edge oscillations were detected below the stability range and slot mode oscillations were encountered above the stability range. SN 103 exhibited the increased stability which the additional slot loss was intended to provide. The tube was operated at rated beam current and beam voltage with zero to saturated drive across the entire cold passband without instability.

Figure 6-27 shows output power versus frequency at indicated drive levels with beam voltage of 15.6 kV and beam current of 630 mA. The slightly higher than nominal beam voltage was chosen to achieve band centering at 12.2 GHz. These are pulsed measurements at 1% duty. The measured maximum peak beam interception at full drive was 10 mA.

The measured small signal gain is lower than anticipated. Other measurements at 15.2 kV and at 15.0 kV show a small signal gain very nearly equal to that measured at 15.6 kV; i.e., approximately 33 dB at 12.2 GHz. Figure 6-28 shows the small signal gain and the large gain versus frequency with the tube operated at 15.2 kV at 2% duty. The results at this beam voltage are not significantly different from those taken at 15.6 kV. The midband small signal gain is approximately 33 dB and the large signal gain is 26 to 27 dB. The measured maximum power was 1.9 kW which corresponds to a conversion efficiency of 20%.

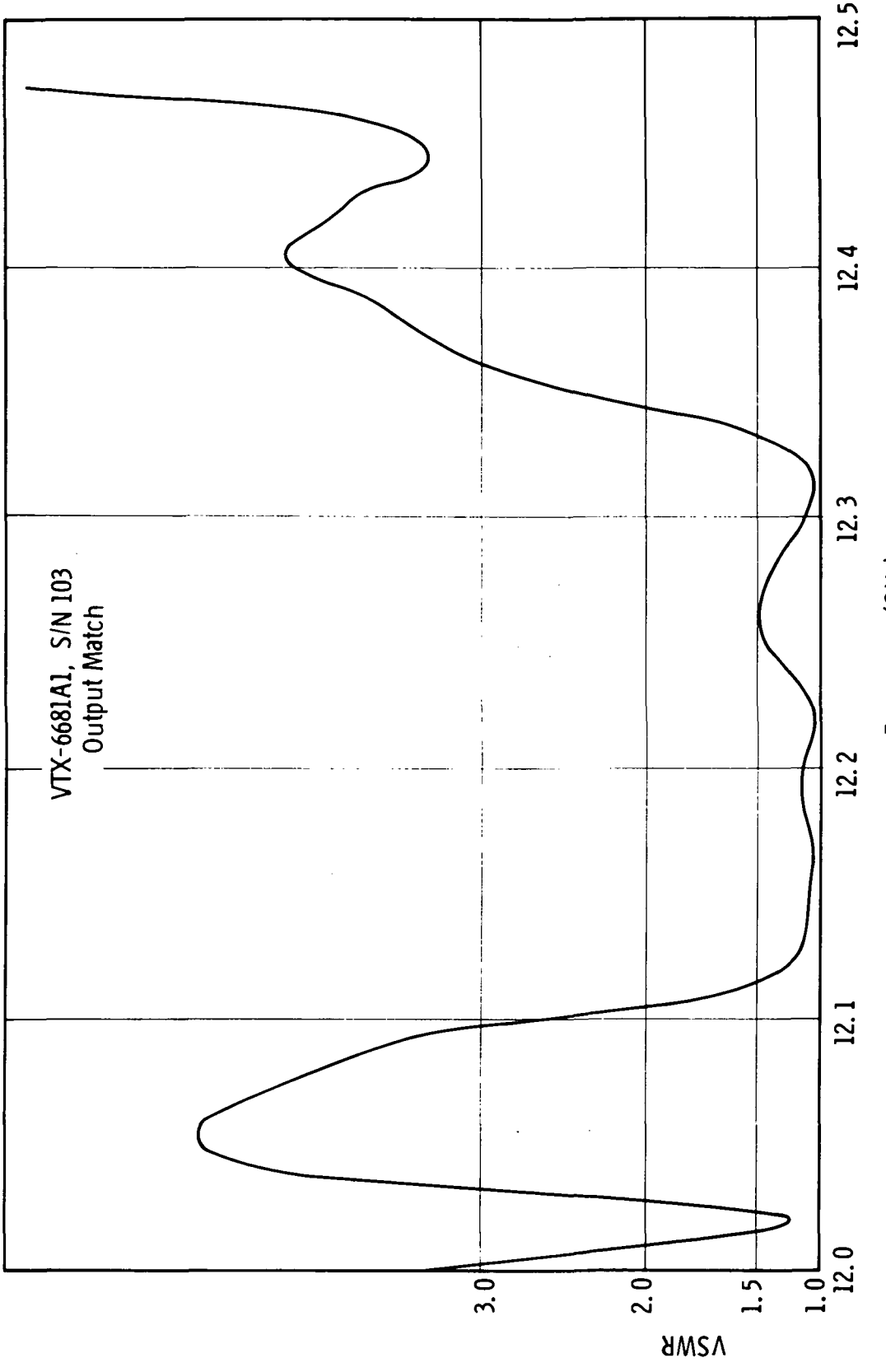

TP L-7947

Figure 6-26. Rf Match at Output of Tube Before Hot Test

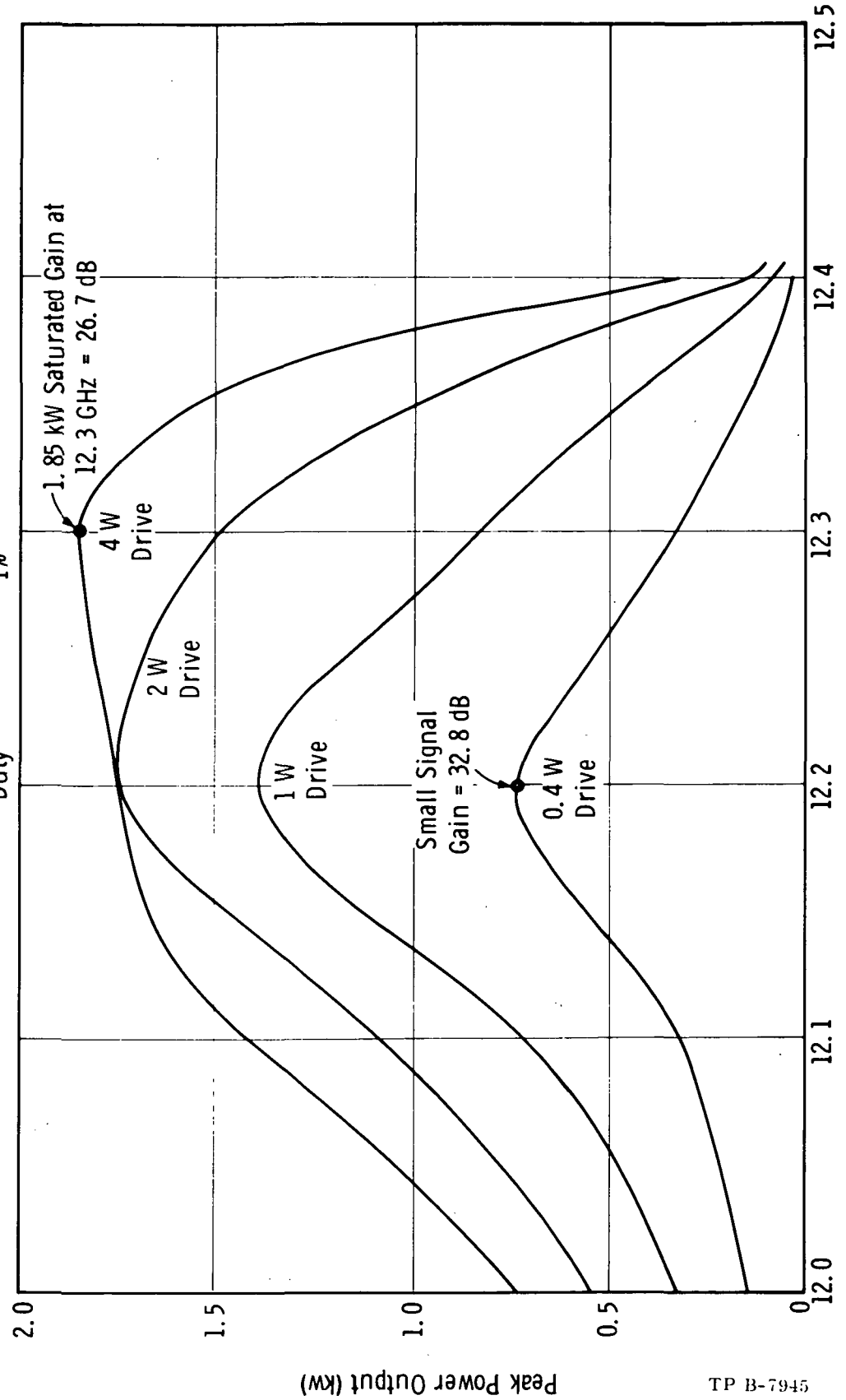

Figure 6-27. Power Output vs Frequency with Rf Drive as a Parameter

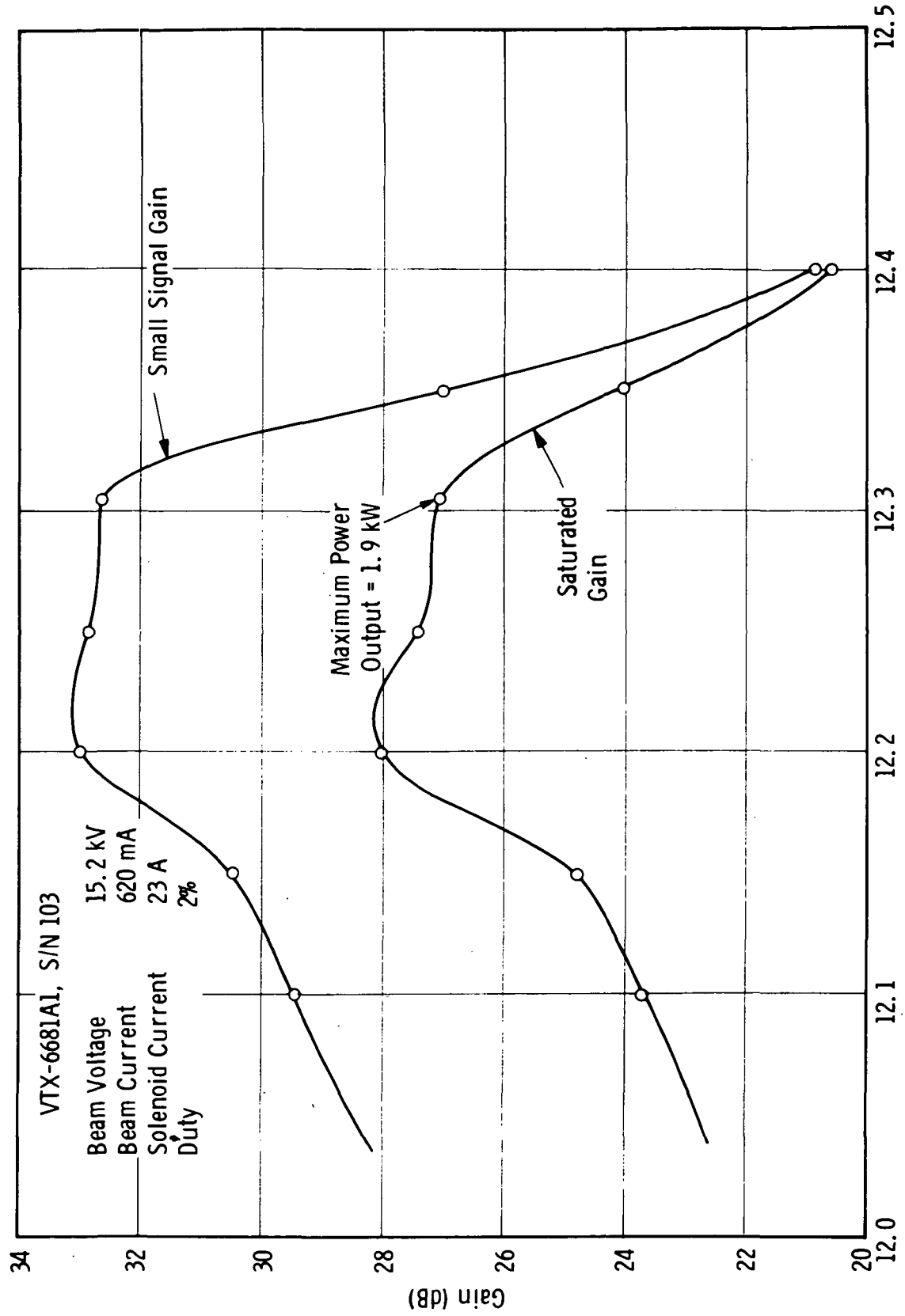

Figure 6-28. Small Signal Gain and Large Signal Gain vs Frequency

Figure 6-29 shows the rf match looking into the output of the tube. The excellent midband match deteriorates abruptly at both ends of the passband giving almost the appearance of a passband within a passband. A similar difficulty in obtaining a good rf match over the entire cold passband was recently encountered in the development of a 10 kW, X-band coupled-cavity traveling wave tube at Varian. The difficulty was found to be the result of a failure to achieve sufficient accuracy in cutting coupling slots; i.e., there was a slight random distribution of coupling slot lengths. The tube was redesigned with slightly increased cold bandwidth (initial tests having shown insufficient hot bandwidth) particular care being taken to achieve uniformity of coupling slot length. The resultant tube exhibited 5 dB greater small signal gain than its predecessor, although it would otherwise have been expected to lose approximately 2 dB in small signal gain, because of the increase in bandwidth.

The degree to which the slot tolerance problem may have affected the performance of the third experimental tube is not known. The fact that SN 103 has much narrower bandwidth than the tube described earlier would tend to make it less tolerant of circuit imperfections. Spraying some of the slots with iron powder, as was done, would tend to aggravate the problem.

Cw testing of the third experimental tube was undertaken to verify the pulsed tests and to investigate thermal stability. Beam interception versus beam voltage at constant solenoid current is shown in Figure 6-30. Beam interception at 15 kV without drive is approximately equal to that measured under full drive during pulse testing. At 13 kV the tube was found to oscillate at the band edge, whereas under pulse testing, band edge oscillation started below 11 kV. With power output displayed on the oscilloscope and drive swept across the 12.0 to 12.5 GHz band, the beam voltage and magnet current were adjusted for optimum performances. Initially, the power output curve closely resembled that measured during the pulse tests. Within 15 minutes the oscilloscope trace showed three power peaks whereas formerly there had been only one. Soon thereafter, the power output trace exhibited an abrupt discontinuity which was associated with drive-induced oscillation. Hot testing was discontinued pending analysis of the cause of the deteriorating performance.

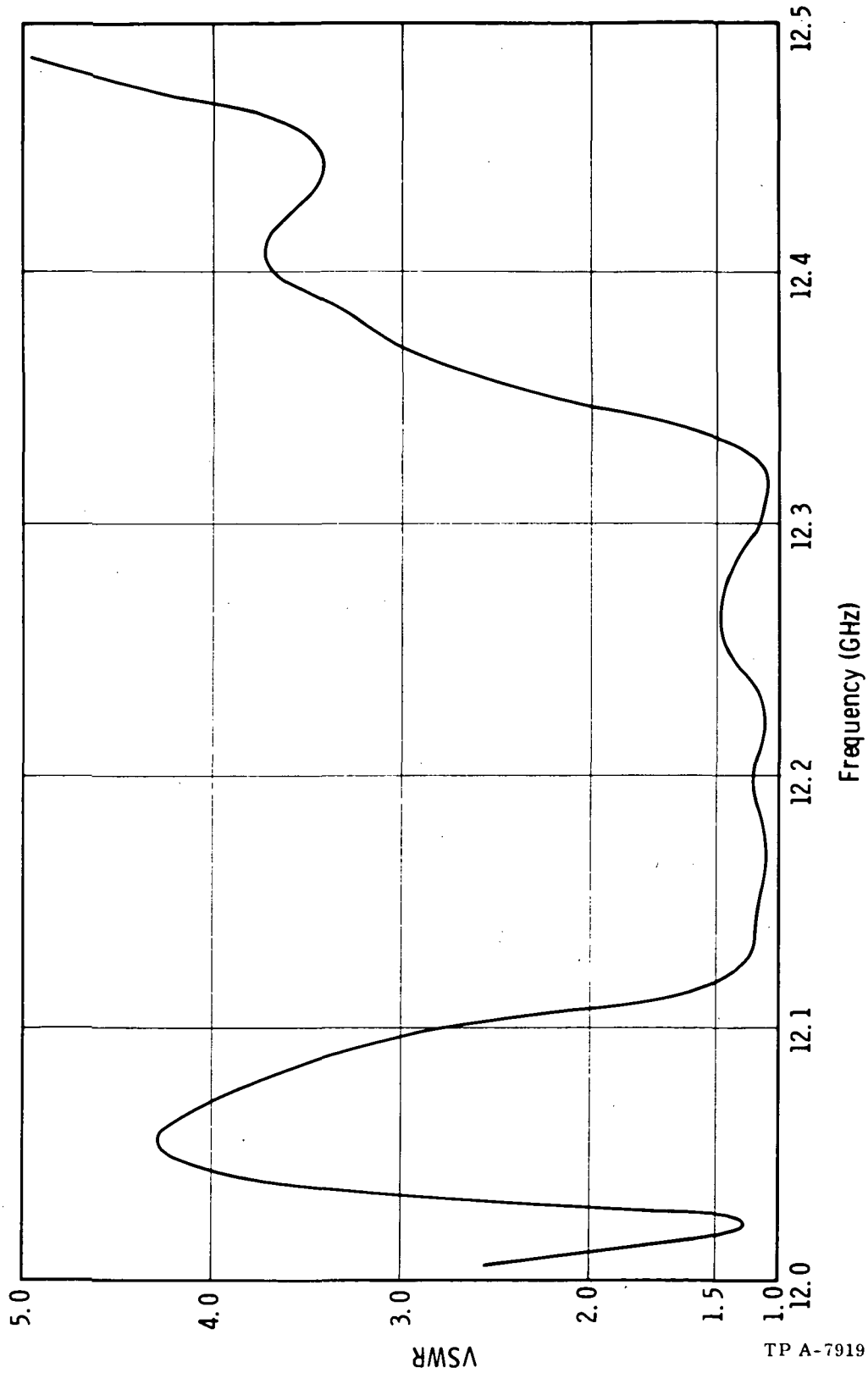

Figure 6-29. Rf Output Match of Third Experimental Tube

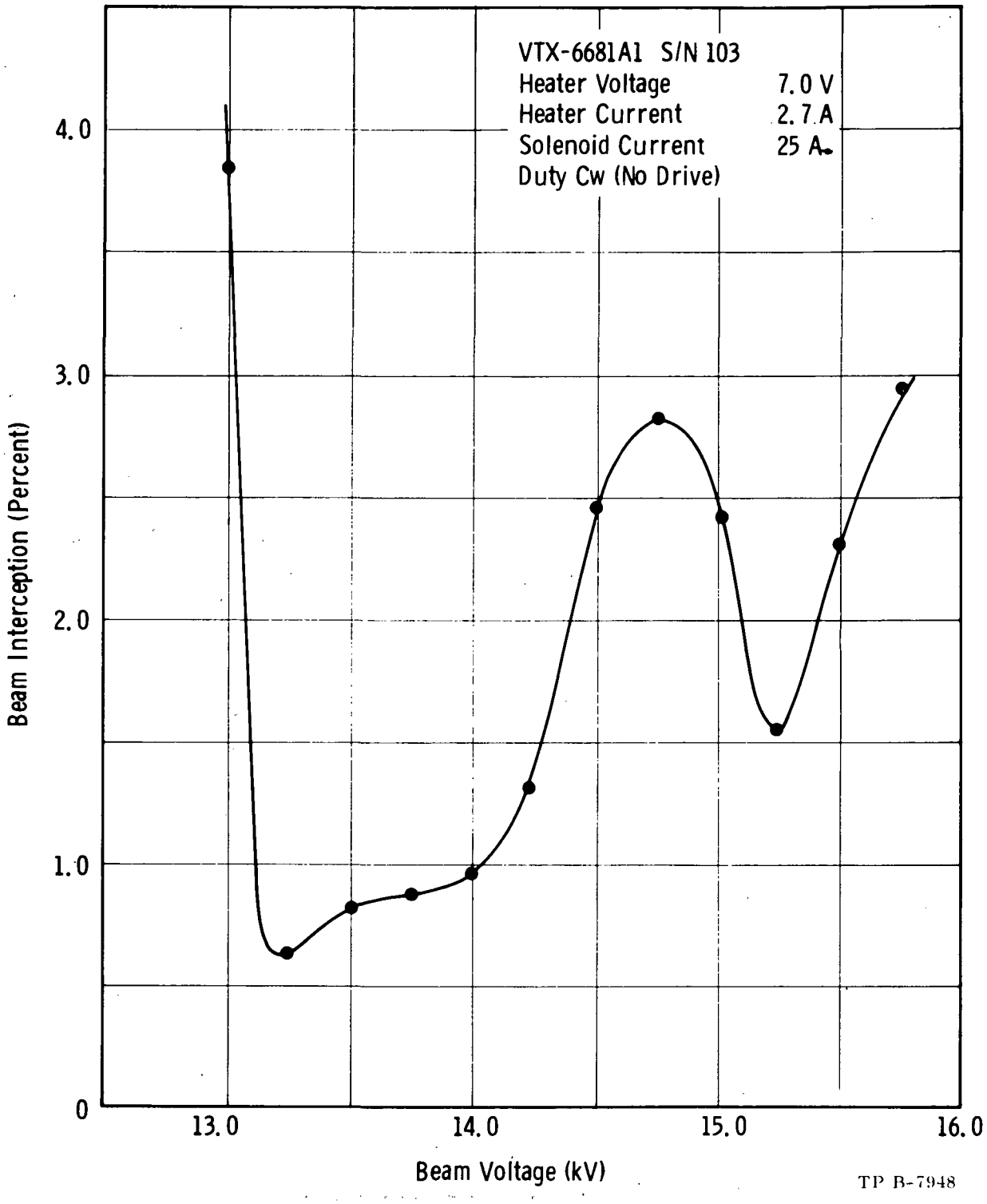

Figure 6-30. Beam Interception vs Beam Voltage

Figure 6-31 shows the rf match of the output of the tube after cw test. The match had deteriorated to such an extent that further hot testing could not be expected to give interpretable results. The collector was removed in order to investigate what had happened to the output circuit to cause the noted change in rf match. By inserting a mandrel in the drift tubes it was determined that drift tube melting had probably not occurred. Feeler gauges were inserted to determine whether the gap spacings had changed. It was found, surprisingly, that the first two gaps, counting from the output, had changed less than 0.001 in. relative to their original spacing of 0.050 in.; the third and fourth gaps had become 0.002 to 0.003 in. shorter, and the fifth gap approximately 0.005 in. longer. The warpage of cavity walls near the middle of the output section of the circuit would not result from rf defocusing of the beam in a nonoscillating tube. Even in an oscillating tube, the beam confinement provided in the present design should be sufficient to prevent rf defocusing effects in the middle of the output section. It must be concluded that imperfect alignment of the solenoid magnetic field relative to the axis of the circuit has produced a marginal focusing condition in which the beam comes very close to the circuit at the middle of the output circuit section. Therefore a relatively small rf perturbation of the beam was sufficient to cause interception which thermally overstressed the cavity wall.

Experimental tests have established four problem areas in the design of a high efficiency, high power narrow bandwidth coupled-cavity traveling wave tube:

1. Thermal stability
2. Electronic stability
3. Beam focusing
4. Circuit uniformity

1. The resolution of the thermal stability problem will require an increase in the thickness of the cavity web. Thickening the web will decrease the thermal gradient, at the same time increasing its mechanical strength. For fixed power flow the radial compressive force in a disc is independent of thickness since the pressure decreases because of the reduction in

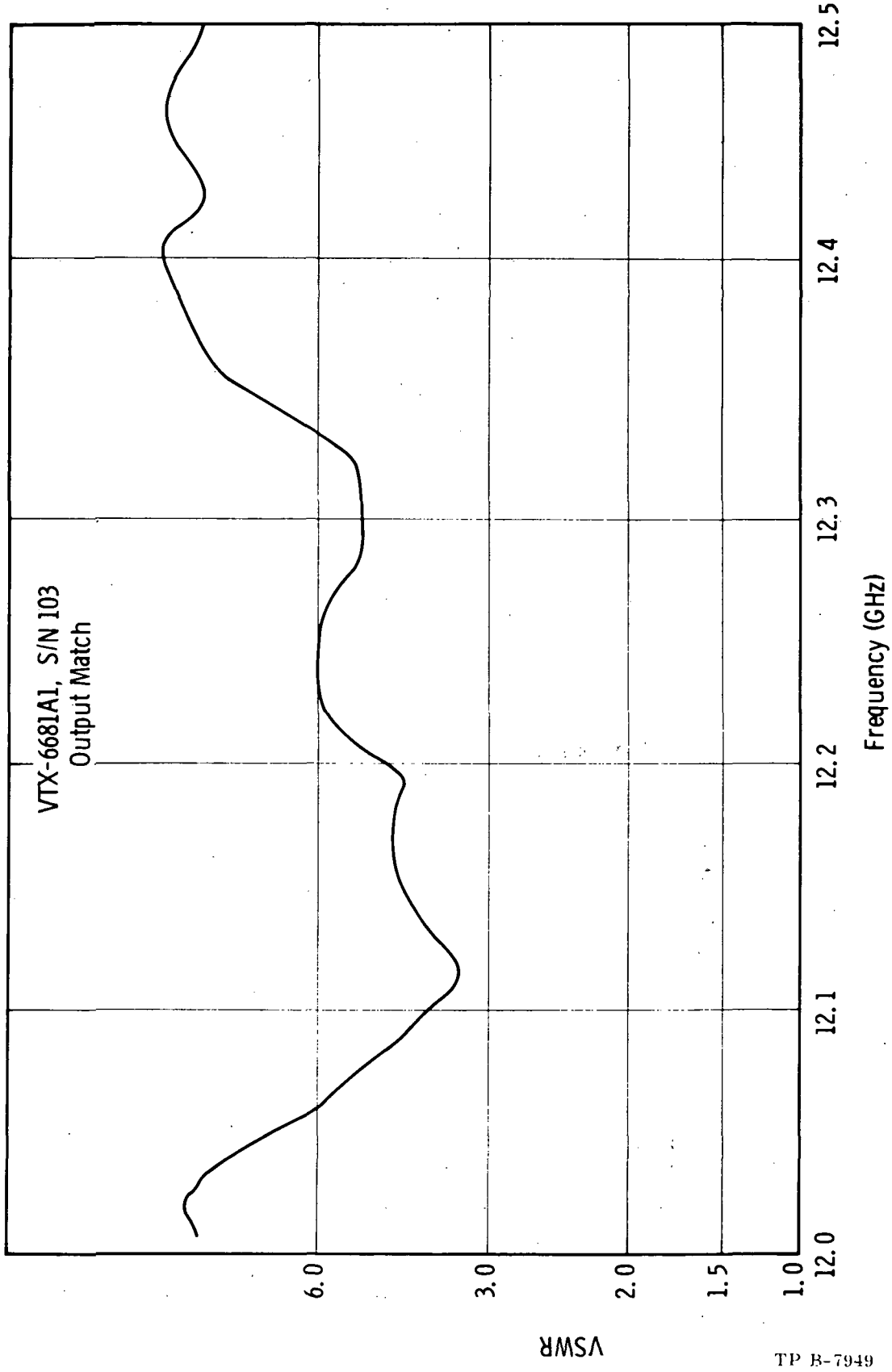

Figure 6-31. Rf Match at Output of Tube After Hot Test

thermal gradient at the same rate as the area increases. The deformation of a disc under fixed loading varies inversely as the cube of the thickness. Hence by doubling the thickness it should be possible to reduce deformation by a factor of eight.

2. Electrical stability can be maintained by providing adequate rf matching and by loading the circuit to reduce gain in the higher modes. Increased thermal stability will help maintain adequate rf matching during thermal cycling. Careful control of tolerances will be required to obtain the requisite circuit uniformity.

3. The present electron gun and beam focusing design is fundamentally sound. It will be necessary to maintain high enough beam transmission to guarantee satisfactory operation.

4. The effective beam coupling impedance is degraded by circuit nonuniformity. A painstaking effort must be made not only to achieve the best obtainable accuracy on the individual machined parts, but also to ensure that the parts are assembled with sufficient care to obtain the best possible overall circuit uniformity.

6.1.4 Serial Number 104 Test Results

In order to achieve thermal stability the two final tubes, SN 104 and SN 105 were designed with a cavity web thickness of 0.040 in. The estimated thermal capacity of the 0.040 in. web is between 50 and 100 W.

It was found that by electroplating the cavity walls with a 0.0001 in. film of iron, a cavity Q of 200 could be achieved, corresponding to a midband insertion loss of 1.3 dB/cavity. The use of iron plating would eliminate the dimensional tolerance problems encountered in SN 103, which employed a relatively thick film of powdered

iron, the thickness of which was difficult to accurately control. The uniformity of the iron plating should improve the rf match to the circuit thereby increasing electronic stability. The new circuit employs coupling slots of higher resonant frequency thereby reducing the probability of slot mode instability. The drift tube diameter has been increased from 0.0625 to 0.067 in. to improve beam transmission.

Cold test work for the final design was done on a 5X scale model of the circuit. The cold passband of this circuit extends from 2.416 to 2.498 GHz, a bandwidth of 3.3%. Figure 6-32 shows the rf match looking into the terminated circuit. The worst match inside the band occurs at 2.475 where the VSWR reaches 1.3:1. Figure 6-33 shows the measured interaction impedance on the cold test circuit. The impedance is approximately 90% of that measured on the circuits with 0.020 in. webs.

Figure 6-34 shows the cavity and coupling slot configuration for SN 104. The measured Brillouin Diagram is shown in Figure 6-35.

The two-cavity taper employed in SN 104 and SN 105 is illustrated in Figure 6-36. Due to the increased web thickness it was not possible to obtain as much circuit velocity reduction as was obtained in the thin web case. The two step taper used has velocity reduction ratios of 0.90 and 0.78.

Small signal calculations show that a nine-cavity output section with five lossy cavities and four lossless cavities will provide adequate gain to ensure efficient operation. In order to use the existing focusing solenoid, the fourth and fifth tubes will be two section tubes, employing eight cavities in the input section and nine cavities in the output section. Figure 6-37 shows the computed small signal gain. To demonstrate the required 40 dB gain it would be necessary to build a three-section tube employing a longer focusing solenoid. Some modification of the design would be required to bring the total gain variation within specification. The present design is intended to demonstrate a reliable high efficiency tube.

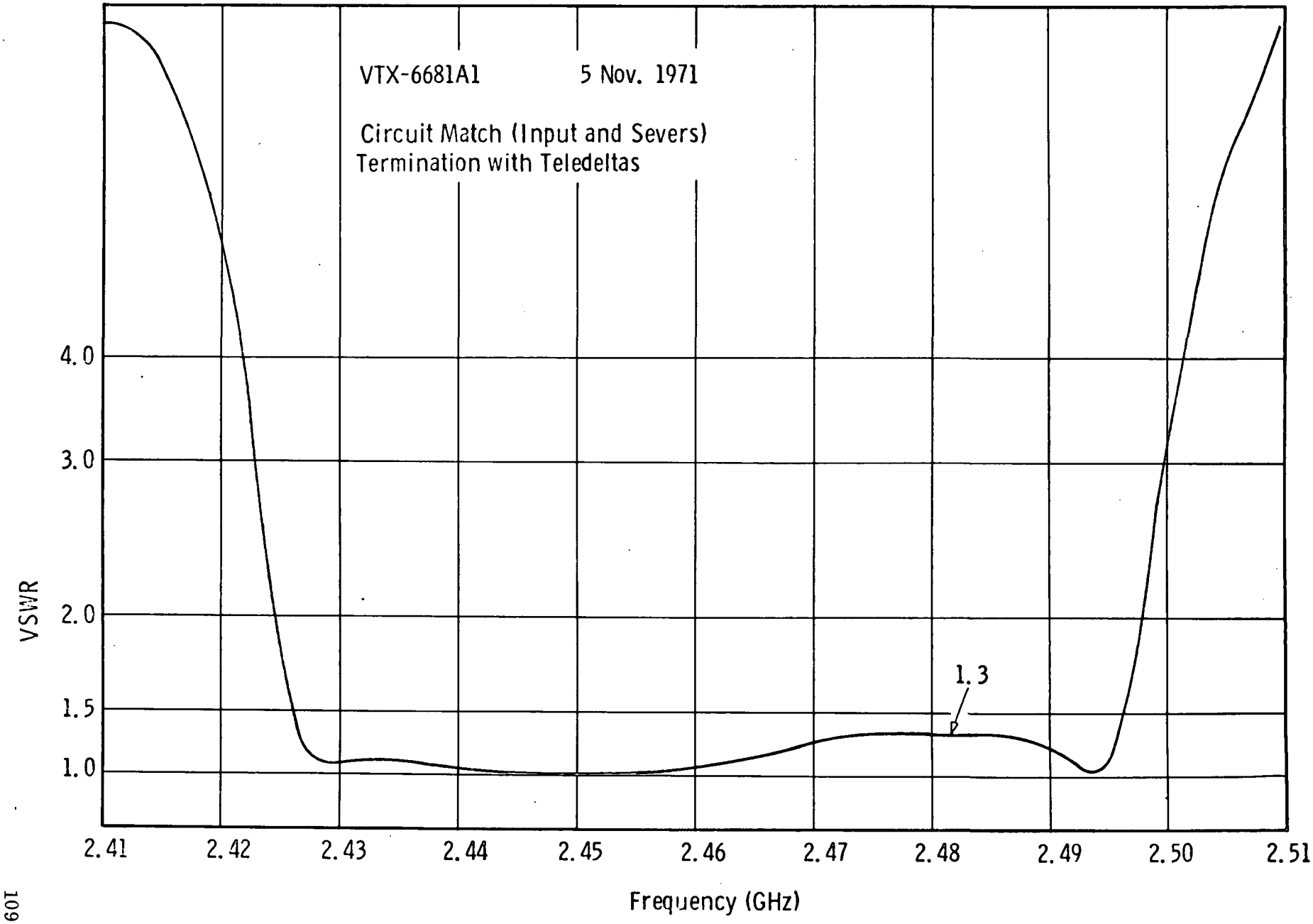

Figure 6-32. Rf Match Looking Into Terminated Cold Test Circuit

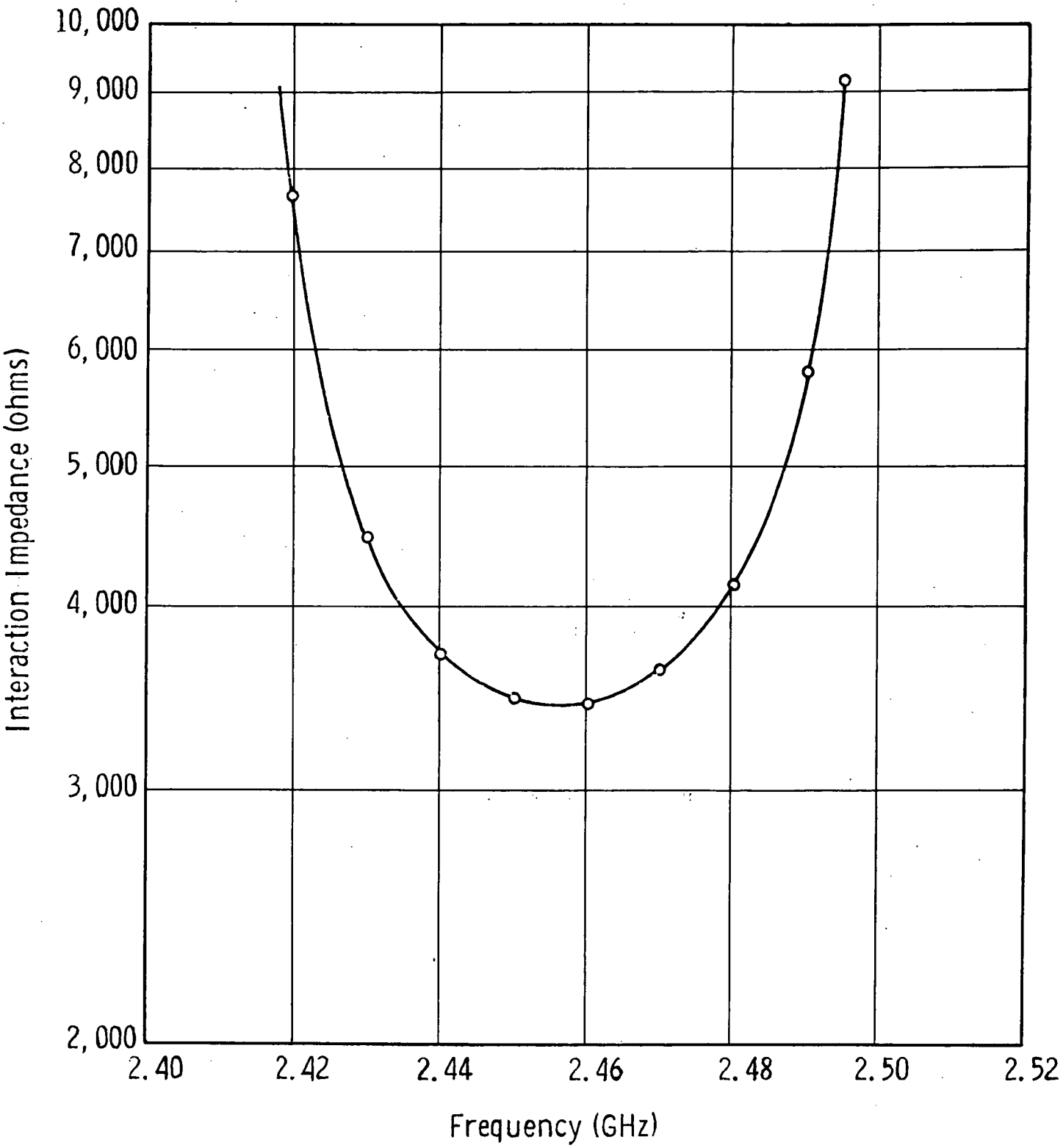

Figure 6-33. Measured Interaction Impedance of Scaled Cold Test Circuit

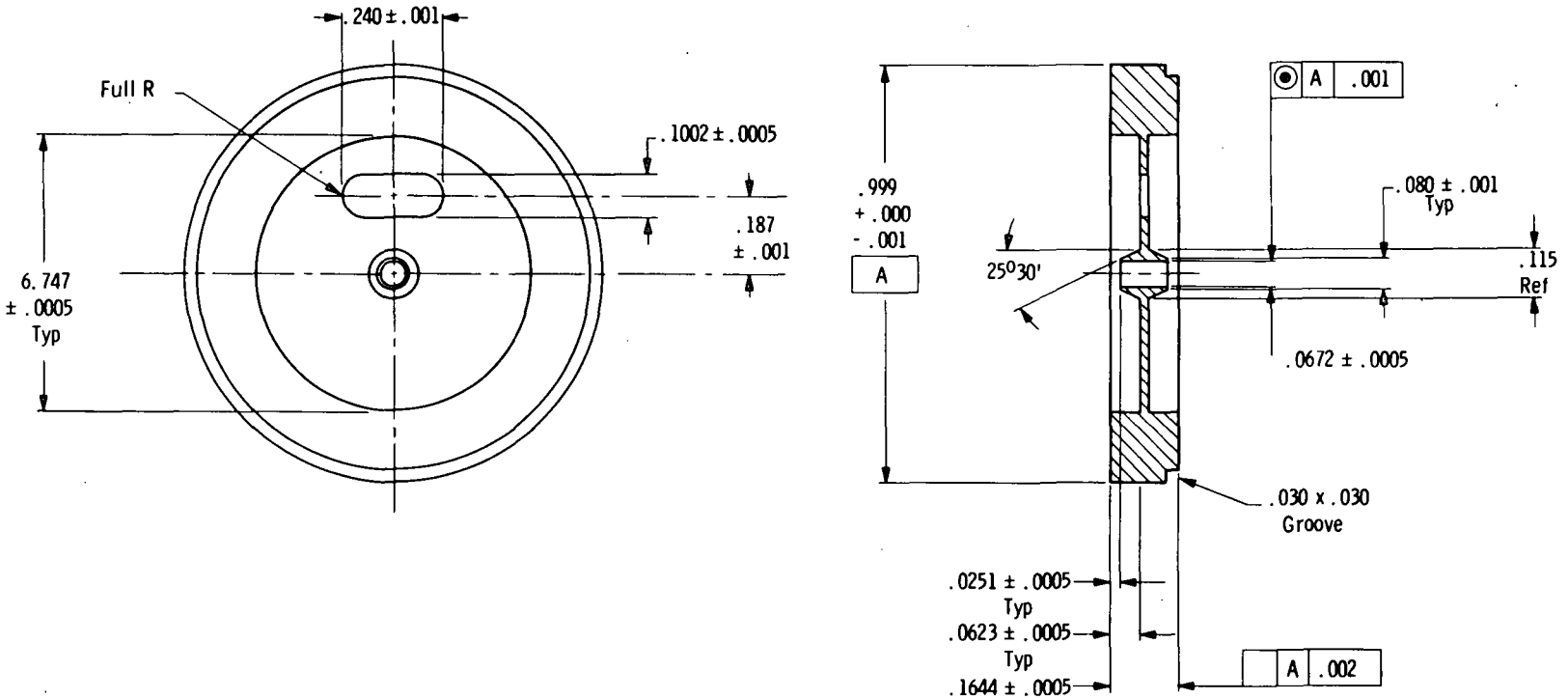

Figure 6-34. Cavity Web and Coupling Slot for VTX-6681A1, S.N. 104

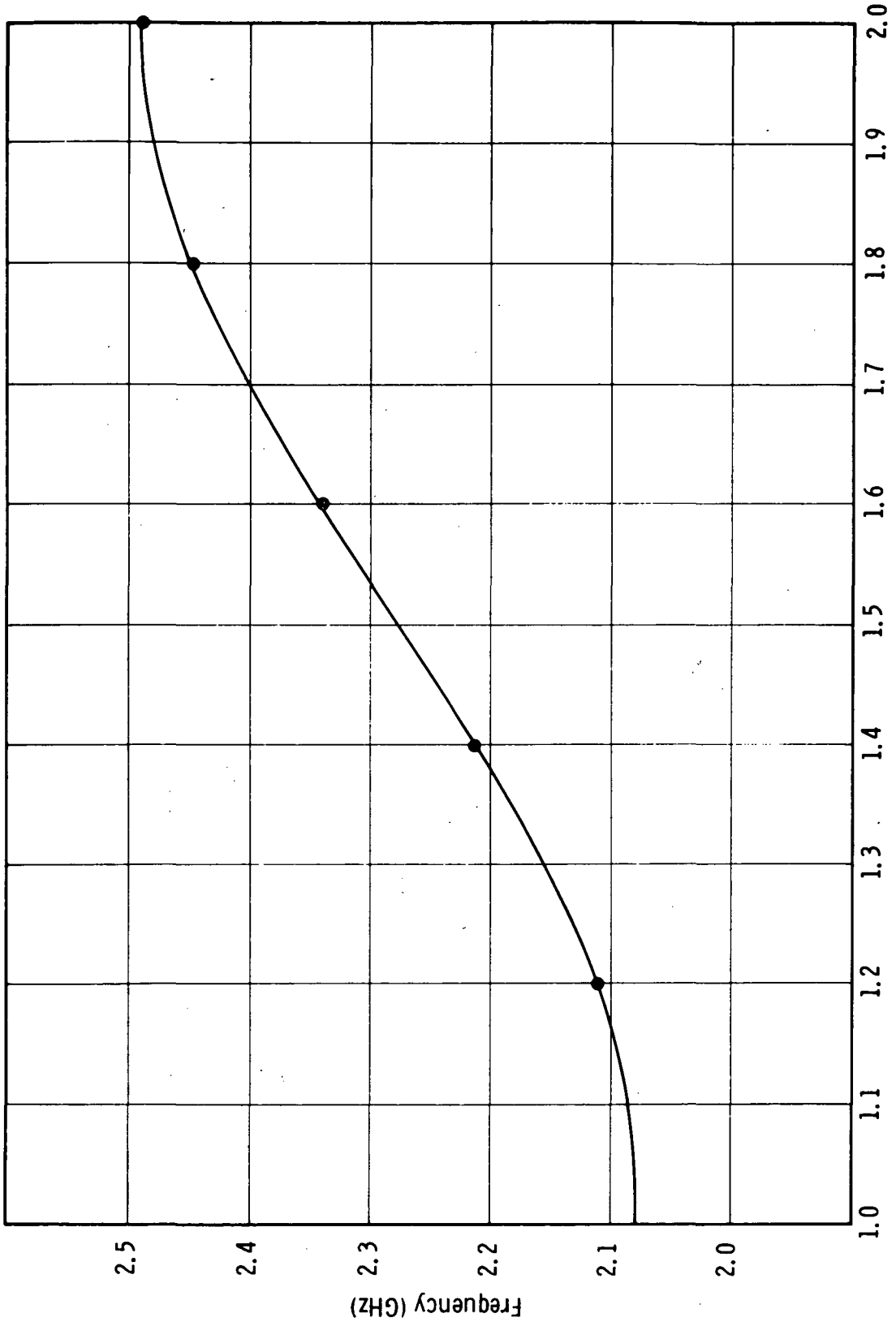

Figure 6-35. Brillouin Diagram for VTX-6681A1, S.N. 104

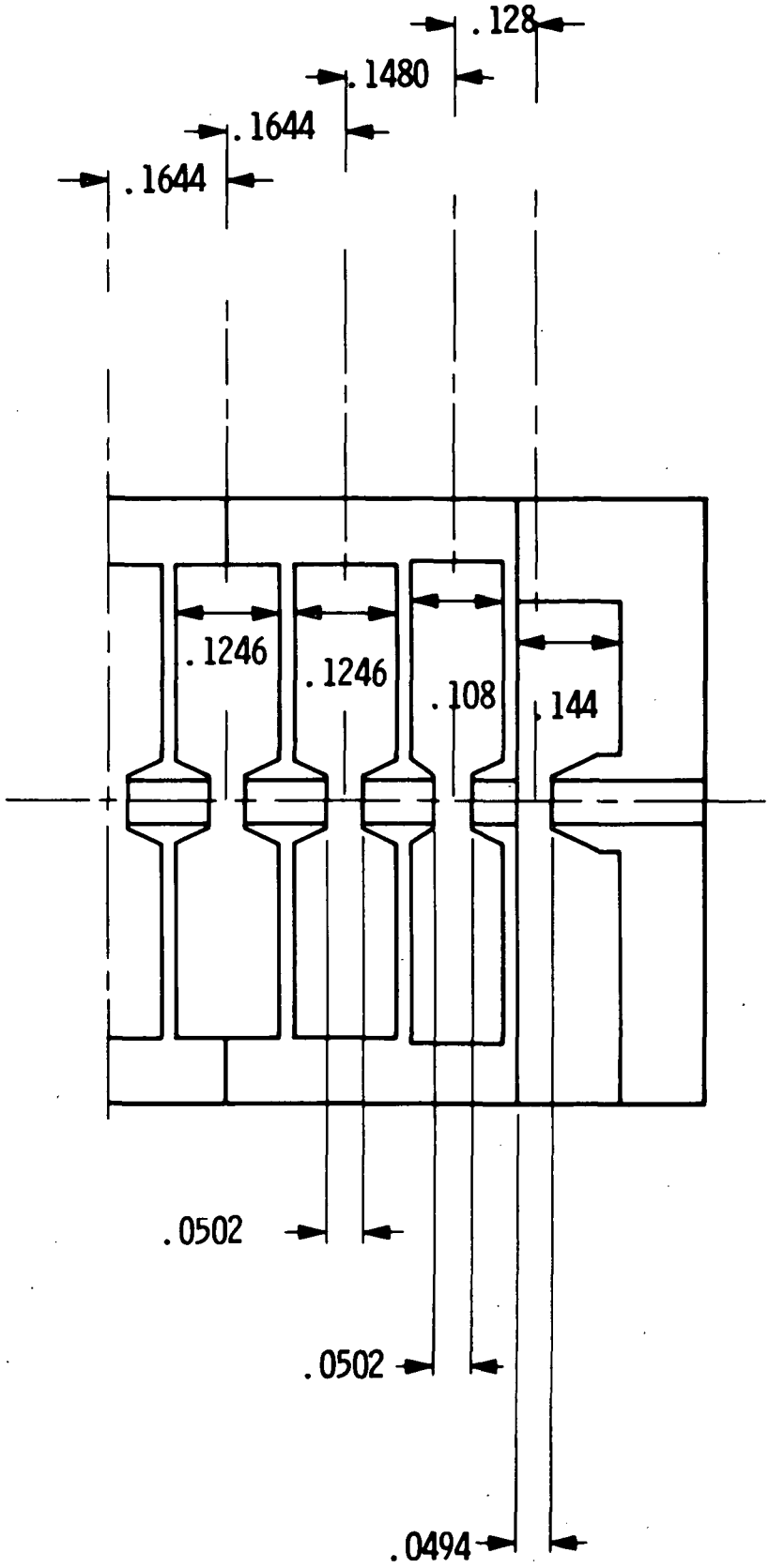

Figure 6-36. Schematic of Output Velocity Taper for VTX-6681A1 S.N. 104 and 105

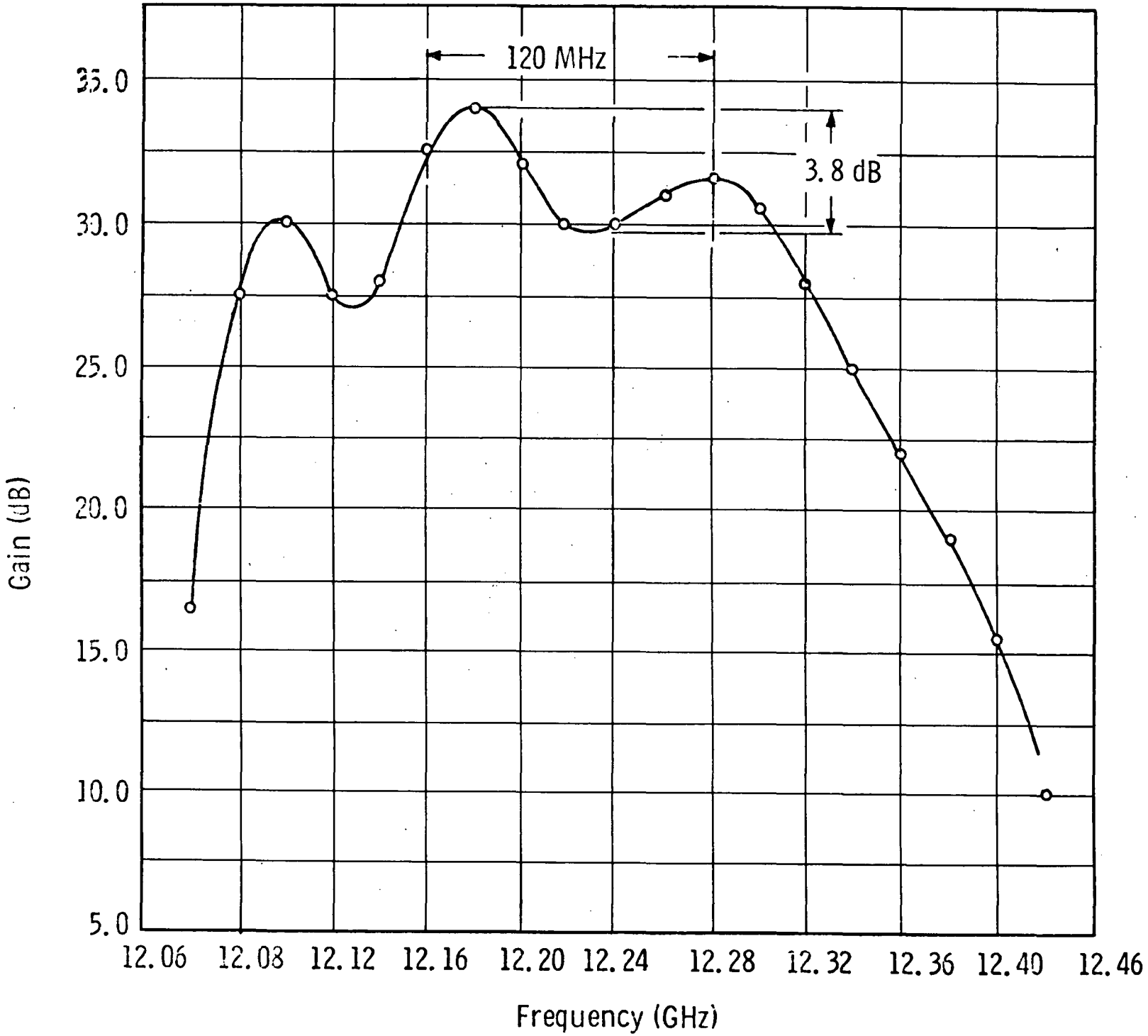

Figure 6-37. Computed Small Signal Gain for VTX-6681A1, S. N. 104

The computed start oscillation current for band edge oscillation is plotted in Figure 6-38. This design is predicted to be stable at all beam voltages above 10 kV.

The input and output rf matches for SN 104 were measured just prior to initial hot test. The results are shown in Figure 6-39.

Figure 6-40 shows the beam current as a function of beam voltage with heater voltage as a parameter. The beam perveance at a heater voltage of 6 V is 0.37 μperv which is somewhat higher than the design value of 0.33 μperv.

Under pulse testing at 1% duty the beam transmission was found to be very poor. Attempts were made to improve beam transmission by varying the position of the tube in the solenoid and by use of a bucking coil on the gun. These tests were not successful. Beam transmission was found to be very critical with respect to solenoid current adjustment. Figure 6-41 shows beam transmission as a function of solenoid current. Only by very careful adjustment of the solenoid current was it possible to obtain beam transmission better than 97%. It was concluded from these results, and the indicated higher than anticipated beam perveance, that the cathode to focus electrode spacing must have been less than it was intended to be.

During initial pulse testing the tube was found to be completely stable at all beam voltages above 10 kV.

Figure 6-42 shows peak power output vs frequency at four different drive levels. The measured maximum body current at each drive level is indicated. The frequency at which the body current peaks is dependent on drive level in an apparently random manner. The maximum body interception is 30 mA which is approximately 4% of the beam current.

The maximum conversion efficiency measured in these tests was 28%. Later cw tests show these results to be in error. A malfunction in the pulser was found after these tests had been completed which showed that under some conditions extra pulses were being generated.

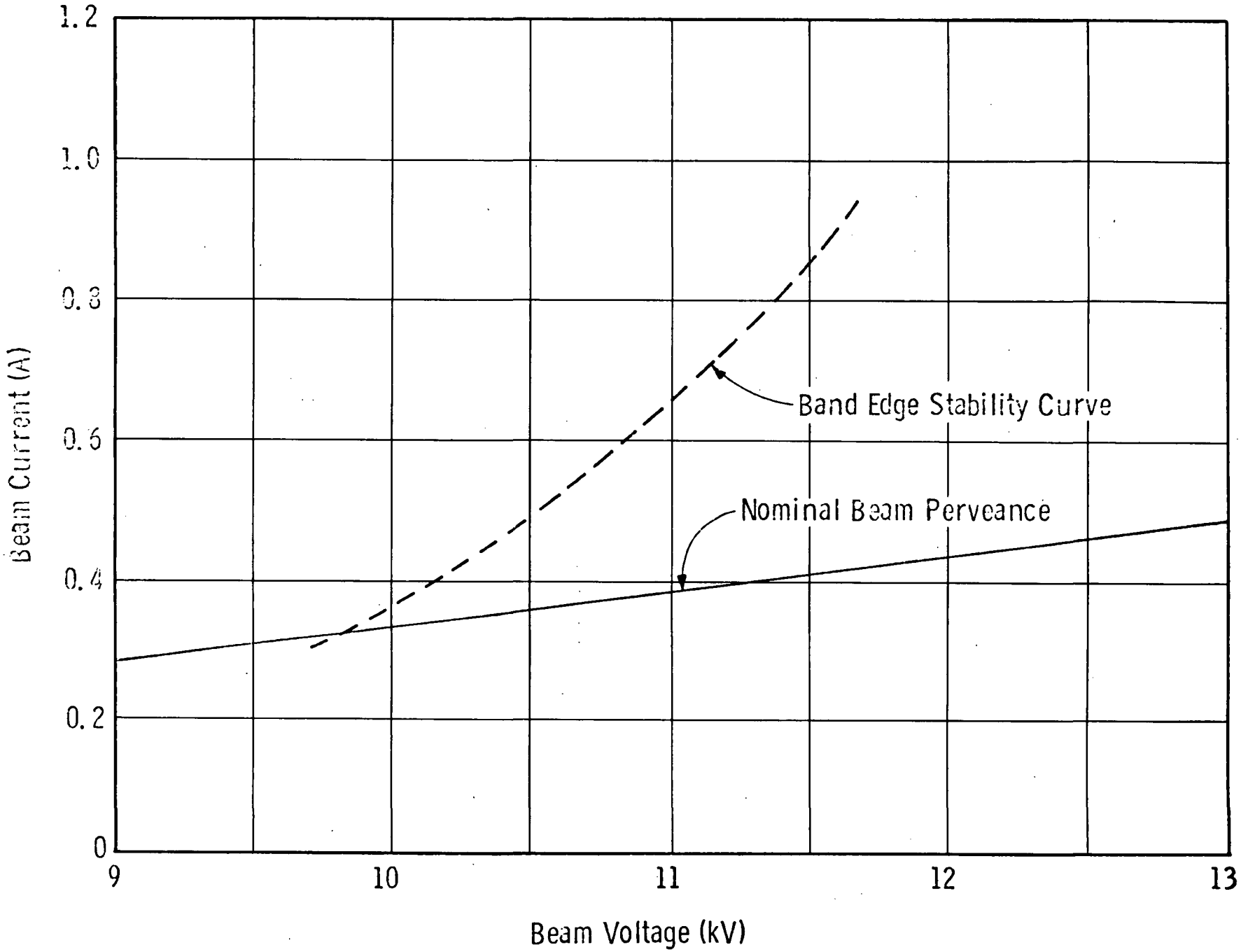

Figure 6-38. Computed Start Oscillation Current vs Beam Voltage for VTX-6681A1, S. N. 104

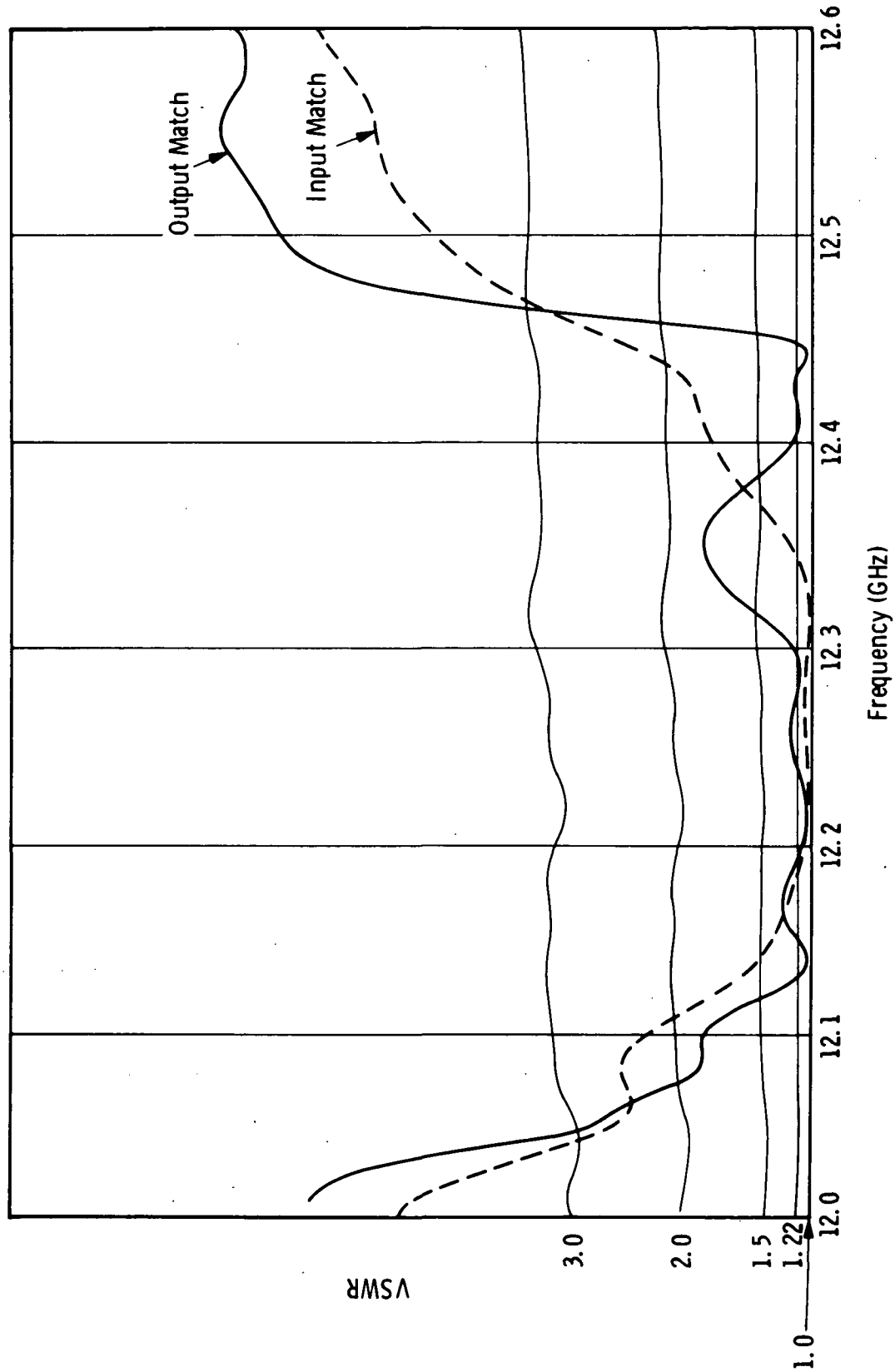

Figure 6-39. Measured Rf Matches at Input and Output of VTX-6681A1, S. N. 104

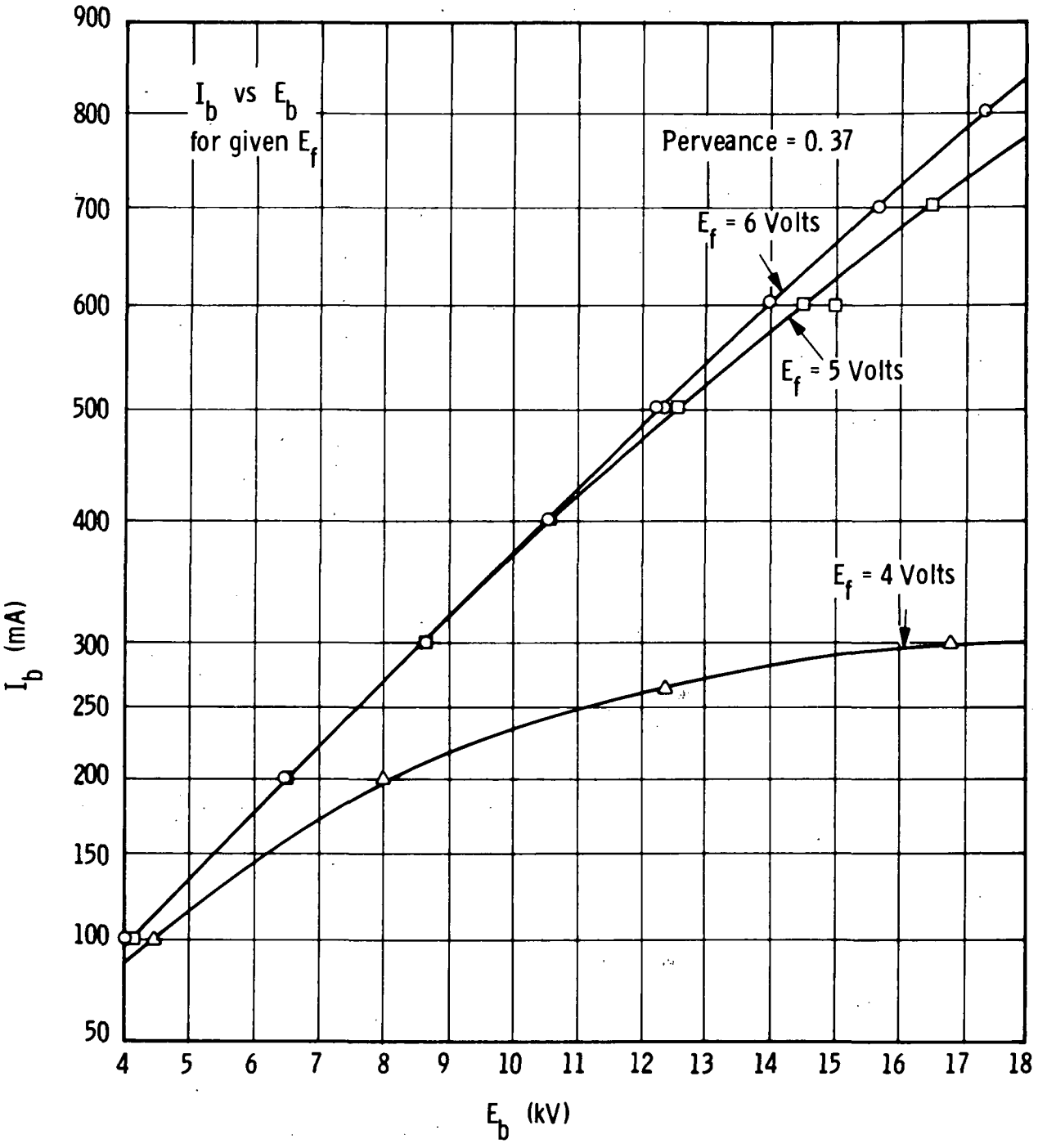

Figure 6-40. Measured Beam Current vs Beam Voltage with Heater Voltage as a Parameter for VTX-6681A1, S.N. 104

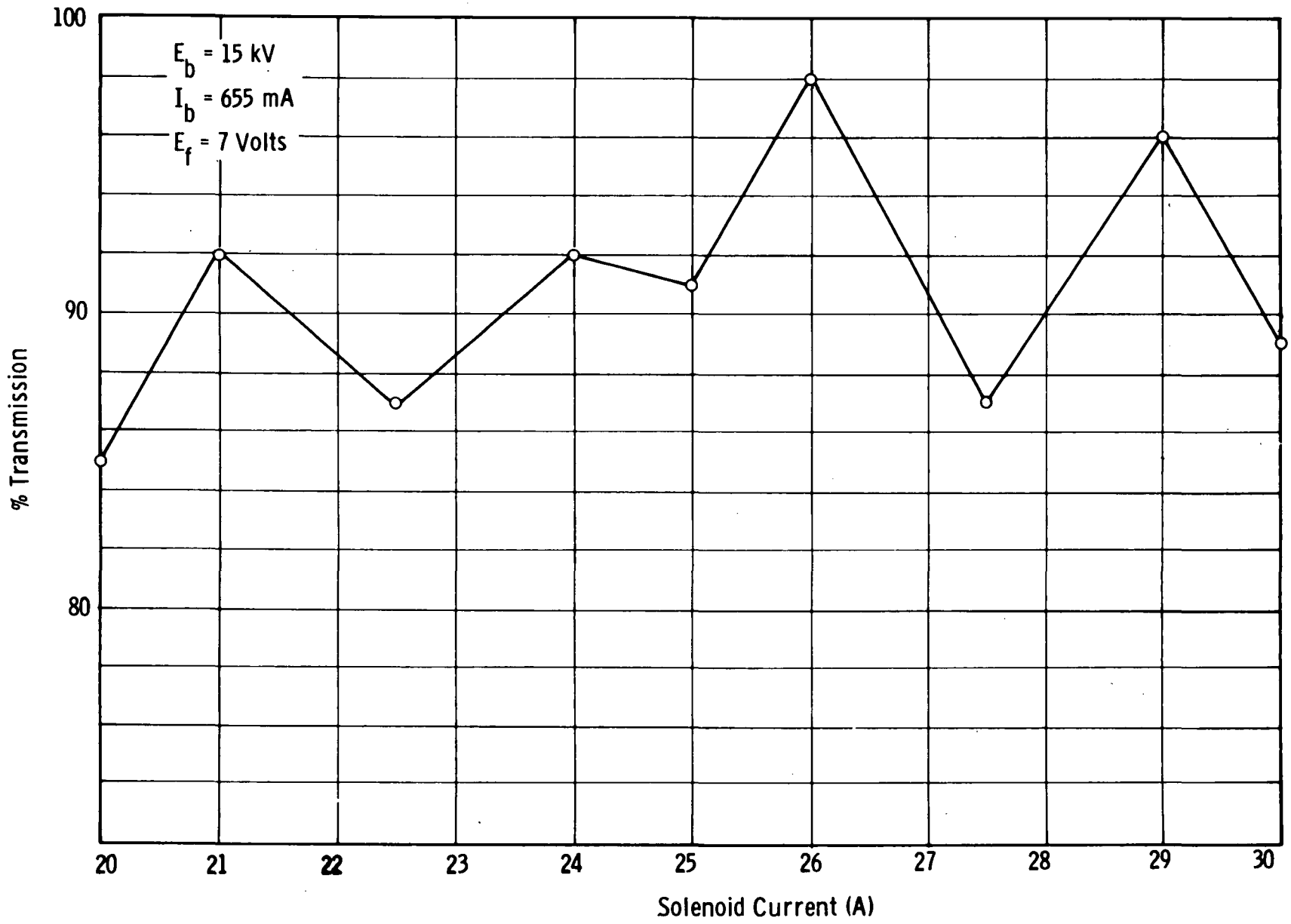

Figure 6-41. Beam Transmission as a Function of Solenoid Current for VTX-6681A1, S. N. 104

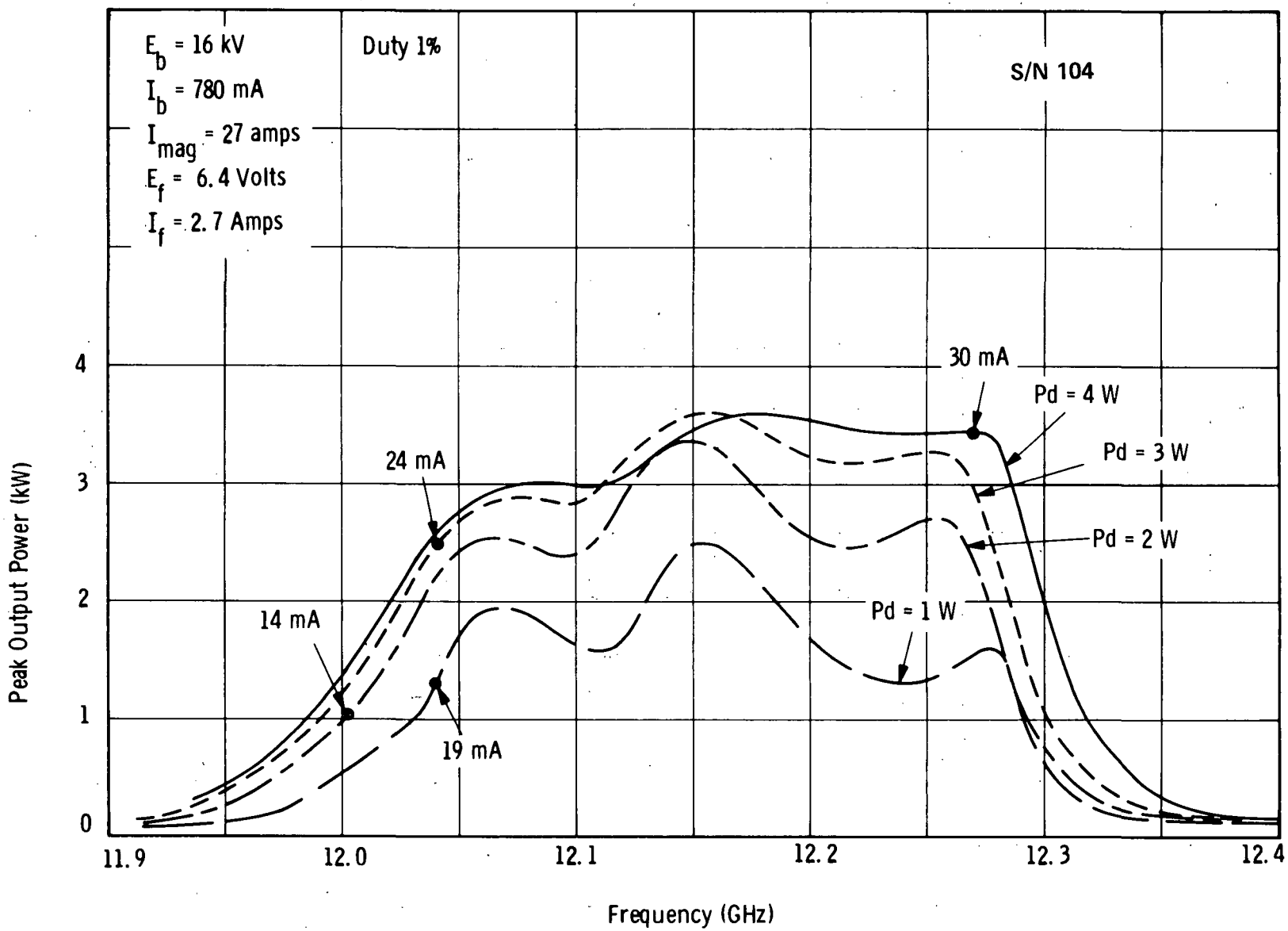

Figure 6-42. Peak Output Power vs Frequency with Drive Level as a Parameter

Although poor beam transmission was a major problem it was decided to test the tube under cw conditions. Since beam transmission was very sensitive to drive level and frequency, solenoid current was adjusted in each case to maintain a maximum of 50 mA of body current.

Figures 6-43, 6-44, and 6-45 show cw power output vs drive for three different beam voltages. At 15 kV the maximum power output occurs at 12.3 GHz. At 16 kV maximum output power occurs at 12.2 GHz although it would appear that if more drive power had been available the maximum output would have occurred at 12.3 GHz. At 17.5 kV the maximum power output occurs at 12.2 GHz. These data show the relatively slow rate at which the hot passband is shifted as a function of beam voltage. These data also show that the conversion efficiency is an increasing function of beam voltage, a certain indication that the velocity taper is nonoptimum.

Figure 6-46 shows the measured input and output rf matches after completion of cw testing. No significant change in the match has occurred although the tube had been operated with up to 14 kW of beam power and with perhaps as much as 800 W of intercepted beam power.

In a test at 16 kV with saturated rive at 12.2 GHz the calorimetrically measured body power was 600 W. Since the intercepted beam current was only 10 mA, the power attributed to beam interception could not have been more than 160 W, hence rf dissipation on the circuit must have been at least 500 W. These data are consistent with the measured low efficiency and point to excessive rf loss in the output circuit section.

6.1.5 Serial Number 105 Test Results

SN 105 was designed with one less lossy cavity than SN 104; i.e., the nine-cavity output circuit has four lossy cavities followed by five lossless cavities. A small change in the position of the focus electrode was made to bring the gun perveance down to design value, with the expectation that this change would

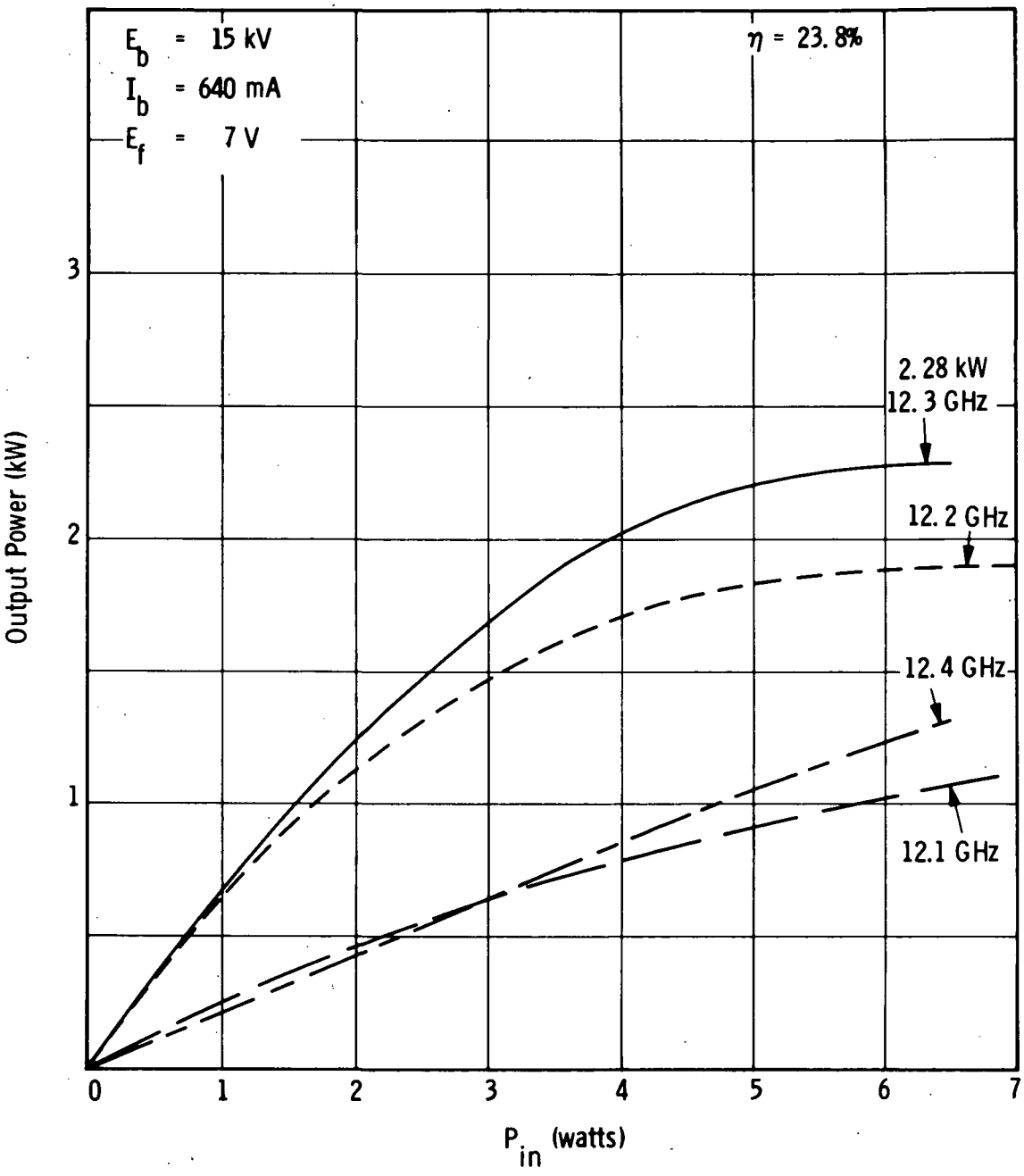

Figure 6-43. Cw Power Output vs Input Power for VTX-6681A1, S. N. 104

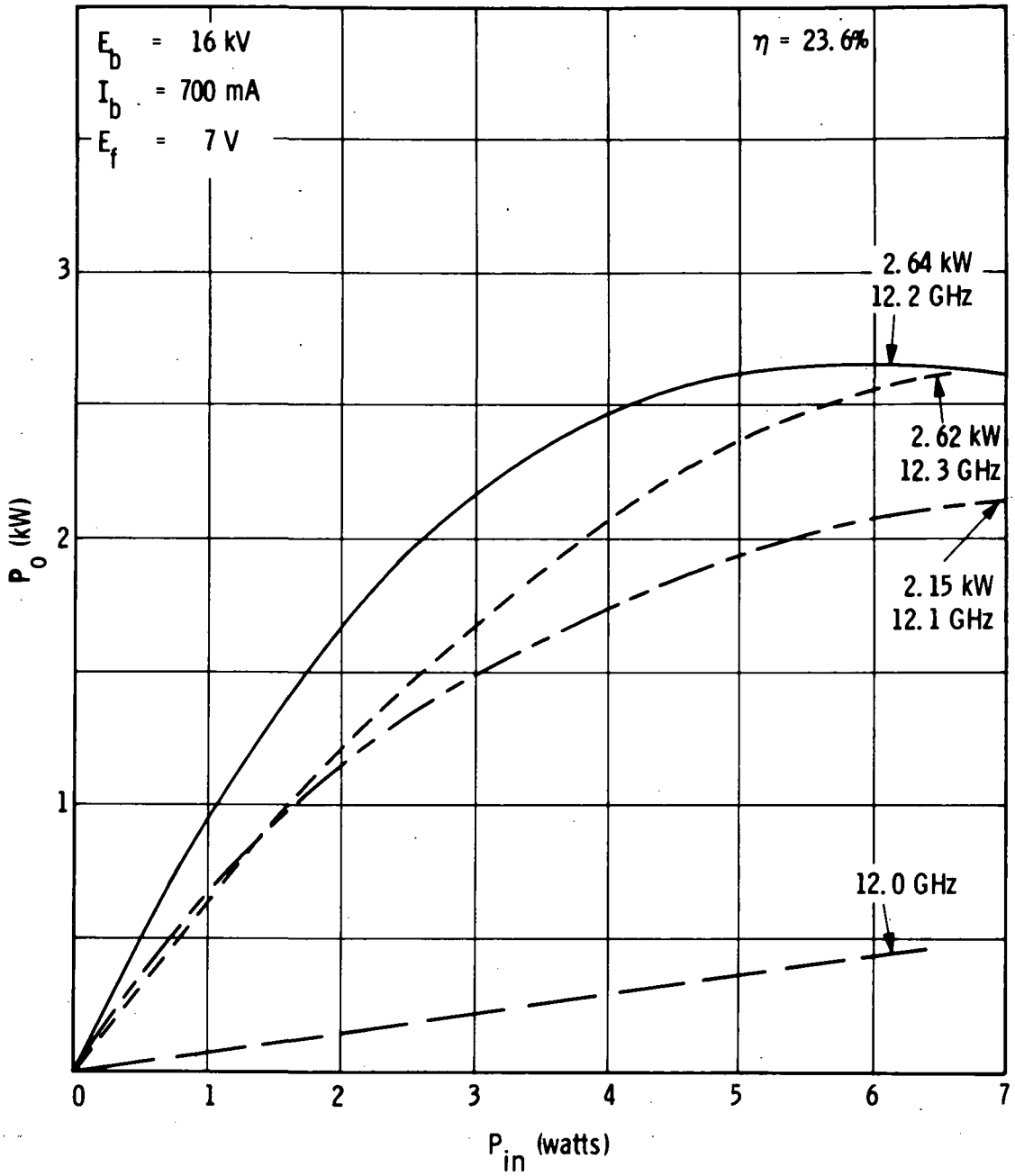

Figure 6-44. Cw Power Output vs Input Power for VTX-6681A1, S. N. 104

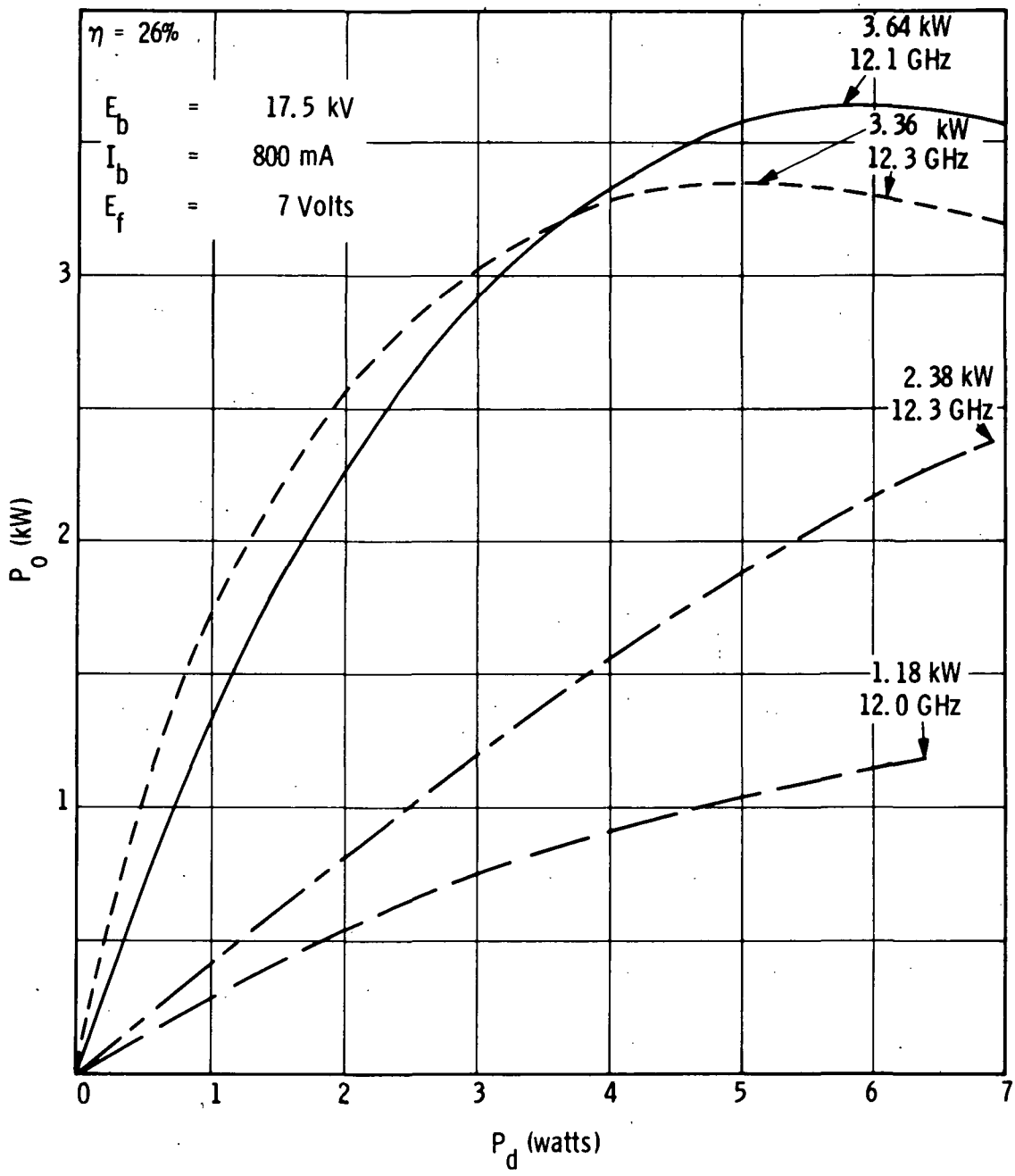

Figure 6-45. Cw Power Output vs Input Power for VTX-6681A1, S. N. 104

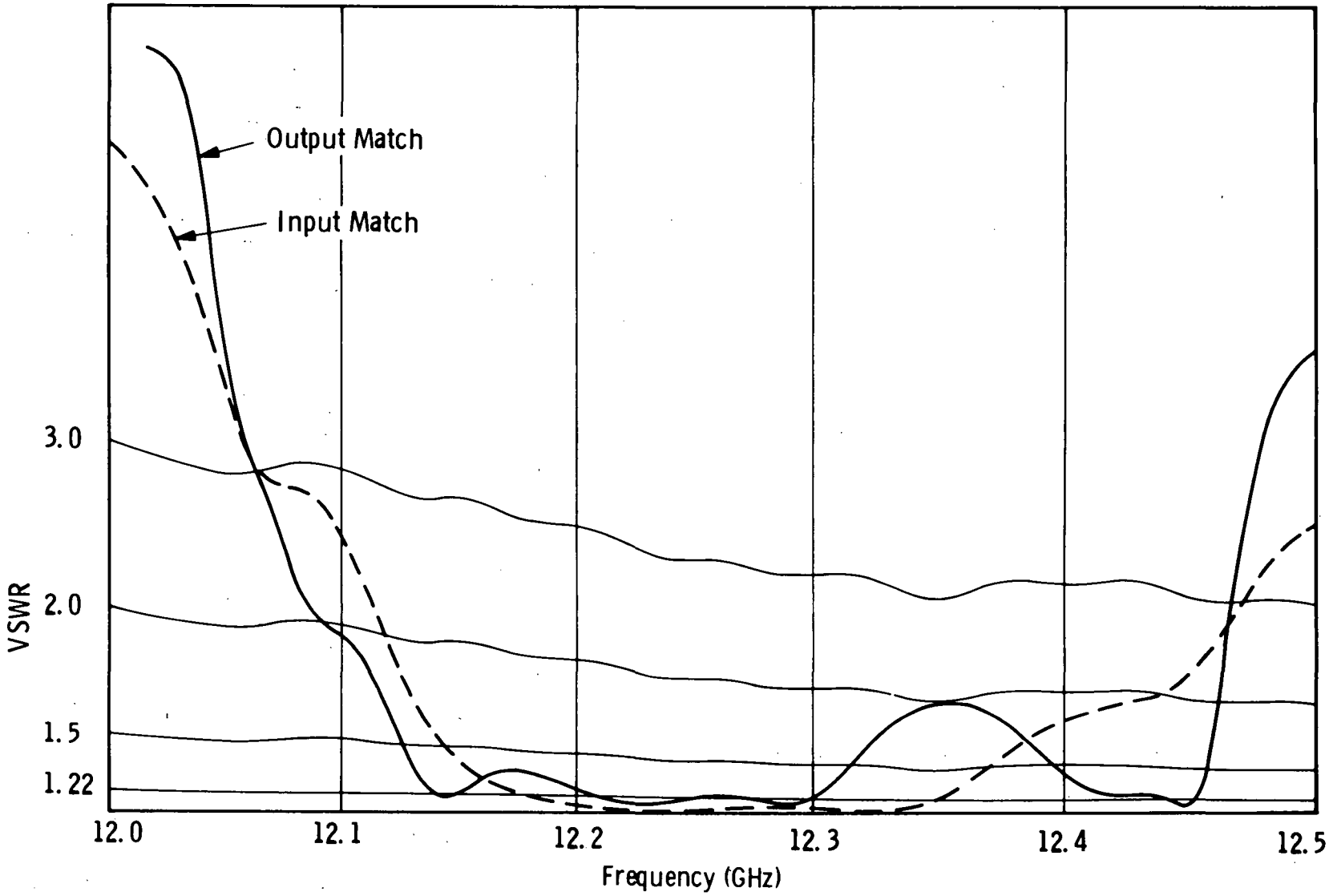

Figure 6-46. Measured Rf Matches at Input and Output of VTX-6681A1, S. N. 104 after Cw Test

improve beam transmission. In all other respects these two tubes were made identical.

Figure 6-47 shows the input and output rf matches for SN 105. The output match of this tube is not quite as good as was obtained with SN 104.

During initial test at 10% duty the tube was electronically stable at all voltages above 11 kV. Beam transmission without drive was 99.9% and perveance agreed very closely with the design value of 0.33 μperv.

Figures 6-48 and 6-49 show power output as a function of frequency at 10% duty. The maximum conversion efficiency is 35%, but, as was the case in the pulse tests of SN 104 this high value of efficiency was not borne out in cw testing. The saturated gain is seen to be flat within less than 1 dB over the frequency range 12.1 to 12.3 GHz.

The cw performance of the tube is shown in Figures 6-50, 6-51, 6-52, 6-53, and 6-54. As the beam voltage is increased the hot passband moves to slightly lower frequencies and the maximum conversion efficiency is generally seen to increase. These data confirm the results on SN 104 and indicate an insufficient circuit wave velocity reduction in the taper section. In an ideal taper the efficiency should be maximum at the design voltage and should slowly fall off both above and below this voltage.

A solenoid was placed over the gun to increase the flux density in the cathode and expand the beam. Figures 6-55 and 6-56 show the results of these tests. There is an increase in the small signal gain and maximum power output which would seem to indicate that the beam had been too small. The fact that beam interception did not appreciably change as a result of expanding the beam would tend to imply that the beam optics could be improved. The maximum measured conversion efficiency in these tests was 28.9%. Taking into account thermal losses in the output waveguide, the estimated efficiency at the output cavity is 31%.

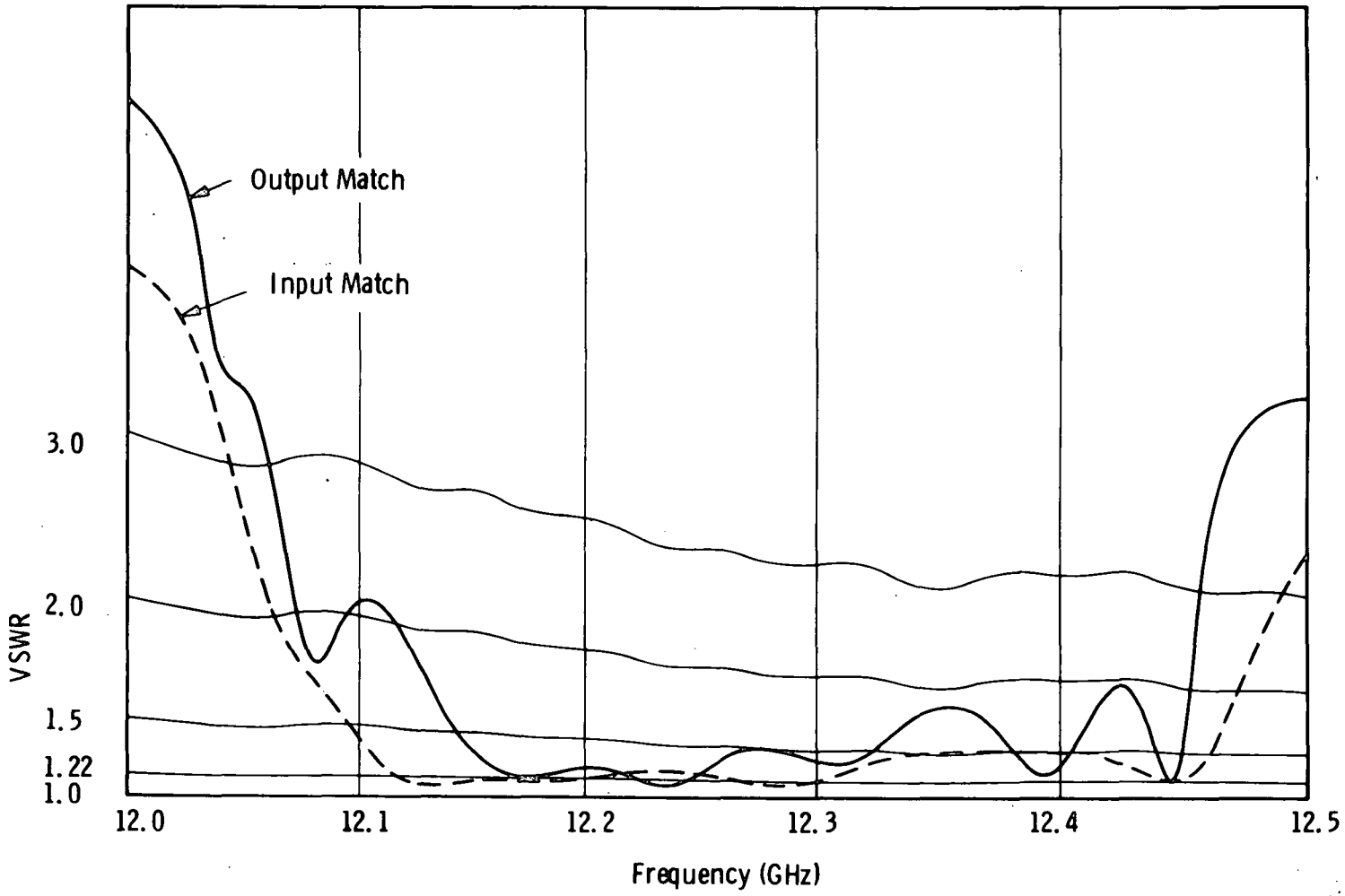

Figure 6-47. Measured Rf Matches at Input and Output of VTX-6681A1, S. N. 105

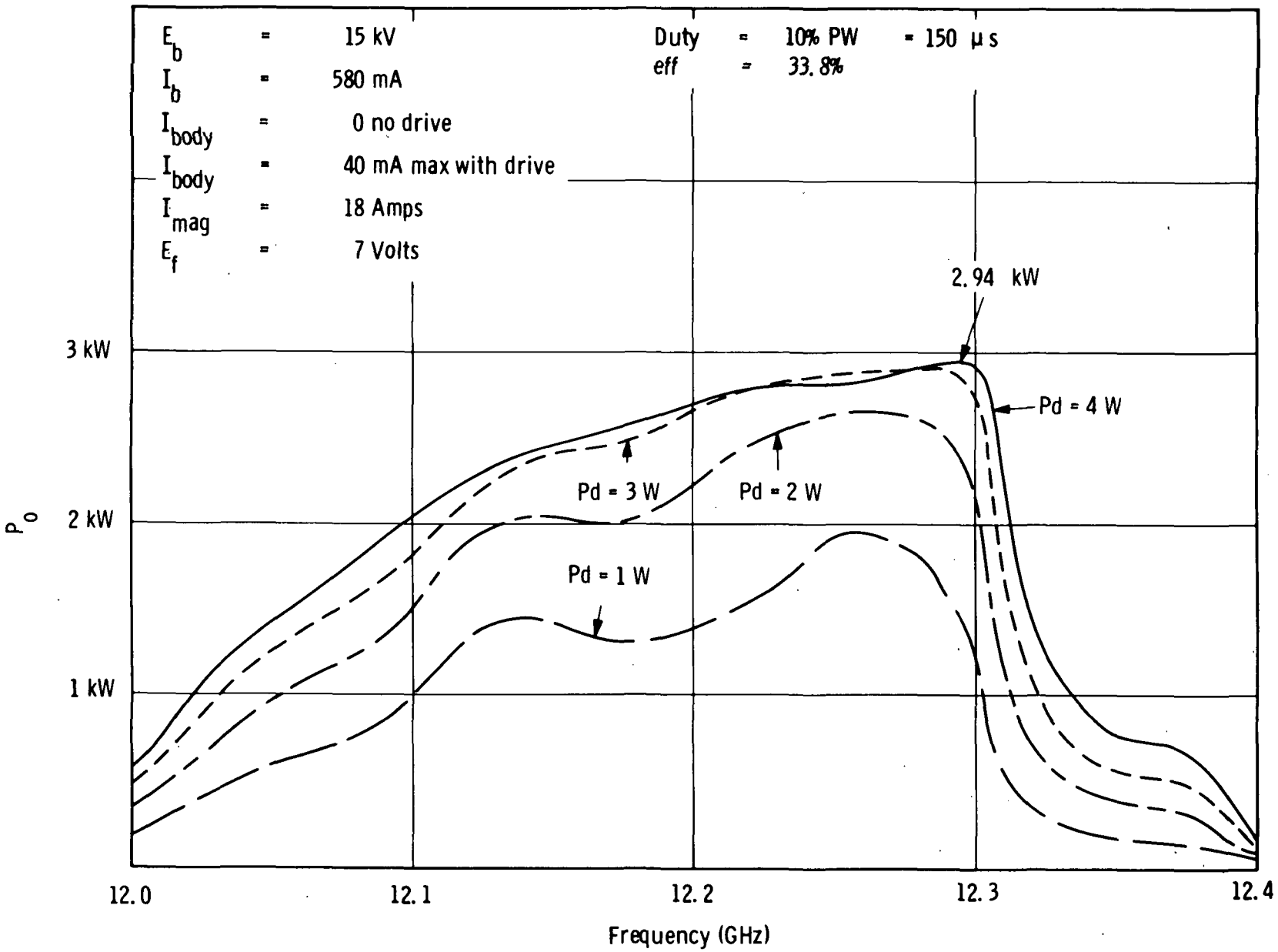

Figure 6-48. Power Output vs Frequency at 10% Duty. VTX-6681A1, S. N. 105

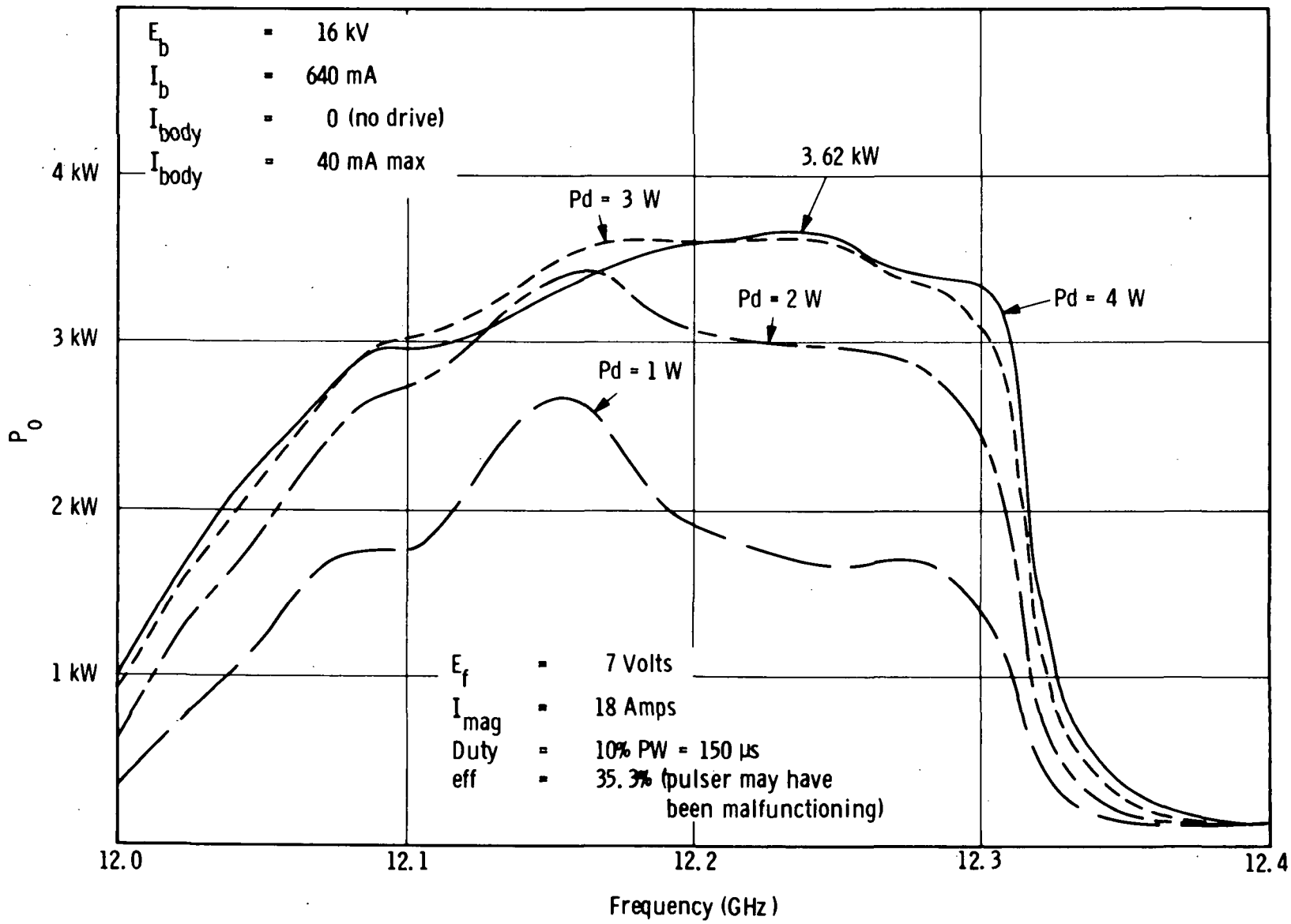

Figure 6-49. Power Output vs Frequency at 10% Duty. VTX-6681A1, S. N. 105

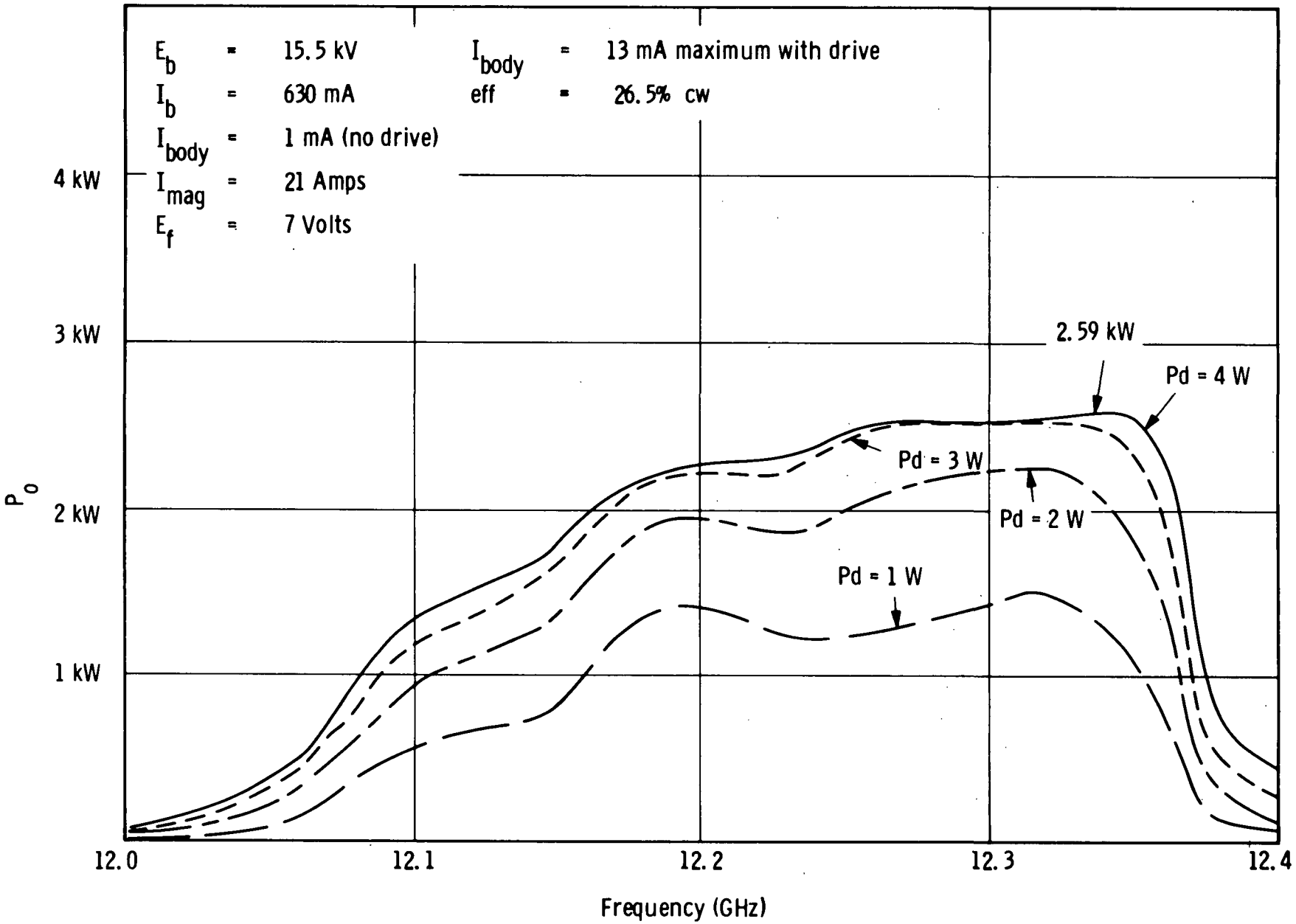

Figure 6-50. Cw Power Output vs Frequency for VTX-6681A1, S. N. 105

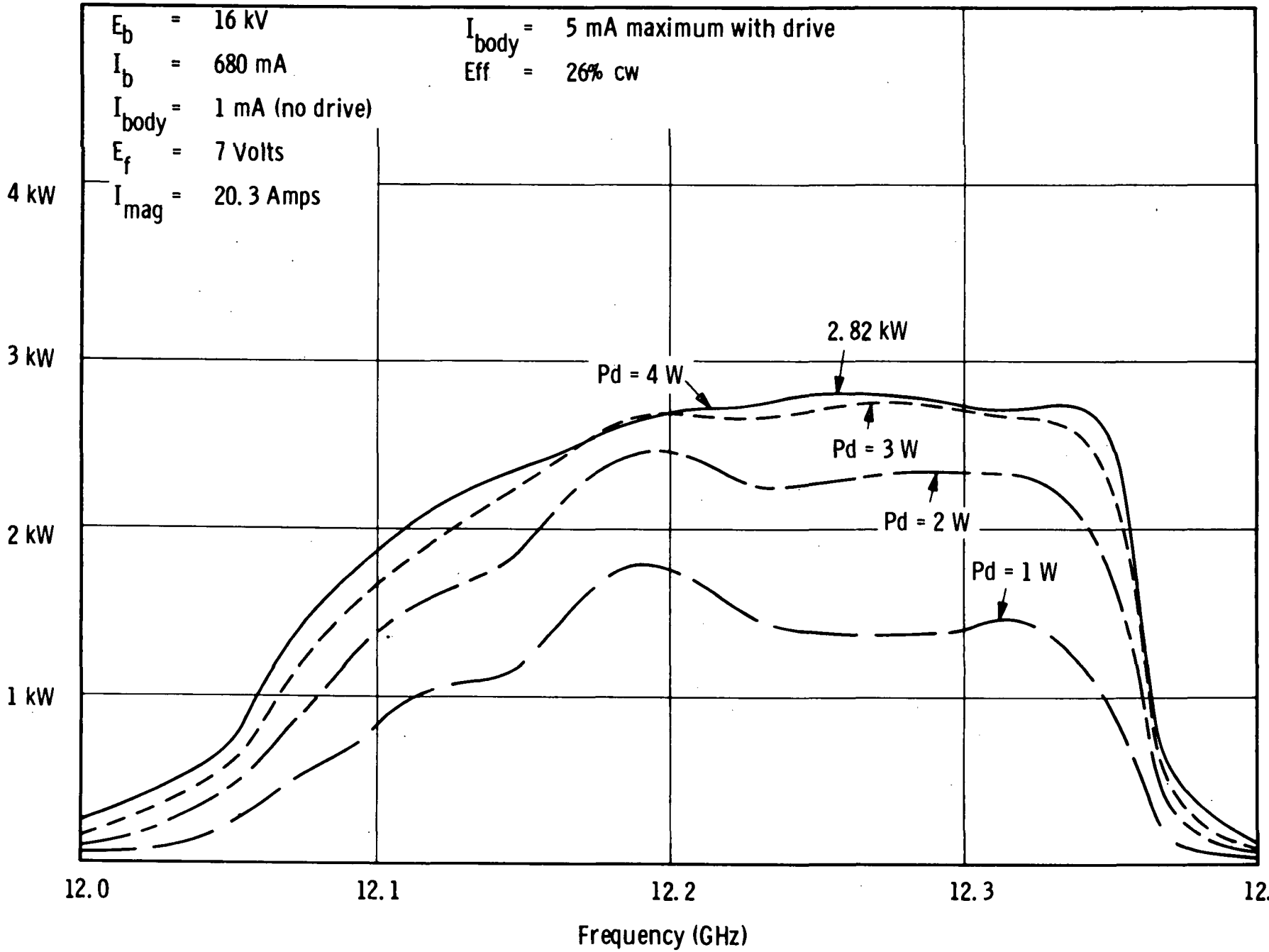

Figure 6-51. Cw Power Output vs Frequency for VTX-6681A1, S. N. 105

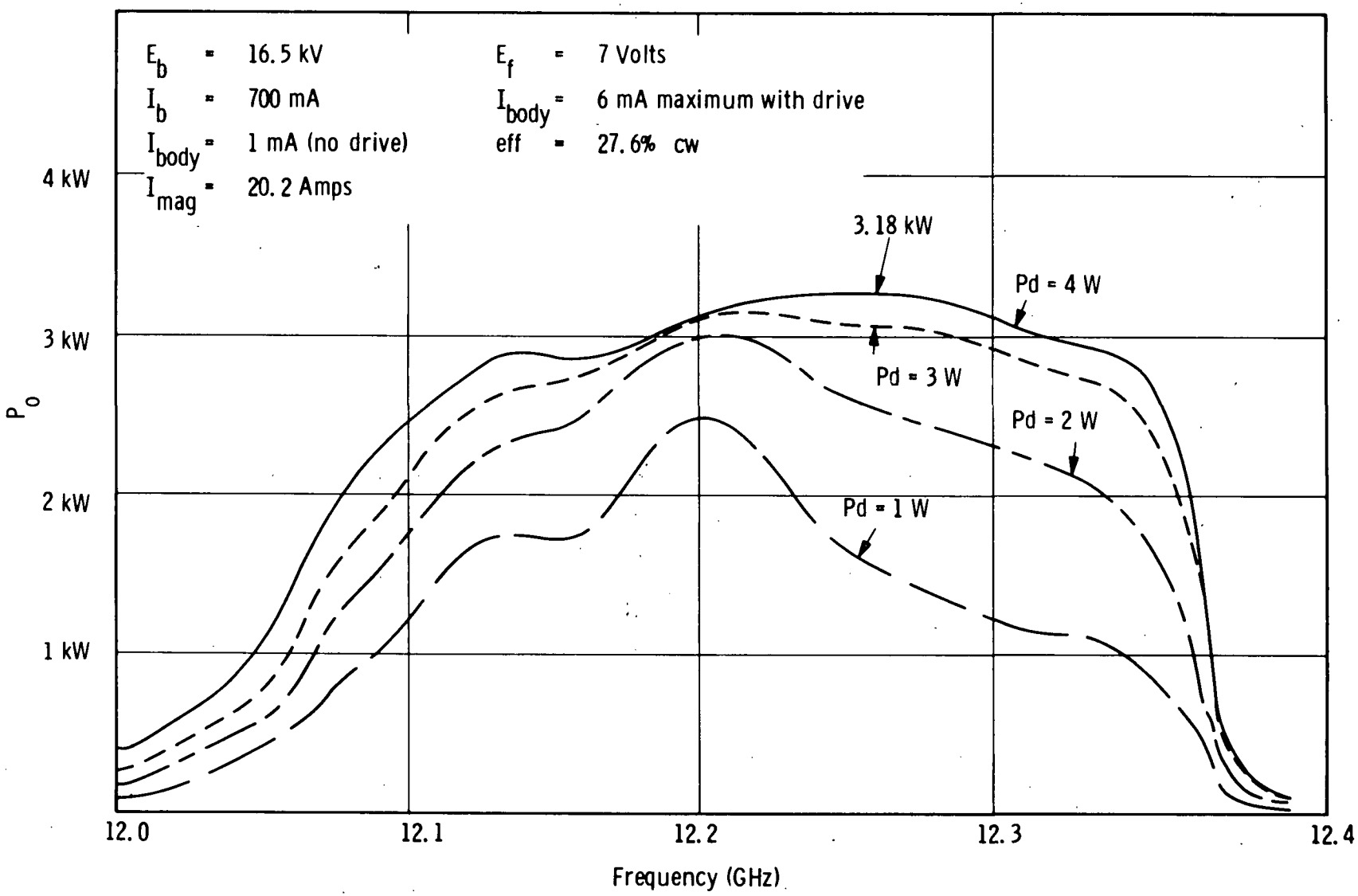

Figure 6-52. Cw Power Output vs Frequency for VTX-6681A1, S. N. 105

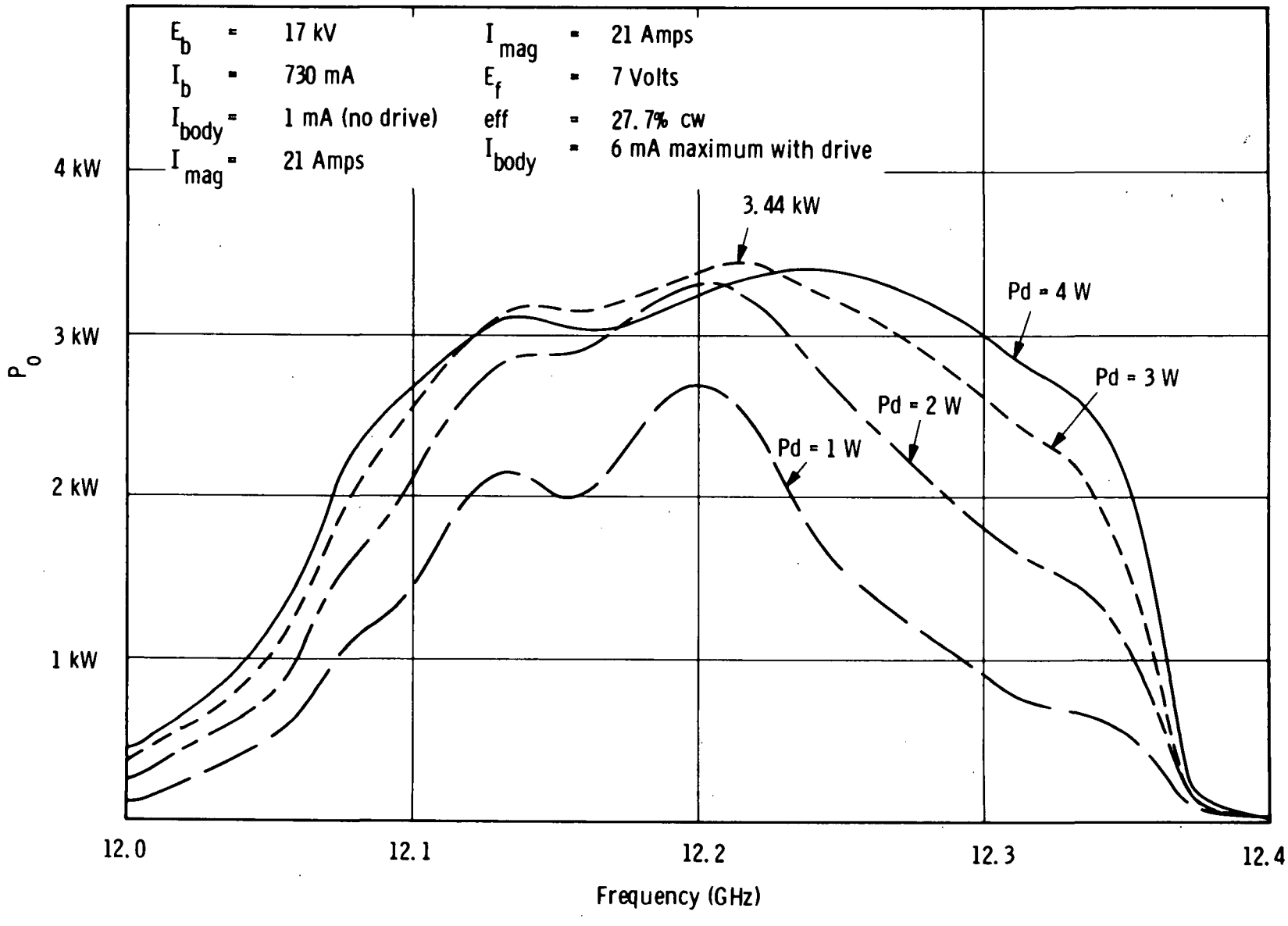

Figure 6-53. Cw Power Output vs Frequency for VTX-6681A1, S. N. 105

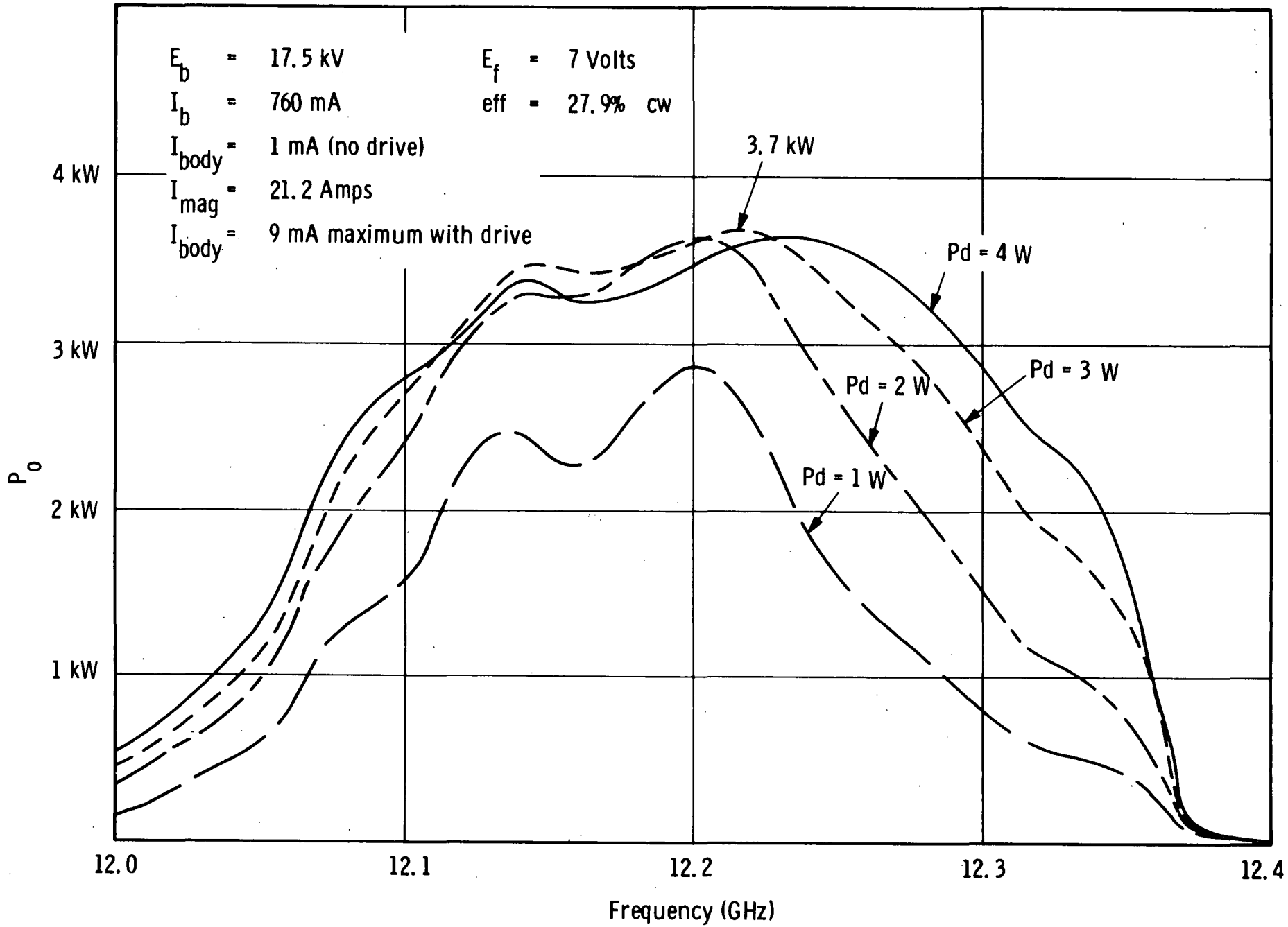

Figure 6-54. Cw Power Output vs Frequency for VTX-6681A1, S. N. 105

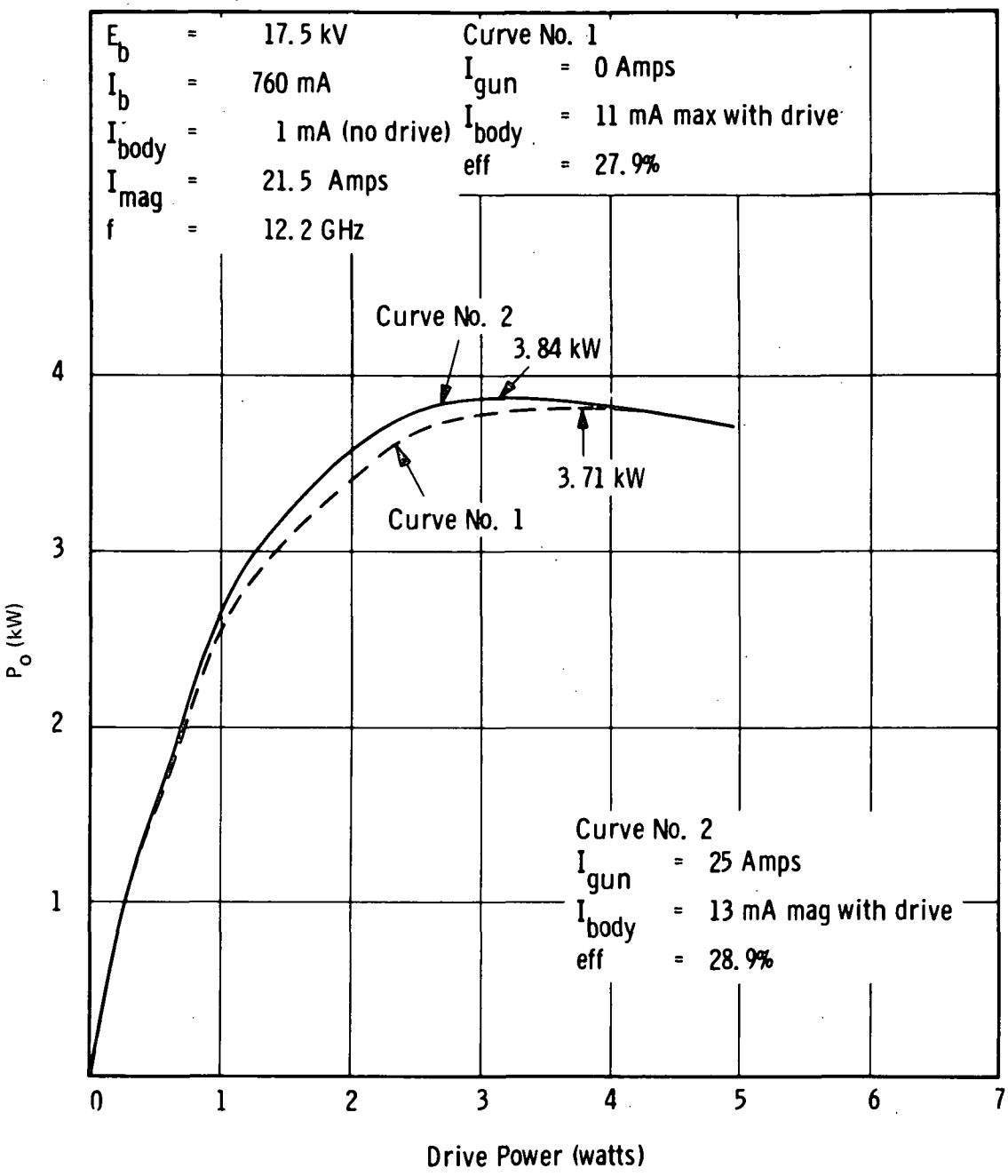

Figure 6-55. Cw Power Output vs Drive for VTX-6681A1, S. N. 105

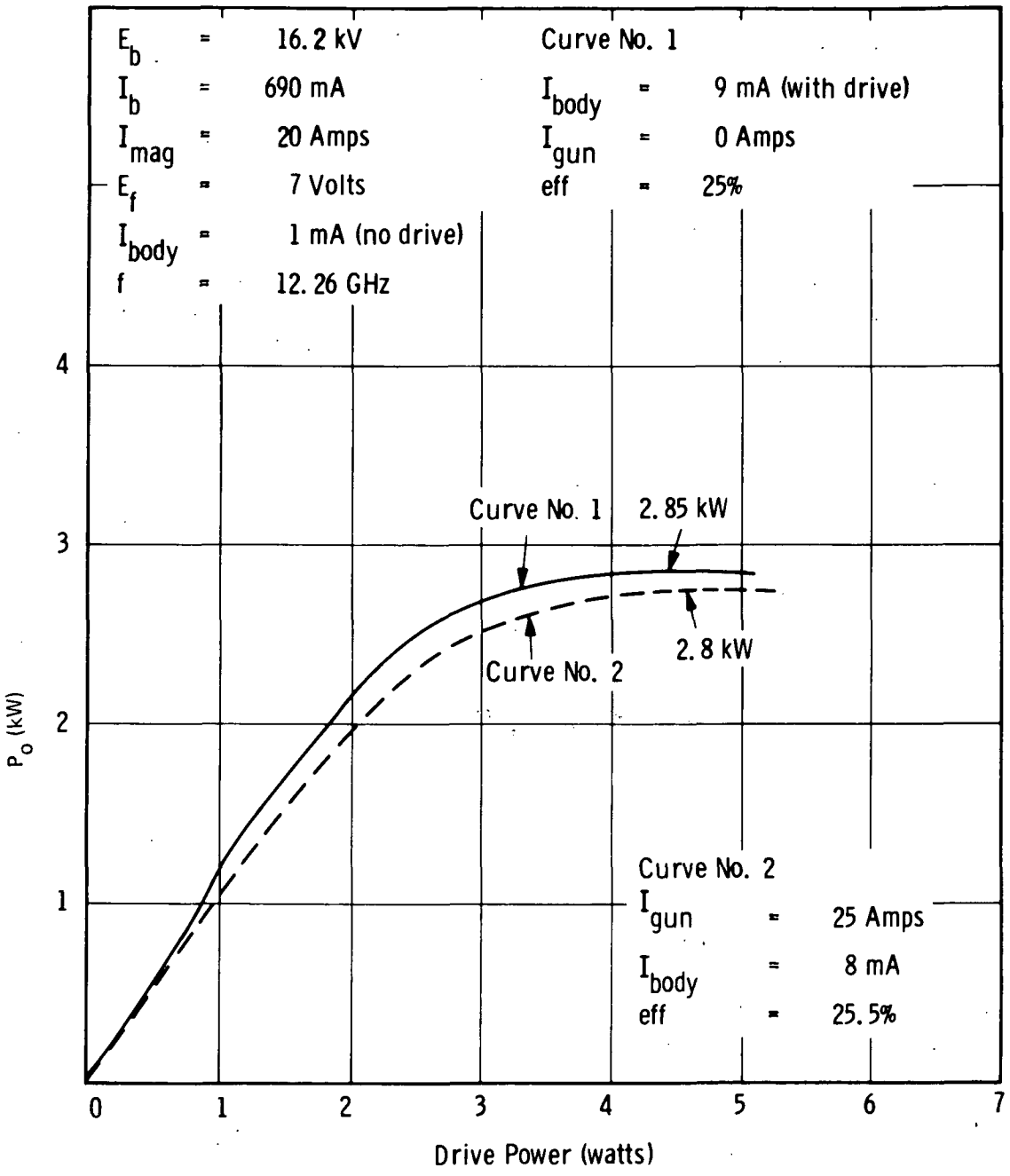

Figure 6-56. Cw Power Output vs Drive for VTX-6681A1, S. N. 105

During final test a small vacuum leak developed in one of the coolant channels on the body of the tube. It was not possible to repair this leak although it was still possible to operate the tube at full power with the vacuum appendage pump connected.

6.2 RESULTS OF COMPUTATIONAL ANALYSIS

The computational tools at Varian which were available for use in studying techniques which could aid in carrying out the objectives of the program were described in Section 4. These included both small signal and large signal computer programs as well as a number of peripheral programs which aided in the analysis of coupled-cavity traveling wave tube performance.

These tools were used for the initial tube design work, for checking the measured performance data against theoretical predictions, and for systematic refinement of the experimental designs. In addition, numerous computer experiments were conducted to investigate the details of the coupled-cavity interaction process in order to determine factors which either limited or enhanced the achievement of high interaction efficiency. The scope of the present study program, combined with the extreme complex nature of the coupled-cavity tube, precluded our being able to resolve completely the individual parameters for optimizing interaction efficiency. However, a great deal of further insight into the behavior of high efficiency coupled-cavity tubes was obtained.

Some of the specific areas in which large signal computer experiments were conducted are the following:

1. Effect of cavity Q (circuit loss) on efficiency
2. Optimum synchronization for bunching
3. Voltage jump resynchronization vs velocity tapering in the output circuit
4. Effect of interaction impedance on efficiency
5. Effect of interaction impedance on beam modulation
6. Effects of backward wave on efficiency

7. Optimization of velocity tapers
8. Effect of output gain after the sever
9. Adjustment of individual gap phases for more favorable interaction
10. Effect of circuit phase on the interaction process

Although the small signal program was an important tool for calculating gain, phase ripple, stability, etc., these have been primarily reported on in earlier sections. The following paragraphs relate only to large signal experiments on efficiency phenomena.

6.2.1 Voltage Jump vs Velocity Taper

Fundamentally, energy is extracted from a traveling wave tube by modulating the beam to have a large component of rf current which is then passed through a region of circuit fields in a phase which will extract maximum energy from the beam through the slowing down of electrons. The amount of energy given up depends upon the magnitude of the rf beam current and upon the amplitude and phase of the circuit fields. Since the bunching mechanism in the beam is one that tends to produce a modulation current which lags appreciably behind the phase for maximum extraction of energy, high efficiency tubes generally employ a resynchronizing technique for advancing the phase of the electron bunches with respect to the circuit fields. This can be done either through a slowing down of the circuit wave by means of a velocity taper or by increasing the velocity of the beam by means of a voltage jump.

Figure 6-57 is an illustration of achieving efficiency through both means. Calculations were with the initial 17-cavity design example consisting of a four-cavity input section, a six-cavity intermediate section and a seven-cavity output section. With no resynchronization an efficiency of 19.6% was calculated under the condition of nearly synchronous bunching; i.e., dc beam velocity and rf circuit velocity equal. A single cavity velocity taper in the output circuit increased the efficiency to 36.5% whereas a taper in the last two cavities of the circuit increased the efficiency to 48%. A voltage jump in the last two cavities in place of the velocity

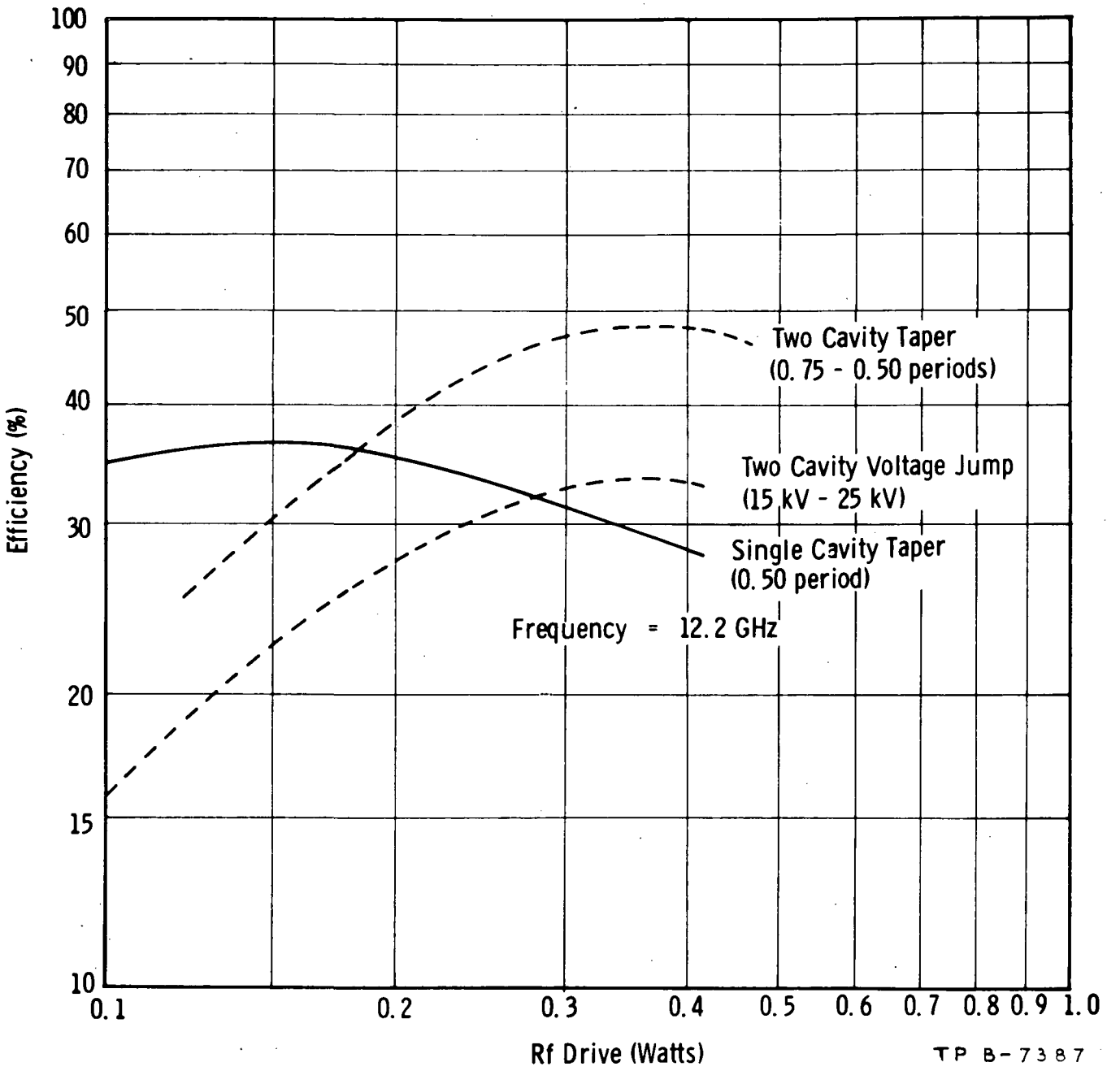

Figure 6-57. Calculated Midband Efficiencies of the 17-Cavity Design Example for Several Different Output Configurations

taper produced an efficiency of 33.4%. In each of these cases the I_1/I_o ratio of rf to dc beam current reached essentially the same value of slightly over 1.4:1. The enhancement in efficiency with each of the resynchronization schemes resulted from a more favorable phasing of the rf beam current with respect to the circuit fields for the extraction of energy.

On the basis that true conversion efficiency (based on actual beam power within the circuit region) is not fundamentally higher for voltage jump tubes than for velocity tapered tubes, we chose to concentrate our optimization on the velocity taper approach for reasons of simplicity and reliability. The near equivalent performance capability of the two schemes is apparent when one considers that if the high voltage output section of a voltage jump tube is driven by a beam with a given level of rf modulation, the only difference in performance between the case of a driving beam obtained from a section operating at the same voltage or from one operating at a lower voltage than the given output circuit would be slight differences in the quality of the modulation. Theoretical advantages could be cited in the case of either approach.

6.2.2 Optimization of the Velocity Taper

Numerous computer experiments were performed on a number of design models to determine optimum velocity tapers for maximum efficiency in given circuit designs. The number of cavities involved in any given taper depends upon the circuit impedance level as it affects the gain per cavity. Generally, two to three cavities were involved in the examples studied. This usually represented about the last 5 to 6 dB of large signal gain in the tube.

Table 6.1 summarizes the optimum tapers that were obtained in several different design configurations studied.

A number of complicated factors are involved in arriving at a taper for optimum efficiency. Since nearly all of the exchange in energy occurs in the last few gaps it is essential that the rf beam current and gap voltage be phased for

TABLE 6.1

SUMMARY OF OPTIMUM VELOCITY TAPERS FOR SEVERAL DIFFERENT DESIGN CONFIGURATIONS

Case	Description	No. of Cavities per Section	Gap Impedance Level (Ohms)	Velocity Taper (gap-to-gap)	I_1/I_o Max	Calculated Efficiency (%)
1	Preliminary Design Model Narrow Band Hi Impedance Two-Cavity Taper	4 – 6 – 7	6524	0.875 – 0.625	1.44	48.0
2	Wider Band Circuit Model All Cavities Lower Impedance Two-Cavity Tapers	5 – 5 – 8	4763	0.80 – 0.70 0.75 – 0.75	1.42 1.43	39.0 40.1
3	Similar to Case 2 Except Three-Cavity Taper	5 – 5 – 8	4763	0.90–0.85–0.70	1.38	41.6
4	Similar to Case 3 Except 50% Higher Impedance in Tapered Cavities	5 – 5 – 8	4763/7145	0.90–0.80–0.65	1.39	47.2
5	Similar to Case 3 Except 50% Higher Impedance in Last 7 Output Cavities	5 – 5 – 8	4763/7145	0.90–0.80–0.65	1.37	43.9
6	Similar to Case 2 Except Nonoptimum Taper (Closest Simulation to Final Tube Configuration)	5 – 5 – 8	4763	0.90 – 0.85	1.41	31.0
7	Low Impedance Case	4 – 6 – 9	2000	0.875–0.625	1.34	35.0
8	Similar to Case 1 Except Voltage Jump Resynchronization (Not Completely Optimized)	4 – 6 – 7	6524	Voltage Jump	1.46	33.4

maximum energy exchange in this region. In particular, the last gap should be positioned such that at saturation the beam is slowed to a point where the rf current and voltage are very nearly in phase. Some distance back from the end of the tube the gap voltages should lead the rf beam current phase by something less than 90° in order that a favorable bunching process is formed within the beam.

Figure 6-58 is an illustration of a type of plot which proved quite useful for analyzing velocity taper configurations. In this figure the phasing referred to above is quite clearly illustrated. To understand more fully the data presented it should be pointed out that a reference phase is taken to be that of a signal propagating at the dc beam velocity. Consequently, dc electrons move horizontally in the figure. In the vicinity of the final output cavities one notes a sudden falling back in the phase of the rf beam current as the beam gives up its energy to the circuit. The more or less constant negative slope to the current phase observed in the earlier cavities does not represent any appreciable slowing down of the electrons, but merely reflects the fact that most of the rf current is in the slow space charge wave, which has a velocity below that of the dc electrons.

The illustration presented is Case No. 4 of Table 6.1, and is for an 18-cavity (5-5-8 configuration) tube in which the last three cavities were tapered to 80% — 80% — 50% of the normal cavity period. Since the computer program uses only symmetrical cavities, whereas physical tapers can be produced by offsetting the gaps with respect to the cavity boundaries, a more significant set of parameters to use is the gap-to-gap spacing in the tube. For the above example this becomes 90% — 80% — 65% of the normal cavity period, as noted in the table. Note that the normalized rf beam current reaches a maximum value inside the penultimate cavity where it interacts in a favorable phase with the normalized gap voltage to produce a large normalized gap voltage in the output cavity. The energy exchange in the final cavity occurs under most optimum conditions with a high gap voltage in near perfect phase with the fundamental component of rf beam current. Note that the current amplitude drops rapidly near the exit of the tube as the interaction process is completed and the electron bunches become destroyed.

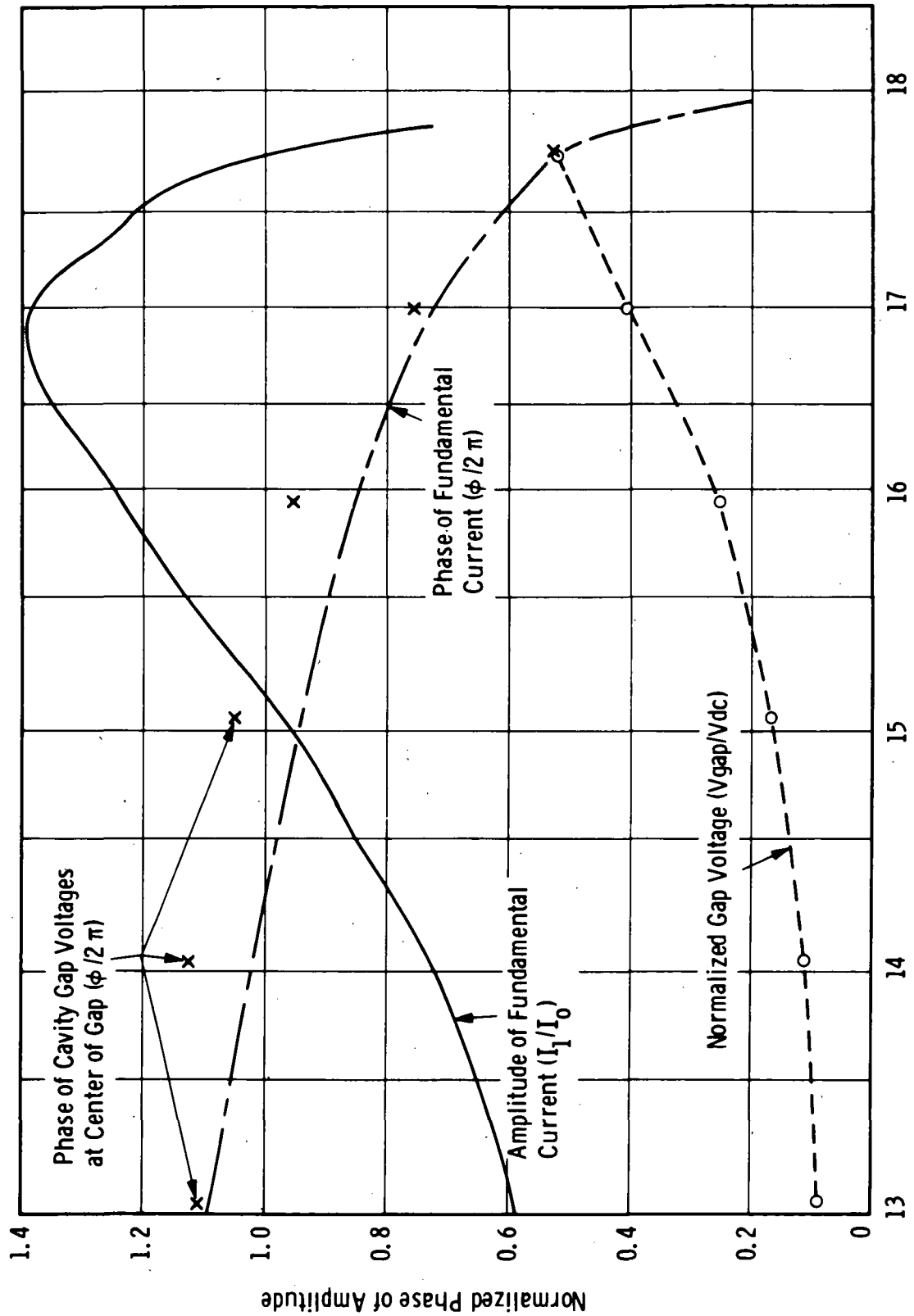

Figure 6-58. Calculated Parameters in an Optimally Tapered High Efficiency Coupled-Cavity Tube

The above case is presented as an example of an optimally tapered tube. With plots similar to the one shown in Figure 6-58 it is possible to visualize most of the interaction process, particularly with regard to phasing, and to make the appropriate adjustments in the taper to produce an optimum resynchronization condition. Unfortunately, except for the output gap, the optimum phasing between gap voltages and beam current is not a simple relationship to define. The picture is further complicated by the amplitude and phase effects resulting from large amounts of backward wave power on the circuit. Experiments with some of these effects are described in Section 6.2.3.

6.2.3 Backward Wave Effects in Coupled-Cavity Tubes

An effect often ignored in the analysis of traveling wave tubes, but which plays a dominant role in a high gain per cavity tube, is that of the backward wave power generated in the circuit. In any given cavity, the effect of the beam is to induce a pair of equal amplitude waves traveling in both directions away from the gap along the propagating circuit. Wavelets traveling in the forward direction add up to the final output wave whereas the phasing of the backward wavelets is such that they may either add to or subtract from the forward wave voltage in any given gap. Depending upon their respective amplitudes and phases, these backward wavelets may or may not represent significant losses in energy, either at a sever or input terminal, or due to lossy attenuator cavities in the tube. Their nature is such that the addition of a cavity to an already existing circuit may have the effect of either increasing the gain of the circuit, leaving the gain unchanged, or even decreasing the gain of a given section.

Since the space-harmonic coupled-cavity tube nominally has a phase shift of the order of $1.5\ \pi$ per cavity, there is a tendency for forward and backward components to alternately reinforce and cancel each other in succeeding gaps. This effect is clearly illustrated by the plots of the gap voltages shown in Figure 6-59. The cases shown here are the same three examples appearing in Figure 6-57. Interestingly enough, all three cases had similar circuits with

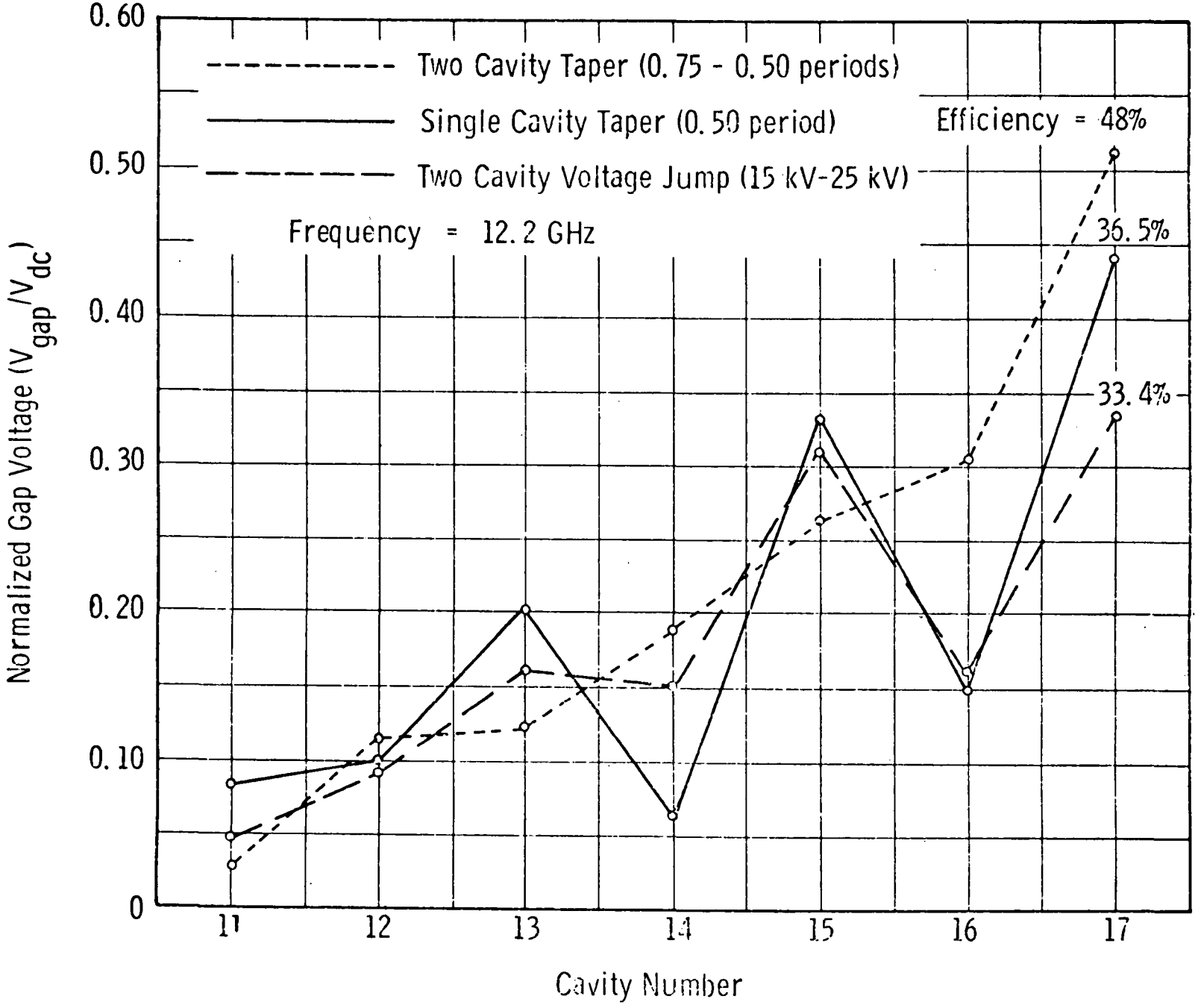

Figure 6-59. Normalized Gap Voltages in Tube Output Section Under Saturated Drive Conditions

identical output gap impedances, each achieved nearly identical I_1/I_o maximums (of the order of 1.45), and each had the output gap voltage phased with the rf beam current in the gap under saturated conditions. Yet, vastly different efficiencies were obtained.

Part of the answer lies in the fact that even though the output gaps were favorably phased, the voltage amplitude in the highly critical penultimate gap was drastically lowered as the result of backward wave cancellation effects, in each of the lower efficiency cases. The effect of the backward wave upon the amplitudes of the various gap voltages is also generally accompanied by corresponding variations in the phase of the gap voltages with respect to the rf beam current. Most of these effects can be overcome with appropriate adjustments of the gap voltage phases in a properly tapered circuit.

Even in the case of the 48% efficiency example shown in Figure 6-59, some backward wave effect is apparent. Figure 6-60 shows the variations in the gap phases that accompanied this case, as well as the improvement in efficiency that occurred when the cavity periods were adjusted to further reduce these variations.

A few experiments were conducted to determine what effect the total phase shift per cavity (BL) might have upon the phasing of the backward wave on the circuit. This factor did not appear to be significant as a means for eliminating backward wave effects. This is not surprising when one considers the fact that the efficiency of most tubes is not highly sensitive to frequency over their operating bands.

6.2.4 Tube Parameters Effecting Efficiency

Many different tube parameters effect the efficiency of a traveling wave tube. In a program where high efficiency is an objective it is desirable to know the sensitivity of efficiency vs various parameters used in the design.

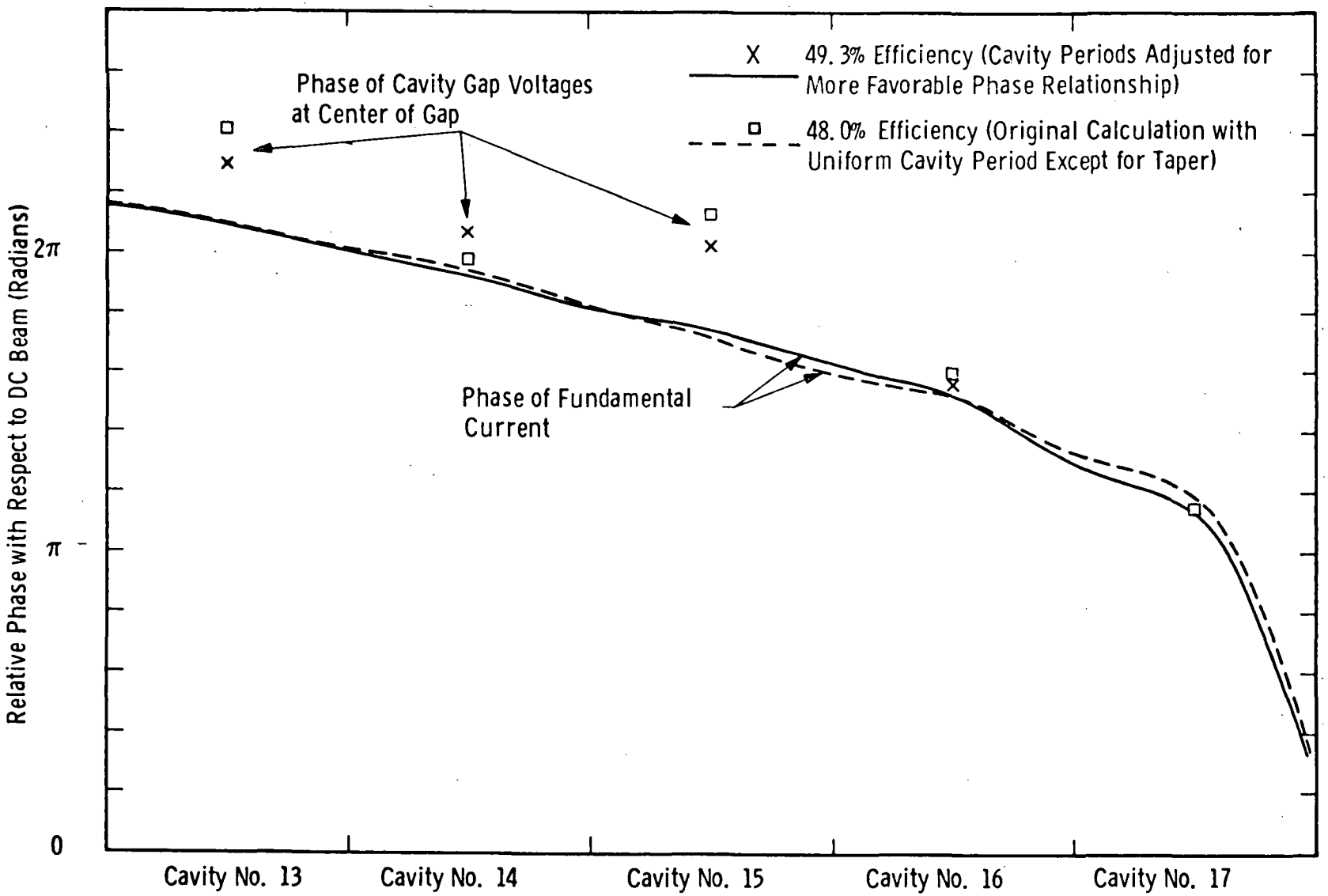

Figure 6-60. Calculated Phase Relationships Between Cavity Gap Fields and Beam Current Modulation for Typical Design Examples

As an example, it is known that insufficient gain past the sever in the output of a traveling wave tube will severely limit the efficiency achievable with that design (Ref. 11). Net saturated gain of 20 dB was typically achieved in the computer models studied on this program. In the preliminary design model, the effect of increasing the 7-cavity output to 8 cavities increased the efficiency by only 1.0%, from 48% to 49%. At the same time, the saturated gain increased by approximately 4 dB indicating that very little loss in efficiency was occurring due to sever losses. Since the added cavity was a "lossless" cavity it also indicated that the lossy attenuator cavities were not seriously effecting the efficiency. In this design the lossy cavities ended where the circuit amplitude was approximately 10 dB down from the saturated power level at the end of the tube.

In another experiment an analysis was made on the effect of small amounts of circuit loss in the so-called "lossless" cavities used in the tube output.

In most of the computer experiments the cavity Q of the final output cavities was typically set at 2000. In the narrow band design this represented approximately 0.2 dB loss per cavity. In practice, cavity Qs higher than this are readily achieved at these frequencies.

In a high output impedance version of the wider band prototype model, efficiency was calculated as the cavity Q was varied from 2000 to 4000. Efficiency increased from 49% to 51% in this case. The cavity loss was assumed to vary from 0.2 dB per cavity to 0.1 dB per cavity with 5 of the 8 cavities making up the output section being of the "lossless" type.

Experiments were also performed with respect to the degree and quality of the electron bunching process. Figure 6-61, although done without backward waves present, is typical of the electron trajectories obtained in a large signal calculation. These plots, obtained directly from the computer, are similar to the phase plots shown in Figures 6-58 and 6-60. Again, dc electrons

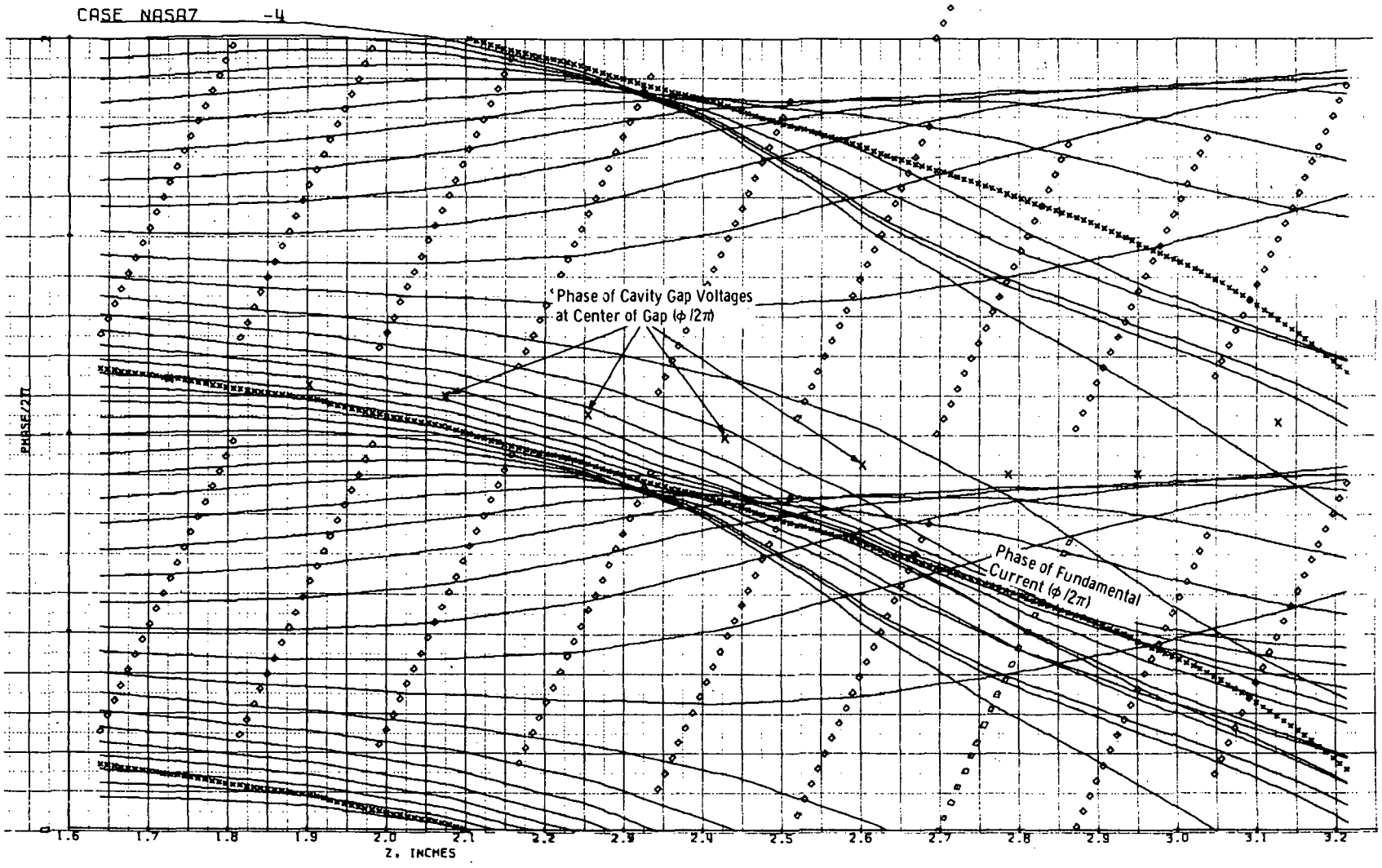

Figure 6-61. Plot of Electron Phase vs Distance Showing Typical Bunching in Output Section of Tube

are simply horizontal lines and become the reference phases from which all other phases are calculated. The electrons are introduced initially at equally spaced phase intervals throughout the rf cycle. Electrons with negative trajectory slopes are traveling at less than dc velocity whereas those with positive slope are traveling above the dc velocity.

Although I_1/I_o reached a maximum value of 1.425 at Z = 2.525 the large spread in the electron velocities forming the bunches, as well as electron crossovers, is apparent from the figure.

Experiments were performed in which various length drift sections were incorporated after the last sever. In other experiments both the circuit impedance level and the velocity for synchronization with the circuit were varied to determine their effects upon the bunching process.

The additional drift region after the sever had some effect in reducing the degree of electron crossover, but somewhat lower values of I_1/I_o were obtained.

Varying the synchronization parameter u/v (ratio of dc velocity to rf circuit phase velocity) around unity, in a number of cases, showed that the maximum value of I_1/I_o generally occurred for a value of u/v just slightly less than unity. The maximum value of I_1/I_o for high impedance circuits (i.e., gap impedances of the order of 6500 ohms) was found to be 1.48 with u/v = 0.91. Lower impedance circuits produced slightly lower maximum I_1/I_o values with optimum u/v values somewhat closer to unity. However, even at gap impedance levels of only 2000 ohms, (a factor 3.25 times lower than in the above case) the I_1/I_o maximum reached a value of 1.39 with u/v = 0.96. Although these low impedance circuits were capable of producing relatively high modulation in the beam, the efficiency in these examples dropped to levels of around 35%.

In studying the quality of the bunching it was found that high impedance circuits tended to overbunch the beam and produce large amounts of

crossover. A comparison between the results of high and low impedance bunching is made in Figure 6-62. In this figure the integrated kinetic potential spectrum for the bunched electron beam is presented for two cases of rf beam modulation resulting from high and low impedance bunching. Although the low impedance case produces a lower value of fundamental beam current it has a significantly narrower velocity spectrum. Theoretically, the bunch produced by the low impedance circuit is capable of giving up more energy to a circuit than that produced by the high impedance circuit. These results indicate than an optimum design would utilize different impedance circuits, in the driving or bunching regions of the tube, from that used in the final output cavities.

The parameters used in calculating cases 2, 3, 4, and 5 in Table 6.1 form a consistent set in which only the cavity impedances were varied. In these examples the gap impedance for the high impedance cavities (7145 ohms) was only 50% greater than that of the low impedance cavities (4763 ohms). The best two-cavity taper with all low impedance cavities gave 40.1% efficiency. A three-cavity taper at this impedance level produced 41.6% efficiency. By employing 50% higher impedance cavities in only the tapered output the efficiency increased dramatically to 47.2%. (This case is also the example presented in Figure 6-58.) By employing high impedance cavities throughout the entire output section (except for one lossy cavity immediately following the sever) the highest efficiency that could be achieved was 43.9%. Thus, while high impedance output cavities are needed to convert beam energy into useful output power, the above experiments would indicate that more optimum impedance levels may be found for initially bunching the beam. One would expect this optimum bunching impedance to be a function of the beam perveance.

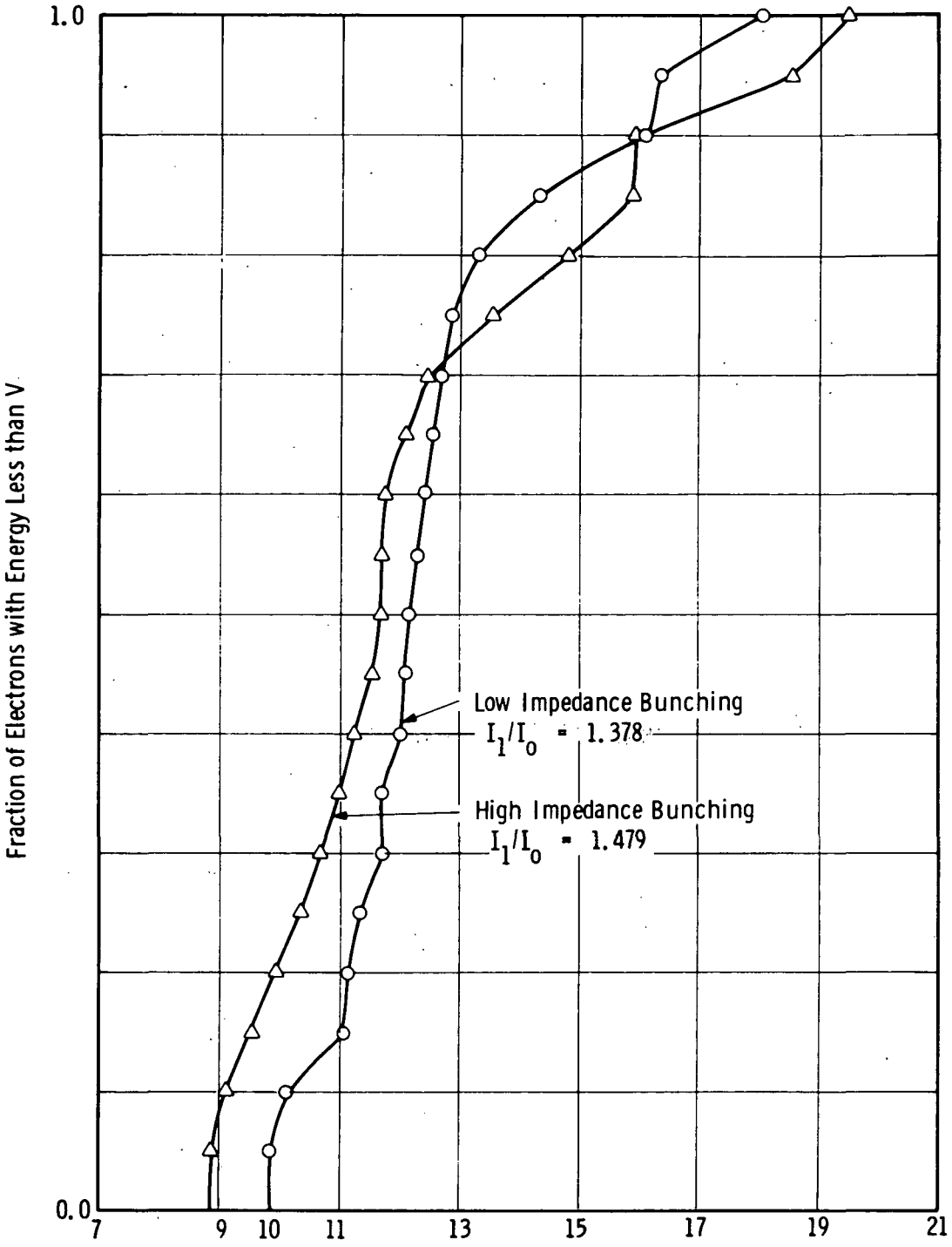

Figure 6-62. Integrated Kinetic Potential Spectrum for Tubes with High- and Low-Impedance Bunching

7.0 CONCLUSIONS

An experimental and analytical program has been undertaken to demonstrate techniques for achieving high conversion efficiency in a 4 kW, cw traveling wave tube at 12.2 GHz.

The initial tubes employed thin webbed cavities in order to maximize interaction impedance, since analysis had shown that high interaction impedance was essential to the achievement of high conversion efficiency. These designs proved to be thermally inadequate.

The first tube built employed a very narrow bandwidth (2%) circuit. Analysis showed this to be the highest impedance configuration which would provide the required 1% operating bandwidth. The thermal failure of this circuit led us to believe that a wider bandwidth circuit would be required, since a wider bandwidth circuit would suffer less from the effects of thermal detuning. This conclusion led to the use of wider bandwidth circuits in all subsequent tests.

Thermal detuning problems were completely resolved in the fourth and fifth tubes by the use of a 0.040 in. thick cavity web. The price paid for the use of a thick web, wide bandwidth circuit, was a significant loss in conversion efficiency. The computed efficiency for the original circuit with optimum velocity taper was 48% compared with a computed optimum efficiency of 38% for the final circuit. It is now believed that a thick web, narrow bandwidth circuit, would have provided the requisite thermal stability with maximum conversion efficiency.

Analysis has shown that high conversion efficiency requires good rf bunching followed by optimum velocity resynchronization. Optimum bunching requires that the circuit wave should travel at approximately the same velocity as the beam. This is called synchronous bunching. The rf current in the beam must be allowed to build to near its maximum value before resynchronization is begun, otherwise bunching will not be complete. Resynchronization is achieved by slowing the circuit wave or by speeding up the beam so that the electron bunch may move into the maximum decelerating

field where it gives up energy to the circuit. Bunching cannot continue in the resynchronized circuit because the phase of the rf field, being right for power extraction, is wrong for bunching. For maximum efficiency it is vital that power be extracted from the bunch rapidly; otherwise space charge forces will obliterate the bunch before the maximum energy is extracted. To achieve rapid extraction of energy from the beam it is essential that the interaction impedance of the resynchronized circuit section be as high as possible.

In the experimental tubes, a less than theoretical taper was employed, in order to maintain the highest possible circuit impedance. This choice was shown to be non-optimum. The best compromise between velocity taper and interaction impedance remains to be found. To solve this problem it would be necessary to estimate or to measure the manner in which the cavity impedance varies as a function of cavity height, assuming a fixed optimum gap length. A large signal computer analysis could then be carried out, in which the interaction impedance changes would automatically be taken into account, as the velocity taper was varied in a search for maximum conversion efficiency.

The 48% computed conversion efficiency of the initial design is probably not attainable. The interaction impedance that was assumed for the taper section could not be achieved in practice, without thinning the cavity web to a point which has been demonstrated thermally infeasible, for a 4 kW TWT operated at 12.2 GHz. The computed conversion efficiency for the final design employing a thicker webbed wider bandwidth circuit was 38%. During the mechanical design phase it was found that the required optimum taper could not be achieved without compromising the circuit impedance. It was decided instead to compromise the taper velocity in order to maintain the impedance. The result was a tube with measured efficiency (referred to the output cavity of the tube) of 31%. The conversion efficiency of the tube actually built was never computed; however, a very nearly identical design had previously been computed to have 31% efficiency. (See Case No. 6 Table 6.1.)

This program has provided a clear understanding of the problems in the design and fabrication of a high efficiency TWT at 12.2 GHz. It has improved our knowledge

of the design of low perveance electron guns. Thermal tuning problems, unusual in traveling wave tubes, have been encountered and resolved. The adequacy of computer simulation of high efficiency traveling wave tubes has been verified. The ability to compute the stability threshold for band edge oscillation has been demonstrated. A better understanding has been gained of the way in which the backward wave interferes with the interaction process in high gain per cavity traveling wave tubes.

Varian Associates
Palo Alto Tube Division
Palo Alto, California, March 20, 1973

8.0 REFERENCES

1. Kavanagh, Francis E.; Alexovich, Robert E.; and Chomos, Gerald J.: Evaluation of Novel Depressed Collector for Linear-Beam Microwave Tubes. NASA TM X-2322, 1971.

2. Kosmahl, Henry G.: A Novel, Axisymmetric, Electrostatic Collector for Linear Beam Microwave Tubes. NASA TN D-6093, 1971.

3. Pierce, J. R.: Traveling Wave Tubes. D. Van Nostrand Co., Inc., 1954.

4. Gerchberg, R. W.; Niclas, K. B.: New Concepts for Achieving High Efficiency in Traveling-Wave Tubes. Q.P.R. No. 4, Feb — Apr 1965; No. 5, May — July 1965; No. 6, Aug — Oct 1965. (Contract No. DA28-043 AMC-00076(E), DA Project No. 5624-11-905-05-65, USAEL, Fort Monmouth, New Jersey) Watkins-Johnson Co., Palo Alto, California.

5. Curnow, H. J.: A General Equivalent Circuit for Coupled-Cavity Slow-Wave Structures. IEEE Trans., MTT-13, No. 5, Sept 1965, pp. 671-675.

6. Tien, P. K.: A Large Signal Theory of Traveling Wave Amplifiers. BSTJ, Vol. 35, No. 2, Mar. 1956, pp 349-374.

7. Lien, Erling L.: High Efficiency Klystron Amplifiers. Eighth International Conference on Microwave and Optical Generation and Amplification, Amsterdam, Sept 1970, Section II, pp. 21-27.

8. Gittens, J. F.: Power Traveling-Wave Tubes. American Elsevier Publishing Co., 1965, pp. 99-100.

9. Pierce, J. R.: Theory and Design of Electron Beams. D. Van Nostrand Co., Inc., 1954.

10. Pierce, J. R.: Op. cit., 3, p. 95.

11. Scott, A. W.: Why a Circuit Sever Affects Traveling Wave Tube Efficiency. IRE Trans., PGED, Vol. ED-9, Jan. 1962, pp. 35-41.

APPENDIX A

LIST OF SYMBOLS

a	inner radius of drift tube
b	Pierce's velocity parameter
C	Pierce's gain parameter
E_b	dc beam voltage
E_f	filament voltage
I_o	beam current
I_b	beam current
I_{body}	beam current intercepted by circuit
I_{mag}	focusing solenoid current
I_{gun}	auxilliary focusing coil current
k	free space propagation number, ω/v
K	Pierce's impedance parameter
L	periodic length of circuit
P	power propagating on circuit
P_d	rf input power
P_o	dc beam power
Q	quality factor of resonant cavity
QC	Pierce's space charge parameter
R	Cavity interaction gap shunt resistance
R_o	final radius of magnetic flux tube which intersects edge of cathode
r_o	radius of electron beam
S	beam perveance, $I_o/V_o^{3/2}$
u	dc beam velocity
u_o	dc beam velocity
v	velocity of wave propagation
V	peak gap voltage
V_o	dc beam voltage

V_{gap}	peak gap voltage
β	axial propagation number, ω/v
β_e	electronic propagation number, ω/u
γ	radial propagation number, $\sqrt{\beta^2 - k^2}$
δ	cavity interaction gap length
η	conversion efficiency
μperv	perveance times 10^6
ϕ	rf phase shift
ω	angular frequency
ω_q	reduced plasma angular frequency

APPENDIX B

BIBLIOGRAPHY

A. LARGE SIGNAL ANALYSIS

Putz, J. L.
Non-Linear Effects in Velocity Modulated Beams.
Electronics Research Laboratory, Stanford University, Stanford
TR. No. 33, March 1951.

Putz, J. L.
Non-Linear Phenomena in Traveling-Wave Amplifiers.
Electronics Research Laboratory, Stanford University.
TR No. 37, October 1951.

Nordsieck, A.
Theory of the Large-Signal Behavior of Traveling Wave Amplifiers.
Proceedings of IRE, Volume 41, No. 5, pp. 630-637, May 1953.

Poulter, H. C.
Large Signal Theory of the Traveling Wave Tube.
Stanford University, Electronics Research Laboratory, Tech
Report, No. 73, January 1954.

Hess, R. L.
Some Results in the Large Signal Analysis of Traveling Wave Tubes.
University of California, Institute of Engineering Research,
Tech Report No. 60. December 1954.

Tien, P. K., Walker, L. R., Wolantis, V. M.
A Large Signal Theory of Traveling Wave Amplifiers.
Proceedings of IRE, Volume 43, No. 3, pp. 260-277, March 1955.

Rowe, J. E.
A Large Signal Analysis of the Traveling Wave Amplifier.
University of Michigan, Electron Tube Laboratory, Tech Report
No. 19, April 1965.

Caldwell, J. J., Jr., Hock, O. L.
Large Signal Behavior of High Power Traveling Wave Amplifiers.
IRE Transactions, PGED, Volume ED-3, pp. 6-17, January 1956.

Rowe, J. E.
A Large Signal Analysis of the Traveling Wave Amplifier: Theory
and General Results.
IRE Transactions, Volume ED-3, pp. 39-57, January 1956.

Tien, P. K.
A Large Signal Theory of Traveling Wave Amplifiers.
BSTJ. Volume 35, No. 2, pp. 349-374, March 1956.

Cutler, C. C.
The Nature of Power Saturation in Traveling Wave Tubes.
BSTJ, Volume 34, July 1956.

Webber, S. E.
Electron Bunching and Energy Exchange in a Traveling Wave Tube.
Transactions of IRE, Volume ED-4, PGED, pp. 87-91, January 1957.

Wilson, R. N.
Theory of the Signal Behavior of Traveling Wave Amplifiers.
Microwave Laboratory Stanford University. Internal Memo,
ML Report 359, January 1957.

Wilson, R. N.
A Large Signal Theory of Traveling Wave Amplifiers.
Microwave Laboratory, Stanford University. Internal Memo,
ML Report 360, January 1957.

Sobol, H., Rowe, J. E.
Theoretical Power Output and Bandwidth of Traveling Wave Amplifiers.
Electron Physics Laboratory, University of Michigan,
Tech Report, No. 32, August 1959.

Rowe, J. E.
One-Dimensional Traveling Wave Tube Analyses and the Effect
of Radial Electric Field Variations.
Transactions of IRE, PGED, Volume ED-7, pp. 16-21, January 1960.

Konrad, G. T., et al.
Theoretical and Experimental Investigation of Large Signal
Traveling Wave Tubes.
University of Michigan, Electron Physics Laboratory,
Final Report (February 1953 to August 1960). August 1960.

Rowe, J. E.
N-Beam Non-Linear Traveling Wave Amplifier Analysis.
University of Michigan, Ann Arbor, Michigan, Electron Physics
Laboratory, Tech Report No. 44, January 1961.

Rowe, J. E.
Relativistic Beam-Wave Interaction.
Electron Physics Laboratory, The University of Michigan,
Tech Report No. 48, June 1961.

Rowe, J. E.
N-Beam Non-Linear Traveling Wave Amplifier Analysis.
IRE Transactions, PGED, Volume ED-8, pp. 279-284, July 1961.

Hess, R. L.
Large Signal Traveling Wave Tube Operation: Concepts and Analysis.
University of California Electronic Technology Laboratory,
ASD Tech Report, 61-15, July 1961.

Rowe, J. E., et al.
Theoretical and Experimental Investigation of Large Signal
Traveling Wave Tubes. Electron Physics Laboratory,
The University of Michigan Quarterly Progress Reports,
QPR No. 6: October 1961.

Investigation of Large Signal Traveling Wave Tubes:
Electron Physics Laboratory, University of Michigan, Ann Arbor,
Tech Report, No. RADC, TDR-63-284, August 1963.

Konrad, G. T., et al
Investigation of Large Signal Traveling Wave Tubes.
University of Michigan, Electron Physics Laboratory, TR-No.
RADC TR-64-542, Final Report, February 1965.

Rowe, J. E.
Non-Linear Electron Wave Interaction Phenomena.
Academic Press, New York, 1965.

B. EFFICIENCY STUDY

Rowe, J. E., Sobol, H.
General Design Procedure for High Efficiency Traveling Wave
Amplifiers. Electron Tube Laboratory, University of Michigan.
Tech Reports, No. 24, Part 1.

Rowe, J. E., Sobol, H.
General Design Procedure for High Efficiency Traveling Wave
Amplifiers. Transactions IRE, PGED, Volume ED-5, pp. 288-300,
October 1958.

Birdsall, C. K., Johnson, C. C.
Traveling Wave Tube Efficiency Degradation Due to Power Absorbed
in the Attenuator. IRE Transactions, Volume ED-6, pp. 6-8,
January 1959.

Ruetz, J. A., Robinson, D., Pavkovich, J.
The Effect of Tapered Circuits on Efficiency for High Power Traveling
Wave Tubes. Electron Device Meeting, Washington, D.C., October 1960.

Rowe, J. E., Meeker, J. G.
Interaction of Premodulated Electron Streams with Propagating Circuits. Journal of Elect. and Control., Volume 9, pp. 439-467, December 1960.

Meeker, J. G.
Phase-Focusing in Linear-Beam Devices.
Electron Physics Laboratory, University of Michigan,
Tech Reports, No. 49, August 1961.

Scott, A. W.
Why a Circuit Sever Affects Traveling Wave Tube Efficiency.
IRE Transactions, PGED, Volume ED-9, pp 35-41, January 1962.

Meeker, J. G., Rowe, J. E.
Phase-Focusing in Linear-Beam Devices.
IRE Transactions, PGED, Volume ED-9, pp. 257-266, May 1962.

Lichtenberg, A. J.
Prebunched Beam Traveling Wave Tube Studies.
IRE Transactions, PGED, Volume ED-9, pp. 345-350, July 1962.

Bates, D. J., Scott, A. W.
The Effect of Circuit Tapering on the Efficiency, Bandwidth Characteristics of Dispersive Traveling Wave Tubes. IRE Transactions, PGED, Volume ED-10, p. 89, March 1963.

Haddad, G. I., Rowe, J. E.
General Velocity Tapers for Phase-Focused Forward Wave Amplifiers.
IEEE Transactions, PTGED, Volume ED-10, p. 212, May 1963.

Rowe, J. E., Brackett, C. A.
Velocity Tapering in Microwave Amplifiers.
University of Michigan, Electron Physics Laboratory,
Tech Reports, No. RADC-TR-64-554, March 1965.

Rowe, J. E., Brackett, C. A.
Velocity Tapering in Microwave Amplifiers.
IRE Transactions, PGED. Volume ED-12, No. 8, pp 441-447,
August 1965.

Pond, N. H., Twiggs, R. J.
Improvement of Traveling Wave Tube Efficiency Through Period Tapering.
IEEE Transactions, Volume ED-13, pp. 956-961, December 1966.

Sanseng, O. G., Basiulis, A., Tammaru, I.
Analytical Study Program to Develop the Theoretical Design of Traveling Wave Tubes. Final Report. NASA, CR No. 72450, October 1968.

FINAL REPORT MAILING LIST

1. National Aeronautics & Space Administration
   Headquarters
   Washington, DC 20546

   Attn: ED/L. Jaffe 1
   ECC/A.M.G. Andrus 10
   EC/R.B. Marsten 1

2. NASA – Lewis Research Center
   21000 Brookpark Road
   Cleveland, Ohio 44135

   Attn: H. W. Plohr (MS 54-1) 1
   R. E. Alexovich (MS 54-5) 1
   Dr. H. G. Kosmahl (MS 54-5) 1
   Tech. Utilization Officer (MS 3-19) 1
   Contract Section B (MS 500-313) 1
   Library (MS 60-3) 2
   Report Control Office (MS 5-5) 1
   N. T. Musial (MS 400-311) 1
   G. J. Chomos (MS 54-5) 50

3. Communication Systems Inc.
   5817 Columbia Pike
   Falls Church, Virginia 22046

   Attn: J. Bisaga 1

4. Rand Corporation
   1700 Main Street
   Santa Monica, California 90404

   Attn: Dr. J. Holt 1

5. NASA – George C. Marshall Space Flight Center
   Huntsville, Alabama 35812

   Attn: RASTR-A/E.C. Hamilton 1
   Library 1

6. NASA – Goddard Space Flight Center
   Greenbelt, Maryland 20771

   Attn: 733/R. Pickard 1
   Library 1

7. NASA – Ames Research Center
   Moffett Field, California 94035

   Attn: OART-MAO/E. Van Vleck (MS 202-6) 1
   Library 1

8. NASA – Langley Research Center
   Langley Station
   Hampton, Virginia 23365

   Attn: B. Kendall (MS-173) 1
   Library (MS-185) 1

9. NASA – Manned Spacecraft Center
   Houston, Texas 77001

   Attn: Library 1

10. Jet Propulsion Laboratory
    4800 Oak Grove Drive
    Pasadena, California 91103

    Attn: L. Derr 1
    Library 1

11. NASA Scientific and Technical Information
    Facility
    P.O. Box 33
    College Park, Maryland 20740

    Attn: NASA Representative 3

12. TRW Systems
    One Space Park
    Redondo Beach, California 90278

    Attn: W. A. Finley/Space Vehicle Division 1
    Alfred P. Fay 1

13. General Dynamics, Convair Division
    P.O. Box 1128
    San Diego, California 92112

    Attn: F.J. Dore/Advanced Programs Laboratory 1

14. Hughes Aircraft Company
    Space Systems Division
    1194 W. Jefferson Boulevard
    Culver City, California 90230

    Attn: H.A. Rosen/Satellite Systems Laboratory 1

15. General Electric Company
    Missile and Space Division
    Valley Forge Space Technology Center
    P.O. Box 8555
    Philadelphia, Pennsylvania 19101

    Attn: H. Collins 1
    P. Nadler 1

16. Federal Communications Commission
    521 12th Street
    Washington, DC 20554

    Attn: H. Fine 1

17. U. S. Information Agency
    25 M St. S. W.
    Washington, DC 20547

    Attn: IBS/EF/G. Jacobs 1

18. General Electric Company
    Tube Department
    Microwave Tube Operation
    Schenectady, New York 12305

    Attn: R. Dehn 1
    Dr. T. Mihran 1
    Dr. G. Branch 1
    W. Neugebauer 1

19. Litton Industries
Electron Tube Division
960 Industrial Road
San Carlos, California 94070

Attn: Dr. G. Pokorney 1
J. Orr 1
W. Day 1
Dr. O. Sauseng 1
R. Cerko 1
B. D. McNary 1

20. Varian
Eastern Tube Division
Salem Road
Beverley, Massachusetts 01915

Attn: Dr. G. Farney 1

21. Hughes Aircraft Company
Electron Dynamics Division
P.O. Box 2999
Torrance, California 90509

Attn: Dr. J. Mendel 1
Dr. I. Tammaru 1
J. A. Christensen 1

22. Watkins Johnson Company
3333 Hillview Avenue
Palo Alto, California 94304

Attn: R. Espinosa 1

23. Varian Associates
611 Hansen Way
Palo Alto, California 94303

Attn: Dr. G. Caryotakis 1
Dr. J. Reutz 1
Dr. W. Ayers 1
Dr. W. Harmon 1

24. RCA
Industrial Tube Division
Lancaster, Pennsylvania

Attn: W. P. Bennett 1

25. Raytheon Company
Research Division
28 Seyon Street
Waltham, Massachusetts

Attn: W. Teich 1
Dr. J. M. Osepchuk 1

26. Mr. Lawrence Gasch 1
Aerospace Radar Branch
U.S. NRL
Washington, DC 20390

27. Mr. Robert Richardson 1
Mail No. 1620
Martin-Marietta Corp.
Denver Division
P.O. Box 179
Denver, Colorado 90201

28. Mr. William E. Waters 1
Sr. Engr. Staff Specialist
Philco Ford Corporation
3939 Fabian Way
MS C-70
Palo Alto, California 94303

29. Mr. George Orr 1
Code 733
Goddard Space Flight Center
Greenbelt, Maryland 20771

30. Sperry
Electronic Tube Division
Gainsville, Florida 32601

Attn: H. H. Conners 1

31. Lt. Commander L. Wardel 1
Naval Electronic Systems Command
PME 116
Washington, DC 20360

32. Commanding Officer
Navy Space Systems Activity
Air Force Unit Post Office
Los Angeles, California 90045

Attn: Code 50 1

33. U. S. Air Force Liaison Officer (MS 501-3) 1
c/o NASA – Lewis Research Center
2100 Brookpark Road
Cleveland, Ohio 44135

34. National Technical Information Service 15
Springfield, Virginia 22151